^{19}F PCS NMR Spectroscopy: a Novel Approach to Determine Structures of Protein-Ligand Complexes, Illustrated with Human Carbonic Anhydrase II and Fluorinated Inhibitors

Inauguraldissertation

zur

Erlangung der Würde eines Doktors der Philosophie

vorgelegt der

Philosophisch-Naturwissenschaftlichen Fakultät

der Universität Basel

von

Kaspar Zimmermann

aus Basel (BS)

Basel 2018

Genehmigt von der Philosophisch-Naturwissenschaftlichen Fakultät
auf Antrag von:

Prof. Dr. Thomas R. Ward

PD Dr. Daniel Häussinger

Prof. Dr. Catherine Housecroft

Basel, den 19.04.2016

Prof. Dr. Jörg Schibler
Dekan

Abstract

This thesis presents the structural investigation of human carbonic anhydrase II (hCA-II) inhibitor complexes by pseudocontact shift (PCS) NMR spectroscopy. Five different single cystein mutants of hCA-II were prepared in different isotope labelling schemes. These protein mutants were tagged with LnM8-SPy complexes for the determination of PCS. Triple labelling of one protein mutant allowed the unambiguous assignment of 90 % of the protein backbone. For four out of five protein mutants reasonable PCS were observed and the assignment of the PCS was possible for more than 90 % of the assigned residues. This large number of assigned PCS showed an excellent agreement between the protein structure in solution and the X-ray structure. In order to determine precise $\Delta\chi$-tensor parameters based on the X-ray structure PCS in the neighbourhood of the tag and in fluctional parts of the protein were systematically excluded. ^{19}F PCS were determined for two different fluorinated inhibitors bound to hCA-II, for each of the four protein mutants. Based on the determined $\Delta\chi$-tensor parameters the fluorine position was determined based on the ^{19}F PCS alone. This is the first example of the localization of a fluorine-containing ligand within a protein, based only on one-dimensional ^{19}F-nuclear magnetic resonance (NMR) spectra and the PCS derived from this data.

While the fluorine-fluorine distance in the ligand that contains two F-atoms, was reproduced very precisely by the ^{19}F-PCS, the positioning of the two ligands within the hCA-II protein was significantly different compared to the X-ray structures of the two complexes. For one of the two protein inhibitor complexes, a deviation of up to 8 Å was observed. The most likely reason for this systematic error was identified to be residual anisotropic chemical shift (RACS) that could not be taken in account in the structure calculation. This was supported by the second protein-inhibitor complex, where a higher degree of motional freedom of the fluorine atoms and therefore smaller RACS were observed and consequently the determined PCS position was closer to the X-ray structure. A validation of the PCS structure determination suggested a precision of the proton position from PCS alone of 1-2 Å. Finally, the principle of using an ^{1}H-^{19}F-heteronuclear Overhauser effect spectroscopy (HOESY) spectra to determine ^{1}H PCS of protons close to the fluorine was demonstrated.

Contents

Acronyms

Notation	Description
AcN	aceto nitrile
amp	ampicillin
amp^r	ampicillin resistance
APS	ammonium peroxodisulfate
cm	chloramphenicol
cm^r	chloramphenicol resistance
CSA	chemical shift anisotropy
CV	column volume
DIPEA	diisopropylethylamine
DMSO	dimethyl sulfoxide
DMSO-D_6	deuterated dimethyl sulfoxide
DNA	deoxyribonucleic acid
DNase I	Deoxyribonuclease I
DOTA	1,4,7,10-tetraazacyclododecane-1,4,7,10-tetraacetic acid
DTT	dithiothreitol
EPR	electron paramagnetic resonance
ESI-MS	electrospray ionisation mass spectrometry
EtOAc	ethyl acetate

Notation	Description
EtOH	ethanol
GdmCl	guanidinium chloride
GPS	global positioning system
hCA-I	human carbonic anhydrase I
hCA-II	human carbonic anhydrase II
hetNOE	heteronuclear nuclear Overhauser effect
HOE	heteronuclear Overhauser effect
HOESY	heteronuclear Overhauser effect spectroscopy
HPLC	high performance liquid chromatography
HSQC	heteronuclear single quantum coherence
IPAP	in phase anti phase
IPTG	Isopropyl-β-D-thiogalactopyranosid
LB	lysogeny broth
LCT	lanthanide chelating tag
MeOH	methanol
NEt_3	triethylamine
NMR	nuclear magnetic resonance
NOE	nuclear Overhauser effect

Notation	Description
OD_{600}	optical density at 600 nm
PCR	polymerase chain reaction
PCS	pseudocontact shift
PDB	protein data bank
PMFS	phenylmethanesulfonylfluoride
PRE	paramagnetic relaxation enhancement
pyBOP	benzotriazol-1-yl-oxytripyrrolidinophosphonium hexafluorophosphate
RACS	residual anisotropic chemical shift
RDC	residual dipolar couplings
RMS	root mean square
RMSD	root mean square deviation
RNA	ribonucleic acid
RT	room temperature
SAP	square anti prism
SDS	sodium dodecyl sulfate
SDS-PAGE	sodium dodecyl sulfate polyacrylamide gel electrophoresis
SOC	Super Optimal Broth with Catabolic repressor
TCEP	tris(2-carboxyethyl)phosphine

Notation	Description
TEMED	tetramethylethylenediamine
TFA	trifluoroacetic acid
TOF	time of flight
TROSY	transverse relaxation optimized spectroscopy
TSAP	twisted square anti prism
UV	ultraviolet-visible

CHAPTER 1

Introduction

Nuclear magnetic resonance (NMR) spectroscopy nowadays is a standard method for the structure determination in chemistry and molecular biology. NMR spectroscopy determines the interaction of a nuclear spin with a magnetic field. In order to observe such interactions a nuclear spin is required thus limiting this method to those atoms i.e. to those isotopes with nuclear spin. Especially well suited for NMR spectroscopy are nuclei with a nuclear spin of ½, such as ^{1}H, ^{13}C, ^{15}N and ^{19}F. The interaction of the nuclear spin with the magnetic field strongly depend on the chemical environment of a nucleus and therefore allows to determine structural information.[1]

1.1 Protein NMR spectroscopy

The determination of protein structures in solution[2] as well as the detailed characterisation of dynamic processes, that can be observed for a large range of time-scales (from picoseconds to days)[3] are two of the main advantages of protein NMR spectroscopy. The first protein structure determined by NMR was solved in 1984.[2] The first protein structure solved by X-ray crystallography was determined already 26 years before, in 1958.[4] Today still the vast majority of published protein structures are determined by X-ray crystallography as this can be seen from the RCSB protein data bank (PDB).[5] X-ray structures, however, have the drawback that they only deliver static information about the protein structure. If dynamic processes are involved, NMR spectroscopy remains the only source that can deliver detailed residue specific information.[3]

In order to record multidimensional NMR spectra of protein samples stable isotope labelling of the protein is an important requirement due to the low natural abundance of ^{13}C and ^{15}N. For standard ^{1}H-^{15}N heteronuclear single quantum coherence (HSQC) experiments at least uniform ^{15}N or amino acid selective ^{15}N labelling of the protein is required.[6] For standard triple resonance experiments that are used for protein backbone assignment additionally uniform ^{13}C labelling of the protein is necessary. For larger proteins >20 kDa protein NMR spectroscopy becomes more challenging due to the decreasing transversal relaxation time and consequently smaller signal intensity with increasing molecular weight. Deuteration of the protein decreases the relaxation rates of the remaining protons and therefore improves the signal intensity.[7]
Nuclear Overhauser effects (NOEs) are one of the major restraints used for protein structure determination. Although they deliver more or less precise structural information due to their distance dependence of $1/r^6$ they are limited to a distance of 5 Å. Because the median protein size for human proteins is in the order of 60 Å[8] it becomes obvious that with increasing protein size NOE restraints lose more and more significance because they deliver only local structural information. Especially with regard that this number only represents the size of monomeric proteins and does not consider protein-protein complexes that are observed in many important biological processes. In the last century different methods have been developed to enable solution state NMR studies of large proteins and protein-protein complexes, among them paramagnetic restraints have gained a very important role because they deliver unique long-range information for protein structure determination.[3]

1.2 Paramagnetic NMR

Paramagnetic ions, especially paramagnetic lanthanide ions induce several long range effects on nuclear spins that can be used for structure determination. Several of these effects are known for a long time in NMR spectroscopy. For example pseudocontact shift (PCS) have been observed for the first time in 1960.[9] And the use of paramagnetic relaxation enhancement (PRE) for the study of biological systems has already been proposed in 1971.[10]
PRE is an effect observable for every paramagnetic center. The interaction of a nuclear spin with a paramagnetic center leads to a increased relaxation rate and therefore to

an increase of the linewidth of the corresponding NMR signal.[11] PRE depend with $1/r^6$ on the distance of the nuclear spin to the paramagnetic center and are observable for distances up to 30 Å.[12] In general for every paramagnetic effect, it is very important to determine an experimental parameter with respect to a suitable diamagnetic reference, in order to cover for every interaction of the paramagnetic center that is not related with paramagnetism.
If the unpaired electrons have an anisotropic distribution, which is the case for all trivalent paramagnetic lanthanide ions apart from gadolinium, then additional effects such as PCS, residual dipolar couplings (RDC) and residual anisotropic chemical shift (RACS) can be observed.

1.3 Pseudocontact shifts

PCS are differences in the chemical shift of a nuclear spin that are induced by the interaction of a paramagnetic ion with anisotropic distribution of the unpaired electrons.[13] PCS can be described according to the following equation:[14]

$$\delta^{PCS} = \frac{1}{12\pi r^3}\left[\Delta\chi_{ax}\left(3\cos^2\theta - 1\right) + \frac{3}{2}\Delta\chi_{rh}\sin^2\theta\cos 2\phi\right] \tag{1.1}$$

Where δ^{PCS} is the observed PCS and $\Delta\chi_{ax}$ and $\Delta\chi_{rh}$ are the axial and rhombic components of the anisotropic magnetic susceptibility tensor ($\Delta\chi$-tensor). And r, θ and ϕ are the polar coordinates describing the position of the nuclear spin with respect to the paramagnetic center. Due to the $1/r^3$ distance dependence PCS are observable for much larger distances than NOE or PRE. PCS have been observed for distances of 70 Å and theoretically they should last as far as 150 Å.[15] The angular dependence of the PCS illustrates why a tight attachment of the paramagnetic ion is necessary in order to observe large PCS, because residual motion of the paramagnetic ion with respect to the protein leads to averaged and only very small PCS. The solutions of equation 1.1 for a given PCS, $\Delta\chi_{ax}$ and $\Delta\chi_{rh}$ for the polar coordinates r, θ and ϕ deliver an isosurface describing all positions where a certain PCS can be observed as displayed in figure 1.1

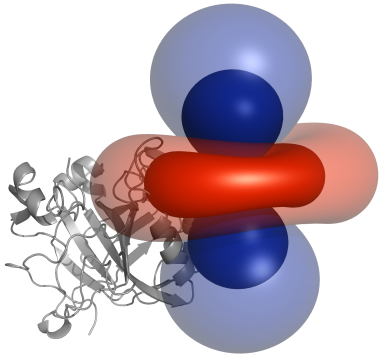

Figure 1.1: Isosurfaces representing the solutions of equation 1.1 of an arbitrary tensor for a PCS of 0.5 ppm (transparent) and 2 ppm (solid). Blue surfaces represent a positive and red a negative PCS.

1.4 Residual dipolar couplings

Paramagnetic ions with an anisotropic $\Delta\chi$ tensor weakly align in the magnetic field. When such ions are tightly bound to a protein this leads to partial alignment of the whole protein and therefore compared to the isotropic case residual dipolar couplings are observable. These couplings add to the scalar coupling constant of two coupled nuclei. Such RDC can be described by the following equation:[14,16]

$$D_{IS} = -\frac{B_0^2 \gamma_I \gamma_S \hbar}{120 k T \pi^2 r_{IS}^3} \left[\Delta\chi_{\mathrm{ax}} \left(3\cos^2\theta - 1\right) + \frac{3}{2}\Delta\chi_{\mathrm{rh}} \sin^2\theta \cos 2\phi \right] \tag{1.2}$$

where D_{IS} is the observed RDC between the coupled nuclear spins I and S, B_0 the magnetic field, γ_I and γ_S the gyromagnetic ratios of two spins, $\hbar$ the reduced Planck constant, r_{IS} the internuclear distance between the coupled spins. $\Delta\chi_{\mathrm{ax}}$ and $\Delta\chi_{\mathrm{rh}}$ are again the axial and rhombic components of the $\Delta\chi$-tensor and θ and ϕ the polar angles describing the orientation of the IS vector with respect to the orientation of the $\Delta\chi$-tensor. RDC do not depend on the distance to the paramagnetic center that is responsible for the molecular alignment and therefore can be observed for every pair of coupled nuclear spins in a protein.

1.5 Residual anisotropic chemical shifts

For partially aligned protein small chemical shift changes are observable, because similar to the RDC, the chemical shift anisotropy (CSA) is not completely averaged to an isotropic chemical shift any more which results in small shift changes depending on the orientation of the nuclear spin in the protein. These shifts, called RACS, have been studied in proteins aligned by an external alignment media.[17] In the case of an alignment due to anisotropic paramagnetic metal ion these small shifts add to the effective PCS resulting in the experimentally observed PCS. RACS can be determined according to the following equation:

$$\delta^{\mathrm{RACS}} = \frac{B_0^2}{15\mu_0 kT} \sum_{i,j\in\{x,y,z\}} -\sigma_{ii}^{\mathrm{CSA}} \cos^2\theta_{ij} \Delta\chi_{jj} \tag{1.3}$$

where B_0 is the magnetic field, μ_0 the permeability of vacuum, k the *Boltzmann* constant, T the temperature, $\sigma_{ii}^{\mathrm{CSA}}$ the principal components of the CSA-tensor, $\Delta\chi_{jj}$ the principal components of the $\Delta\chi$-tensor and θ_{ij} the angle between the corresponding principal axis of the CSA-tensor and the $\Delta\chi$-tensor.[18,19] For protons RACS are negligible small, but not for ^{13}C or ^{15}N. For protein backbone carbonyl depending on the orientation RACS can exceed 0.1 ppm.[20] Similar to the RDC, RACS can be observed throughout an aligned protein.

1.6 Lanthanide chelating tags

Early studies of proteins that included paramagnetic restraints were carried out with metal binding proteins, such as cytochrome c that contains heme group consisting of a paramagnetic Fe^{III}-porphyrin complex[21] or the calcium binding protein calbindin where a calcium binding to the protein was replaced by a lanthanide ion.[22] This approach was restricted to metal binding proteins, but the study on calbindin has shown the large potential of lanthanide ions for paramagnetic restraints.[23] During the first decade of the new millennium several lanthanide chelating tag (LCT) have been developed that allowed the attachment of a lanthanide metal to a protein via a cysteine residue on the protein surface. Such a cysteine residue can be introduced at a desired position in the protein sequence by site directed mutagenesis.[24] This permitted to

determine paramagnetic restraints for theoretically every protein, independent of a metal binding site. Early lanthanide chelating tags showed only poor PCS and RDC in the order of 0.12 ppm and 5 Hz respectively.[25] The reason for the small shifts was the high flexibility of the tags, as well as their low affinities towards lanthanide metals. The low affinity could be resolved by the development of tags based on the 1,4,7,10-tetraazacyclododecane-1,4,7,10-tetraacetic acid (DOTA) framework, that shows an extremely high affinity towards lanthanide ions.[26] To ensure a rigid attachment of the tag to the protein a strategy of a two point anchoring of a DOTA based tag showed a rigid attachment to the protein based on the large PCS that were observed.[27] Nevertheless this approach requires the introduction of two cysteine residues to the protein surface at a defined distance. Therefore a single point attachment of a tag would be much simpler for the production of a corresponding protein mutant.

1.7 DOTA-M8-SPy

DOTA-M8-SPy (**M8-SPy**) is an extremely rigid lanthanide chelating tag, based on the DOTA framework. The stereoselective introduction of eight methyl groups provide only one single confomer of the corresponding lanthanide complex, which has been demonstrated on the diamagnetic LuM8-SPy complex.[28] When the dysprosium-tag is attached to a single cystein mutant of ubiquitin extremely large PCS were observed, that are still unprecedented for such a type of attachment.

The lanthanide complexes of DOTA have a rather complex stereochemistry (shown in

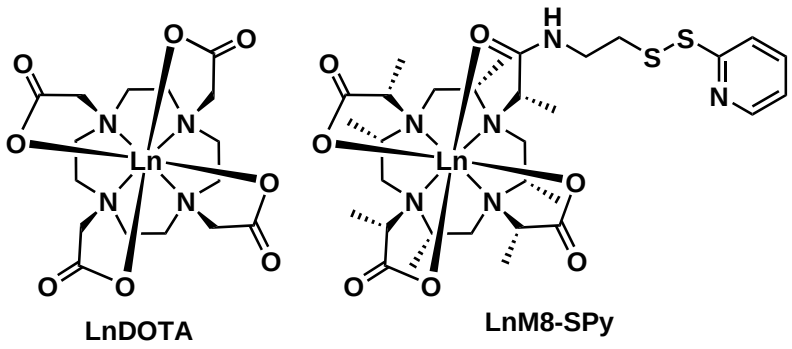

Figure 1.2: Lanthanide complexes of DOTA and M8-SPy.

figure 1.3) with in total four different stereoisomers.[29] Depending on the orientation

of the side-arms and the conformation of the twelve-membered cyclen ring either a square anti prism (SAP) or a twisted square anti prism (TSAP) coordination polyhedron around the metal center is obtained. In the case of the lutetium complexes of M8-SPy, depending on the stereochemistry of the methyl groups only one distinct stereoisomer is obtained. The *S* configuration of the stereocenters at the cyclen ring selectively results in the (δδδδ) conformation of the cyclen ring. Where the *R* and the *S* configuration of the side-arm direct the complex in the Λ and Δ conformation respectively. Therefore for (*8S*)-LuM8-SPy only the TSAP (Δδδδδ) conformation and for the *4R,4S* stereoisomer only the SAP (Λδδδδ) conformation is observed.

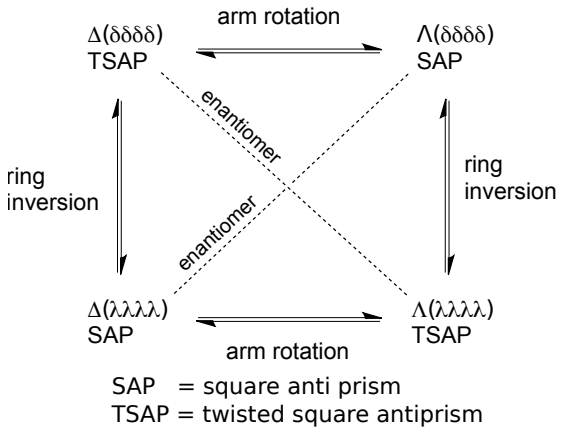

Figure 1.3: Stereoisomers of LnDOTA complexes.

The synthesis of the lanthanide complexes of M8-SPy is carried out in a six step synthesis starting from tetramethylcyclen **1** as shown in figure 1.4. Detailed conditions are given in the experimental section.

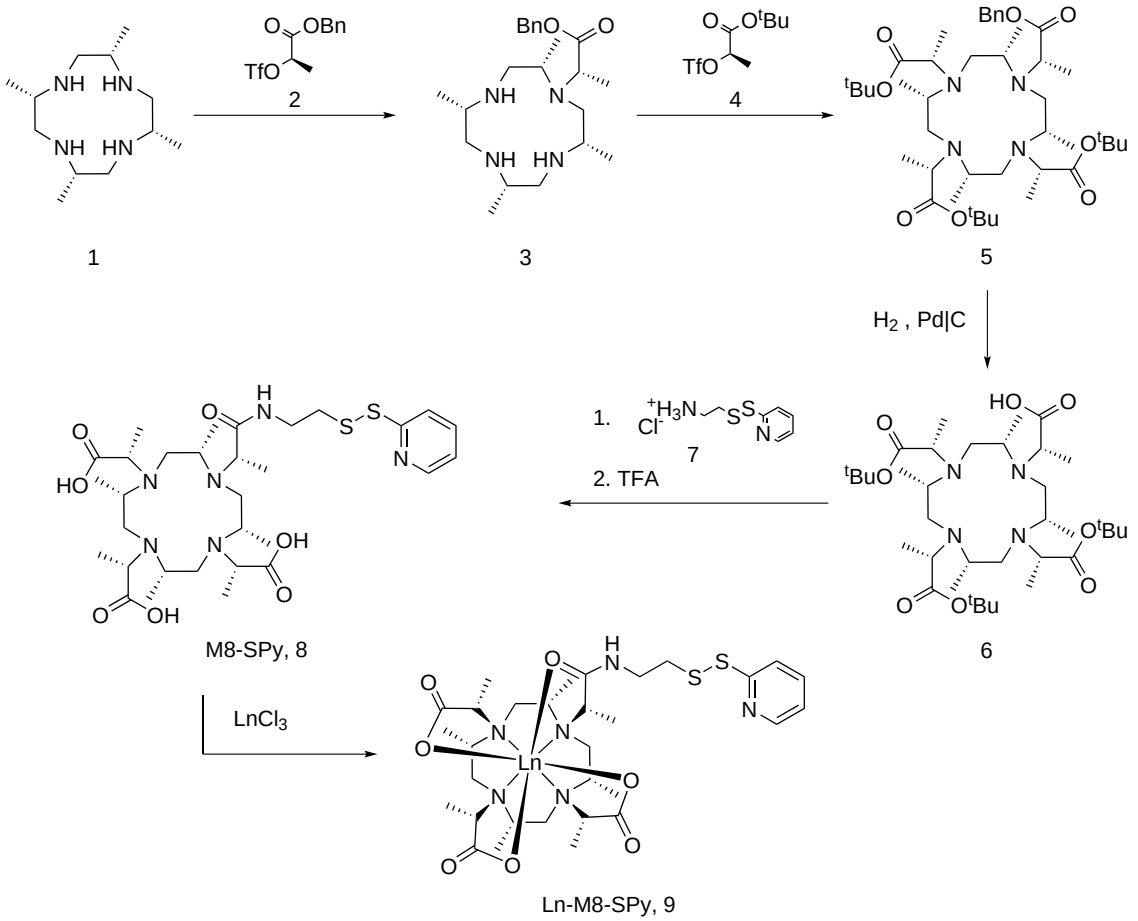

Figure 1.4: Synthesis of lanthanide complexes of M8-SPy.

1.8 GPS-like position determination from PCS of multiple sites

For the determination of the position of one or more atoms in a protein by PCS alone, it is far better to determine the PCS from protein samples that have been tagged at different sites of the protein. When the PCS of different lanthanide metals tagged the same position in the protein are used for the position determination, then the isosurfaces defining the possible positions for a certain PCS are very likely to intersect in a small angle, leading to a poor precision of the position in directions parallel to the isosurfaces. When the position is determined from PCS obtained for different tagging sites the probability of the isosurfaces to intersect in an angle close to 90° is much higher and therefore the position is usually better defined.

In figure 1.5 the principle of determining a position from PCS is illustrated. When

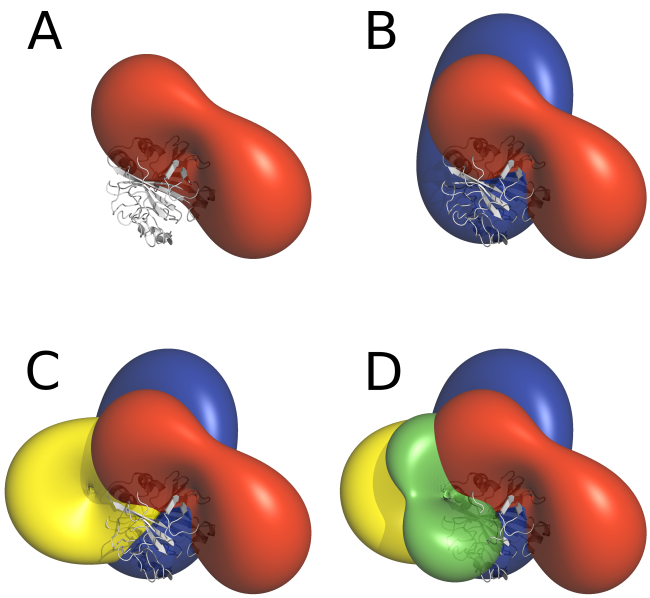

Figure 1.5: Structure determination from PCS of different tagging sites.

PCS of at least three different tagging sites are available for one certain nuclear spin, and for a certain part of the protein, the structure is known to allow the determination the $\Delta\chi$-tensor parameters, the position of the nuclear spin can be determined similar to the global positioning system (GPS).[30] Due to the more complex shape of the isosurfaces for PCS a larger number of positions is possible. Usually up to four distinct positions can be obtained when three isosurfaces intersect with each other. This can be recognised when the possible solutions from the intersection of two isosurfaces are considered (figure 1.5 B). These are represented by a circular line with a particular three dimensional shape, very often this shape resembles to the line that is found on a tennis ball. When a third isosurface intersects with this circular line it becomes clear that it is possible that only two solutions are obtained for the position, but in most cases four solutions are obtained. Therefore it is useful to determine at least four different PCS for the determination of a position. This reduces the possible solution to only one position which is better defined as well, because an additional data point

is available. In the unlikely case that still more than one solution is found normally only one of them is reasonable.

1.9 Artificial metalloenzymes

Artificial metalloenzymes are designed proteins that combine the selectivity of enzymes with the broad substance range of homogeneous transition metal catalysts.[31] Artificial metalloenzymes can be formed by anchoring an achiral metal catalyst in the binding pocket of a protein. The chiral environment of the protein enables stereoselective catalysis. Furthermore, point mutations of the protein sequence allow to enhance the selectivity as well as the activity of such a system.[32] An artificial metalloenzyme that allows different stereoselective or regioselective conversions has been presented on the base of iridium catalysts that are bound to streptavidin by a biotin anchor.[33] Recently a similar approach was presented, where such iridium catalysts were anchored to human carbonic anhydrase II (hCA-II) by a sulfonamide linker.[34,35] For this system computational optimization was successfully applied to improve the selectivity as well as the activity of this artificial metalloenzyme.[36] Such optimisations have been carried out on basis of the X-ray structures determined for the corresponding protein-inhibitor complex, because a solution state structure of hCA-II is not available. Because the catalytic reactions are processes running in solution, structural information determined by NMR spectroscopy in solution could reveal important information about such a system. Therefore such an hCA-II-inhibitor complex has been chosen for the investigation by PCS NMR spectroscopy.

1.10 Human carbonic anhydrase II

HCA-II is a 29 kDa protein consisting of 260 amino acids. In vivo the protein catalyses extremely efficiently the reaction from CO_2 to bicarbonate (equation 1.4). The catalytic turnovers of this reaction are among the highest known for proteins.

$$CO_2 + H_2O \rightleftharpoons HCO_3^- + H^+ \tag{1.4}$$

hCA-II is a monomeric globular protein with a diameter of size 40 Å to 55 Å. The structure consists of a dominant ten stranded twisted anti-parallel β-sheet. Seven α-helices surround this central structure. Only very small structural differences were observed for a wide range of pH (5.7 - 8.4) and upon binding of ligands. The catalytic site consists of a zinc atom bound to three histidine side-chains and to a hydroxide ion or to a water molecule. Phenyl-sulfonamide inhibitors have a very high affinity to hCA-II (K_d in the nM range are reported, and even down to 30 pM).[37]

1.11 Objectives of the thesis

DOTA-M8 showed very large PCS when the corresponding dysprosium complex is tagged to Ubiquitin.[28] In this thesis we planned to further characterise the utility of this LCT on a medium sized protein. The 29 kDa protein hCA-II was chosen as viable candidate, because the group of Prof. Tom Ward already targeted this protein for the generation of artificial metallo enzymes. Structural information of such protein constructs usually is gained from X-ray crystal structures, because no solution state structure of this protein is available. Therefore it was decided to:

- Prepare different single cystein mutants of the protein in order to attach LnM8-SPy complexes to different sites of the protein.
- Assign PCS based on a available X-ray structure in order to determine $\Delta\chi$-tensor parameters for the determination of further structural information.
- Determine ^{19}F PCS of two different fluorinated inhibitor in complex with hCA-II.
- Determine the position of these fluorines based only on PCS

Up to now only few studies are presented where PCS are determined for different tagging sites of a protein. Therefore this study will contribute to the characterisation of the usefulness of PCS for protein structure determination. Furthermore, fluorinated small molecules play an important role as drugs[38] and the potential determination of the site of such ligands within a protein receptor is highly relevant for medicinal chemistry.

CHAPTER 2

Results

In the following Chapter the sections 2.3, 2.4, 2.6 and 2.7 were carried out in collaboration with Dr. Elisa S. Pereira Nogueira and are described as well in her PhD thesis[39]. Throughout the whole thesis the numbering system for the residues of human carbonic anhydrase I (hCA-I) was used for hCA-II, where Thr-125 is followed directly by Lys-127. hCA-I has an additional alanine residue at the position 126 which is missing for hCA-II.[40] And the ligand M8-SPy and it's corresponding lanthanide complexes refer to the (*8S*) stereoisomer, if not stated otherwise.

2.1 LnM8-SPy Synthesis

The synthesis of M8-SPy was repeated based on published procedures[28] and for two steps reaction conditions could be improved. An overview of the five step synthesis is given in figure 1.4 in the introduction. In step three, the duration of the benzyl deprotection reaction could be reduced by 95 %, from 20 h to 1 h when 0.5 L of hydrogen gas was bubbled directly through the solution over the period of 1 h, instead of stirring the reaction mixture under an hydrogen atmosphere. In the fourth step the reaction time of the initial amide coupling reaction could be reduced from 2 h to 1 h when 2 eq. of diisopropylethylamine (DIPEA) were used as base instead of 1 eq. of triethylamine (NEt_3). One equivalent of the base is needed for the deprotonation of the ammonium salt, leaving another equivalent, required for the amide coupling. The subsequent deprotection step was also subject of optimization but all attempts like purification

of the intermediate after the amide coupling or different deprotection conditions (H_2SO_4 in CH_2Cl_2) led to a significant reduction of the overall yield. Therefore the deprotection was carried out according to the described conditions and was followed closely by electrospray ionisation mass spectrometry (ESI-MS) in order to find the optimal reaction time. As shown in figure 2.1 the progress of the reaction could be

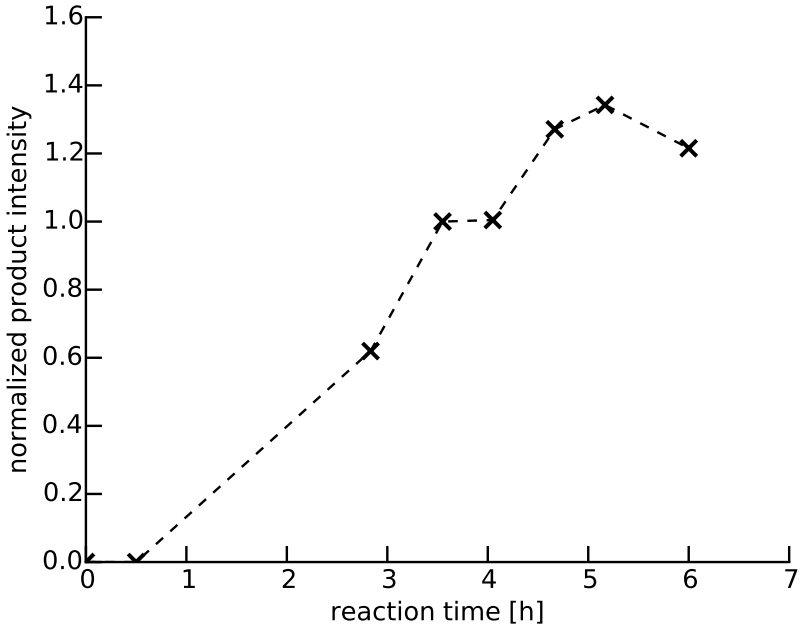

Figure 2.1: Progress of the ^{t}Bu deprotection step of the M8-SPy synthesis followed by ESI-MS. The product peak intensity is normalized by the intensity of an unaffected peak at m/z 515.

monitored, when the intensities of the product signals at m/z 685 ($[M+H]^+$) and 707 ($[M+Na]^+$) were normalised by the intensity of the signal at 515 which is not affected during the course of the whole deprotection step. This signal is expected to be a byproduct of the coupling reagent, benzotriazol-1-yl-oxytripyrrolidinophosphonium hexafluorophosphate (pyBOP), used in the initial amide coupling step. According to this data, the deprotection reaction is terminated when the intensity of the product started to reach a plateau after 6 h. In the final metallation step of M8-SPy with the according lanthanide metal it could be shown that a buffered solution (100 mM ammonium acetate) is required for a complete reaction. When the metallation was

carried out in pure aqueous solution only partial conversion could be observed. For the (*8S*)-LnM8-SPy complexes in the final high performance liquid chromatography (HPLC) purification step two fractions for the product could be separated both containing the same product as detected in the ESI-MS spectra. When the two fractions were conjugated later to hCA-II_S50C_C206S, exactly the same ^{1}H-^{15}N HSQC spectra was observable. The ratio of these two fractions depends on the lanthanide metal, for Gd a ration of 8:2 was observed for the earlier to the later fraction, for Dy 6:4, for Tm 1:19 and for Lu only the second fraction was observable. This was in good agreement with published findings.[41] In contrast to this, for the (*4R,4S*)-LnM8-SPy complexes only one fraction was observable in the HPLC for each Lanthanide mentioned above.

2.2 Selection of the mutation sites

For the tagging of proteins with Ln-M8-SPy complexes a solvent exposed cysteine residue in the protein is required. We decided to introduce such a cysteine residue at the position of a native serine residue. Serine and cysteine residues have a similar shape in terms of their covalent radius as well as comparable polarity and electronic properties, therefore the protein structure is not expected to be affected significantly from such kind of mutation. An X-ray crystal structure (PDB code 3KS3) was used to select five different solvent exposed serine residues at the edge of a secondary structure element (compare to figure 2.2). These positions were chosen because the cystein residues should be in a well structured part of the protein to promote a rigid attachment of the tag to the protein. Additionally the mutation must not influence the overall tertiary structure of the protein to ensure the comparability of all different mutants. Residues at the beginning or the end of a secondary structure element are less likely involved in significant interactions defining the overall fold of the protein.

Because the protein already contains a cysteine residue the introduction of a second cystein to the protein sequence can lead to the formation of an undesired disulfide bond during the expression of the protein and thus to miss-folded protein. To avoid this the present cysteine at position 206 was planed to be replaced by a serine residue. Serine was chosen because bovine carbonic anhydrase II, an isocyme of hCA-II with 81 % sequence similarity contains a serine at this position. Additionally this mutation was already reported not to affect either the stability or the activity of the protein.[42,43]

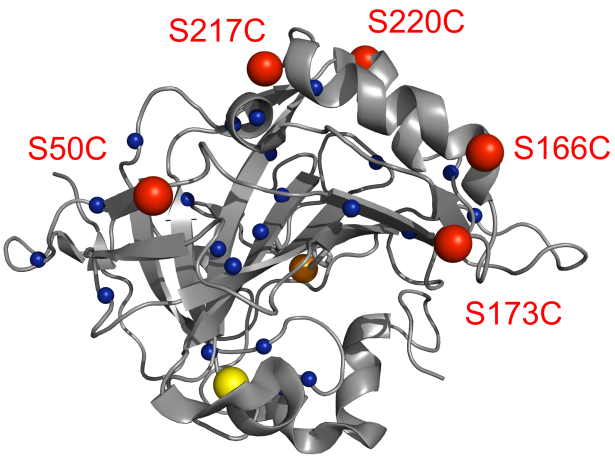

Figure 2.2: X-ray structure of hCA-II (3KS3), the colours correspond to: red: selected serine to cysteine mutation sites, yellow: native cysteine residue, blue: leucine residues and orange: catalytic zinc.

To have an alternative in case of difficulties due to the mutation of Cys-206 to serine we decided to prepare also a second set of mutants where the Cys-206 is replaced by an alanine residue. This resulted in ten different double mutants, listed in the following table 2.1.

Table 2.1: List of all planed hCA-II mutants.

hCA-II_S50C_C206S	hCA-II_S50C_C206A
hCA-II_S166C_C206S	hCA-II_S166C_C206A
hCA-II_S173C_C206S	hCA-II_S173C_C206A
hCA-II_S217C_C206S	hCA-II_S217C_C206A
hCA-II_S220C_C206S	hCA-II_S220C_C206A

2.3 Mutation of the pACA plasmid encoding for human carbonic anhydrase II

The pACA plasmid used for the production of hCA-II was generous gift from Prof. Carol A. Fierke (University of Michigan, USA).[44] It consists of the hCA-II gene[45] behind a T7 ribonucleic acid (RNA) polymerase promoter, a f1 origin of replication,[46] and an ampicillin resistance (amp^r) gene as well as a chloramphenicol resistance (cm^r) gene in a pMa5-8 vector.[47] The gene for hCA-II has an alanine instead of a serine at position 2 which does not affect the expression of the protein nor its catalytic activity. Starting from this plasmid, site-directed mutation was carried out according described procedures.[24] In a first step C206 was mutated either to serine or alanine and in the second step the five different serine to cysteine mutations were introduced to the plasmid. Primers and details to the procedure are given in the experimental section.

2.4 Expression of uniformly ^{15}N labelled hCA-II mutants

Test expression showed no differences between the C206S and the C206A mutants, therefore we decided to use use only the C206S mutants for over-expression. The C206A constructs were not investigated further.
Optimised protocols for the expression of hCA-II were derived by E. Nogueira from protocols provided by Prof. Carol A. Fierke. Uniform ^{15}N labelling was achieved by the use of minimal medium containing ^{15}N ammonium chloride as the sole nitrogen source. This resulted in yields of 60 mg to 95 mg of protein per litre medium. All details are given in the experimental section.

2.5 Tagging of ^{15}N-hCA-II mutants

To ensure having only monomeric protein present, with accessible thiol groups for the tagging with Ln-M8-SPy, a solution of 300 µM to 350 µM protein was reduced using 1 mM tris(2-carboxyethyl)phosphine (TCEP) at 4 °C over night. Buffer exchange to reduce the TCEP concentration was achieved by ultrafiltration followed by a single use size exclusion column. To keep the dimerisation of the protein by the formation

of a disulfide bond as low as possible, the protein was eluted from the size exclusion column directly into a solution of the desired Ln-M8-SPy. The tagging of the protein could be followed by ESI-MS. After one hour already more than 70 % conversion was observed (figure 2.3 B). For complete conversion the reaction continued at 4 °C over night. The resulting ESI-MS spectra showed more than 98 % conversion (figure 2.3 C). This was confirmed by the ^{1}H-^{15}N-HSQC spectrum where only traces of untagged protein were observable. Tagging with Ln-M8-SPy was possible for all five different hCA-II mutants with yields in a range of 60 % to 90 %. Observation of the protein concentration after each step of the tagging procedure (see experimental section) by ultraviolet-visible (UV) absorption showed that the amount of protein decreased only during the ultrafiltration steps before and after the tagging reaction. This is attributed to the tendency of hCA-II to aggregate[37] During the entire tagging reaction the protein concentration remained constant.

Figure 2.4 shows the overlay of hCA-II_S50C_C206S tagged either with the paramagnetic Tm-M8-SPy or the diamagnetic Lu-M8-SPy. Almost all signals show a significant PCS. For some isolated peaks, the assignment of the PCS was straight forward, but for the majority of the peaks this was not the case. The main reason was the large number of peaks clustering in the central region of the spectrum. This could lead to false PCS assignments which could result in a self consistent but wrong assignment of the PCS. Furthermore NMR assignment of hCA-II was only available for the wild type protein[48] and not for the double mutants we prepared. Therefore we can expect some of the peaks of residues in the vicinity of the mutation sites to be shifted compared to the wild type protein. Although this is only an issue for a small number of peaks, it further increases the possibility of a false PCS assignment. In order to avoid these problems we decided to prepare selectively ^{15}N labelled protein samples, where only one type of amino acid is ^{15}N labelled. This will reduce significantly the complexity of the spectrum when only a fraction of the peaks are observable. In addition to this, we decided to fully assign the protein backbone of one double mutant to exclude any wrong assignments for this mutant and thus to simplify the assignment of the other protein mutants.

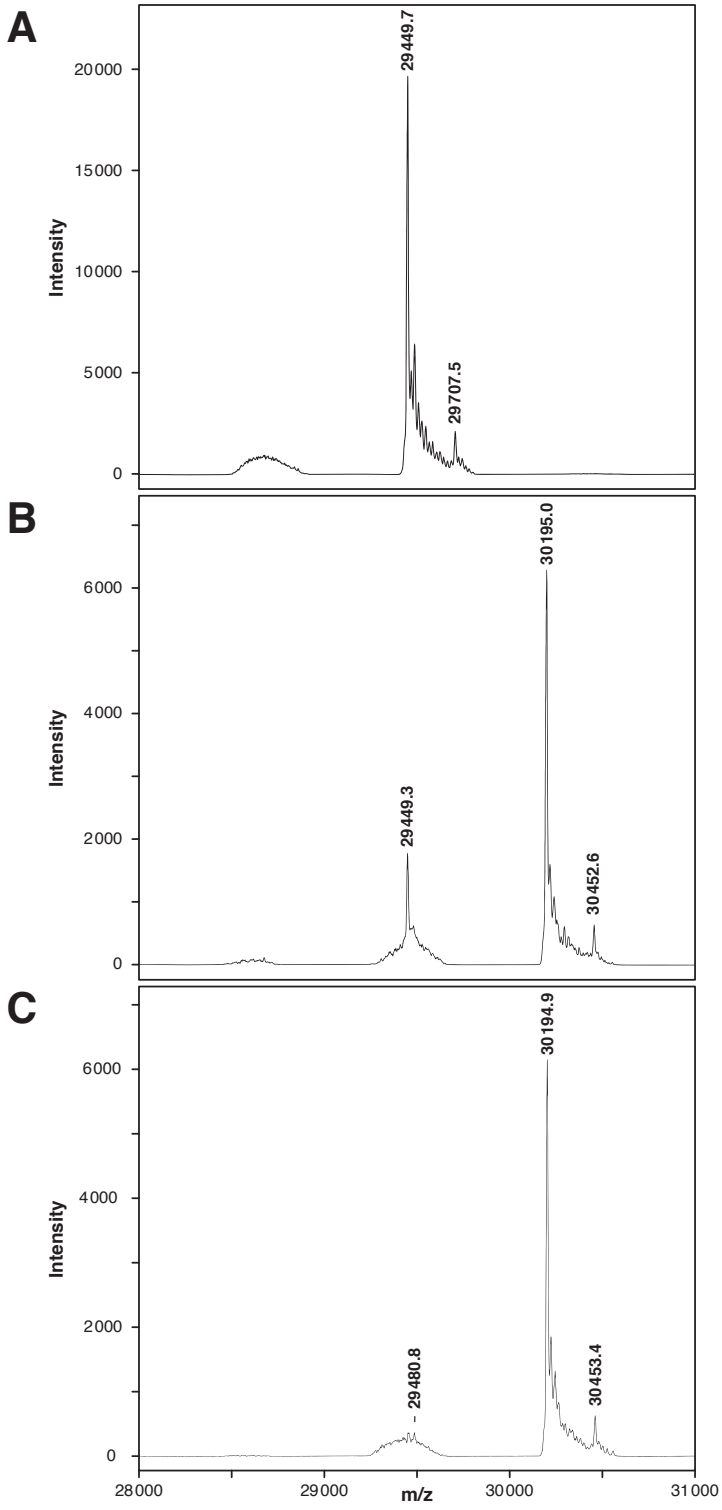

Figure 2.3: Deconvoluted ESI-MS spectra of uniformly ^{15}N labelled hCA-II showing the progress of the tagging reaction. **A** Protein before reaction, **B** after one hour reaction time and **C** after overnight reaction.

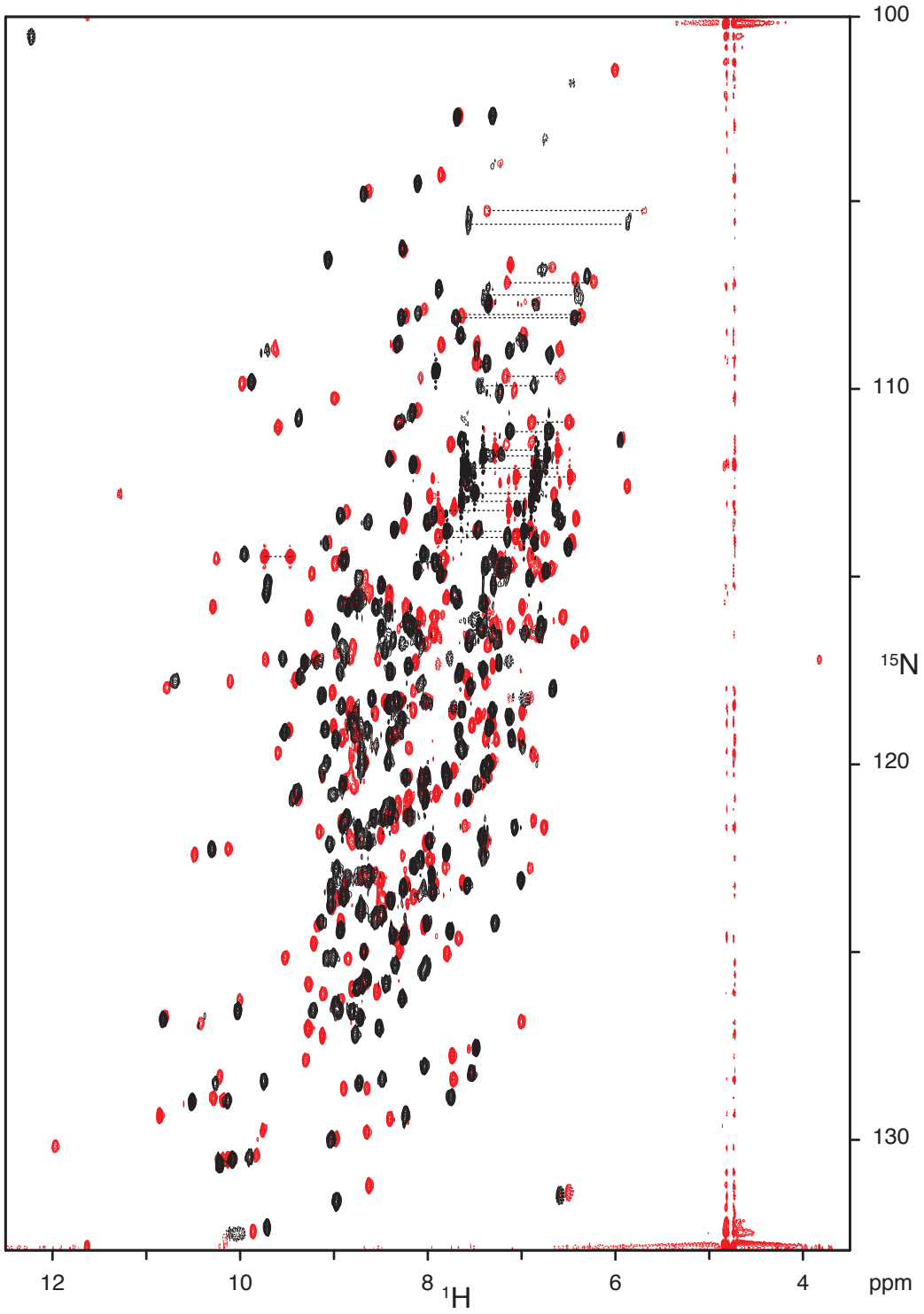

Figure 2.4: Overlay of the ^{1}H-^{15}N-HSQC spectra (600 MHz, 298 K) of uniformly ^{15}N labelled hCA-II_S50C_C206S-LuM8 (black) and hCA-II_S50C_C206S-TmM8 (red). Artefacts from non perfect water suppression are observable at 4.7 ppm in the ^{1}H-dimension. NH_2-groups are indicated with dashed lines.

2.6 Expression of selectively ^{15}N-Leu labelled hCA-II mutants

With a number of 26 residues leucine is the most abundant amino acid in hCA-II, therefore we decided to express the protein selectively ^{15}N-leucine labelled. The protocol for expression of selectively ^{15}N labelled hCA-II was based on the protocol for uniformly ^{15}N labelled protein where instead of ^{15}N ammonium chloride a mixture of all unlabelled amino acid apart from leucine is used for the media. ^{15}N labelled leucine is added to the media at the time of induction to avoid isotope scrambling by biochemical conversion of leucine to other amino acids like isoleucine. The expresion yielded 140 mg to 230 mg of protein per litre media for all five mutants. The resulting ^{1}H-^{15}N-HSQC spectra showed exactly the expected 26 signals for all five mutants and no isotope scrambling from the expression was observable. The assignment based on the shifts for wild type hCA-II was straight forward for all five mutants. The signals of Leu-79 and Leu-120 showed strong overlap for all mutants, with the exception of S50C where these peaks were separated but Leu-47 and Leu-212 were overlapping instead. This assignment could be also confirmed by the later backbone assignment of hCA-II_S50C_C206S.

2.7 Expression of uniformly ^{2}H, ^{15}N and ^{13}C labelled human carbonic anhydrase II

Triply labelled protein was prepared for the construct S50C_C206S using media prepared from D_2O instead of H_2O containing ^{15}N ammonium chloride and D_7-^{13}C-glucose as the sole nitrogen source and carbon source respectively. Expression in shaking flasks provided the desired protein but only in poor yields (below 20 mg protein per litre media. Therefore the expression was carried out in a 2 L bench-top fermenter. This allowed better control of parameters like temperature and oxygen content of the media and on top of that it even allowed to control the addition of D_7-^{13}C-glucose optimizing the amount of protein which is produced per gram of glucose. All details to the procedure are given in the experimental section. From 1 L media 84 mg triple labelled protein were obtained. The determined molecular weight of 32 157 Da corresponds to a deuteration level of 85 % assuming the cleavage of the N-terminal methionine and uniform labelling of ^{13}C and ^{15}N. 1D proton spectra

confirmed this assumption when the residual intensity of the signals in the aliphatic region is compared to the spectra of a fully protonated protein.

2.8 Backbone assignment of triply labelled hCA-II_S50C_C206S

2.8.1 Refolding of hCA-II

Protons were reintroduced to the deuterated protein by refolding of the protein using guanidinium chloride as chaotropic agent. This procedure replaces all exchangable deuterons by protons. Based on published conditions[49] the protein was denatured in 5 M guanidinium chloride (GdmCl) and refolding was initiated by a subsequent fast dilution to 0.3 M GdmCl. The conditions were optimised using selectively ^{15}N leucine labelled protein. In the best case 50 % of ^{15}N labelled protein could be recovered after refolding. In order to cope with the large volume of buffer after the dilution step it was decided to load the protein on a sulfonamide affinity column, which results in around 120 mL of solution. In addition this method selectively separates only correctly folded active protein, because unfolded protein would not bind to the column. The detailed conditions are given in the experimental section. Unfortunately when these conditions were applied to a larger amount of protein, 17 mg instead of 2 mg to 5 mg, the final yields turned out to be only 20 %. Monitoring of the protein concentration by UV after every step the whole process showed that around 40 % of the protein is lost during the denaturation and renaturation steps. Another 30 % was lost in the affinity column and additional 10 % was lost in the final dialysis and concentration steps. Nevertheless an NMR sample of refolded triply labelled hCA-II was obtained and the ^{1}H-^{15}N-HSQC spectra showed that out of 193 well separated signals only 25 showed a significant increase in signal intensity of more than 1.5 times the intensity that was measured before refolding (see figure 2.5). This means that only for a small number of residues the signal intensity improves due to the refolding. Because of limited amount of triple labelled protein we decided therefore to carry out the backbone assignment with non refolded protein.

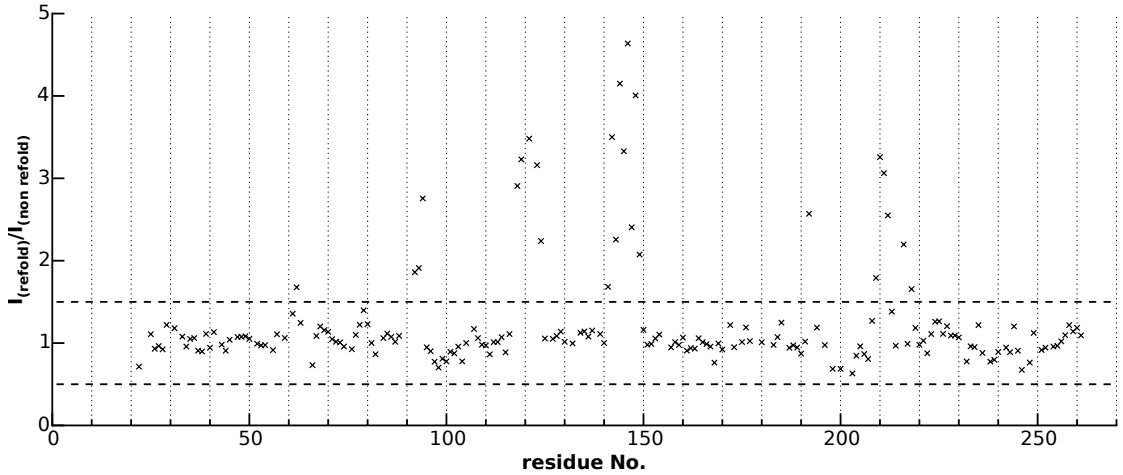

Figure 2.5: Comparison of signal intensity of triply labelled hCA-II_S50C_C206S before and after refolding of the protein. Out of 193 signals only 25 residues show an increase in signal intensity by a factor of more than 1.5

2.8.2 Backbone assignment

For the backbone assignment triply labelled hCA-II_S50C_C206S was tagged with LuM8-SPy following the procedure described in the experimental section. A NMR sample with a concentration of 460 µM was prepared and transverse relaxation optimized spectroscopy (TROSY) based ^{1}H-^{15}N-HSQC, HNCO, HNCA, HN(CO)CA, HN(CA)CO as well as HNCACB spectra were recorded. Backbone assignment was carried out according to described procedures.[50]. Using ^{15}N leucine labelled protein it was possible to confirm the correct assignment of the leucine residues. 90 % of the protein backbone was successfully assigned. Residues 2 to 20 were not assigned as well as H64, I91, P155, G156, T199, T200, P201 (The N-terminal methionine was assumed to be cleaved based on the molecular weight obtained from the ESI-MS spectra. For Thr-200 later an assignment was found based on PCS.) For the N-terminal residues (Ala-2 to Phe-20) some sequential assignments were possible for remaining unassigned peaks in the spectra but an unambiguous assignment of these segments to the protein sequence was not possible. On top of that for some of the unassigned peaks *cis-trans* isomerisation was observable, indicating a certain flexibility of this part of the protein, which is unfavourable for a reliable assignment of PCS. The assignment of hCA-II_S50C_C206S-LuM8 could be transferred directly to the other mutants except

for residues in close vicinity to the cysteine mutation site which were shifted either due to the Ser→Cys mutation or due to interactions with the tag bound to this cystein. For these residues a tentative assignment could later be confirmed using the PCS.

2.9 PCS assignment

For convenience, in the following section only a part of the figures for the different protein mutants are shown. All remaining figures for the other mutants are given in the appendix section (see Figures A.1 - A.6). Every determination of magnetic susceptibility tensor parameters was carried out using the same X-ray structure (PDB code: 3KS3). Because X-ray structures do not contain protons, their position had to be added to the protein structure file. There are several different algorithm available for this task. We decided to use the HAAD algorithm, because of its higher accuracy compared to other widely used programs.[51] All other X-ray structures used were aligned to the 3KS3 X-ray structure meaning all given coordinates in this thesis are given in the coordinate system of this structure.
As already described in section 2.5 tagging with LnM8-SPy was possible for all five different mutants. However when the S173C mutant was tagged with TmM8-SPy two peaks were observable for each residue. This can easily be shown for the selectively ^{15}N-leucine labelled protein (see figure 2.6) The spectra of the uniformly labelled protein turned out to be very crowded and is therefore not shown. The reason for these two sets of signals has to be the tag, which orients in two different directions either at the same or at different positions when bound to Cys-173. Therefore for each residues two different PCS are observable. Although the two sets of signals showed different intensities it turned out to be much more demanding than this was the case for the other mutants. On top of this the signals of the set with higher intensity were broader than the signals of the other set. This could be either explained by a higher dynamic of the tag or by another set of signals overlapping with these signals which could be well seen for Leu-185. Because all other mutants showed reasonable spectra when tagged with TmM8-SPy we decided to leave out the S173C mutant for the determination of the PCS.

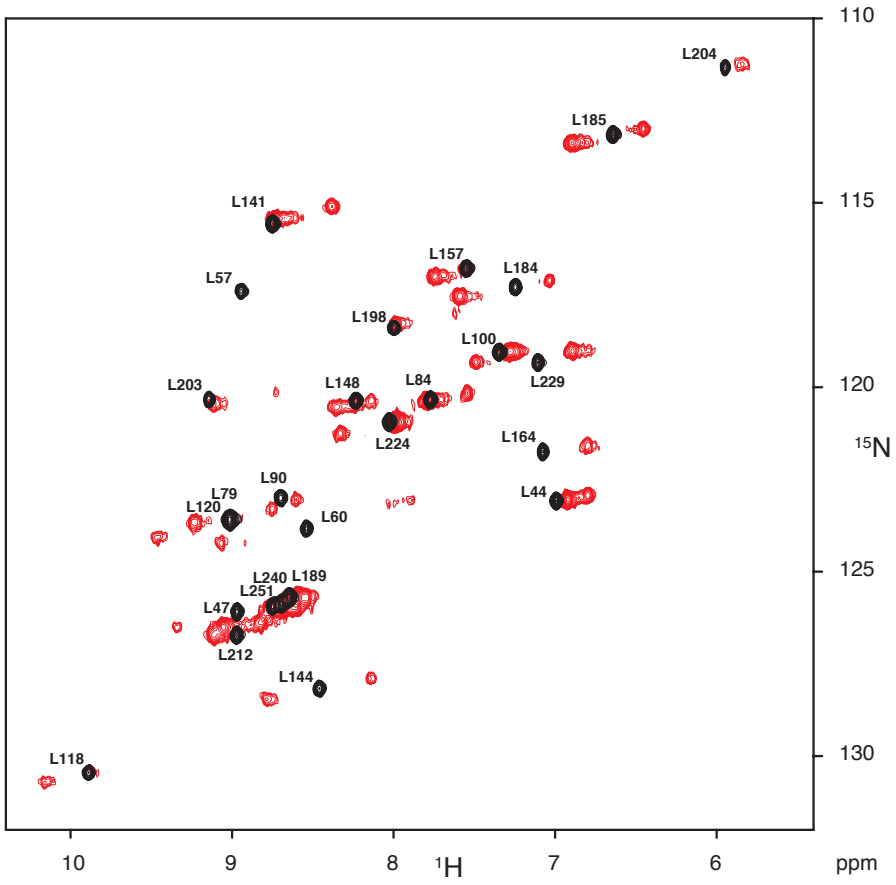

Figure 2.6: Overlay of the ^{1}H-^{15}N-HSQC spectra (600 MHz, 298 K) of selectively ^{15}N leucine labelled hCA-II_S173C_C206S-LuM8 (black) and hCA-II_S173C_C206S-TmM8 (red). Two sets of PCS are observable.

Having selectively ^{15}N leucine labelled protein and a reliable assignment of uniformly ^{15}N labelled protein in hand, assignment of the PCS was carried out as follows. Form an overlay of LuM8 and TmM8 tagged selectively ^{15}N leucine labelled protein (see figure 2.7 and Appendix) more than eight shifted peaks could readily be assigned for each mutant. Parameters describing the magnetic susceptibility tensor of the lanthanide metal were determined from the program Numbat[18] using this initial set of PCS. This tensor set allowed to back calculate the expected PCS for the remaining leucine residues. This allowed the unambiguous assignment of all remaining shifted peaks apart from those leucine residues close to the tag, where the signals were either

broadened beyond the limit of detection due to PRE or shifted outside of the spectral window (for S50C this is the case for Leu-79). From this larger set of PCSs refined tensor parameters could be calculated, since a larger set of data points was used.

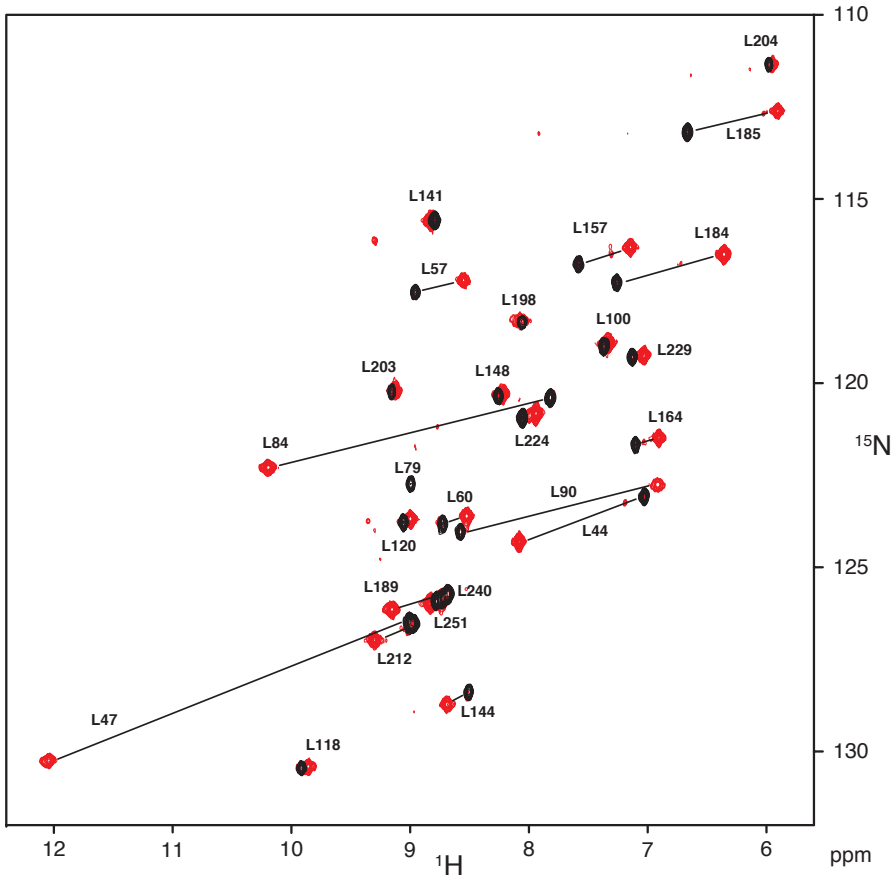

Figure 2.7: Overlay of the ^{1}H-^{15}N-HSQC spectra (600 MHz, 298 K) of selectively ^{15}N leucine labelled hCA-II_S50C_C206S-LuM8 (black) and hCA-II_S50C_C206S-TmM8 (red). Assignment and PCS are indicated.

The tensors obtained from the leucine PCS could be transferred to the uniformly ^{15}N labelled samples and allowed to assign further PCS following the same strategy of calculating expected PCS based on current tensor, assigning further shifted peaks and recalculating refined tensors including the newly assigned PCS. Backbone assignment delivered for the S50C_C206S mutant 221 signals in the ^{1}H-^{15}N-HSQC for which a

reliable assignment was available. The assignment of the PCS was restricted to these residues. For 205 residues a shifted peak could be assigned which corresponds to 93 % of these considered signals or to 84 % of the total number of backbone amide NH groups in the protein. The remaining residues where an assignment in the diamagnetic spectra was available but no PCS could be assigned, were found close to the tag in the protein structure. Due to the PRE these signals were not observable any more in the paramagnetic spectra. For the S166C mutant the PCS of 208 residues could be assigned which corresponds to 97 % of the residues where a reliable assignment was possible or to 86 % of all backbone amide NH groups. For the S217C mutant these ratios turned out to be 91 % or 82 % respectively. And for the S220C mutant these were 90 % and 81 %. For reasons of clarity in figure 2.8 only well separated peaks are assigned. A table with all PCS assigned is given in the Appendix (see table A.2).
In all spectra of TmM8 tagged protein of the four considered mutants a minor second shifted species was observable analogue to ubiquitin where this already has been observed.[28] The intensity of this species in the order of 10 % of the main peak intensity apart from the S220C mutant where up to 15 % have been observed, independently of the protein sample. In figure 2.7 the second species can be observed for example for residue 141. Because these small peaks for most residues were not observable, no assignment was carried out. Due to the low intensity this second species never interfered with the assignment of the main peaks.

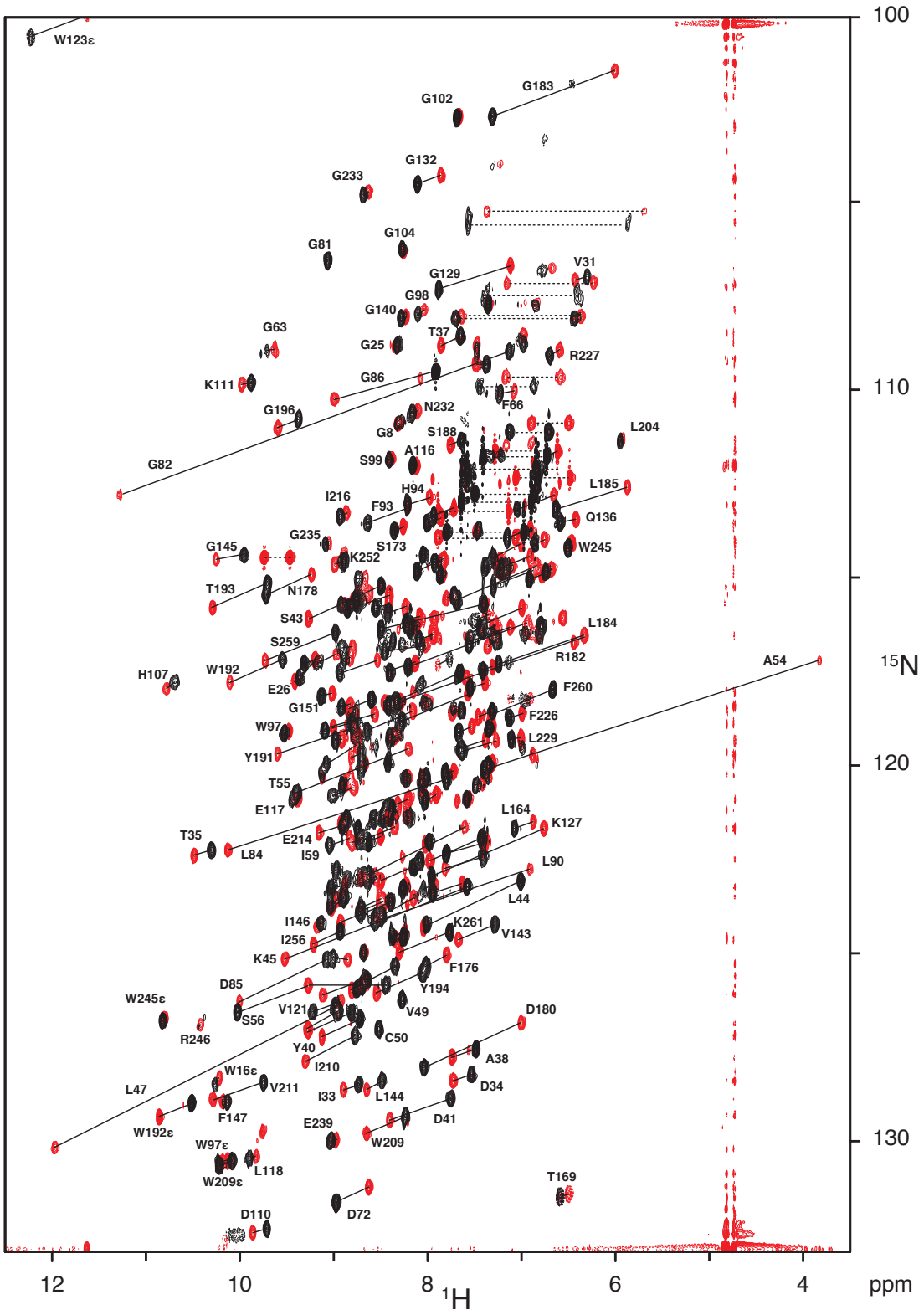

Figure 2.8: Overlay of the ^{1}H-^{15}N-HSQC spectra (600 MHz, 298 K) of uniformly ^{15}N labelled hCA-II_S50C_C206S-LuM8 (black) and hCA-II_S50C_C206S-TmM8 (red). Aliased signals with negative intensity are shown with dashed contour lines. PCS are indicated with solid and NH_2 groups with dashed lines.

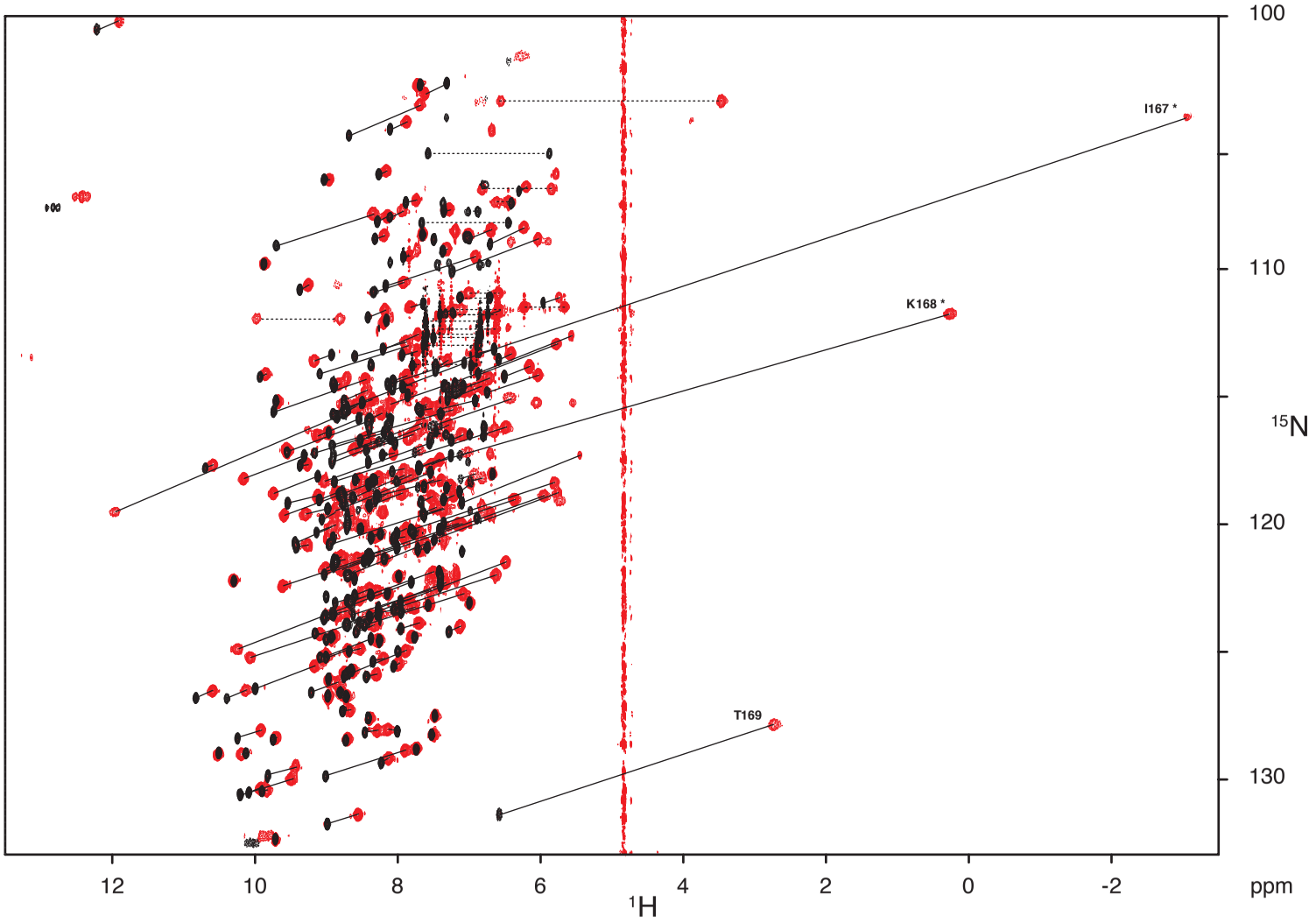

Figure 2.9: Overlay of the ^{1}H-^{15}N-HSQC spectra (600 MHz, 298 K) of uniformly ^{15}N labelled hCA-II_S166C_C206S-LuM8 (black) and hCA-II_S166C_C206S-TmM8 (red). Aliased signals with negative intensity are shown with dashed contour lines. PCS are indicated with solid and NH_2 groups with dashed lines. Only signals on the right side of the spectra are assigned. Assignment of the left side of the spectra is given in the appendix. Tentative assignments are marked with an asterisk.

2.10 Determination of the magnetic susceptibility tensors

Magnetic susceptibility tensors were determined using the program Numbat[18], using the X-ray structure (PDB code: 3KS3). As starting point to the tensor fit, for each mutant the coordinates of the side-chain oxygen of the corresponding serine in the X-ray structure were used. The *Euler* angles defining the orientation of the magnetic susceptibility tensor, were applied in the ZYZ' convention (default in Numbat) and a value of 0° was used fore every angle as initial orientation for the optimisation. Correction for RACS, small shifts which arise from partial alignment of the protein in the magnetic field[20], was applied at the corresponding spectrometer frequency. It was found that the resulting errors of the tensor were slightly smaller when the RACS correction was applied, showing a small improvement of the agreement between PCS and X-ray structure. The uncertainties of the tensors were estimated by the application of a *Monte-Carlo* protocol which is implemented in Numbat. Described procedures for the error analysis were applied.[18] For each tensor the uncertainties were estimated twice with two different methods. The first was a structure variation, where the atomic coordinates of the x-ray structure were varied according to a Gaussian distribution with a standard deviation σ of 0.5 Å which results in a average displacement of each atom by 0.8 Å. The second method was the random selection of PCS subsets, where only 20 % of all PCS were used to recalculate the tensor. For each method and tensor 1000 samples were calculated and the average values and their standard deviation were reported. To avoid artefacts arising from the use of the same set of random numbers, for each mutant a different random seed was chosen. In order to be able to compare different tensors, calculated for one specific protein mutant, always the same seed was used for this construct. For the S220C mutant the γ *Euler* angle turned out to be close to 0° or 180°. According to the ZYZ' convention for the *Euler* angles implemented in Numbat and because of the symmetry of the magnetic susceptibility tensor a rotation of the γ angle by 1° is equivalent to a rotation by 181°. When during the 1000 iterations of the *Monte-Carlo* procedure for the γ angle angles close to 0° as well as to 180° were found the angles were corrected manually by either addition or subtraction of 180° to obtain proper average values and corresponding standard deviation. For two mutants (S217C and S220C) when tensor parameters were determined with the full set of PCS for

10 % of the iterations of the *Monte-Carlo* procedure two or even all three *Euler* angles showed a large difference to the average value. This happens when the optimisation converges in a different local minimum. But this was only the case for the full sets of PCS for these two mutants, later for the subsets this was not observed any more, indicating one single coherent minimum for each optimisation. For convenience those iterations were excluded from the error analysis of the full tensor sets for these mutants.

Table 2.2: Magnetic susceptibility tensor parameters for the different hCA-II mutants. All PCS that could be assigned were used. The values and their uncertainties are calculated by a *Monte-Carlo* protocol applying two different random inputs given below.

		S50C	**S166C**	**S217C**	**S220C**
$\Delta\chi_{ax}$	[10^{-32}m^3]	20.2 ± 1.9	38.7 ± 2.0	18.9 ± 1.0	24.6 ± 2.2
$\Delta\chi_{rh}$	[10^{-32}m^3]	8.1 ± 1.0	7.5 ± 1.2	11.4 ± 0.5	2.9 ± 0.6
x	[Å]	-27.6 ± 0.4	-16.1 ± 0.5	-23.9 ± 0.3	-14.6 ± 0.4
y	[Å]	13.5 ± 0.4	-3.5 ± 0.3	-16.5 ± 0.3	-26.5 ± 0.5
z	[Å]	18.9 ± 0.3	-11.2 ± 0.4	20.2 ± 0.3	3.9 ± 0.4
α	[°]	107.0 ± 2.7	51.5 ± 2.0	148.4 ± 1.4	3.6 ± 2.2
β	[°]	140.9 ± 1.2	123.1 ± 1.3	65.7 ± 1.2	151.1 ± 1.4
γ	[°]	116.8 ± 2.2	143.1 ± 5.0	126.9 ± 1.4	164.3 ± 8.4
Monte Carlo structure variation with a $\sigma = 0.5$ Å					
$\Delta\chi_{ax}$	[10^{-32}m^3]	19.8 ± 1.5	37.3 ± 1.2	22.7 ± 4.3	23.2 ± 4.7
$\Delta\chi_{rh}$	[10^{-32}m^3]	7.7 ± 0.9	7.8 ± 0.9	12.3 ± 1.7	3.7 ± 1.2
x	[Å]	-27.3 ± 0.4	-16.1 ± 0.3	-24.2 ± 0.7	-13.7 ± 0.9
y	[Å]	13.4 ± 0.4	-3.5 ± 0.2	-16.9 ± 1.4	-26.0 ± 1.2
z	[Å]	18.6 ± 0.3	-10.9 ± 0.2	19.8 ± 0.6	3.5 ± 0.9
α	[°]	106.8 ± 2.8	52.7 ± 1.5	144.6 ± 3.3	13.0 ± 7.7
β	[°]	141.1 ± 1.2	122.7 ± 0.9	68.7 ± 3.8	153.5 ± 3.0
γ	[°]	117.1 ± 2.8	142.7 ± 3.6	125.6 ± 2.5	176.6 ± 19.2
Monte Carlo protocol where random subsets consisting of 20 % of the available PCS were used					

Table 2.2 lists the tensor parameters obtained for the the different protein mutants and the two *Monte-Carlo* methods. All metal coordinates turned out to be found in a reasonable distance of 5 Å to 8 Å to the γ-oxygen of the serine residue at the position where the corresponding sulfur atom of the protein mutant is expected. For the mutants S50C, S217C and S220C similar values for $\Delta\chi_{ax}$ were found, whereas this value was almost twice as large for the S166C mutant. This was also reflected in the PCS where significantly larger shifts were found for the S166C mutant. Values of $\Delta\chi_{rh}$ did not vary to the same extend, here the largest value was found for S217C and the smallest for S220C. The smaller $\Delta\chi_{rh}$ the closer is the magnetic susceptibility tensor to having axial symmetry. This explains why for the S220C mutant the largest differences in the *Euler* angels with the biggest uncertainties were observed. Because the closer a tensor is to axial symmetry the larger the number of orientations that become more and more equivalent. The orientation of a perfect axial symmetrical tensor eventually can be described by two *Euler* angles alone.
The agreement of the experimental PCS with the back calculated values is shown in figures 2.10 and 2.11 for the two different *Monte-Carlo* methods applied to the tensor calculation. The given Q-factors are calculated according the following equation:

$$Q = \sqrt{\frac{\sum(PCS_{exp} - PCS_{calc})^2}{\sum PCS_{exp}^2}} \tag{2.1}$$

Q-factors basically are the root mean square deviation (RMSD) of experimental and calculated PCS divided by the root mean square (RMS) of the experimental PCS, they are getting smaller the better the agreement is between experimental and calculated PCS and the larger the average PCS is in a certain dataset. The Q-factors show an excellent agreement of experimental and calculated PCS for the S166C mutant. For this mutant the largest number of PCS could be assigned and all of them showed a smaller deviation than 0.2 ppm compared to the calculated PCS. Only 5 PCS diverged more than 0.15 ppm and 6 additional PCS showed a deviation in the range of 0.1 ppm to 0.15 ppm. This mutant has also the largest range of PCS with −11.20 ppm to 3.73 ppm, whereupon it has to be mentioned, that the four largest negative PCS corresponding to residues 167 and 168 were assigned only based on their predicted PCS. Large chem-

ical shift changes of the residues in this region of the protein due to the Ser to Cys mutation and the subsequent conjugation with the tag were observed. These made an unambiguous assignment of the diamagnetic peaks close to residue 166 impossible for this mutant.

The mutant with the second smallest Q-factor and the second most assigned PCS is

Table 2.3: Number of PCS per mutant with deviations between experimental and calculated PCS in the given ranges.

PCS Deviation	S50C	S166C	S217C	S220C
>0.2 ppm	5	0	23	6
0.2 ppm to 0.15 ppm	11	5	19	6
0.15 ppm to 0.1 ppm	21	4	44	12
Total >0.1 ppm	**37**	**9**	**86**	**24**
Total no. of PCS:	**410**	**416**	**398**	**394**

S50C. Here the number of differing PCS already is larger (compare to table 2.3) The largest PCS deviation with 0.32 ppm was found for residue A54. For this residue the second largest PCS of this mutant (−3.57 ppm) was recorded.
Although the Q-factor indicates a lesser agreement between experimental and calculated PCS of S220C compared to S50C, the S220C mutant shows a smaller total number of PCS with deviations exceeding 0.1 ppm. This can be explained by the smaller range of PCS which is with −1.44 ppm to 0.85 ppm more than 3 times smaller than for S50C (−3.57 ppm to 4.15 ppm). With smaller absolute PCS the average distance increases to the paramagnetic center and consequently the absolute PCS deviation decreases too in general because of the r^{-3} distance dependence of the PCS. For the S220C mutant the largest PCS deviation was found for residue S99 with 0.44 ppm.

In the case of the S217C mutant which showed the largest Q-factor and by far the largest number of deviating PCS (more than a fifth of all PCS) also the largest PCS deviation was found for residue L148 exceeding 1.2 ppm for both (^{1}H and ^{15}N) PCS. These two PCS clearly stick out in figures 2.10 and 2.11. In the selectively ^{15}N-Leu labelled protein

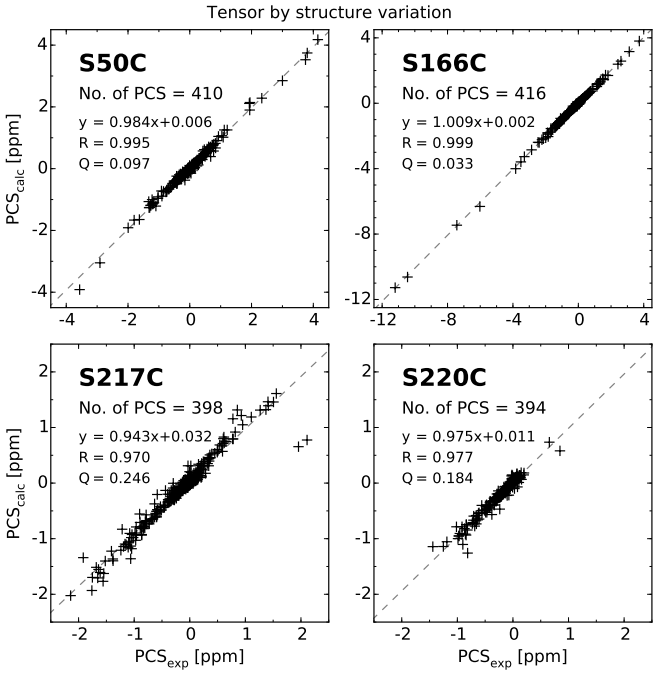

Figure 2.10: Correlation of experimental and back calculated PCS obtained from tensors determined with the given type of *Monte-Carlo* protocol. All assigned PCS were used.

the PCS of L148 could be assigned unambiguously, because for each of the 26 leucine residues a corresponding PCS was found. Therefore these PCS were included in the tensor calculation for this mutant. This mutant also shows the biggest differences in the tensor parameters calculated with the two different *Monte-Carlo* methods (see table 2.2) which indicates that either the variation of the atomic coordinates in the X-ray structure or the exclusion of some of the PCS from the tensor calculation has an impact on the tensor. Both reasons point out that the X-ray structure does not agree for every residue with the determined PCS. When subsets consisting of 20 % of all PCS are randomly selected then the probability that both L148 PCS are excluded from the tensor calculation is 64 % and the probability that at least one of these PCS is excluded is 96 % this means that these PCS have none or only very small influence on the majority of the 1000 calculated tensors. The fact that the PCS deviation increases (1.2 ppm to 1.8 ppm) for residue L148 when the PCS are calculated using the tensor obtained by random selection of 20 % subsets (see figure 2.11) supports the assumption

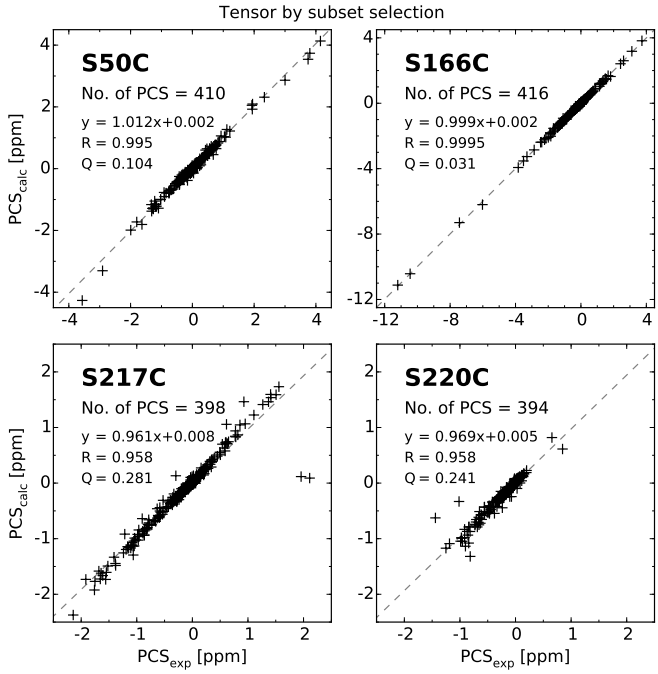

Figure 2.11: Correlation of experimental and back calculated PCS obtained from tensors determined with the given type of *Monte-Carlo* protocol. All assigned PCS were used.

that indeed this residue's position seems to differ from the X-ray structure. This is in accordance to the X-ray structure where the residue L148 is found very close to the mutation site of the S217C mutant. L148 is located at the end of a β-sheet which crosses the β-sheet where residue 217 is present. Therefore it is likely that the mutation or the tagging as well can have an effect on the position of L148, which would explain the deviation in the corresponding PCS. From this it follows that the large number of differing PCS for S217C can at least partially be explained by the circumstance that the two PCS of the residue L148 which were included in the tensor calculation, resulted in biased tensor parameters and thereby caused increased PCS deviations for some of the residues. Other deviating PCS could as well differ in their position observed by PCS compared to the X-ray structure but the effect was not that obvious as for L148 in the case of the S217C mutant, therefore the next step was finding a method to sort out such PCS from the tensor calculation in order to refine the tensor parameters.

2.11 Refinement of the magnetic susceptibility tensors

The magnetic susceptibility tensors obtained from the PCS assigned as described in the section above allowed to calculate in Numbat the expected shifts based on the X-ray structure (PDB code: 3KS3). When these calculated PCS were compared with the experimental shifts apart from the S166C mutant, for all other mutants, some PCS showed deviations of more than 0.2 ppm. After close examination of the NMR spectra and the X-ray structure possible reasons explaining these deviations were found:

- The approach in this thesis is based on the assumption that the protein structure in buffered solution is comparable to the X-ray structure used for the determination of the magnetic susceptibility tensor. Based on the large number of PCS that could be assigned, the protein in solution has to have high structural similarity to the available X-ray structure. This is not necessarily true for every part of the protein. Crystal artefacts arising from the crystal packing, as well as dynamic behaviour of flexible loop regions in solution are both well known phenomena explaining structural differences in certain parts of the protein.
- The X-ray structure available was recorded form wild type protein. But the PCS were determined from double mutants which were tagged with LnM8-SPy. Both, the tagging as well as the mutations can cause small structural differences. Especially for residues close to the tag only a very small displacement in their position compared to the X-ray structure can lead to large differences in the PCS due to their r^{-3} distance dependence.
- In the ^{1}H-^{15}N-HSQC spectra of uniformly labelled protein peak overlap can limit the precision of the determined PCS. This is more pronounced for the ^{15}N dimension because of lower resolution and a larger spectral window.

Based on these considerations we defined three criteria upon which we excluded some PCS from the final tensor calculation:

(i) If the weighted chemical shift distance of LuM8 tagged compared to untagged protein is larger than 5σ, where σ is the standard deviation of unaffected residues, ^{1}H and ^{15}N PCS were removed regardless of the according PCS deviation.

(ii) If the PCS deviation is larger than a defined cut off and if the residue is either in a flexible loop region of the protein or at the edges of a secondary structure element close to the tag, ^{1}H and ^{15}N PCS were removed.

(iii) If the PCS deviation is larger than a defined cut off and peak overlap in the ^{1}H-^{15}N-HSQC spectra could explain the observed PCS deviation. In this case only the PCS of the concerned nucleus was removed.

The aim of the first criterion is to detect residues whose position could be affected by the tagging with LnM8-SPy. We decided to follow the approach of chemical shift mapping, where chemical shift differences are used to determine and characterise protein ligand or protein protein interaction sites.[52] In this case the site where the tag is bound to the protein is already known, but information could be obtained about which residues are strongly affected by the tagging. Chemical shift changes show changes in the chemical environment of the observed nuclei. This has not necessarily to be caused by a structural change in the protein, but nevertheless it is a possibility. The number of PCS compared to the full set, that were excluded based on this criteria, consisted of only 5 % or even less PCS. Therefore priority was laid on exclusion of candidates whose structure may differ instead of maximising the number of PCS per subset. Chemical shift changes between untagged and LuM8 tagged protein were determined as weighted chemical shift distance with a weighting factor of 0.25 for the nitrogen shift according to equation 2.2.

$$\Delta\delta = \frac{1}{2}\sqrt{(\Delta\delta_{^{1}H})^2 + (0.25\Delta\delta_{^{15}N})^2} \tag{2.2}$$

Well separated peaks in the ^{1}H-^{15}NHSQC spectra which were not shifted after tagging were used to determine the standard deviation of the chemical shift differences (σ) of unaffected peaks. Only residues showing a larger weighted shift differences than 5σ were excluded from the PCS set (see figures 2.12 to 2.15). The value of 5σ was obtained experimentally by comparing different sizes of this cut-off, in order to keep the number of excluded residues as small as possible, but still observe a significant

improvement of the determined tensor values.
The second criterion takes the possibility into account that loop regions of a protein in solution can adopt a different conformation than in the X-ray structure. As well as to cover for possible structural changes due to the serine to cysteine mutation, which could not be approached by chemical shift changes, because no wild type protein was available for such a comparison.
The third criterion considers residues where the corresponding peak in the ^{1}H-^{15}N-HSQC overlaps with another signal either the diamagnetic or in the paramagnetic spectra. It was found that in several cases one of the two PCS (in most cases the ^{1}H-PCS) fitted well to the tensor whereas the deviation of the other PCS could be explained by the lowered accuracy of the shift in the respective dimension due to the overlap. Therefore only the deviating PCS was removed.
To see whether the exclusion of different number of PCS has a large influence on the tensor we decided to define three different subsets of PCS each with a different cut off for the PCS deviation. The values chosen were 0.2 ppm, 0.15 ppm and 0.1 ppm respectively. The three corresponding subsets will be called further on set 1 to 3 where for set 1 all PCS with deviations exceeding 0.2 ppm were excluded leaving set 3 to be the one with the smallest PCS deviations.
In the following sections it will be discussed in detail for each mutant individually, which PCS have been removed and what impact on the tensor the three different subsets have.

2.11.1 S50C tensor

For this mutant a total of 410 PCS (^{1}H and ^{15}N) for 205 residues could be assigned unambiguously. This corresponds to 85 % of all residues or to 95 % of those residues where a reasonable assignment was available.

Set 1

In total 28 PCS were removed for set 1 to obtain a set where the largest PCS deviation was below 0.2 ppm. This set consists of 93 % of all available PCS.

- Residues 22, 23, 36, 47, 54, 72, 74, 82, 87, 88, 95 and 198 showed a shift of more than 5σ when the protein was tagged with LuM8-SPy (see figure 2.12). Of these residues 47 to 88 are all found in the β-sheet where the tag is attached, in the parallel β-sheet or in the adjacent loop regions to the two β-sheet. Except residue 88 is the first residue of the second next β-sheet. For all these residues it is very likely that they are influenced by the attachment of the tag. Residues 22, 23, 36, 95 and 198 were found further away from the tag. Nevertheless they were removed from the tensor set to exclude all residues with possible structural changes. Of these residues both PCS (^{1}H and ^{15}N) were removed.
- After excluding the residues mentioned above, residues 71 and 89 still showed a PCS deviation of more than 0.2 ppm. Both residues were found in a loop region close to the tag and next to a residue that showed a large chemical shift change. Therefore both PCS of these residues were excluded from set 1.

Set 2

In total 32 PCS were removed for set 2 (all PCS that were excluded for set 1 and 4 additional), to obtain a set where the largest PCS deviation was below 0.15 ppm. This set consists of 92 % of all available PCS.

- Residue 189 was found in a loop region close to the tag. Both PCS of these residue were excluded.
- The the deviation of ^{15}N PCS of residue 197 could be explained by peak overlap in the ^{1}H-^{15}N-HSQC spectra.
- After exclusion of all PCS above, the ^{15}N PCS of residue 119 still showed a PCS deviation of more than 0.15 ppm. For this PCS no explanation of the deviation could be found. Nevertheless it could be shown, that the exclusion of this PCS did not have an influence on the tensor parameters. Therefore it was decided to remove this PCS too in order to exclude any possible source of errors.

Set 3

In total 44 PCS were removed for set 3 (all PCS that were excluded for set 2 and 12 additional), to obtain a set where the largest PCS deviation was below 0.10 ppm. This

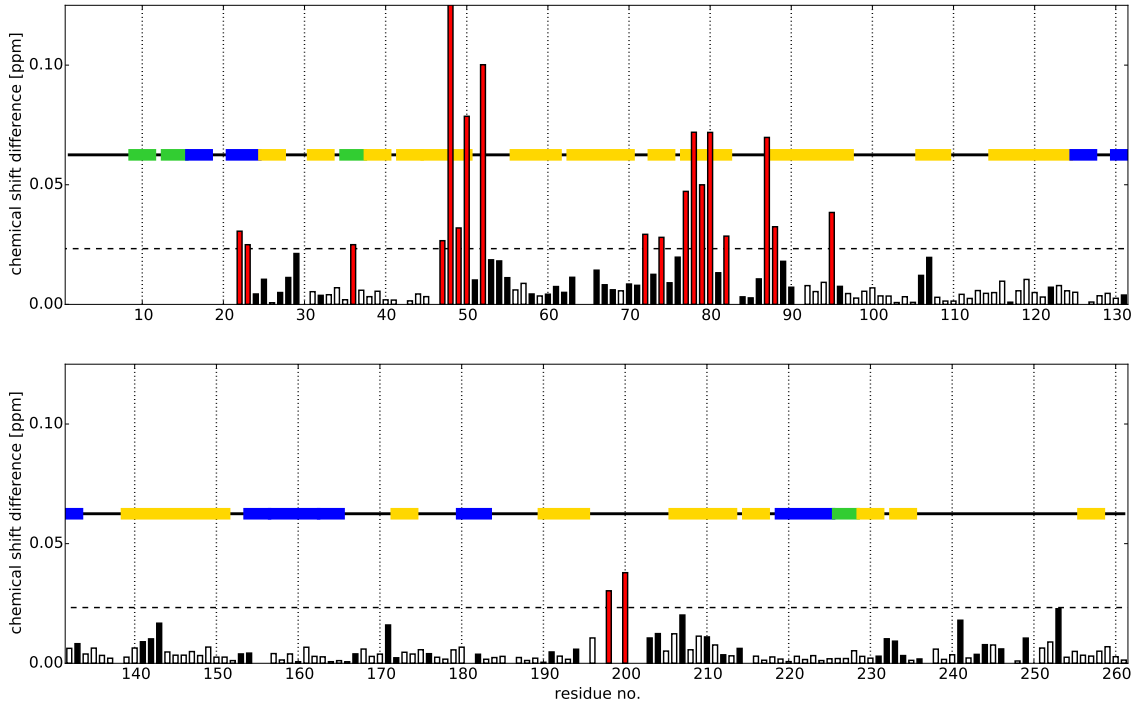

Figure 2.12: Plot of weighted chemical shift differences of hCA-II_S50C_C206S-LuM8 compared to untagged protein, calculated using $0.5[(\Delta\delta_{^1H})^2+(0.25(\Delta\delta_{^{15}N}))^2]^{0.5}$. Residues with well separated signals in the ^{1}H-^{15}N-HSQC spectra used for calculation of the standard uncertainty (σ) of the peak position are shown in white. The dashed line indicates the 5σ cut off. Residues exceeding this value (shown in red) were excluded from tensor calculation. Residues with black and white bars remained in the tensor set with respect to this criterion. Secondary structure elements of the protein are indicated (β-sheets: yellow, helices: blue and hydrogen bonded turns: green).

set consists of 89 % of all available PCS.

- Residue 84 and 190 were found in a loop region close to the tag. Both PCS were removed for these residues.
- The the deviation of ^{15}N PCS of residues 32, 60, 96, 106, 128 and 203 could be explained by peak overlap in the ^{1}H-^{15}N-HSQC spectra.
- After exclusion of all PCS above, the ^{15}N PCS of residues 29 and 135 still showed a PCS deviation of more than 0.1 ppm. For these PCS again no explanation of the deviation could be found. Nevertheless it could be shown, that the exclusion of these PCS did not have an influence on the tensor parameters. Therefore it

was decided to remove these PCS too in order to exclude any possible source of errors.

Magnetic susceptibility tensors of the different subsets

when the tensor parameters obtained from the different subsets were compared with each other, only very small effects on the tensor parameters were found (see table 2.4). Obviously the determined uncertainties decreased when a more consistent set of PCS was used for the tensor calculation. The differences in the tensor parameters for the two *Monte-Carlo* methods were much smaller for the three subsets than for the full set of PCS for this mutant (compare to table 2.2).

Table 2.4: Tensors of the S50C mutant for the different subsets of PCS

S50C		**Set 1**	**Set 2**	**Set 3**	**Set 1**	**Set 2**	**Set 3**
$\Delta\chi_{ax}$	[$10^{-32}m^3$]	20.8 ± 1.2	21.1 ± 1.2	21.6 ± 1.2	20.7 ± 1.1	20.9 ± 1.1	21.1 ± 0.9
$\Delta\chi_{rh}$	[$10^{-32}m^3$]	8.4 ± 0.7	8.4 ± 0.7	8.5 ± 0.7	8.5 ± 0.7	8.5 ± 0.7	8.5 ± 0.6
x	[Å]	-27.5 ± 0.3	-27.6 ± 0.3	-27.8 ± 0.3	-27.3 ± 0.4	-27.4 ± 0.4	-27.5 ± 0.3
y	[Å]	13.7 ± 0.3	13.7 ± 0.3	13.7 ± 0.3	13.7 ± 0.3	13.7 ± 0.3	13.6 ± 0.2
z	[Å]	18.3 ± 0.3	18.3 ± 0.3	18.1 ± 0.3	18.3 ± 0.3	18.3 ± 0.3	18.2 ± 0.2
α	[°]	104.8 ± 1.6	104.8 ± 1.6	104.1 ± 1.6	103.9 ± 2.3	103.8 ± 2.2	104.0 ± 1.8
β	[°]	141.8 ± 1.1	141.8 ± 1.1	142.3 ± 1.1	141.8 ± 1.0	141.7 ± 1.0	141.8 ± 0.8
γ	[°]	116.4 ± 1.7	116.4 ± 1.7	116.2 ± 1.7	116.2 ± 2.1	115.9 ± 1.9	115.9 ± 1.7
Error analysis:		*Monte-Carlo* structure variation with a $\sigma = 0.5$ Å			*Monte-Carlo* protocol for random subset selection of 20 % of PCS		

2.11.2 S166C tensor

For this mutant in total 416 PCS corresponding to 208 residues could be assigned. These are 86 % of all residues that show a resonance in the ^{1}H-^{15}N-HSQC spectra, or 97 % of those residues, where a reasonable assignment was available.

Set 1

Only 2 residues (4 PCS) were removed for this set. It consists of 99 % of all available PCS. Residue 167 and 168 both showed a PCS deviation smaller than 0.2 ppm but their

PCS could only be assigned tentatively, because unambiguous assignment of their corresponding peaks in the diamagnetic spectra was not possible due to the large change in the chemical shift upon tagging. Anyway these residues would have been excluded due to the criteria that was defined based on the change in the chemical shift. Every possible candidate in the diamagnetic spectra for these two residues would have shown a change in the chemical shift of more than 5σ compared to the untagged protein.

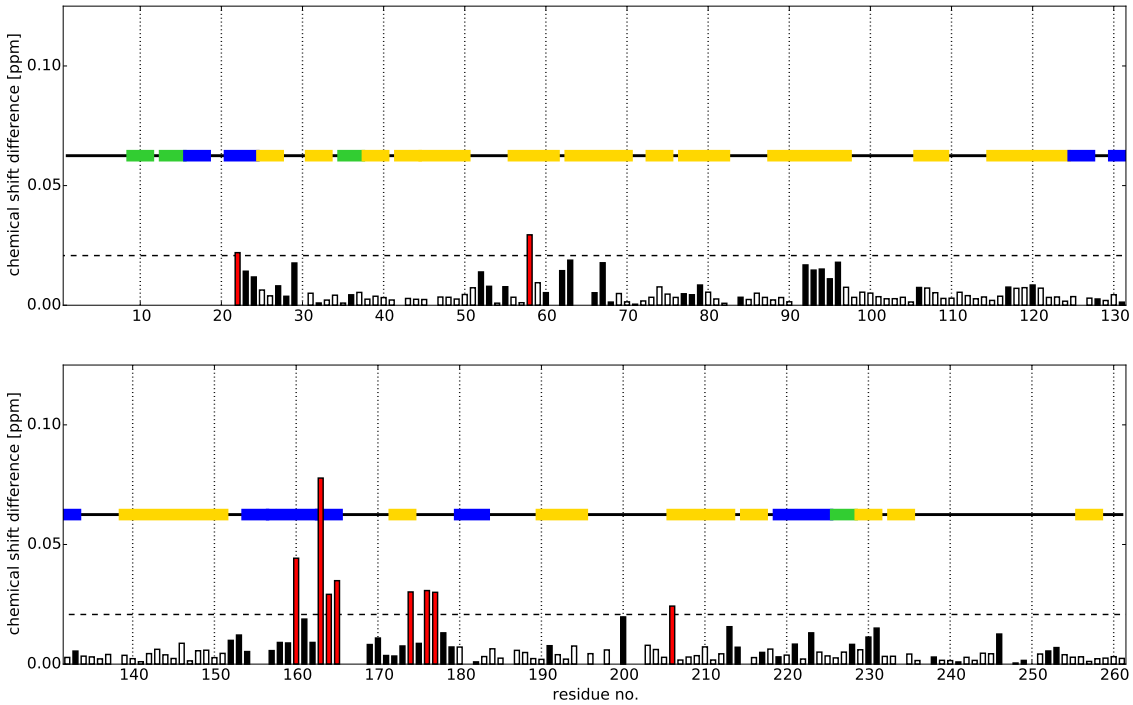

Figure 2.13: Plot of weighted chemical shift differences of hCA-II_S166C_C206S-LuM8 compared to untagged protein. For further details, compare to figure 2.12.

Set 2

Set 2 consists of 402 PCS which corresponds to 96 % of all assigned PCS. In total 14 PCS of 7 different residues were excluded (The two from set 1 and 5 additional).

- Residues 22, 58, 160 and 206 were removed due to the chemical shift change (compare to figure 2.13).
- Residue 172 was excluded according criteria (ii) as it was found at the edge of a

β-sheet close to the tag.

Set 3

In total 19 PCS were removed for this set, all from set 2 and 5 additional PCS which showed a PCS deviation of more than 0.1 ppm. This set consists of 95 % of all available PCS.

- The ^{15}N PCS of residues 75, 79, 197 and 235, as well as the ^{1}H PCS of residue 171 were excluded due to peak overlap.

Magnetic susceptibility tensors of the different subsets

The tensor parameters in table 2.5 show almost no differences, depending on the different PCS subsets and even compared to the full set (see table 2.2). This shows the excellent agreement of PCS and protein structure for this mutant. Compared to the S50C mutant larger differences are found for the two *Monte-Carlo* methods. Where the uncertainties for the subset selection were in the same range as for S50C, the uncertainties for the structure variation turned out to be around twice as large. This supports the good agreement between X-ray structure and experimental PCS since the distortion of the protein structure leads to an decreased agreement to the recorded PCS. This effect could be amplified by the larger average PCS determined for this mutant, because the larger a PCS the higher the sensitivity to structural changes.

2.11.3 S217C tensor

In total 398 PCS could be assigned for this mutant, these cover 82 % of all backbone amide NH groups or 91 % of the residues where a reasonable assignment was possible.

Set 1

Set 1 consists of 94 % of all assigned PCS. 22 PCS were excluded.

- Residues 62, 93, 113, 116, 148, 190, 220, 221, 223 and 246 were removed due to their chemical shift change (compare to figure 2.14).
- Residue 112 was found in a loop region close to the tag.

As already discussed in section 2.10 residue 148 showed a strong indication that the determined PCS does not fit to the position in the X-ray structure. Here this residue

Table 2.5: Tensors of the S166C mutant for the different subsets of PCS

S166C	**Set 1**	**Set 2**	**Set 3**	**Set 1**	**Set 2**	**Set 3**
$\Delta\chi_{ax}$ [$10^{-32}m^3$]	38.7 ± 2.0	38.7 ± 1.9	38.5 ± 2.0	37.3 ± 1.2	37.6 ± 1.0	37.4 ± 0.9
$\Delta\chi_{rh}$ [$10^{-32}m^3$]	7.5 ± 1.2	8.4 ± 1.0	8.0 ± 1.0	7.8 ± 0.9	8.3 ± 0.8	7.8 ± 0.6
x [Å]	-16.1 ± 0.5	-16.4 ± 0.4	-16.3 ± 0.4	-16.1 ± 0.3	-16.3 ± 0.3	-16.2 ± 0.2
y [Å]	-3.5 ± 0.3	-3.6 ± 0.4	-3.6 ± 0.4	-3.5 ± 0.2	-3.6 ± 0.2	-3.6 ± 0.2
z [Å]	-11.2 ± 0.4	-11.2 ± 0.4	-11.2 ± 0.4	-10.9 ± 0.3	-11.0 ± 0.2	11.0 ± 0.2
α [°]	51.5 ± 2.0	52.8 ± 1.8	52.2 ± 1.8	52.7 ± 1.5	53.3 ± 1.4	52.7 ± 1.2
β [°]	123.1 ± 1.3	123.6 ± 1.4	123.6 ± 1.4	122.7 ± 0.9	123.0 ± 0.8	123.1 ± 0.7
γ [°]	143.1 ± 5.0	140.5 ± 5.6	140.3 ± 5.6	142.7 ± 3.6	141.5 ± 3.0	141.1 ± 2.7
Error analysis:	*Monte-Carlo* structure variation with a $\sigma = 0.5$ Å			*Monte-Carlo* protocol for random subset selection of 20 % of PCS		

was excluded because of the chemical shift change. This shows that this method is suitable to sort out residues which are affected by structural changes due to the tagging of the protein.

Set 2

For set 2 all PCS of set 1 and 4 additional, in total 26 PCS were removed. Set 2 consists of 93 % of all available PCS.

- Residue 147 was found at the edge of a β-sheet close to the tag. This residue is next to L148 which already showed several indications for a very likely structural change.
- Residue 191 was found in a loop region close to the tag.

Set 3

This set consists of 91 % of all assigned PCS. In total 34 PCS were excluded (all from set 2 and 8 additional).

- Residues 101, 109, 110 and 111 were removed according to criteria (ii), due to their PCS deviation which exceeded 0.1 ppm and in addition because they were

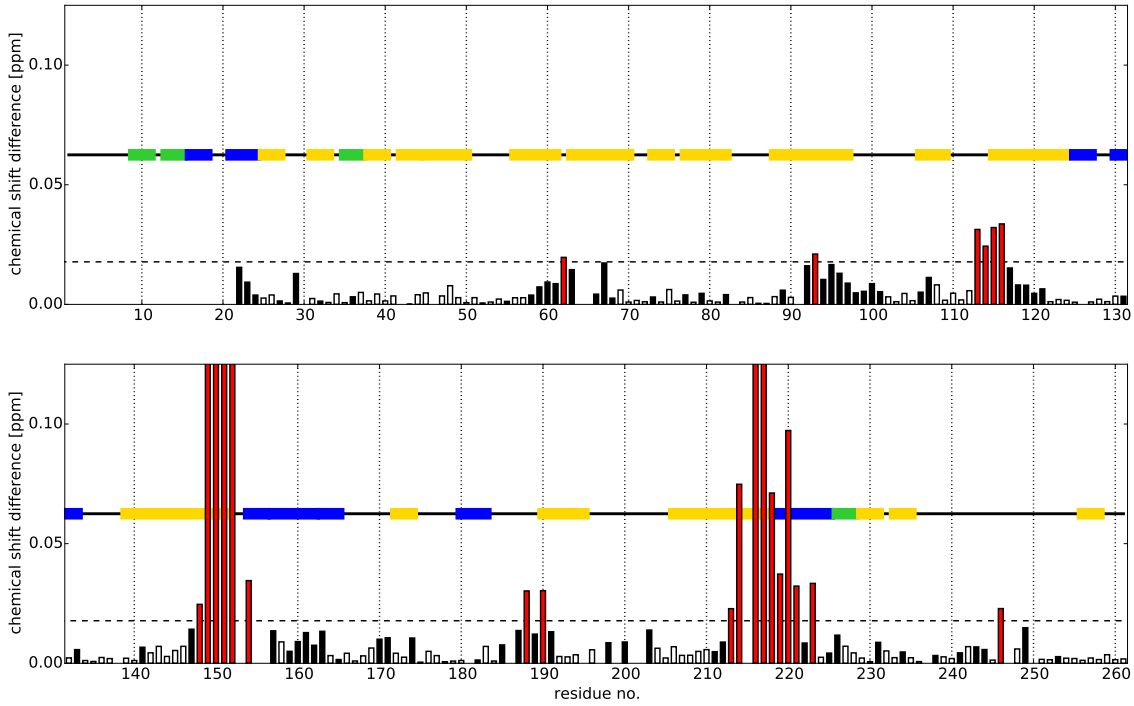

Figure 2.14: Plot of weighted chemical shift differences of hCA-II_S217C_C206S-LuM8 compared to untagged protein. For further details, compare to figure 2.12.

found in a loop region close to the tag .

For this subset 34 PCS were removed to obtain a set where the largest PCS deviation is below 0.1 ppm. In contrast to 86 PCS that showed a PCS deviation larger than 0.1 ppm when the full set of PCS was used (see table 2.3). This clearly shows that it was possible to increase the overall agreement of PCS and X-ray structure by a proper selection of the right subset.

Magnetic susceptibility tensors of the different subsets

The tensor parameters of the different subsets for this mutant (compare to table 2.6) do not show differences worth mentioning. Whereas the differences to the tensor parameters determined for the full set of PCS (see table 2.2) clearly show the effect of the refinement. The tensor parameters showed clear differences depending on the *Monte-Carlo* method, when the full set of PCS was used. This was not the case any more for the three subsets, showing that PCS and protein structure become more

consistent and less dependant on the mode of error estimation.

Table 2.6: Tensors of the S217C mutant for the different subsets of PCS

S217C		**Set 1**	**Set 2**	**Set 3**	**Set 1**	**Set 2**	**Set 3**
$\Delta\chi_{ax}$	[10^{-32}m^3]	26.0 ± 1.0	25.8 ± 1.0	25.7 ± 1.0	25.5 ± 1.4	25.4 ± 1.3	25.5 ± 1.1
$\Delta\chi_{rh}$	[10^{-32}m^3]	13.4 ± 0.6	13.4 ± 0.5	13.2 ± 0.6	13.2 ± 0.7	13.2 ± 0.7	13.1 ± 0.6
x	[Å]	-24.9 ± 0.2	-24.9 ± 0.2	-24.9 ± 0.2	-24.7 ± 0.3	-24.7 ± 0.3	-24.8 ± 0.2
y	[Å]	-17.9 ± 0.3	-17.8 ± 0.3	-17.7 ± 0.3	-17.6 ± 0.4	-17.6 ± 0.3	-17.5 ± 0.3
z	[Å]	19.6 ± 0.2	19.7 ± 0.3	19.6 ± 0.2	19.7 ± 0.3	19.7 ± 0.3	19.6 ± 0.2
α	[°]	143.7 ± 0.8	143.7 ± 0.8	143.7 ± 0.8	143.4 ± 1.0	143.3 ± 0.9	143.3 ± 0.8
β	[°]	70.4 ± 0.6	70.3 ± 0.5	70.9 ± 0.5	70.6 ± 0.9	70.7 ± 0.8	71.2 ± 0.7
γ	[°]	126.1 ± 1.0	126.2 ± 1.1	125.5 ± 1.0	125.7 ± 1.3	125.7 ± 1.3	125.1 ± 1.1
Error analysis:		*Monte-Carlo* structure variation with a $\sigma = 0.5$ Å			*Monte-Carlo* protocol for random subset selection of 20 % of PCS		

2.11.4 S220C tensor

For this mutant 396 PCS were assigned, covering 81 % of all possible backbone amide PCS, or 90 % of those residues where an assignment was available.

Set 1

For set 1 in total 7 residues (14 PCS) were excluded. The set consists of 96 % of all assigned PCS.

- Residues 99, 102, 104, 148, 150, 153 and 161 showed a large chemical shift change, when the protein was tagged (compare to figure 2.15) All of these residues are found close to the tag.

Set 2

All residues of set 1 and 4 additional residues (in total 22 PCS) were removed for set 2. It consists of 94 % of all available PCS.

- Residues 96, 98 and 114 were removed also because of their chemical shift differences. Because both, their PCS deviation (between 0.2 ppm and 0.15 ppm)

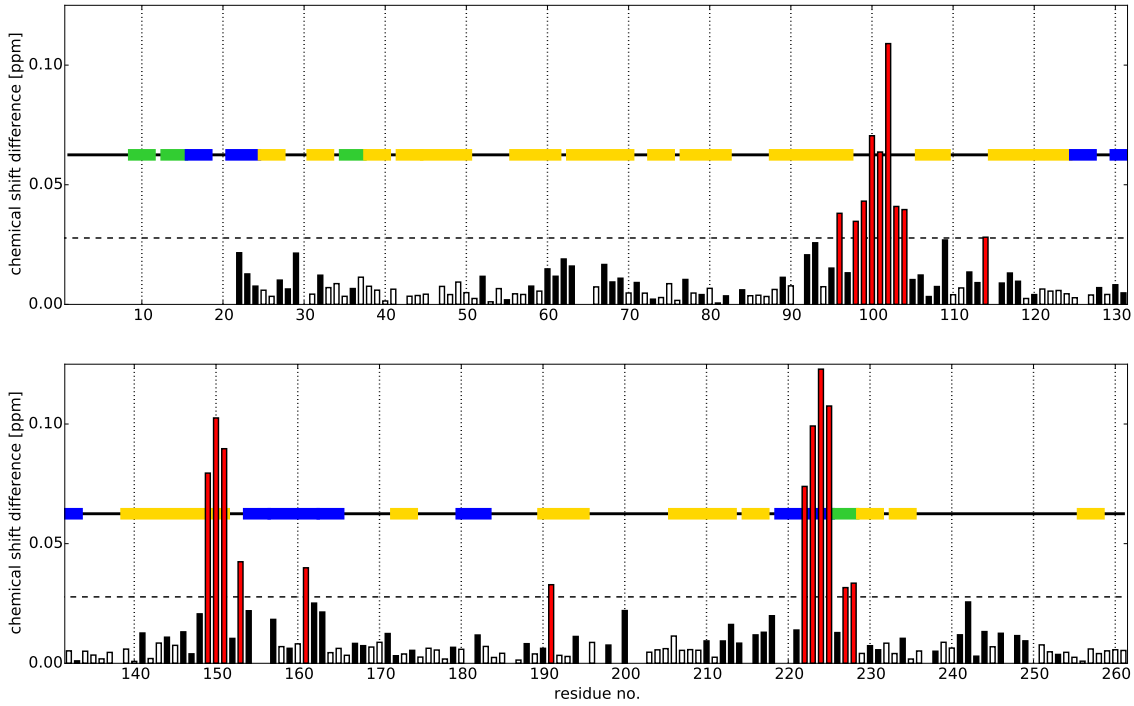

Figure 2.15: Plot of weighted chemical shift differences of hCA-II_S220C_C206S-LuM8 compared to untagged protein. For further details, compare to figure 2.12.

as well as their chemical shift differences (between 7σ and 5σ) were smaller, compared to the residues removed for set 1, these residues were kept for set 1.

- Residue 116 was excluded due to the PCS deviation and because it was found in a loop region close to the tag (according to criteria (ii)).

Set 3

For set 3 in total 28 PCS were removed (all from set2 and 6 additional). It consists of 93 % of all assigned PCS.

- Residue 157 was found at the edge of a α-helix close to the tag.
- Residue 229 was found in a loop region close to the tag.
- The ^{15}N PCS of residues 58 and 197 were excluded due to peak overlap in the HSQC spectrum.

Magnetic susceptibility tensors of the different subsets

Compared to the tensor parameters determined with the full set of PCS (compare to table 2.2) the values in table 2.7 clearly show smaller uncertainties. When the different subsets are compared with each other the differences in the values of the tensor parameters are only marginal. Except for the *Euler* angles, where the differences and larger uncertainties (especially for γ) are attributed to the smaller $\Delta\chi_{rh}$ and hence a tensor closer to axial symmetry. But what attracts attention is the fact that the uncertainties for the parameters determined by structure variation are more than twice as small as the uncertainties determined by random subset selection. This is the other way round as found for the S166C mutant before. Possibly the uncertainties determined by structure variation are dependent on the size of the corresponding PCS. For S166C the largest average absolute PCS were determined, where S220C these were the smallest of all four mutants (for S50C and S217C these were in the same order in between the other two mutants). An explanation for the smallest uncertainties obtained for this mutant from the structure variation could be that structure variation with the same magnitude has a smaller effect on the resulting tensor parameters if the average absolute PCS are getting smaller.

Table 2.7: Tensors of the S220C mutant for the different subsets of PCS

S220C		**Set 1**	**Set 2**	**Set 3**	**Set 1**	**Set 2**	**Set 3**
$\Delta\chi_{ax}$	[10^{-32}m^3]	23.2 ± 1.0	23.6 ± 0.9	23.6 ± 0.9	22.5 ± 2.4	22.9 ± 2.3	23.0 ± 2.1
$\Delta\chi_{rh}$	[10^{-32}m^3]	4.0 ± 0.3	4.3 ± 0.3	4.3 ± 0.3	4.1 ± 0.9	4.4 ± 0.9	4.4 ± 0.8
x	[Å]	-13.0 ± 0.2	-13.4 ± 0.3	-13.1 ± 0.3	-13.0 ± 0.7	-13.3 ± 0.7	-13.0 ± 0.6
y	[Å]	-26.2 ± 0.3	-26.6 ± 0.3	-26.7 ± 0.3	-26.0 ± 0.7	-26.3 ± 0.6	-26.4 ± 0.6
z	[Å]	3.1 ± 0.2	3.3 ± 0.2	3.2 ± 0.2	3.1 ± 0.6	3.2 ± 0.6	3.2 ± 0.5
α	[°]	16.7 ± 1.6	14.9 ± 1.3	14.9 ± 1.4	17.8 ± 4.7	16.7 ± 4.0	16.2 ± 3.5
β	[°]	154.2 ± 0.6	154.3 ± 0.6	153.6 ± 0.6	154.3 ± 1.8	154.4 ± 1.7	153.7 ± 1.5
γ	[°]	1.2 ± 3.0	1.8 ± 2.6	1.0 ± 2.6	4.7 ± 8.1	5.4 ± 7.1	3.9 ± 6.6
Error analysis:		*Monte-Carlo* structure variation with a $\sigma = 0.5$ Å			*Monte-Carlo* protocol for random subset selection of 20 % of PCS		

2.11.5 Comparison of tensor parameters for the different protein mutants

As it was is shown in tables 2.4 to 2.7 there was no significant difference depending on which subset was used for determination of the sensor parameters. For convenience in this section the comparison between the four mutants is based only on the tensor parameters determined with the PCS set 3. All other tensor parameters are already given above, and all corresponding correlation plots (compare to figure 2.16 and 2.17) are given in the appendix section.
After the refinement, the magnitude of the tensor parameters remained the same as for the full set of PCS. $\Delta\chi_{ax}$ for S166C is still almost twice as large as for the other three mutants, where for $\Delta\chi_{rh}$ the biggest value was found for S217C and the smallest for S220C. The most likely reason for the differences would be that for the S166C the paramagnetic metal has the least motional freedom with respect to the protein. For the other mutants residual dynamic behaviour of the tag could allow different orientations of the lanthanide metal which would result in averaged and therefore reduced tensor parameters. Interestingly this motional freedom has to be similar for all three mutants, to result in such comparable tensor parameters.

As shown in table 2.8 even the smallest subset (set 3) still contains a very large number of PCS as compared to other tensors reported in the literature[18,23,30,53–56]. Set 3 for the mutants S50C, S217C and S220C still contains 75 % and S166C even covers 82 % of all possible backbone amide PCS for the whole protein. For every mutant we have an excellent agreement between experimental and back-calculated PCS as shown in figures 2.16 and 2.17. The plot is shown for both tensor parameters obtained with the different *Monte-Carlo* methods to show again that there is basically no difference any more between these two approaches of the error analysis. The higher Q-factor for the S220C mutant is mainly affected by the fact that this mutant shows the smallest RMS of the PCS which can be seen directly from the smallest range of PCS for this mutant.

Table 2.8: Number of PCS total assigned and finally used for the different subsets. Number of removed PCS are given in brackets.

		S50C	**S166C**	**S217C**	**S220C**
Full Set		**410**	**416**	**398**	**396**
Set 1	1H	191 (14)	206 (2)	188 (11)	191 (7)
	15N	191 (14)	206 (2)	188 (11)	191 (7)
	Tot.	382 (28)	412 (4)	376 (22)	382 (14)
Set 2	1H	190 (15)	201 (5)	186 (13)	187 (11)
	15N	188 (17)	201 (5)	186 (13)	187 (11)
	Tot,	378 (32)	402 (10)	372 (26)	374 (22)
Set 3	1H	188 (17)	200 (8)	182 (17)	185 (13)
	15N	178 (27)	197 (11)	182 (17)	183 (15)
	Tot.	**366 (44)**	**397 (19)**	**364 (34)**	**368 (28)**

Table 2.9: Refined magnetic susceptibility tensor parameters The values and their uncertainties are calculated by a *Monte Carlo* protocol applying two different random inputs given below.

		S50C	**S166C**	**S217C**	**S220C**
$\Delta\chi_{ax}$	[10^{-32}m^3]	21.6 ± 1.2	38.5 ± 2.0	25.7 ± 1.0	23.6 ± 0.9
$\Delta\chi_{rh}$	[10^{-32}m^3]	8.5 ± 0.7	8.0 ± 1.0	13.2 ± 0.6	4.3 ± 0.3
x	[Å]	-27.8 ± 0.3	-16.3 ± 0.4	-24.9 ± 0.2	-13.1 ± 0.3
y	[Å]	13.7 ± 0.3	-3.6 ± 0.4	-17.7 ± 0.3	-26.7 ± 0.3
z	[Å]	18.1 ± 0.3	-11.2 ± 0.4	19.6 ± 0.2	3.2 ± 0.2
α	[°]	104.1 ± 1.6	52.2 ± 1.8	143.7 ± 0.8	14.9 ± 1.4
β	[°]	142.3 ± 1.1	123.6 ± 1.4	70.9 ± 0.5	153.6 ± 0.6
γ	[°]	116.2 ± 1.7	140.3 ± 5.6	125.5 ± 1.0	1.0 ± 2.6
Monte Carlo structure variation with a $\sigma = 0.5$ Å					
$\Delta\chi_{ax}$	[10^{-32}m^3]	21.1 ± 0.9	37.4 ± 0.9	25.5 ± 1.1	23.0 ± 2.1
$\Delta\chi_{rh}$	[10^{-32}m^3]	8.5 ± 0.6	7.8 ± 0.6	13.1 ± 0.6	4.4 ± 0.8
x	[Å]	-27.5 ± 0.3	-16.2 ± 0.2	-24.8 ± 0.2	-13.0 ± 0.6
y	[Å]	13.6 ± 0.2	-3.6 ± 0.2	-17.5 ± 0.3	-26.4 ± 0.6
z	[Å]	18.2 ± 0.2	-11.0 ± 0.2	19.6 ± 0.2	3.2 ± 0.5
α	[°]	104.0 ± 1.8	52.7 ± 1.2	143.3 ± 0.8	16.2 ± 3.5
β	[°]	141.8 ± 0.8	123.1 ± 0.7	71.2 ± 0.7	153.7 ± 1.5
γ	[°]	115.9 ± 1.7	141.1 ± 2.7	125.1 ± 1.1	3.9 ± 6.6
Monte Carlo protocol where random subsets consisting of 20 % of the available PCS were used					

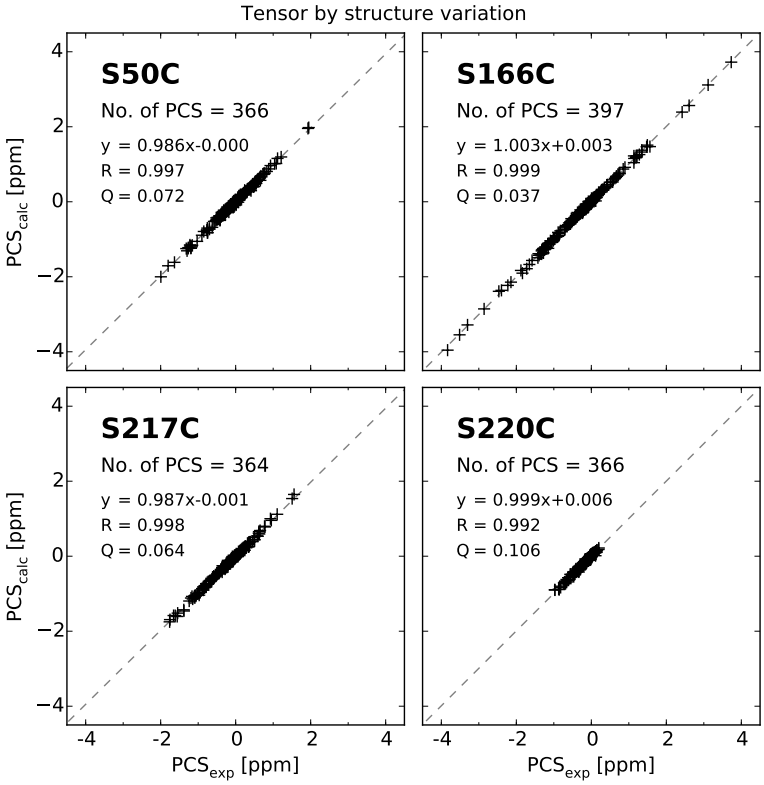

Figure 2.16: Correlation of experimental and back calculated PCS obtained from tensors determined with the given type of *Monte-Carlo* protocol using the PCS of set 3.

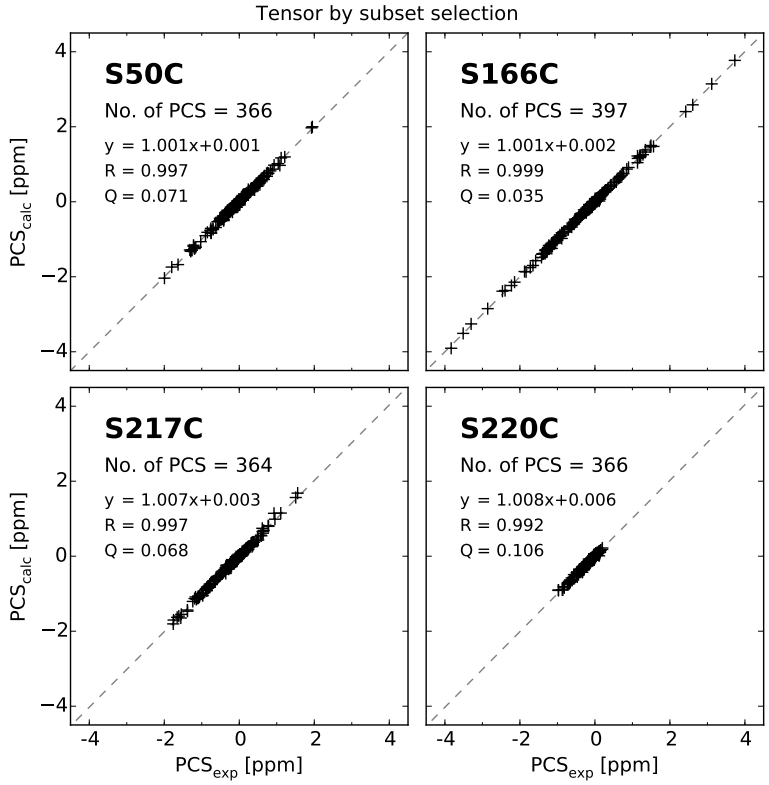

Figure 2.17: Correlation of experimental and back calculated PCS obtained from tensors determined with the given type of *Monte-Carlo* protocol using the PCS of set 3.

2.12 Comparison of (*4R,4S*)-LnM8-SPy with (*8S*)-LnM8-SPy

Depending on the configuration of the lactic acid used for the synthesis of M8-SPy the resulting ligand can be obtained as (*8S*) or as (*4R,4S*) stereoisomer. At the beginning of the project described in this thesis only the (*8S*)-M8-SPy was available, therefore this isomer has been selected for the detailed PCS analysis. (*4R4S*)-M8-SPy as well as protein samples tagged with (*4R,4S*)-TmM8-SPy and (*4R,4S*)-DyM8-SPy respectively, were synthesized by Dr. Roché Walliser in the course of his masters thesis.[57] Here the comparison of these samples with the corresponding (*8S*)-M8-SPy analogues is presented.

Figure 2.18 shows the ^{1}H-^{15}N HSQC spectra of (*4R,4S*)-TmM8-SPy and (*8S*)-TmM8-SPy tagged to ^{15}N-leucine labelled hCA-II_S50C_C206S. With (*4R,4S*)-TmM8 several PCS with opposite sign are observable compared to (*8S*)-TmM8-SPy. This already indicates that for the two tags different orientations of the $\Delta\chi$ tensor can be expected. In contrast to the (*8S*) tagged protein where a minor second species was observable, as already discussed in section 2.9, for the (*4R,4S*) samples only one peak was observable per residue in the paramagnetic spectra.

For a more detailed comparison the magnetic susceptibility parameters based only on the leucine PCS were determined. Leucine residues that were excluded for the uniformly labelled protein from PCS were excluded as well. These residues were number 47, 84 and 189. All of them are close to the tagging site. With this condition reasonable PCS can be expected for the (*4R,4S*) sample as well when determined as the difference from (*8S*)-LuM8 tagged protein, because (*4R,4S*)-LuM8 tagged protein as reference was not available. In total 44 PCS corresponding to 22 residue were used for tensor determination. Due to the small set of PCS and because for the comparison the size of the tensor parameters was sufficient, no error discussion was carried out.

As shown in table 2.10 the tensor parameters for (*8S*)-TmM8 determined from leucine PCS only are very close to the full set of PCS from the uniformly ^{15}N labelled protein. Therefore the tensors for the other three tags can be expected to be representative as well. As already expected the Tm tensors of the two stereoisomers indeed show a large difference in their orientation. Furthermore, the size of the (*4R,4S*) tensor is larger than than (*8S*) tensor which is in agreement with the on average larger PCS that are

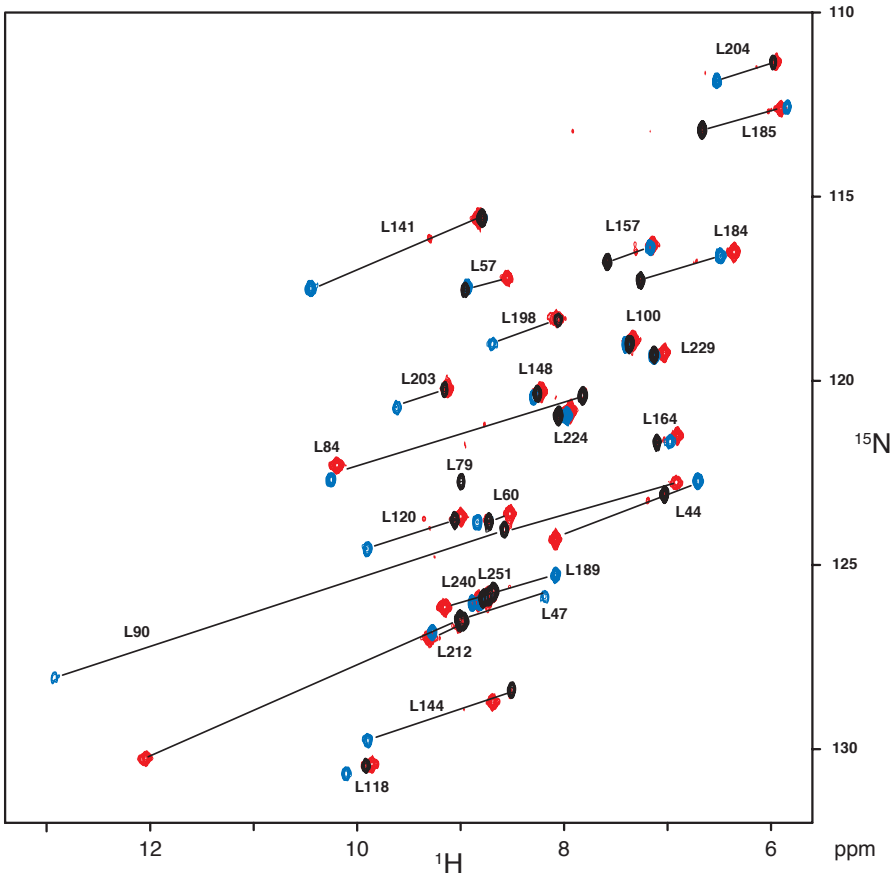

Figure 2.18: Overlay of the ^{1}H-^{15}N-HSQC spectra (600 MHz, 298 K) of selectively ^{15}N leucine labelled hCA-II_S50C_C206S-(*8S*)LuM8 (black), hCA-II_S50C_C206S-(*8S*)TmM8 (red) and hCA-II_S50C_C206S-(*4R,4S*)TmM8 (blue). Assignment and PCS are indicated.

observed for this stereoisomer. The Dy tensors were in both cases smaller than for Tm as opposed to the general trend in the literature where for the Dy larger susceptibility tensors are expected than for Tm.[58] Again the tensor for the (*4R,4S*) Dy sample is larger compared to the (*8S*) stereoisomer. The difference in the orientation of the tensors for the two setereoisomers in the case of Dy is much smaller compared to the Tm samples.

Table 2.10: Tensor parameters determined from selectively ^{15}N-leu labelled hCA-II_S50C_C206S tagged with two different stereoisomers of M8-SPy and two different lanthanide metals. The same set consisting of 22 Leu-Residues (44 PCS) was used for each tensor.

S50C tagged with		***8S*-TmM8**	***4R,4S*-TmM8**	***8S*-DyM8**	***4R,4S*-DyM8**
$\Delta\chi_{ax}$	[10^{-32}m^3]	22.1	30.5	-12.1	-20.6
$\Delta\chi_{rh}$	[10^{-32}m^3]	8.6	11.7	-5.0	-6.9
x	[Å]	-27.9	-28.8	-30.9	-30.4
y	[Å]	13.5	13.1	9.4	12.3
z	[Å]	18.2	20.9	20.1	20.2
α	[°]	104.7	176.1	6.7	5.8
β	[°]	142.1	85.2	107.9	93.9
γ	[°]	115.6	121.1	59.8	81.9

2.13 ^{19}F PCS of hCA-II inhibitors

To access PCS of protein inhibitors NMR signals of the inhibitor have to be determined unambiguously. This is usually not a trivial task. Proton signals overlap with the signals of the protein making an assignment very difficult. Especially for inhibitors which strongly bind to the protein. They have the same rotational correlation time as the protein and their signals therefore are broadened to a similar extend as the protein. This usually makes a discrimination between protein and inhibitor signals impossible. Isotope filtered experiments are very demanding, because isotope enrichment of the inhibitor carbon and heteroatoms in the normal case includes time consuming chemical modification of the inhibitor. However NMR active isotopes such as ^{19}F or ^{31}P have a high natural abundance, and therefore no isotope enrichment is necessary for these elements. If inhibitors containing ^{19}F are used, their signals can be recorded directly from one dimensional ^{19}F NMR spectra, where for aqueous solutions no solvent signal suppression has to be applied.

Two sulfonamide inhibitors containing fluorine atoms were selected for the determination of ^{19}F PCS(see figure 2.19). For F2-Inh bound to hCA-II an X-ray structure (PDB

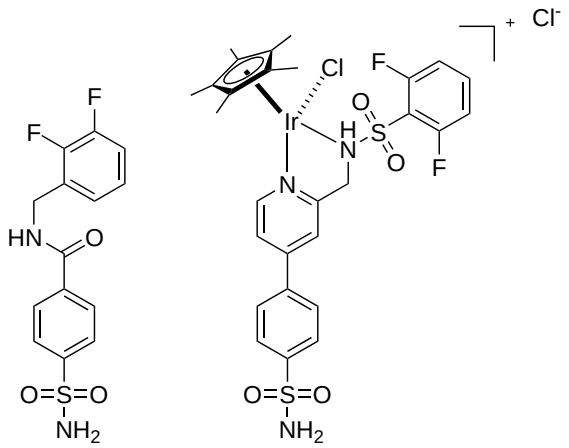

Figure 2.19: Structures of sulfonamide inhibitors containing fluorine atoms.

code: 1G52) was available[59], therefore this compound was selected to validate the method of obtaining structural information from ^{19}F PCS of a protein ligand complex. F2-complex is an analogue of an Ir-complex used for the formation of an artificial metallo enzyme, which is capable of catalysing enatioselective transfer hydrogenation reactions, when bound to hCA-II.[60] Structural information of this protein ligand complex in solution is very important for the further optimisation of this artificial enzyme. The two fluorine atoms were introduced to the inhibitor in order to be able to approach this protein ligand complex by ^{19}F PCS.

The inhibitors were added to the protein as a dimethyl sulfoxide (DMSO) solution with concentrations in the order of 25 mM in a small excess of 1.1 eq. to ensure complete loading of the protein with inhibitor. F2-complex was found to be only soluble in aqueous solution at pH below 3.5 and even in DMSO the solution had to be acidified by bubbling some gaseous HCl through the solution to ensure complete solubility. Nevertheless when this solution was added to the protein at pH 6.8 complete loading of the protein with inhibitor was possible as confirmed by ^{1}H-^{15}N-HSQC spectra. The excess of inhibitor could be removed by ultafiltation without removing any bound inhibitor showing that both inhibitors have a very high affinity to hCA-II. This is usually observed for phenyl-sulfonamide compounds.[37] For F2-Inh the dissociation constant

(K_d) is reported to be 0.29 nM.[61,62] For the F2-complex this is expected to be in the nM range as well but experimental data is not available. In the ^{1}H-^{15}N-HSQC spectra both inhibitors are found, as expected from dissociation constants in such an order of magnitude, in the slow exchange regime in terms of their exchange rates. When subequivalent amounts of the inhibitor were added to the protein, those residues that show a chemical shift changes due to the inhibitor binding, clearly show two distinct peaks in the spectra and the intensity is dependant on the amount of inhibitor. Otherwise only one averaged signal would be observable whose chemical shift depend on the ligand concentration. Chemical shift changes upon inhibitor binding are only observed for the residues in the binding pocket of the protein, which indicates that the overall structure of the protein does not change due to the interaction with the inhibitor. This is very important because the magnetic susceptibility tensors that are later used for structural calculation are determined form protein without any bound inhibitor.

Figure 2.20 shows the ^{19}F spectra of free and bound F2-Inh. For all four protein mutants the spectra with the inhibitor bound to LuM8 tagged protein show the same chemical shift for the two fluorine atoms. The same shift is observed, when the inhibitor is bound to untagged protein. This demonstrates that the inhibitor is not affected by the tagging of the lanthanide complex to the protein. ^{19}F PCS were determined for all four protein mutants and are given in figure 2.19. ^{19}F chemical shift was calibrated to the fluorine signal of internal trifluoroacetic acid (TFA) at −79.0 ppm. For the full fluorine spectra including the TFA reference see Figure A.11 in the Apendix section. The largest PCS was found for the S166C mutant where the tag is the closest to the binding site. For the TmM8 tagged S50C mutant still some traces of free inhibitor were observable which was not removed completely from the protein sample. Small signals attributed to the minor second species, arising from reorientation of the tag, as discussed in section 2.9 are observable for S166C and S220C. Again for the S220C mutant these signals are significantly larger. For the other two residues these signals are not observable due to peak overlap.

For the F2-complex the two fluorine atoms are symmetry equivalent and show therefore only one signal in the ^{19}F NMR spectrum of the free inhibitor (not shown). This has been observed as well, when the complex is bound to the protein (see figure 2.21).

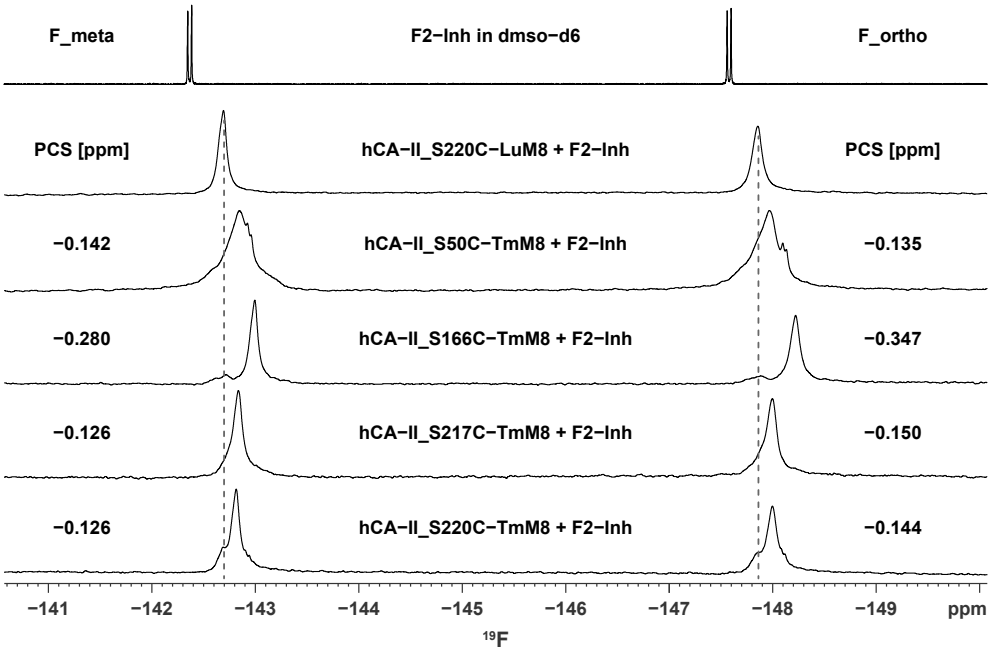

Figure 2.20: 1D ^{19}F NMR spectra (600 MHz, 298 K) of F2-Inh and F2-Inh in the presence of different hCA-II constructs. Spectra of LuM8 tagged hCA-II with F2-Inh did not show any differences, therefore only one diamagnetic reference spectra is displayed.

Therefore the aromatic ring with the fluorine atoms still has to be able to rotate freely, otherwise two different signals would be observable for the two fluorine atoms due to the chiral environment in the protein. Consequently only one averaged ^{19}F PCS can be observed for the F2-complex corresponding to an averaged position of the two fluorines.

Because no differences for the untagged protein and all four LuM8 tagged proteins were observed for the F2-Inh, we decided to use untagged protein as a diamagnetic reference for the F2-complex. PCS are given with respect to internal TFA at −79.0 ppm. Reasonable ^{19}F PCS could be observed for three of the four mutants. For the S217C mutant a shift very close to 0 ppm was observed. This is possible when the fluorine atom is located exactly on a nodal plane between two cones of the tensor with opposite signs. Therefore in this case even a PCS of 0 ppm bears structural information when the atom is within a reasonable distance to the tag. This clearly is the case because for

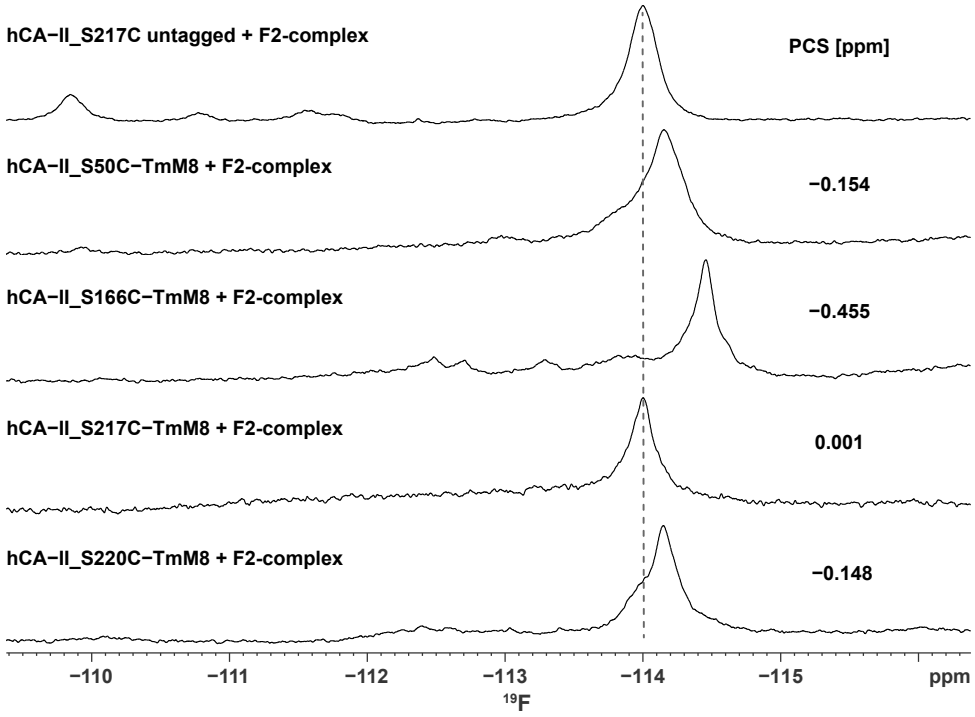

Figure 2.21: 1D ^{19}F NMR spectra (600 MHz, 298 K) of F2-complex in the presence of different hCA-II constructs. As diamagnetic reference untagged hCA-II with F2-complex is used.

the other mutants the PCS are not zero. Unfortunately the tensor has a large gradient in terms of the position for PCS close to zero. Hence a small difference in the PCS can have a large influence on the determined position. This will be discussed again in section 2.14. Excess of F2-complex that was not removed completely is still observable in the topmost spectra of untagged protein and F2-complex in figure 2.21. Most likely this was caused due to the lower solubility of the complex at the pH it was added to the protein.

^{1}H-^{19}F-HOESY experiments for ^{1}H PCS of the inhibitor and the protein side-chain

^{1}H-^{19}F-Heteronuclear Overhauser effect spectroscopy (HOESY) allows to determine proton signals which are close in space to the fluorine atoms. When these spectra are determined of the protein inhibitor complex, F2-Inh ⊂ hCA-II, this would not only result in intramolecular correlations of the inhibitor alone but also in intermolecular

correlations to protons of the protein. The most likely intermolecular correlations are expected to be interactions with sidechain protons of the protein. These signals have not been assigned, so far especially not for the protein inhibitor complex, where significant chemical shift changes due to the inhibitor can be expected. Nevertheless PCS offer a possibility to obtain structural information of the neighbouring protons of the fluorine. PCS of these protons can be determined directly from HOESY spectra of the Lu and Tm tagged protein-inhibitor complex. In this context the fluorine atom act as relay stations delivering selectively proton signals in their vicinity. This circumvents the problem of signal overlap which is often encountered when proton signals of fully protonated protein are determined.

HOESY spectra were recorded of hCA-II in complex with F2-Inh for all four mutants tagged with TmM8 and for the S217C mutant tagged with LuM8. As already discussed above for the protein inhibitor complex one diamagnetic reference is expected to be sufficient. To increase the resolution in the indirect dimension for the proton chemical shift, only a small spectral window of 3.5 ppm was recorded centred to 7 ppm. Signals lying outside of this window still appear in the spectra at a corresponding aliased frequency, which depends on the original chemical shift. PCS which are determined as shift differences can still be determined precisely from aliased signals and benefit from higher resolution of the signals. Figure 2.22 shows the section for the *meta*-fluorine where the most intensive signals were observed. The *ortho*-fluorine showed only two weak correlations at the same proton frequency as the two most intensive signals for the *meta*-fluorine. In total four different signals with variable intensities were observable. A second experiment with a spectral window of 4 ppm allowed to determine the original shift of the aliased signals. This revealed that only the topmost signal at 7.12 ppm was not aliased. This signal was the most intensive and is considered to be the correlation to the proton in *para* position of the benzylic ring in the F2-Inh. For aliased signals an original shift in the aliphatic region between 0.4 ppm and 0.75 ppm was determined. Therefore they were expected to be correlations to neighbouring methyl groups.

Unfortunately at the time when these HOESY spectra were recorded the protein samples used were more than two years old and for two samples partial degradation of the protein was observable. Therefore these experiments serve only as a proof of

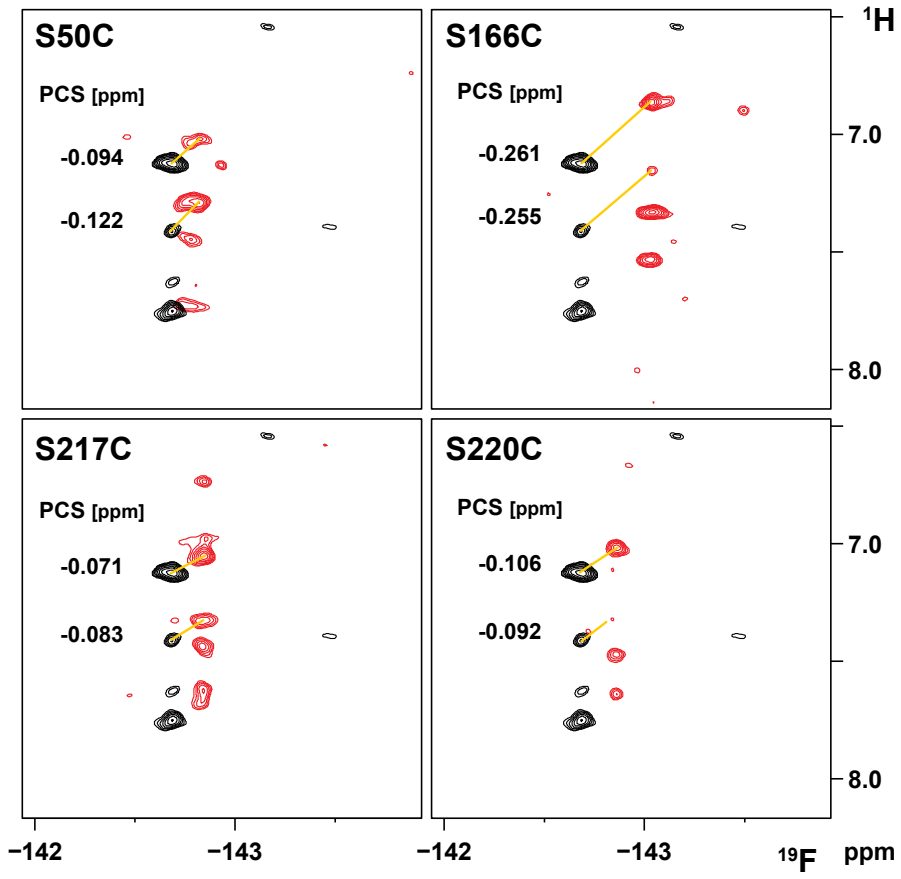

Figure 2.22: HOESY spectra (600 MHz, 298 K) of F2-Inh ⊂ hCA-II showing trough space interaction of ^{19}F with ^{1}H. Determined PCS are indicated. All signals, appart from the one at 7.12 ppm appear at their aliased frequency, due to the small sweep width.

principle, for the feasibility of such experiments. It was clearly possible to demonstrate that additional PCS information could be obtained from HOESY experiments but the obtained structural information should be interpreted with utmost care.

2.14 Determination of fluorine position from PCS

When structural information would be obtained form recorded PCS the following considerations have to be taken into account: All PCS of a certain value lie on top of a

so called isosurface defined by equation 2.3

$$\delta^{\mathrm{PCS}} = \frac{1}{12\pi r^3}\left[\Delta\chi_{\mathrm{ax}}\left(3\cos^2\theta - 1\right) + \frac{3}{2}\Delta\chi_{\mathrm{rh}}\sin^2\theta\cos 2\phi\right] \tag{2.3}$$

Where δ^{PCS} is an experimentally determined PCS and $\Delta\chi_{\mathrm{ax}}$ and $\Delta\chi_{\mathrm{rh}}$ are the axial and rhombic components of the magnetic susceptibility tensor. The solutions for a given PCS, $\Delta\chi_{\mathrm{ax}}$ and $\Delta\chi_{\mathrm{rh}}$ of this equation for the polar coordinates r, θ and ϕ deliver the mentioned isosurface. The position and orientation of this isosurface within a reference coordinate system has to be specified additionally. Here this is given by three euclidean coordinates of the corresponding lanthanide metal and three *Euler* angles (α, β, γ) in the ZYZ' convention respectively.
When two PCS for two different tensors are available for the same nucleus then the position is restricted to the intersection of these two isosurfaces. This intersection usually is one circular line which very often has a shape similar to the line that is found on a tennis ball. Depending on the shape and the size of the isosurfaces it is even possible to obtain two individual circular lines as intersections if two isosurfaces. Thus when three PCS from different tensors are available, the position is restricted to two or more points in space which are represented by the intersections of three isosurfaces. Consequently from four different PCS one unique position can be obtained, unless the isosurfaces intersect in a way that still allows more than one point as solution which is very unlikely.
According to these considerations, when at least four PCS of different tensors are are available for one certain nucleus the position is overdetermined and can be obtained by the method of least squares. A sum of square residuals was defined according to equation 2.4

$$s(x,y,z) = \sum_{i=1}^{n}\left(\delta_i^{\mathrm{PCS}}(\tilde{x}_i,\tilde{y}_i,\tilde{z}_i) - \delta_i^{\mathrm{PCS}}(\mathrm{exp})\right)^2 \tag{2.4}$$

where i is the index of a corresponding tensor and n is the total number of individual tensors available (here n was 4). $\delta_i^{\mathrm{PCS}}(\mathrm{exp})$ is the experimental PCS for the different

tensors and $\delta_i^{\mathrm{PCS}}(\tilde{x}_i,\tilde{y}_i,\tilde{z}_i)$ is defined by equation 2.5

$$\delta_i^{\mathrm{PCS}}(\tilde{x}_i,\tilde{y}_i,\tilde{z}_i)=\frac{1}{12\pi r_i^3}\left[\Delta\chi_{\mathrm{ax}_i}\frac{2\tilde{z}_i^2-\tilde{x}_i^2-\tilde{y}_i^2}{r_i^2}+\frac{3}{2}\Delta\chi_{\mathrm{rh}_i}\frac{\tilde{x}_i^2-\tilde{y}_i^2}{2r_i^2}\right] \tag{2.5}$$

$\tilde{x}_i,\tilde{y}_i,\tilde{z}_i$ are the coordinates x,y,z transformed into the according tensor frame. This transformation is carried out by translation of the reference coordinate system to the position of the corresponding metal center and rotation of the coordinate system by the three *Euler* angles (α,β,γ) which are given for each tensor. $\Delta\chi_{\mathrm{ax}_i}$, $\Delta\chi_{\mathrm{rh}_i}$ and r_i are the axial and rhombic tensor components and the distance between lanthanide metal and the observed position (x,y,z) respectively.
The coordinates of the fluorine atoms were determined from the four different PCS that were determined for each fluorine atom as described in section 2.13 and the described method of least squares. The optimised position was determined by minimisation of the function $s(x,y,z)$ defined in equation 2.4. All calculations of fluorine positions from PCS were carried out in Matlab.[63] Minimisation of the target function $s(x,y,z)$ was executed using the internal "fminsearch" routine. Error analysis of the determined fluorine position was performed applying a *Monte-Carlo* protocol where the tensor parameters were varied for every iteration according to the uncertainties determined in Numbat (as described in section 2.10). For each fluorine position 1000 iterations were carried out with the same random seed in order to ensure comparability. The resulting values and uncertainties were the average and standard deviation of these 1000 iterations. It could be shown that 1000 iterations were sufficient for reasonable results, neither the average position nor the standard deviation did change significantly, when 10 000 or 100 000 iterations were used for the calculation.

Fluorine positions of F2-Inh

The fluorine position was calculated for all tensors determined in section 2.11. As shown in table 2.11 the position did not change significantly with the different PCS subsets. Compared to the X-ray structure of F2-complex the determined fluorine positions differed by as much as 8 Å. Interestingly the determined fluorine fluorine

distance was very close to the expected 2.8 Å from the X-ray structure. The fluorine fluorine distance and the corresponding uncertainty were determined directly during the *Monte-Carlo* simulation. The distance was determined for every single iteration individually and then the average distance and the standard deviation was evaluated. Because the same random seed was applied for both fluorine calculations the distances were determined with respect to exactly the same pair of tensor parameters. This procedure gave results closer to the expected value and with much lower uncertainties as obtained when different random seeds were applied or when the fluorine fluorine distance was determined from the two fluorine positions in table 2.11.

The large difference between X-ray structure and PCS position can be explained in two

Table 2.11: Flourine positions of F2-Inh calculated for the 6 different tensor sets (of the 3 different pcs subsets and the the 2 *Monte-Carlo* methods), the corresponding F-F distance and the deviation from the position in the X-ray structure (1G52). All coordinates and distances are given in Å with respect to the coordinate system of the X-ray structure 3KS3.

PCS Set:		**Set 1**	**Set 2**	**Set 3**	**Set 1**	**Set 2**	**Set 3**
		Tensor by structure variation			Tensor by subset selection		
	x	-7.4 ± 1.7	-7.4 ± 1.7	-7.3 ± 1.7	-7.5 ± 1.7	-7.4 ± 1.5	-7.3 ± 1.4
F_*ortho*	y	6.1 ± 0.8	6.1 ± 0.8	6.0 ± 0.8	6.0 ± 0.9	6.0 ± 0.8	6.0 ± 0.8
	z	15.5 ± 0.7	15.7 ± 0.7	15.7 ± 0.7	15.6 ± 0.5	15.7 ± 0.5	15.7 ± 0.4
	x	-7.1 ± 2.5	-7.0 ± 2.5	-6.8 ± 2.5	-7.1 ± 2.4	-6.9 ± 2.1	-6.7 ± 1.8
F_*meta*	y	8.4 ± 0.8	8.5 ± 0.8	8.3 ± 0.8	8.3 ± 0.9	8.4 ± 0.8	8.4 ± 0.7
	z	16.7 ± 0.7	16.9 ± 0.8	16.9 ± 0.7	16.8 ± 0.6	16.9 ± 0.5	16.9 ± 0.5
F-F dist.		2.9 ± 0.3	2.9 ± 0.3	2.9 ± 0.4	2.8 ± 0.3	2.8 ± 0.2	2.8 ± 0.2
F_*ortho* dev.		7.9 ± 1.2	8.0 ± 1.2	8.0 ± 1.1	8.0 ± 1.3	7.9 ± 1.1	7.9 ± 1.0
F_*meta* dev.		8.0 ± 2.0	8.1 ± 2.0	8.0 ± 1.9	8.1 ± 2.0	7.9 ± 1.7	7.8 ± 1.4

ways: either the structure of the protein inhibitor complex in solution is different from the crystal structure, or there has to be an error on the fluorine PCS that is responsible for the deviation.

Figure 2.23 shows the point clouds for the two fluorine atoms from the *Monte-Carlo* calculation. It can be seen that when the phenyl ring with the two fluorines is rotated

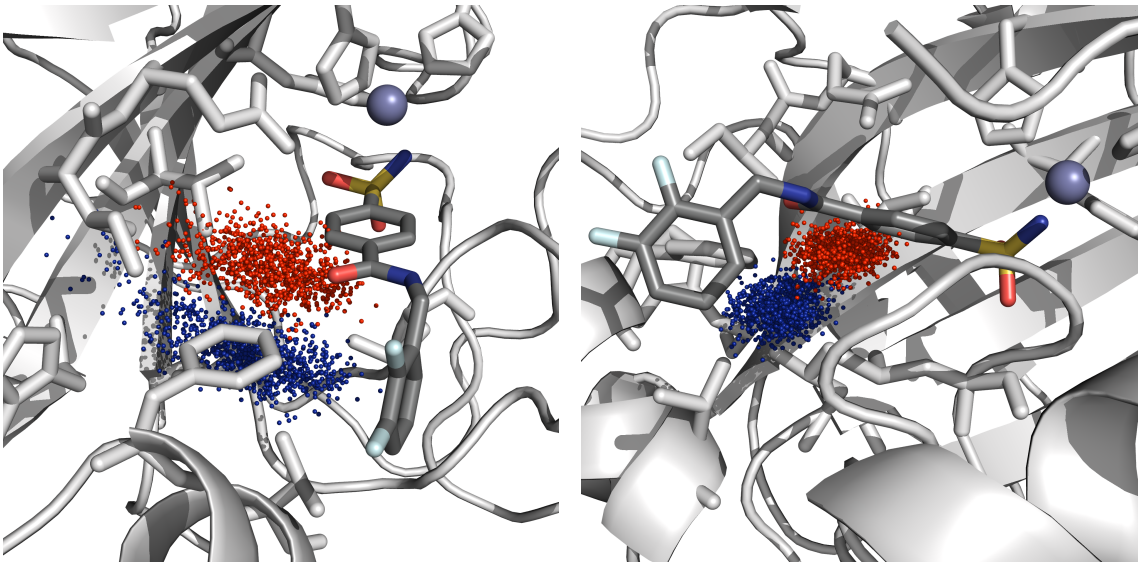

Figure 2.23: Point cloud of the *Monte-Carlo* fluorine position calculation for F2-Inh ⊂hCA-II. Red points are obtained from the PCS of the *ortho*-F and the blue points from the *meta*-F PCS respectively.

by 180° around the benzylic C-C bond the deviation to the calculated position would be smaller, but the fluorines would still lie outside of the point cloud. Other conformational changes that would bring the fluorines closer to the PCS position would include reorientation of the protein side chains, especially of the phenyl ring of F-131. Docking simulations where the determined PCS position were taken into account were not able to support the assumption of a larger reorientation of the inhibitor and the protein side chains. The structures from the docking experiments were in agreement with the crystal structure.

A possibility for a systematic error on the fluorine PCS are RACS, these are small chemical shift changes due to partial alignment of the protein in the magnetic field. They were not considered so far because prior knowledge of the structure is necessary for their determination. This subject will be discussed in more detail later in this section. The very close agreement of the PCS fluorine fluorine distance with the X-ray structure, where 2.8 Å are measuerd, supports this assumption. A small error on both PCS of the two fluorines which is equally large would still allow the determination of a reasonable distance between them, because both positions would be affected to a similar extent,

provided the gradient of the isosurfaces is not too large. This can be assumed since the difference in the back calculated PCS for the X-ray position and the determined PCS position was in the order of 0.02 ppm, except for S217C where this was as large as 0.1 ppm (see table 2.14).

Proton position from ^{1}H-^{19}F HOESY PCS of F2-Inh

As already mentioned in section 2.13 due to partial degradation of the protein sample after two years in storage, these results should be interpreted with care. However they are presented in order to show the potential of this new method.
Proton positions from the PCS determined in the ^{1}H-^{19}F HOESY experiment were calculated by the same procedure as for the fluorine. For the H_{para} position three outliers of the 1000 iterations were removed before determining the average position. The determined proton positions relative to the X-ray structure (1G52) are shown in figure 2.24.

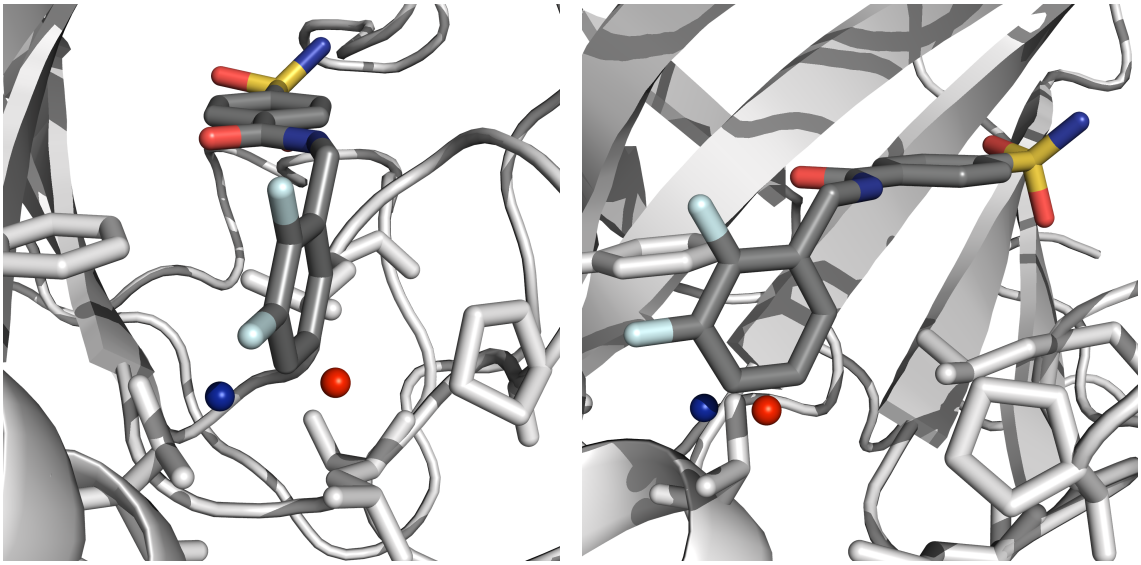

Figure 2.24: Average proton positions from PCS determined in the ^{1}H-^{19}F-HOESY experiment of F2-Inh ⊂ hCA-II. In red the position of H_{para} and in blue the proton in the aliphatic region.

The distances to the expected proton position in the X-ray structure are given in

table 2.12. For the signal at 7.12 ppm indeed the expected aromatic proton was the closest candidate. For the aliphatic signal at 0.41 ppm the closest candidate were the methyl protons of V-135. The second next candidate was the H^{α} of G-132 with a deviation of 3.2 Å to the determined proton position. But for the α proton of glycine a different chemical shift, in the order of 3.9 ppm would be expected.

Table 2.12: Proton positions from ^{1}H-^{19}F-HOESY PCS of F2-Inh ⊂ hCA-II calculated using the tensor parameters obtained from PCS set 3 with subset selection. The deviation to the closest proton in the X-ray structure (1G52) is given. All coordinates are given with respect to the coordinate system of PDB structure 3KS3.

Assign.	δ	**x**	**y**	**z**	**Dev.**
	[ppm]	[Å]	[Å]	[Å]	[Å]
H_{para} F2-Inh	7.12	-0.1 ± 1.2	10.2 ± 1.0	14.8 ± 0.8	1.4
$H^{\gamma 2}$ V-135	0.41	-2.1± 1.2	11.1 ± 0.8	15.6 ± 0.7	2.3

Fluorine positions of F2-Complex

In the case of the F2-complex ⊂ hCA-II no X-ray structure was available but for the analogue complex without the two fluorines a structure was published in 2015.[35] It was assumed that for the F2-Complex the structure would be very similar. The terminal phenyl ring at the sulfonamide group that binds to the iridium metal, in the PDB structure (3ZP9) showed two different conformations in the crystal structure. This is in agreement with the observation that for the F2-Complex, the corresponding phenyl ring has to be able to rotate freely in solution, even when the complex is bound to hCA-II. Due to the free rotation only one fluorine signal could be observed and therefore only an average fluorine position was determined from the corresponding PCS. For the comparison of the X-ray structure with the PCS position for the fluorine position in the X-ray structure the average position of the quaternary carbon of the terminal phenyl ring for the two different conformations was selected.

The initially determined PCS position for the F2-complex showed a deviation of more than 15 Å compared to the expected fluorine position. In a direction that could not possibly be adopted by the fluorine when the F2-Complex binds as expected

Table 2.13: Flourine positions of F2-Compex calculated for the 6 different tensor sets (of the 3 different pcs subsets and the the 2 *Monte-Carlo* methods), the deviation from the expected average fluorine position in the X-ray structure (5BRV). All coordinates and distances are given in Å with respect to the coordinate system of the X-ray structure 3KS3.

	Tensor by structure variation			Tensor by subset selection		
PCS Set:	**Set 1**	**Set 2**	**Set 3**	**Set 1**	**Set 2**	**Set 3**
No. of solutions:	130	76	156	120	67	97
x	-5.2 ± 1.6	-5.3 ± 1.8	-4.9 ± 1.7	-5.4 ± 1.7	-5.8 ± 1.8	-5.3 ± 1.4
y	11.1 ± 0.9	11.1 ± 0.9	11.0 ± 0.9	10.8 ± 1.0	11.1 ± 1.0	11.0 ± 0.9
z	6.6 ± 1.0	6.3 ± 1.2	6.7 ± 1.1	7.1 ± 1.3	7.0 ± 1.3	7.1 ± 1.1
F dev.	3.5 ± 0.8	3.8 ± 0.9	3.5 ± 0.8	3.2 ± 1.0	3.2 ± 1.1	3.0 ± 0.9

with the sulfonamide to the zinc of the protein. Additionally this position was found below the protein surface right next to the residue 55. When the starting point for the fluorine position calculation was set exactly to the expected fluorine position for around 10 % of the iterations of the *Monte-Carlo* position calculation a second minimum appeared much closer to the expected fluorine position as shown in table 2.13 and figure 2.25. The intersection of the four isosurfaces corresponding to the four PCS of the F2-complex (figure 2.25 lower left) have indeed the closest intersection at the position where the majority of points were found for the fluorine position. But for three isosurfaces (for S50C,S166C and S220C) a second intersection is observed closer to the expected fluorine position. This explains why the second minimum with much smaller deviation was found. The PCS determined for the S217C mutant was 0.001 ppm implying that the fluorine lies in a node plane of the corresponding tensor where the isosurfaces have the largest gradient with respect to their position compared to the PCS. This could be illustrated by plotting the isosurface of the S217C mutant for a PCS that is only 0.05 ppm smaller than the experimentally determined PCS (figure 2.25 lower right). This isosurface already lies exactly where the second minimum is found. This indicates that only a small difference of the PCS can have a large influence on the position determined from the PCS. This again supports the theory that there is an unascertained systematic error that has not been considered so far.

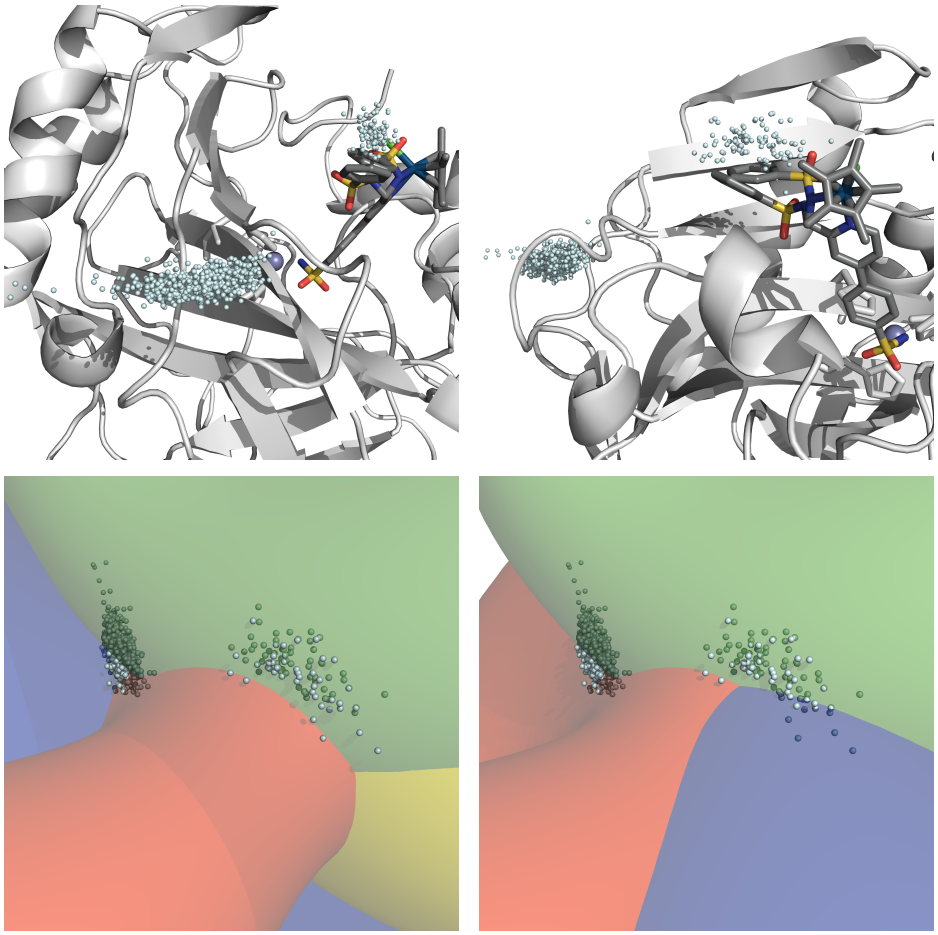

Figure 2.25: Point cloud of the *Monte-Carlo* fluorine position calculation for F2-Complex ⊂ hCA-II. Lower left figure shows the isosurfaces of the four different tensors and their corresponding PCS (Red: S50C, green: S166C, blue: S217C and yellow: S220C). Lower right figure: same isosurfaces except for S217C (Blue) which represents a PCS of −0.049 ppm instead of 0.001 ppm.

2.14.1 RACS as a potential source of systematic error

Paramagnetic lanthanide metals with an anisotropic $\Delta\chi$ tensor weakly align in the magnetic field. When bound to a protein this leads to partial alignment of the whole protein and therefore the CSA is not completely averaged to an isotropic chemical shift any more which results in small shift changes due to the alignment of the protein.[18] These shifts are called RACS and they add to the effective PCS resulting in the experimentally observed PCS. RACS can be determined according to the following equation:

Table 2.14: Expected PCS of the X-ray fluorine position and the calculated PCS position using the tensor parameters of set 3 and subset selection. For F2-Inh the PDB structure 1G52 was used. For F2-Complex 5BRV was used where for the fluorine position the average position of the quaternary carbon of the two conformations of the terminal phenyl ring was assumed. All values are given in ppm.

		S50C		**S166C**		**S217C**		**S220C**	
F-Position:		X-ray	PCS	X-ray	PCS	X-ray	PCS	X-ray	PCS
F2-Inh:	F_*ortho*	-0.116	-0.135	-0.378	-0.356	-0.061	-0.163	-0.102	-0.108
	F_*meta*	-0.116	-0.145	-0.283	-0.296	-0.061	-0.147	-0.080	-0.085
F2-Complex:		-0.165	-0.126	-0.478	-0.470	-0.059	-0.045	-0.121	-0.119

$$\delta^{\mathrm{RACS}} = \frac{B_0^2}{15\mu_0 kT} \sum_{i,j\in\{x,y,z\}} -\sigma_{ii}^{\mathrm{CSA}} \cos^2\theta_{ij} \Delta\chi_{jj} \tag{2.6}$$

where B_0 is the magnetic field, μ_0 the permeability of vacuum, k the *Boltzmann* constant, T the temperature, $\sigma_{ii}^{\mathrm{CSA}}$ the principal components of the CSA-tensor, $\Delta\chi_{jj}$ the principal components of the $\Delta\chi$-tensor and θ_{ij} the angle between the corresponding principal axis of the CSA-tensor and the $\Delta\chi$-tensor.[18,19] This function is included in Numbat and allows to determine the expected RACS for a given structure and a related set of tensor parameters, for the protein backbone amide proton and nitrogen and for the backbone carbonyl carbon. The values for the CSA-tensors for the three nuclei used by default in Numbat were previously determined from a protein aligned in a liquid crystalline phase.[19] For protons the RACS are negligible, but not for ^{15}N and ^{13}C. For the S166C mutant with the largest tensor, the largest RACS for ^{15}N were in the order of ±0.1 ppm. For the other three mutants they were between ±0.07 ppm and ±0.05 ppm. Values reported for the CSA of aromatic fluorines[64,65] were in a comparable order of magnitude as for ^{15}N, therefore comparable RACS can be expected for ^{19}F. Such RACS could be responsible for the deviation between x-ray structure and PCS position for F2-Inh. Unfortunately for the calculation of RACS in Numbat prior knowledge of the structure is necessary. Which is not the case in the present approach,

where only the position of the fluorine atoms can be determined.
To examine the effect of the RACS on the PCS structure determination, a validation of the structure calculation was performed. For ten residues, the position of amide H and N atoms was predicted using either directly the experimentally determined PCS values or, for comparison, the PCS values that were corrected for RACS by Numbat. The ten different residues were selected to be located either in a secondary structure element or in a loop region that is not expected to be flexible therefore it could be assumed, that x-ray structure and solution structure are in agreement with each other. The residues were selected to be not too close to any of the four tagging sites to avoid structural differences due to the mutation and tagging. In the paramagnetic as well as in the diamagnetic ^{1}H-^{15}N-HSQC spectra for each of the four mutants, the signals of the ten residues were well separated, to ensure that precise PCS are available. For the ten residues the corresponding ^{1}H and ^{15}N PCS were excluded from the PCS set. Tensor parameters were redetermined for the new subset and were found to be very close to the parameters of the previous subset showing that the exclusion of these PCS does not have a significant influence on the determined tensor parameters. For all ten residues the expected RACS were calculated based on the position in the X-ray structure for all four mutants. These values are given together with the experimentally determined PCS in table 2.15. It was expected that the amide H and N position from the experimental PCS alone should be less close to the X-ray position than when the effective PCS is used which is the experimental PCS where the RACS have been subtracted.

For the determined amide H and N positions the deviation from the crystal structure for each of the 20 atoms and for both sets of PCS was determined and is given in table 2.16 together with the calculated N-H distance determined from PCS alone, analogously to the two fluorines of the F2-Inh. As expected, the differences in the position of the protons does not change significantly when the experimental PCS are compared to the effective PCS because the RACS for ^{1}H are negligibly small. For the nitrogen position no consistent effect of the RACS correction was observed. Two residues, G-25 and E-205 show a significantly larger deviation from the X-ray position than the other residues. In addition these two residues have the largest uncertainties

Table 2.15: PCS and RACS of residues selected for validation of structure calculation from PCS. The PCS were determined experimentally from ^{1}H-^{15}N HSQC spectra and the RACS were calculated based on their orientation in the pdb structure 3KS3 using tensor parameters where these residues have been excluded. All values are given in ppm.

Mutant	**Residue**	**^{1}H**		**^{15}N**		**Residue**	**^{1}H**		**^{15}N**	
		PCS	**RACS**	**PCS**	**RACS**		**PCS**	**RACS**	**PCS**	**RACS**
S50C	G-25	0.026	0.000	0.033	-0.014	G-183	-1.296	-0.001	-1.218	0.023
S166C		-0.124	0.000	-0.146	-0.047		0.307	-0.001	0.410	0.039
S217C		-0.141	0.001	-0.189	-0.032		-0.079	0.000	-0.068	-0.002
S220C		-0.080	-0.001	-0.045	0.031		-0.319	-0.001	-0.334	-0.015
S50C	V-31	0.135	-0.002	0.083	0.025	T-193	0.591	-0.002	0.646	0.047
S166C		-0.096	-0.003	-0.178	0.066		-0.030	0.000	0.025	0.037
S217C		-0.592	0.001	-0.538	-0.021		-0.865	0.003	-0.864	-0.004
S220C		-0.087	0.000	-0.080	-0.022		-0.006	-0.002	0.015	0.038
S50C	F-66	-0.149	-0.003	-0.079	0.047	E-205	-0.004	0.001	-0.035	-0.007
S166C		-1.196	-0.003	-1.299	0.062		-0.151	0.005	-0.119	-0.039
S217C		0.011	0.000	-0.019	-0.009		-0.145	0.002	-0.167	-0.003
S220C		-0.447	0.000	-0.395	0.011		-0.083	-0.001	-0.095	0.005
S50C	G-132	-0.243	-0.003	-0.236	0.024	T-208	0.307	-0.003	0.385	0.048
S166C		-0.228	-0.004	-0.297	0.060		-0.137	-0.005	-0.110	0.061
S217C		-0.055	0.002	-0.077	-0.026		-0.275	-0.001	-0.329	-0.013
S220C		-0.092	0.000	-0.094	-0.019		-0.085	0.000	-0.063	0.013
S50C	Q-136	-0.162	-0.001	-0.089	0.030	W-209	0.418	0.000	0.469	-0.019
S166C		-0.167	-0.004	-0.230	0.062		-0.101	-0.001	-0.186	-0.039
S217C		-0.091	0.002	-0.111	-0.027		-0.456	0.004	-0.513	-0.062
S220C		-0.078	0.002	-0.092	-0.010		-0.067	0.002	-0.061	-0.004

which is in agreement with the fact that these two residues have the smallest PCS of the ten residues and have the largest overall distance to the four different metal centres. Both factors lead to less well defined positions in the PCS structure determination. For the other eight residues an average deviation of 2.0 Å for the experimental PCS and 1.9 Å for the effective PCS was observed for the proton position and for nitrogen this was 3.5 Å and 4.2 Å respectively. The lower agreement for the nitrogen position in both cases was attributed to the lower resolution and larger range of the nitrogen chemical shift in the ^{1}H-^{15}N-HSQC spectra.

Table 2.16: Validation of structure calculation by PCS. The deviation from the expected position in the X-ray structure (3KS3) is given for the position determined from experimental PCS as well as from effective PCS which have been calculated by subtraction of the expected RACS (see table 2.15) from the experimental PCS. All distances are given in Å.

Residue		**PCS$_{exp}$**	**PCS$_{eff}$**	**Residue**		**PCS$_{exp}$**	**PCS$_{eff}$**
G-25	H	7.1 ± 4.6	6.9 ± 4.6	**G-183**	H	2.2 ± 1.1	2.2 ± 1.1
	N	9.5 ± 3.4	13.0 ± 4.0		N	2.4 ± 1.3	2.3 ± 1.3
N-H dist.		12.4 ± 4.5	9.5 ± 4.8	N-H dist.		1.3 ± 0.8	1.1 ± 1.0
V-31	H	2.1 ± 1.5	2.0 ± 1.5	**T-193**	H	1.9 ± 1.2	1.8 ± 1.2
	N	3.8 ± 1.5	5.7 ± 2.2		N	5.3 ± 1.5	2.2 ± 2.0
N-H dist.		2.1 ± 0.7	4.1 ± 1.9	N-H dist.		5.4 ± 1.0	1.1 ± 1.4
F-66	H	1.6 ± 0.9	1.6 ± 0.9	**E-205**	H	4.0 ± 2.6	4.1 ± 2.5
	N	2.3 ± 1.0	1.6 ± 0.9		N	7.6 ± 1.7	8.5 ± 1.3
N-H dist.		2.1 ± 0.4	1.2 ± 0.2	N-H dist.		6.6 ± 3.9	7.8 ± 3.2
G-132	H	2.6 ± 1.6	2.4 ± 1.4	**T-208**	H	1.8 ± 1.1	1.6 ± 1.1
	N	3.8 ± 1.1	8.2 ± 1.7		N	2.0 ± 0.7	3.4 ± 1.1
N-H dist.		3.4 ± 0.5	6.6 ± 0.9	N-H dist.		2.8 ± 0.5	2.4 ± 0.6
Q-136	H	2.2 ± 1.5	2.2 ± 1.7	**W-209**	H	1.6 ± 1.2	1.7 ± 1.3
	N	5.3 ± 1.1	7.9 ± 1.2		N	3.2 ± 0.8	2.2 ± 1.0
N-H dist.		4.8 ± 0.6	7.5 ± 1.0	N-H dist.		3.3 ± 1.0	2.2 ± 0.6

2.15 Assignment of sidechain NH resonances of arginine and tryptophan based on PCS

Sidechain NH resonances in the diamagnetic spectra for tryptophan and arginine sidechain NH groups were identified based on the list of average reported chemical shift taken from the Biological Magnetic Resonance Data Bank[66] (list updated on the 17th of March 2016). The reported ^{1}H and ^{15}N chemical shift values were 7.46±0.60 and 84.59±1.62 for the arginine sidechain NH at the ε-position and 10.08±0.64 and 129.29±2.08 for the aromatic sidechain NH of tryptophan. For both residues seven different resonances were expected. Because the resonances for the arginine NH are outside of the spectral window in the indirect dimension these residues were easily identified as aliased peaks with negative intensity in the range of 116 ppm to 117 ppm in the ^{15}N dimension. Tryptophan sidechain resonances were identified indirectly as those resonances in the lower left region in the ^{1}H-^{15}N HSQC spectra which showed no correlation in the HNCO spectra due to the absence of a carbonyl carbon next to the nitrogen.

For such a small number of residues unambiguous assignment of the corresponding PCS was possible for several resonances. These could directly be identified by comparison of their experimental PCS with the back calculated PCS based on the tensor obtained from the backbone amide PCS and the x-ray structure. In a second iteration the remaining ambiguous resonances were assigned by comparing the predicted PCS for those residues, thus allowing eventually the unambiguous assignment of every resonance of the identified groups.

Alternatively the position of the resonance could be calculated as described in section 2.14. Here again the position determined for the ^{1}H PCS turned out to give better results analogue to the findings in section 2.14.1. This would even allow the assignment of resonances where the type of residue has not been identified, provided at least three PCS were determined.

2.16 RDC measurements

RDC can be observed for partially aligned proteins in solution. The dipolar coupling is not averaged to zero any more, as it is the case for an isotropically oriented sample, and therefore adds to the scalar coupling between two nuclei. NH-RDC can be described by the following equation:[14,16]

$$D_{NH} = -\frac{B_0^2 \gamma_H \gamma_N \hbar S}{120 k T \pi^2 r_{NH}^3} \left[\Delta\chi_{\mathrm{ax}} \left(3\cos^2\theta_{NH} - 1\right) + \frac{3}{2}\Delta\chi_{\mathrm{rh}} \sin^2\theta_{NH} \cos 2\phi_{NH} \right] \quad (2.7)$$

where D_{NH} is the observed RDC, B_0 the magnetic field, γ_H and γ_N the gyromagnetic ratios of ^{1}H and ^{15}N, $\hbar$ the reduced Planck constant, r_{NH} the distance between proton and nitrogen and S the order parameter which covers for the effect of local mobility of the NH-bond with respect to the metal center[67]. $\Delta\chi_{\mathrm{ax}}$ and $\Delta\chi_{\mathrm{rh}}$ are the axial and rhombic components of the magnetic susceptibility tensor and θ_{NH} and ϕ_{NH} the polar angles describing the orientation of the NH bond vector with respect to the orientation of the magnetic susceptibility tensor.

RDC were determined using triply labelled S50C protein samples tagged either with LuM8 or with TmM8. An in phase anti phase (IPAP) variant of the ^{1}H-^{15}N HSQC experiment was recorded for both samples, with an NMR spectrometer operating at 900 MHz.[68] In this experiment no decoupling is applied in the indirect dimension thus resulting in spectra with two peaks for every residue separated in the indirect dimension by the corresponding ^{1}J coupling constant. A second experiment where the two peaks resulting from the coupling are obtained with opposite sign then allows either by addition or subtraction of the first spectra to selectively obtain spectra with either only the upper or the lower signal. This reduces the number of peaks in the spectra by a factor of two which is especially helpful in crowded regions. The coupling constant is then determined from the shift difference in the indirect dimension of the two spectra. Subsequently the RDC are determined as the difference in the coupling constant of the paramagnetic and the diamagnetic protein sample. This requires that the diamagnetic as well as the paramagnetic spectra are assigned. In total 178 RDC could be assigned this corresponds to 74 % of all residues or to 81 % of the assigned residues.

RDC-tensors were determined using the program FANTEN[16] which is available online. The program allows the determination of $\Delta\chi$ parameters from individual RDC and PCS data sets as well as from combined PCS and RDC data sets. For the calculated tensors in table 2.17, PCS were equally weighted as RDC for the combined sets, and for the RDC an order parameter of 1.0 and an uniform N-H bond length of 1.02 Å was applied. Because RDC do not depend on the distance to the lanthanide metal, only the orientation and the size of $\Delta\chi_{ax}$ and $\Delta\chi_{rh}$ of the tensor could be determined for the sets where only RDC were used. In contrast to Numbat, in FANTEN *Monte-Carlo* error analysis is only possible for $\Delta\chi_{ax}$ and $\Delta\chi_{rh}$ and the three *Euler* angles but not for the lanthanide metal position. Therefore no error analysis was applied to the tensors below. It was expected that the tensor parameters would have comparable uncertainties to the tensor parameters determined in Numbat. Also the convention for principal tensor components is different in FANTEN than in Numbat therefore a different set of tensor parameters is obtained but they describe a comparable $\Delta\chi$-tensor. Q factors for RDC were determined analogously to the PCS as described in equation 2.1 in section 2.10.

Very similar tensor parameters to the set with only PCS were obtained for the RDC-tensor and the combined PCS and RDC tensor when for the RDC an order parameter of 1.0 was used. Usually the $\Delta\chi$ tensors parameters determined from RDC are 10 % to 20 % smaller compared to the tensors calculated from PCS[69], which is attributed to the local mobility of the NH bond vectors[16] or to residual flexibility of the paramagnetic tag with respect to the protein.[28] To compensate for this effect order parameters (S) in the order of 0.9 are applied to obtain comparable tensor parameters.[70,71] On this background it is remarkable that in the present case with an order parameter of 1.0 the same tensor parameters were obtained for PCS and RDC For the optimised set, where all RDC with a deviation of more than 10 Hz were excluded the values for $\Delta\chi_{ax}$ and $\Delta\chi_{rh}$ are even larger compared to the set with only PCS.

Table 2.17: Tensors determined using the program FANTEN for PCS, RDC and combined data sets. PCS of subset 3 were used only. For the optimized set of RDC all couplings with a deviation larger than 10 Hz to the predicted values were excluded.

S50C		**PCS only**	**RDC only**	**PCS and RDC**	**RDC opt. only**	**PCS and RDC opt**
$\Delta\chi_{ax}$	[10^{-32}m^3]	21.1	21.2	21.2	23.3	23.3
$\Delta\chi_{rh}$	[10^{-32}m^3]	-8.4	-9.0	-9.0	-9.2	-9.2
x	[Å]	-27.6	-	-27.3	-	-27.8
y	[Å]	13.6	-	14.5	-	14.7
z	[Å]	18.2	-	18.4	-	18.4
α	[°]	26.5	164.6	164.6	160.0	160.0
β	[°]	-142.0	-39.0	-39.0	-39.2	-39.2
γ	[°]	-75.5	94.1	94.2	96.2	96.2
Q_{PCS}		0.079		0.157		0.139
Q_{RDC}			0.48	0.48	0.31	0.31
No. of PCS		366		366		366
No. of RDC			178	178	161	161

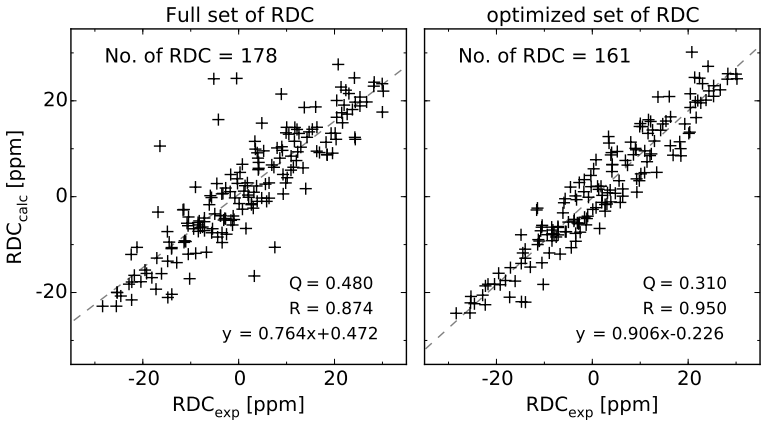

Figure 2.26: Correlation of experimental and back calculated RDC obtained for the tensors determined only with RDC given in table 2.17

CHAPTER 3

Discussion

The results of this PhD thesis cover several different fields, starting from the synthesis of a lanthanide chelate and the corresponding lanthanide complexes, to the design and expression of single cysteine hCA-II mutants with various isotope labelling schemes, to protein backbone assignment, as well as protein conjugation for the determination of PCS on protein-inhibitor complexes and the subsequent analysis and application of the PCS for structure determination. In the following section, these results will be discussed in approximately the same chronological order as presented in the results section.

3.1 LnM8-SPy Synthesis

The synthesis of M8-SPy (see figure 1.4), that was repeated for the first time in the course of my masters thesis previous to this PhD thesis, was further improved. Mainly optimization of reaction time was achieved as described in section 2.1. The amide coupling reaction and the subsequent ^{t}Bu deprotection step, with 40 % overall yield, remained the most crucial step of the whole synthesis. Different deprotection conditions (H_2SO_4 in CH_2Cl_2) or the purification of the intermediate followed by the usual TFA deprotection both resulted in very poor yields in the order of 1 %. Of course this step was not yet fully optimized, but main focus was laid on the preparation of the final lanthanide complexes and there further application. The deprotection in TFA was monitored by ESI-MS, following the peak intensity of the products normalized

by an internal signal that was attributed to a byproduct of the previous amide coupling and remained unaffected under deprotection conditions. The intensity of the product peaks reached a plateau after 6 h thus confirming the reported reaction time. Reasons for this could be that the reaction is already completed at this point of time, but the fact that never more than 40 % yield was obtained shows that it is more likely to expect the presence of a side-reaction competing with the desired deprotection reaction. This could be confirmed by the observation that the overall intensity of the peaks in the mass spectra corresponding to the desired product, starting material and to the two mono- and di-deprotected intermediates, decreased over time. Because no characteristic signals in the mass spectra were observable this side-reaction was expected to be either the cleavage of the disulfide bond and thereby the loss of the group in the molecule that is protonated most easily and therefore mainly responsible for the inthensity observed in the ESI-MS, or the degradation of the macrocycle. This confirmed the optimal reaction time for the TFA deprotection to be 6 h as reported.[28] For the final metallation step yielding the desired lanthanide complexes only partial conversion was observed when, in contrast to the described procedure, only water as solvent was used. When the LnM8-SPy complex is formed, three protons are released which lowers the pH of the reaction mixture and evidently preventing the deprotonation of the carbonic acids of the ligand. This was found to be important for the coordination of the ligand to the lanthanide metal. This confirms the importance of the described ammonium acetate buffer. Already an 100 mM ammonium acetate buffered soulution with a pH of 5.6 for a ligand concentration of 2 mM to 4 mM was enough to compensate for the released protons enabling complete conversion. The complexation was carried out with four different lanthanide metals, Gadolinium, Dysprosium , Thulium and Lutetium. Dysprosium was selected because for this lanthanide metal the largest PCS are expected.[58] On a ubiquitin sample tagged with TmM8 very large PCS were observable for residues close to the tag. The corresponding signals in the spectra of ubiquitin tagged with DyM8 were not observable any more. Either these signals were shifted outside the spectral window and/or they were broadened beyond the limit of detection due to the PRE. This shows that with the Tm tag information could be obtained of regions of the protein much closer to the tagging site. Lutetium was selected because the Lu^{3+} ion has no unpaired electrons and therefore is diamag-

netic. It is used as diamagnetic reference, which compensates for all effects that are not related with paramagnetism, such as chemical shift perturbation of residues close to the tag. Gd^{3+} has a half filled f-shell and therefore seven unpaired electrons, these electrons have an isotropic distribution around the metal center and consequently Gd^{3+} induces no PCS. The Gd^{3+} metal complex was prepared for its application for PRE and for its applications in electron paramagnetic resonance (EPR) spectroscopy, both are not presented in this thesis.
In the course of the Masters thesis of Dr Roché M. Walliser the (*4R,4S*) stereoisomer of M8-SPy was prepared which allowed the comparison with the (*8S*) stereoisomer. At the beginning of this thesis only (*8S*)-M8-SPy was available and because the corresponding (*8S*)-TmM8 tag soon showed satisfying results it was decided to carry out the main body PCS analysis only with this tag. A more limited comparison of the two stereoisomers is discussed later in this section.

3.2 Site directed mutation of human Carbonic Anhydrase II

In order to demonstrate the feasibility of structural analysis of a medium sized protein ligand complex human Carbonic Anhydrase (EC 4.2.1.1.), hCA-II, was selected. This protein has applications in the context of artificial metalloenzymes, where solution structure information can be very useful. Up to now no solution state structure exists of this protein. The reason for this seems to be the that the protein is very well characterised by X-ray crystallography, up to the 9th of March 2016, in the RCSB protein data bank[5], 582 structures of hCA-II were reported, almost every structure solved by X-ray diffraction. Only four structures were solved by neutron diffraction and for one structure neutron diffraction in combination with solution state NMR was used. Here the NMR information was used exclusively to characterise the protonation state of thyrosine residues.[72] Nevertheless solution state information of the protein structure could still reveal some differences to the X-ray structure. Especially for artificial metalloenzymes where the enantioselective catalysis is carried out in solution, information could be obtained that is not possible to determine by X-ray crystallography, e.g. when dynamic processes are involved.
For the attachment of the LnM8-SPy tag to a protein only one single cysteine residue at

the protein surface is necessary for the formation of a disulfide bond. Single cysteine mutants of hCA-II were prepared successfully and it was shown, that the strategy of replacing a serine at the edge of a secondary structure element on the protein surface by cysteine, combined with a mutation of the native cysteine in the wild type protein either to serine or alanine worked well. The total 10 different double mutants with one single cysteine at different positions on the protein surface all showed reasonable expression levels in a small scale protein expression. This illustrates the advantage of a single point attachment of a paramagnetic tag over the strategy of using two point anchoring to a double cysteine protein mutant.[27] Because only one serine to cysteine mutation is necessary, the possibility that this mutation affects the overall protein structure is lower compared to two cysteine residue that have to be introduced at a well defined distance to enable a two point anchoring. The restriction to only one cysteine residue in the protein sequence avoids the possibility of the formation of undesired disulfide bridges that would lead to misfolded protein.
It was, however, also possible to prepare double cysteine mutants of hCA-II where additionally to the described two mutations a second cystein was introduced on the protein surface, thus allowing the simultaneous attachment of two paramagnetic tags. This type of construct has an application in EPR spectroscopy and is mentioned at this place to illustrate another area of application for this protein that is accessible by these cysteine mutations.
Uniformly ^{15}N labelled protein was expressed successfully for all five protein mutants for the set of C206S mutants. This set of mutants was selected because for bovine carbonic anhydrase II, an isozyme with 81 % sequence similarity shows a serine at position 206. Since both proteins catalyse the same reaction it is very likely that this mutation does not affect the overall protein structure. Furthermore the later determined PCS suggested that this mutation did not affect the local protein structure around residue 206 as well, because the PCS for these residues matched well to the back calculated shifts based on the wild type X-ray structure. The expression was carried out in minimal media with ^{15}N ammonium chloride as the sole nitrogen source and yielded 60 mg to 95 mg of protein per litre medium which was sufficient protein for many NMR samples. For an average protein NMR sample with a final concentration of 200 µM, 2 mg of hCA-II was used.

3.3 Tagging of human carbonic anhydrase II with LnM8-SPy

Tagging of hCA-II with LnM8-SPy complexes worked very well, independently of the protein mutant, showing that all cysteine residues are accessible. With a threefold excess of tag, the reaction was fast, after one hour already 70 % conversion was observed in ESI-MS. The reaction runs under mild conditions at pH 6.80. Conversion was higher than 98 %, based on the ESI-MS spectra as well as in the ^{1}H-^{15}N HSQC spectra, where only traces of untagged protein were observable. The average yields of the reaction were typically in the order 80 % with a range of 60 % to 90 %. Although the exact protein concentration could not be determined during the tagging reaction due to the excess of tag, whose UV absorption overlaps with the proteins, the protein concentration is expected to stay constant during the tagging reaction, indicated by constant absorption intensities observed during the reaction. It merely is expected that protein is lost during the ultrafiltration steps, due to aggregation, because high local concentrations can occur during centrifugation. hCA-II has been reported to be prone to aggregation[37]. Either this was the case or the protein cannot be recovered completely from the filter membrane. When the reaction was carried out at 4 °C over night full labelling of the protein was achieved as well and no side-reactions were observed. At lower pH down to 5.0 the reaction has been reported to proceed as well[28]. Higher pH values have not been examined, but the reaction is expected to succeed at physiological pH as well. It is even expected that with a moderate increase of the pH the reaction could be accelerated along with the higher nucleophilicity of the thiol. At a certain high value, finally, it is likely that the selectivity of the reaction will start to drop, when other nucleophiles start attacking the tag. To summarise, the tagging conditions presented will be applicable for a wide range of other proteins as well and even are suitable for pH or temperature sensitive proteins.

The ^{1}H-^{15}N HSQC spectra of hCA-II tagged with TmM8-SPy showed large PCS for several signals and for almost every peak a significant PCS were detected. Unfortunately, for the S173C mutant at least two main sets of shifted signals were observed. The peaks of the set with the larger intensity had broader linewidth, which was caused either due to a dynamic process or by overlap with an additional set of signals. In

the X-ray structure the residue 173 is located in a β-sheet at the edge of the binding pocket of the protein, where the protein surface is more curved than for the other four tagging sites. It is assumed that the tag can therefore adopt different positions on the protein surface for residue 173 which leads to multiple sets of shifted signals. Because of the large large number of signals which made the correct assignment of the PCS much more difficult it has been decided not to assign this protein mutant, especially because for the other four mutants satisfying PCS were observed.

3.4 Second minor species in HSQC spectra of LnM8-tagged protein

In ^{1}H-^{15}N HSQC spectra with a good signal to noise a small second set of shifted signals was observable for the four TmM8 tagged protein mutants, this can be observed well for residue 141 in figure 2.7 in section 2.9. These peaks were in the order of 10 % of the main signal, except for the S220C mutant these have been slightly larger, with intensities up to 15 % of the main species. This was found independently of the protein sample for this mutant. For the majority of residues this second set was not observable, most likely due to signal overlap with the main peak. This second species was already observed for ubiquitin tagged with DyM8-SPy[28] where the relative intensity was reported to be in the order of 15 % to 20 %. Similar intensities have been observed for DyM8 tagged hCA-II. The second set of signals has to be caused due to a different orientation of the tag on the surface of the protein. It was speculated that this is caused by *cis-trans* isomerisation of the amide bond in the linker of the tag, but this would not explain why different intensities for the second species are observed for the DyM8-SPy tagged protein compared to the protein tagged with TmM8-SPy. Another possibility would be the interconversion of the coordination polyhedron around the metal center from a twisted square anti prism (Δ conformation) to a square anti prism (Λ conformation). If this is the case then it will be in accordance to the observation from HPLC where after the complexation of M8-SPy with a lanthanide metal two fraction with the same mass in ESI-MS were separated. The ratio between these fractions depends on the lanthanide metal and can be explained by by the lanthanide contraction, the reduction in the ionic radius of the lanthanides with increasing atomic number. This could explain the observed intensities between the major and the minor species in

the ^{1}H-^{15}N HSQC of the tagged protein because the same trend observed in the HPLC for Dy and Tm could be observed. For Dy a ratio between the first and the second fraction of 6:4 was observed and for Tm 1:19. When the two separated fractions of the tag were attached to a protein for both samples exactly the same HSQC spectra was obtained[57] this would be in accordance with a slow equilibrium between the Δ and the Λ conformation. Additionally this could explain the intensity difference between the S220C mutant and the other three that were observed because this equilibrium can be affected by interactions between the tag and the protein surface leading to a increase of the second species for this mutant. The same observations are described as well in a recent publication.[41]
Because the second species was smaller for the TmM8 tagged protein than for DyM8 and the observed PCS were comparable in size, and to restrict the number of samples that had to be prepared and analysed it has been decided to carry out the PCS assignment and all subsequent experiment only for the TmM8 tagged protein. For TmM8 it would also be possible to detect PCS of residues closer to the tagging site. These would not be observable for Dy because of the larger number of unpaired electrons and therefore higher PRE which broadens the signals of residues close to the tag beyond the limit of detection.

3.5 Comparison of (*4R,4S*)-LnM8-SPy with (*8S*)-LnM8-SPy

At the beginning of this thesis only (*8S*)-M8-SPy was available, therefore all initial experiments were carried out with this stereoisomer and when reasonable PCS were observed for this tag it was decided to carry out all experiments using this stereoisomer. Later, when the (*4R,4S*)-M8-SPy stereoisomer was prepared by Dr. Roché M. Walliser it was possible to directly compare the two seteroisomers. In contrast to the (*8S*)-LnM8-SPy complexes where two fractions were observed in the HPLC, for the (*4R,4S*)-LnM8-SPy complexes only one fraction was observed. When the *4R,4S* complexes of Dy and Tm were attached to hCA-II there as well only one shifted set of signals was observed (see figure 2.18).
It could be shown that the Δχ tensor for the (*8S*)-TmM8 tagged S50C mutant was orientated differently than for the (*4R,4S*)-TmM8 tagged mutant. In the case of Dy

the differences in the orientation between the two stereoisomers were smaller. In the HPLC for the (*8S*)-DyM8-SPy the earlier fraction was more intensive than the later one and for (*8S*)-TmM8-SPy it was the other way round. For (*4R,4S*)-LuM8-SPy a twisted square anti prism (Λ) was observed[28] If all these observations are combined then it would be possible to assume that for (*8S*)-DyM8-SPy mainly the Λ conformation is observed where for (*8S*)-TmM8-SPy the equilibrium lies on the side Δ conformation. When the size of the tensor is compared as listed in table 2.10 in section 2.11.5 the tensors for the *4R,4S* stereoisomer are larger than these of the corresponding *8S* isomers. Such a comparison is appropriate because for all four tensors PCS for the same set of residues were used. All residues that could be influenced by the attachment of tag were excluded from the tensor determination and therefore the possible difference between the (*4R,4S*)-LuM8 tagged protein compared to the (*8S*)-LuM8 tagged sample could be neglected as well. Only a small set of 44 leucine PCS was used but because for the (*8S*)-TmM8 very similar tensor parameters were obtained for this small set of PCS as for the full set of PCS, the same should be true for the other three constructs where no detailed PCS assignment was carried out. The reason for the different size of the tensors between the two different stereoisomers of the tag, has to be most likely that the *4R,4S* tag is more rigidly attached to the protein and therefore the tensor is less affected by motional averaging. The tensor parameters for Dy are smaller than the corresponding Tm tensor, this is opposed to the literature[58] where a larger tensor for Dy than for Tm is expected. What is consistent is, that the Dy and Tm tensor have the opposite sign and therefore most PCS in a comparable sample are shifted in the opposite direction. About the reasons for the smaller Dy tensor, one can only speculate. Probably the difference in the ionic radius could have an influence in such a way that the whole tag has more motional freedom with respect to the protein, leading to an averaging of of the tensor parameters. Or it could be a direct influence of the differences in the coordination polyhedron on the molecular magnetism.[73] Due to the different ionic radii between the different lanthanides, a slight difference in the coordination polyhedron for the different M8 complexes can be expected and similar to the influence of the molecular magnetism, the anisotropy of the χ-tensor could be affected as well. The tensor values presented in the literature for the different lanthanide metals that expect a larger tensors for Dy than for Tm, are determined

for lanthanide metals bound to a metal binding site of the same protein.[23] As the coordination polyhedron in this protein can be different to the LnM8 complexes, these values not necessarily have to be valid for both systems in the same extend.

3.6 Strategy for PCS assignment

As already discussed above the detailed PCS analysis was carried out using only TmM8-SPy and the four protein mutants S50C, S166C, S217C and S220C. PCS assignment in the uniform ^{15}N labelled protein sample turned out to to be a non trivial task. In the present case of hCA-II a backbone assignment of the residues was available[48] and and this assignment could be transferred for most of the residues. But this assignment was carried out based on the wild type protein and in our case the protein used was a double mutant, this leads at least in the regions of the mutations to uncertainties of the transferred assignment due to changes in the chemical shift of the neighbouring residues. Additionally for hCA-II so far no solution structure of the protein is available. The protein is well characterised by X-ray crystallography, nevertheless, there could be differences between the crystal structure and the structure in solution. Although it was possible to assign PCS in less crowded regions of the spectra to determine an initial tensor based on which the expected PCS can be back calculated based on the X-ray structure, for the assignment of further PCS, this direct approach bears several insecurities. Either wrongly assigned PCS, wrongly assigned residues in the diamagnetic spectra or differences between the effective structure in solution and the x-ray structure can be responsible for a wrong initial tensor that is determined. If based on this deviant tensor further PCS are assigned this can lead in the worst case to a self consistent but wrong solution. Usually at a certain point the discrepancies between the deviant tensor and the recorded spectra that is assigned should become obvious, when it is getting more and more difficult to assign further PCS. Nevertheless this can cost a lot of time, and therefore it would be much easier to start with a smaller set of shifts that have to be assigned, where the assignment of the residues in the diamagnetic spectra are unambiguous and if there were ambiguities in the paramagnetic spectra at least the number of possibilities is limited. Amino acid selective ^{15}N labelled protein would fulfil all these requirements. In order to exclude any wrong assignments

of the diamagnetic protein samples it was decided to assign the backbone residues for on of the four mutants.

3.6.1 Selective ^{15}N leucine labelled hCA-II

In hCA-II the most abundant residue is leucine, which is found 26 times in the whole protein. Selective ^{15}N leucine labelled protein was expressed successfully for all five protein mutants that were already expressed uniformly ^{15}N labelled. The expression was carried out again in minimal media where instead of ammonium chloride a mixture of all amino acids with natural abundance of the nitrogen was added with the exception of leucine. This amino acid was added to the media ^{15}N labelled at the time of induction in order to keep possible isotope scrambling at a minimal level. The yields were with 140 mg to 230 mg per litre of media more than two times as high as for the uniform ^{15}N labelled protein. It is expected that the use of an amino acid mixture instead of only ammonium chloride supports the production of protein in *E.coli* because the amino acids do not have to be prepared trough biosynthetic pathways.

3.6.2 Triply labelled hCA-II for backbone assignment

In order to confirm the assignment of the diamagnetic ^{1}H-^{15}N HSQC spectra is was decided to assign the protein backbone for one mutant. Therefore uniform ^{2}H, ^{15}N and ^{13}C labelled protein of the hCA-II_S50C_C206S mutant was prepared. Because expression in shaking flasks yielded only around 30 mg/L which was less protein than expected the expression was carried out in an 2 L fermenter. This allowed to minimize the amount of deuterated ^{13}C glucose and resulted in better yields. From one litre medium 84 mg triplely labelled protein was obtained. The deuteration level determined by ESI-MS was 85 %.

Refolding of triply labelled protein for reintroduction of exchangeable protons turned out to be difficult. Based on published conditions[49] a protocol was developed that allowed the recovery of up to 50 % of protein after denaturation and refolding. Optimization of this protocol was carried out with 2 mg to 5 mg of protein. Unfortunately when these conditions were applied to 17 mg of triple labelled protein the method

yielded only 20 % of refolded protein. Probably the protein is sensitive towards higher concentration. Higher concentrations could trigger aggregation and hCA-II is known to be prone to aggregation.[37] Despite the low yield of the refolding, the experiment revealed that only for 26 residues out of 193 well separated signals in the ^{1}H-^{15}N HSQC the signal intensity increased significantly after refolding. Showing that for 87 % of the residues the exchangable deuterons have been replaced by protons already when the protein was dissolved in protonated buffer. Therefore backbone assignment was carried out with a 460 µM sample of triply labelled hCA-II_S50C_C206S that was not refolded. Here again the yields were with 67 % below the average for the tagging reaction which could have a relationship with the higher concentration of the protein for this sample than for most of the other samples. In the ^{1}H-^{15}N HSQC spectra of this sample for the residues where the signal intensity increased after refolding a small signal was observable due to the incomplete deuteration of the protein. The intensity of these signals remained low due to the slow exchange rate of the deuterons with protons. Nevertheless, it was possible to assignment several of these signals. In total 90 % of the protein backbone could be assigned. Only the N-terminal residues up to residue 20 were not assigned, as well as residues H64, I91, P155, G156, T199, T200, P201. For the N-terminal residues some sequential assignment were possible, but an unambiguous assignment of these residues was not possible. Additionally for some of these residues a broader linewidth was observed, or the signals showed a typical splitting in two peaks due to *cis-trans* isomerisation of a proline amide bond. Both are indication of a dynamic structure of the protein in this region and shows that for these residues a deviation from the X-ray structure is very likely. This would make the assignment of PCS for these residues more challenging and these PCS could be a source of errors if they are included in the tensor determination. Therefore no further efforts were made for the assignment of these residues. Of the remaining unassigned residues the prolines were unimportant, because they have no resonance in the ^{1}H-^{15}N HSQC spectra. Residue 64 and 91 are both located in the catalytic pocket of the protein and residues next to them have low signal intensity, most likely due to a dynamic process. Therefore, correlations for the sequential assignments were not observable as well. L198 could only be assigned because this was the last leucine residue that could not be assigned and the leucine residues were known from the selective ^{15}N labelled protein

sample. L198 has a low signal intensity due to broad lines. It is located as well in the catalytic pocket of the protein and could be affected as well by dynamic processes in this region. Anyhow, because of the low signal intensities no sequential assignment of the neighbouring T199 was possible. Later residue T200 could be assigned form PCS alone because all PCS determined for for the four protein mutants matched well to the predicted shifts. Regardless assignment of residue 199 was not possible even from this side, therefore it is assumed that the corresponding peak for this residue is affected by similar processes as observed for residue 198 preventing a sequential assignment. The comparison with possible PCS helped also in other cases to unravel ambiguities of the assignment. This illustrates the potential of PCS to support the assignment of proteins. Residue 156 could not be assigned because this residue is next to a proline and from the following leucine no distinct correlation could be found. Here also no peak could be identified from the PCS probably, because this residue is is located in a crowded region of the ^{1}H-^{15}N HSQC.

The assignments of the other mutants using the assignments of the S50C mutant was straight forward apart from the regions around the individual Ser→Cys mutation site. There the residues where the chemical shifts have changed had to be assigned tentatively. For the region around S50 for the other three mutants than S50C, the assignment could again be confirmed from the corresponding PCS. This was not possible for the region around the cysteine in the corresponding mutant, because there the PCS either were not observable for most residues due to PRE or differences in the local structure of this mutant around the cysteine made the predicted PCS inaccurate. The region around the cysteine is anyway not important for the later structure determination from PCS because to cover for the local structural changes caused by the mutation and the tagging of the cysteine an individual structure would have to be determined for each tagged protein mutant, which is not practical at all. Therefore, the proper approach is anyway to exclude those PCS from structure determination, if differences can be expected due to the mutation and the tagging.

3.6.3 PCS assignment and tensor refinement

Having selective ^{15}N leucine labelled protein and a backbone assignment of almost the whole protein in hand, assignment of the PCS in the uniformly ^{15}N labelled protein turned out to be straight forward. The PCS in the ^{15}N leucine labelled protein samples could be assigned unambiguously and an initial tensor was determined. This tensor allowed the prediction and the successive assignment of the PCS in the uniformly ^{15}N labelled samples. The detailed procedure is described in section 2.9. A very large number of PCS for each mutant in the order of 197 to 208 residues could be assigned. In total more tha 1600 PCS. For several PCS a deviation exceeding 0.2 ppm was observed, indicating differences between the X-ray structure and the structure in solution. Criteria were defined for the exclusion of PCS from the final tensor calculation as described in section 2.11 To estimate the effect of the refinement three different subsets of PCS were determined with a smaller cut off for the maximum allowed PCS deviation for each subset. It could be shown that the main effect on the determined tensor parameters was achieved by the exclusion of those residues who showed the largest chemical shift perturbations upon tagging of the protein. The further refinement then only had small influence on the determined tensor parameters. For the smallest subset of PCS still at least 364 PCS (for ^{1}H and ^{15}N) for every mutant and for S166C even 394 PCS, in total almost 1500 PCS restraints, showed a smaller deviation than 0.1 ppm to the predicted PCS. Figure 3.1 shows the high coverage of the PCS for the different residues, comparable samples in the literature with up to four different tagging sites do not reach comparable numbers of PCS or comparable numbers of PCS per residue.[30,54,74]
The assigned PCS prove a close agreement between the structure in solution and the crystal structure otherwise such high numbers of PCS with such a small deviation would not be possible. It should be possible to determine a PCS based solution state structure of hCA-II using this set of data, even if it is very likely that a structure almost identical to the X-ray structure would be obtained. Especially for future testing and validation of algorithms for structure determination or protein assignment which include PCS, such as Xplor-NIH[75] or GPS-Rosetta[30] or PARAssign[76] this data set bears great potential. The utility of the PCS for the shift assignment was additionally demonstrated by the unambiguous assignment of the side-chain NH resonances of arginine

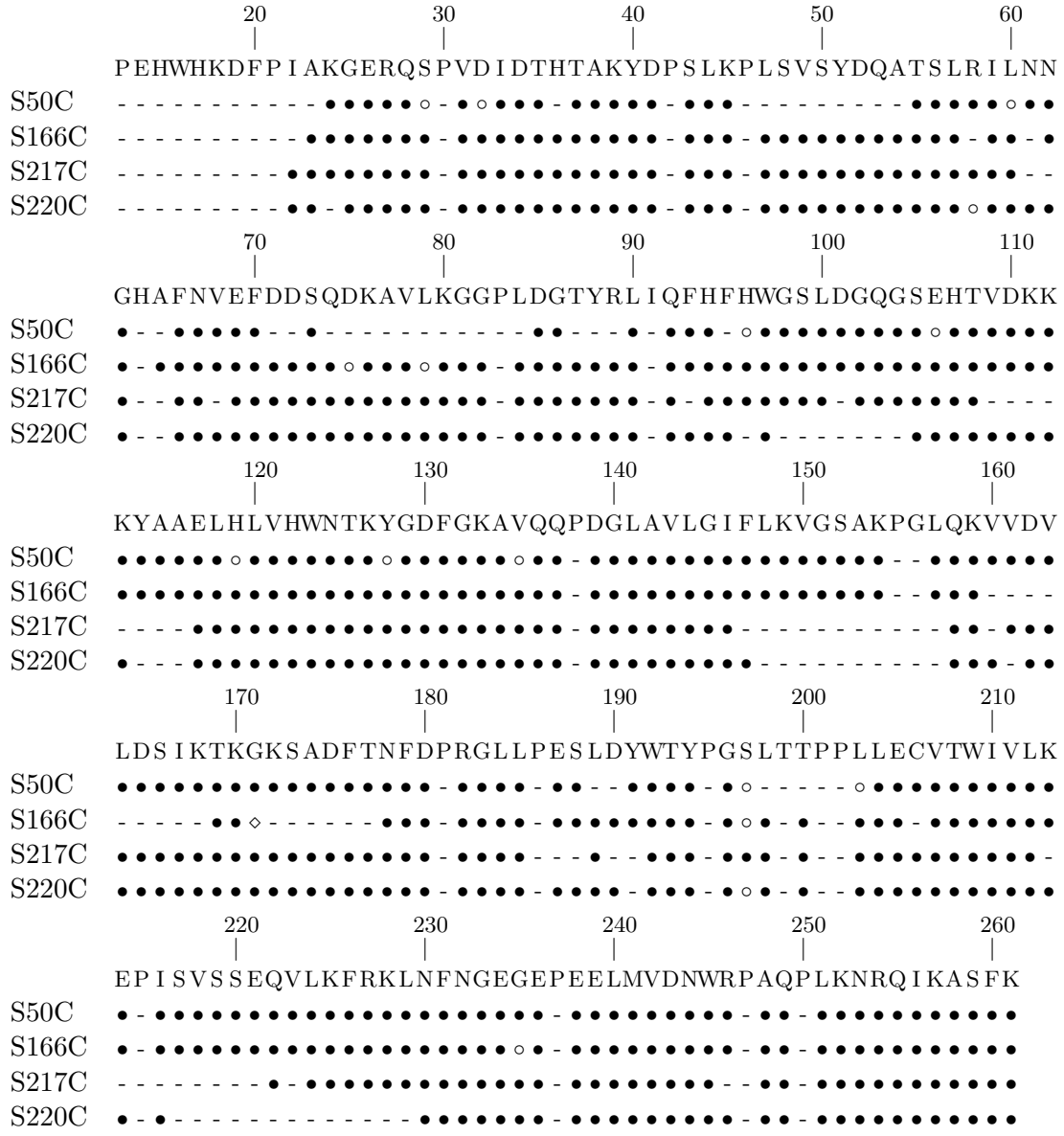

Figure 3.1: Summary for the different protein mutants of the PCS that showed a smaller deviation than 0.1 ppm to the predicted value. Black circles represent residues where both ^{1}H- and ^{15}N-PCS were available, for white circles only the ^{15}N-PCS and for white diamonds only the ^{1}H-PCS was available.

and tryptophan residues as described in section 2.15
An error analysis for the tensor parameters, following published procedures,[18] was performed. Two different random inputs were compared for the *Monte-Carlo* error analysis. The selection of random subsets of only 20 % of the PCS showed the very good consistency of the whole PCS set. With this method comparable uncertainties were detemined as for the introduction random structural noise of 0.5 Å to the atomic position in the X-ray structure, leading to an average displacement of each atom by 0.8 Å.

3.7 ^{19}F PCS of hCA-II inhibitor complexes

Protein ligand complexes with the fluorinated sulfonamide inhibitor, F2-Inh as well as with the F2-Complex (see figure 2.19) were prepared successfully. Excess of inhibitor could be removed by ultrafiltration without removing any of the inhibitor bound to the protein, illustrating the extremely high affinity that is reported for such type of inhibitors.[37] ^{19}F spectra of the protein inhibitor complex show fluorine signals with linewidth in the order of 60 Hz showing that the inhibitor binds tightly to the protein and therefore shares the same rotational correlation time explaining the broad signals. For the F2-complex pH dependent solubility was observed. This complex was only well soluble at low pH. This effect was observed in aqueous solution as well as in DMSO. Once bound to the protein the protein inhibitor complex remained soluble even at pH 6.8 where the ligand complex alone would have precipitated quantitatively as shown by ^{19}F NMR. Because all protein NMR spectra have been recorded at pH 6.8 and the protein inhibitor complex of F2-complex remained soluble at this pH all NMR experiments of this construct were carried out at this pH as well, in order to be able to apply the already determined data to this sample. Nevertheless a closer examination of the influence of the pH could reveal valuable information especially because such protein inhibitor complexes are successfully applied for enantioselective catalysis of [add ref.]. The fluorine spectra of F2-Complex show that even when bound to the protein the aromatic ring with the two flourines has to be able to rotate freely, because only one fluorine signal was observable for this compound. ^{19}F PCS for both protein inhibitor complexes have been recorded by one dimensional ^{19}F spectroscopy

profiting of the high sensitivity of the ^{19}F nuclei and no solvent suppression is required.

3.8 ^{1}H-^{19}F HOESY experiments for additional PCS restraints

In order illustrate the possibility to expand the number of PCS that could be determined from such a sample a ^{1}H-^{19}F HOESY spectra of the protein inhibitor complex of hCA-II with F2-Inh was determined. Due to the ^{19}F detection this experiment does not requires any water suppression. The basic idea of this experiment is to determine ^{19}F-proton distance information. But because most likely heteronuclear Overhauser effect (HOE) contacts that are are expected for such a sample are either intramolecular contacts to the proton of the inhibitor or interactions between the fluorine and sidechain protons of the protein. For side-chain protons in most cases no assignment is available, or most likely is not unambiguous when only the proton frequency is determined. On this basis the idea was developed to determine PCS for these HOE contacts. This would give access to structural information without the requirement of an assignment of protein side-chain protons. Further more even PCS of intramolecular HOE contacts deliver valuable information, because the more restraint for the inhibitor are available the higher the precision of the structure determination.
The major drawback of this experiment has been found to be the low sensitivity of the HOESY type experiment. For a one dimensional ^{19}F experiment of this complex on a spectrometer equipped with a cryo probehead after 6 min of experiment time already a good signal to noise was obtained, where for a ^{1}H-^{19}F HOESY experiment times in the order of 96 h were required for the same sample. The best way to circumvent this would be by increasing the sample concentration. The sample concentration in this case was rather low with 200 µM. In order to achieve a sufficient resolution in the indirect ^{1}H dimension it was decided to record the spectra with reduced sweep width instead of increasing the number of points, because only few signals were expected to be observable. Signals outside of the spectral window were therefore observed at the corresponding aliased frequency in the spectra. On the determined PCS this had no unfavourable influence, because the determined shift difference remains the same whether a peak is aliased or not. Rather precise PCS can be determined the higher the resolution of the spectra. For the unlikely case that two peaks would overlap due to

the aliasing, a second experiment with a different sweep width was recorded to reveal possible peak overlap, as much as it allowed to determine the original shift of the aliased signals. It has to be mentioned that at the time when the HOESY experiments were recorded, the samples used were already more than two years old, and for two samples including the diamagnetic reference significant amount of decomposition of protein was observable. Additionally over this period of time the pH was found to be not as constant as this has been observed for a period of several months. Apparently these were the reasons why of the four sets of PCS only two delivered reasonable shifts that could be used for a structure determination, as discussed later in this section. Therefore the later PCS structure determination was only performed in order to illustrate the potential of this method. For the determination of quantitative data for the structure determination it is recommended to use a different data set.
Theoretically it would be more beneficial to record the HOESY experiment proton detected, because in this case the proton signals are determined with high resolution in the direct dimension and increments in the indirect dimension would only be required as much as necessary for a minimal resolution between the different flourine signals if there are multiple fluorines present at all. Unfortunately for the proton detected HOESY when tested on small molecules much lower sensitivity was observed than for the fluorine detected experiment. It is speculated that the reason for this could be the higher T_1 time for the fluorine than for the proton allowing the magnetisation transfer in one direction but not in the other.

3.9 ^{19}F position determination from PCS

The fluorine position based on the PCS were determined using the X-ray structure and the four different $\Delta\chi$-tensors of the corresponding protein mutant. The PCS assignment of the protein mutants has already shown that the solution structure has to be very close to the X-ray structure therefore the position of the inhibitor can be determined based on the same structure, as it should match equally well as the experimental PCS, provided the protein structure is not affected by the inhibitor binding. That this was not the case could be concluded from the ^{1}H-^{15}N HSQC spectra before and after the inhibitor binding. No changes in the chemical shifts have been observed

nor differences in the PCS, that would accompany a larger change in the protein structure. Only chemical shift changes for the residues in the binding pocket that are expected upon ligand binding, were observed. In the case of the S50C mutant additionally determined RDC did not indicate a major change in the protein structure as well. This would have been very unlikely because for all X-ray structures of hCA-II-inhibitor complexes the basic protein structure is retained. The F2-Inh was selected as model compound, because a X-ray structure of the corresponding protein inhibitor complex was already available[59]. During the course of this thesis a X-ray structure of the complex without the two fluorines corresponding to the F2-complex was published.[36] This allows to bring the determined fluorine position in relation with a position obtained by a different method for both protein-inhibitor complexes.
For the F2-Inh the position determined for the two fluorines from their PCS deviated by as much as 8 Å form the X-ray structure. In contrast the F-F distance between the fluorine in *ortho* and the fluorine in *meta* position could be determined very precisely based on the PCS alone. This situation could be explained by a systematic error on the ^{19}F PCS which has a comparable magnitude for both PCS. A reasonable candidate that could not be taken into account in the presented structure determination were RACS. These small chemical shifts depend on the orientation of a nuclei with respect to the magnetic susceptibility tensor. When the orientation of a nucleus as well as the corresponding $\Delta\chi$-tensor are known, RACS can be predicted for a certain type of nuclei, based on the corresponding CSA. For ^{15}N the possible RACS are already in a range that could be responsible for the deviation in the PCS position from the X-ray structure. The influence of the RACS on the PCS tensor for ^{15}N was already taken into account during the earlier tensor determination. The RACS depend on the CSA and within a rough approximation the maximum CSA depends on the chemical shift range of the nucleus.[77] For aromatic fluorines reported values for the CSA are in a comparable order of magnitude[64,65] than for ^{15}N.[19] From this it follows that for the RACS of fluorine at least similar values than for ^{15}N can be expected but arguing with the larger chemical shift range for ^{19}F compared to ^{15}N, even much larger RACS are possible.
To compensate for the influence of the RACS these have to be determined experimentally, because for the prediction of the RACS from from tensor parameters and

a given CSA previous knowledge of the orientation of the nuclei is required, which is not available if the position is determined from PCS alone. A possibility for the experimental determination of the RACS would be, using the field dependence of the RACS which is quadratic with respect to the magnetic field, compare to equation 1.3. For PCS no field dependence is expected from equation 2.3 and indeed when the field dependence of the PCS has been investigated the only field dependent term that has been found was equivalent to the RACS contribution.[78] Therefore determination of the PCS at different magnetic field strength should allow the order of magnitude of the RACS This experiment has not been carried out so far due to the lowered sensitivity at smaller magnetic fields and limited time during the course of this thesis, and because for accessible NMR spectrometer at higher magnetic field strength the hardware for the determination of fluorine chemical shift was not available.

Another possibility to circumvent the influence of the RACS would be to determine the PCS only for protons, where the influence of the RACS can be neglected.[20] As demonstrated, the ^{1}H-^{19}F HOESY experiment could deliver exactly such PCS for the neighbouring protons to the fluorine. And indeed the calculated proton position from their PCS from the HOESY experiment indicate a much smaller deviation to the X-ray structure as for the fluorines. This interpretation was taken with care, because the sample conditions were not completely comparable any more, for the HOESY experiments.

For the second inhibitor, the F2-Complex, two different minima were found during the fluorine structure determination. One of them was significant closer to the expected fluorine position. For the S217C mutant a PCS of almost 0 ppm was observed. Consequently the fluorine position had to be in the node-plane of this tensor. Unfortunately in this region the tensor has the largest gradient and the position is less well defined than for larger PCS. Already a difference in the PCS of −0.05 ppm would have exclusively delivered the position closer to the tag. This is difference again lies in the same order of magnitude that was observed for the F2-Inh. That in this case a position closer to the expected position in the X-ray structure was obtained can be explained by the higher motional freedom that is observed for the fluorine atoms. Even when the F2-complex is bound to the protein only one fluorine signal is observed, indicating that the phenyl ring with the two fluorine atoms can rotate freely. This rotation would

also average the CSA contribution perpendicular to the rotation axis thereby reducing the size of the RACS. Still the contribution alongside the rotation axis could still be responsible for the observed differences observed in the case of the S217C mutant.
As an indirect proof of the RACS being the source of error, it was tried to determine the amide proton and nitrogen position of ten selected residues based on their PCS. Tensor parameters were redetermined where these ten residue have additionally been excluded. Because the position of these residues was known from the X-ray structure it was possible to calculate the expected RACS. The position of these 20 nuclei was determined twice, one time using the experimental PCS and another time using the effective PCS where the determined RACS were used to correct the experimental PCS. The calculated RACS for the protons were as expected much smaller than for nitrogen. Therefore it was expected that the RACS correction should have a positive influence on the nitrogen position and an negligible effect on the proton position. Unfortunately no effect of the RACS correction was observed. It is likely that the prediction of the RACS is not as precise as necessary. It is reported that RACS used for structural restraints show large errors in the order of 10 % to 20 %.[67] The same would be true for their prediction. Nevertheless this validation showed two different findings: First, the average position for the protons was twice as close to the X-ray structure than for nitrogen and lied within the determined uncertainty. Probably due to the lower precision of the nitrogen chemical shift in the ^{1}H-^{15}N HSQC spectra. Second, the two residues with the largest deviation from the X-ray structure showed the smallest average PCS and the largest average distance to the four different lanthanide tags. This illustrates that the larger a PCS, the preciser its structural information.
In general an uncertainty for the proton position of 1 Å to 2 Å might look only moderate for high resolution spectroscopy, but in this case only the positions of single independent atoms were determined. It has to be emphasized, that when PCS from multiple tagging sites are used, such a precision of the proton position can be obtained almost throughout the entire protein. So PCS from four different tagging sites may not deliver positions with atomic resolution, but if these restraints are used in combination with other restraints for the overall protein structure determination they demonstrate their outstanding value.[54] Especially regarding to the relatively small effort for their assignment compared for example to the clearly much more demanding determination of a

sufficient number of NOE restraints for protein structure determination.
Finally it has to be added that the uncertainties of the tensor parameters were determined conservatively, because the focus was laid on the general use of the presented methods, especially when only an X-ray structure of the protein is available. So the determined uncertainties should clearly be considered as an upper limit. Furthermore, with regard to the possibility that the overall agreement of the determined PCS should further improve if a solution state structure is determined and consequently a better accuracy and higher precision are very likely, even for the position of single atoms.
Eventually, the data presented has been determined using only (*8S*)-TmM8-SPy, representing only one of twelve possible lanthanide metals. Each of the remaining lantanide metals can deliver additional PCS restraints. Furthermore, the comparison with the (*4R,4S*)-LnM8-SPy complexes has proven an equal or even higher potential for PCS NMR spectroscopy, thus doubling the number of PCS restraints that can easily be obtained using the same four protein mutants, once the basic system is well characterised as in the described case.

3.10 RDC of S50C mutant

The determined RDC for the S50C mutant show good agreement between the determined PCS and RDC tensors. As expected a smaller agreement between experimental and predicted RDC is found, reflected in the lager Q-factors of 0.48 and 0.31 of the full set and the optimized set of RDC respectively. This is caused due to the higher sensitivity of RDC towards local mobility, especially because an X-ray structure was used for the prediction of the RDC and the dynamic regions are usually frozen within one of several possible conformations. This would explain the large deviations that have been observed for several residues. Due to their sensitivity towards motion of the RDC usually a smaller tensor is obtained from RDC than from PCS. But this is not the case in the present sample. This would either indicate a very rigid attachment of the lanthanide metal or this is an artefact observed due to the use of an X-ray structure for the determination of the RDC tensor. This could best be differentiated by the determination of a solution state structure of the protein.

CHAPTER 4

Conclusion and Outlook

In the course of this thesis LnM8-SPy complexes were successfully applied for PCS NMR spectroscopy of the medium sized human carbonic anhydrase II (hCA-II). Point mutation of the protein sequence allowed the specific attachment of the paramagnetic tag to five different sites of the protein. Four of these protein mutants showed large and very useful PCS demonstrating the good practicability of the selection criteria for the mutation sites. For one protein mutant 90 % of the protein backbone was assigned in order to ensure the correct assignment of the large number of resonances in the ^{1}H-^{15}N HSQC spectra of the uniformly ^{15}N labelled protein tagged with diamagnetic LuM8-SPy. A very useful strategy for the PCS assignment was presented. Based on the PCS assigned in selective ^{15}N leucine labelled protein initial $\Delta\chi$-tensor parameters were determined. These allowed the successive assignment of the PCS in the uniformly ^{15}N labelled protein. For every mutant PCS for more than 80 % of the residues in the protein were assigned. Overall more than 1600 PCS (^{1}H and ^{15}N) were assigned for the four different mutants. Systematic exclusion of PCS in the neighbourhood of the tag and in flexible parts of the protein allowed to determine a subset of PCS with less than 0.1 ppm deviation between experimentally determined PCS and predicted PCS. This allowed to determine precise $\Delta\chi$-tensor parameters based on the X-ray structure. This subset of PCS still consisted of almost 1500 PCS. This showed an excellent agreement between the protein structure in solution and X-ray structure. The determined PCS should be more than sufficient to determine a low resolution solution state structure of the protein using only PCS as experimentally determined restraints. This would

be the first published solution sate structure of hCA-II. For a protein where such an approach has been demonstrated a far lower number of PCS has been assigned.[30] This set of PCS will provide as well very valuable data for future testing and validation of algorithms that use PCS for structure determination or for protein assignment.

In this study the first example was presented where the fluorine position of fluorinated ligands in complex with a protein were determined alone on the PCS derived from one-dimensional ^{19}F-NMR spectra. For the ligand with two fluorine atoms the fluorine-fluorine distance was reproduced very precisely by the ^{19}F-PCS but for the position of the two fluorines in the protein a deviation of 8 Å to the X-ray structure was observed. The most likely reason for this systematic error was assumed to be residual anisotropic chemical shift (RACS) that could not be taken into account in the structure calculation. This was supported by the second fluorinated ligand, where a smaller deviation to the X-ray structure was observed. The fluorine atoms for this ligand showed higher motional freedom and therefore a reduction of the RACS effect is very likely. To prove this assumption the following future experiments are suggested:

- A ^{15}N edited ^{1}H-^{19}F HOESY experiment should allow to unambiguously identify any NH group in the neighbourhood of the fluorine atoms. Thus allowing to confirm the equivalence between X-ray structure and protein structure in solution.
- The magnetic field dependence of the RACS should allow to determine the order of magnitude of this effect by determination of the PCS at different field strength. This will allow to correct the determined PCS and to determine a position with higher accuracy, if the systematic error is caused by RACS.
- A ligand containing a CF_3-group should show smaller influence of the RACS due to the free rotation of the CF_3-group. Therefore a higher accuracy of the position determined from PCS is expected.
- A repetition of the ^{1}H-^{19}F HOESY experiments with new protein samples should confirm the demonstrated principle of determining ^{1}H-PCS that have a higher accuracy due to the negligible effect of the RACS on the protons.

Once the different tensors are determined the method presented offers quick access to structural information for any kind of fluorine containing inhibitor. This can be used as a general method, provided the overall protein fold is not affected upon binding. For certain protein inhibitor complexes even a deviation of 8 Å could still give valuable information, such as identifying a binding site. In general, detailed 3D structural data can be obtained using only uniform ^{15}N labelled protein with four different tagging sites and a corresponding X-ray structure. Such information would be very demanding to acquire with a different method, e.g. complete side chain assignment of the protein and NOE analysis. Especially for high throughput screening in pharmaceutical industry, this approach would be well suited. Fluorinated pharmacological compounds have been a largely growing field in the last decades, because the introduction of fluorines at specific positions a molecule allows the fine tuning of the pharmacological properties of promising drug candidates.[38,79] And finally if more detailed structural information is desired, with ^{1}H-^{19}F HOESY spectra ^{1}H PCS of the ligands are available allowing to determine PCS that are less affected by RACS and therefore deliver accurate structural information.

CHAPTER 5

Experimental

5.1 Materials and methods

5.1.1 Reagents

All commercial reagents used were of the highest grade available. The quality of the solvents for reactions corresponds to "puriss" or even higher in the case of small scale reactions. For aqueous solutions ultrapure water was used, if not mentioned otherwise. M4-cyclen (**1**) was a gift from Dr. R. A. Byrd (National Cancer Institute, Frederick, USA) and 2-(pyridyldithio)-ethylamine hydrochloride (**7**) was synthesised according to published procedures.[80]

5.1.2 Methods and Devices

Standard methods like primer design, deoxyribonucleic acid (DNA) extraction and purification, gel electrophoresis, protein affinity chromatography and spectroscopic quantification of cell growth were carried out according to published protocols with minor adjustments (when necessary). Commercial kits such as Pd10 ion exchange columns, Sep pak C18 collumns, Amicon ultrafiltration tubes were used according to manufacturer instructions.

NMR spectroscopy: All NMR spectra were recorded either on a Bruker Avance III NMR spectrometer operating at 600.13 MHz, equipped with a 5 mm BBFO+ probe head with z-axis pulsed field gradients or a 5 mm $^{1}H/^{13}C/^{15}N$ TXI probe head with

z-axis pulsed field gradients, or on a Bruker Avance III HD spectrometer operating at 600.13 MHz, equipped with a 5 mm ^{1}H/^{19}F-^{13}C/^{15}N-D QCI cryo probe head with z-axis pulsed field gradients. Experiments for the determination of RDC were performed on a Bruker Avance III HD spectrometer operating at 900.18 MHz, equipped with a 5 mm ^{1}H-^{13}C/^{15}N-D TCI cryo probe head with z-axis pulsed field gradients.

HPLC: HPLC purification was performed on a Prep LC 4000 System in combination with a 2487 Dual λ Absorbance Detector both from Waters (Baden-Dättwil, Switzerland) equipped with a 150×20 mm column packed with ReproSil-Pur 120 ODS-3.5 µm from Dr. Maisch Gmbh (Ammerbach, Germany) using 0.1 % TFA in degassed H_2O as aqueous phase and 90 % aceto nitrile (AcN) with 10 % H_2O and 0.085 % TFA as organic phase. For each purification the following program was used: Flow rate: 10 mL/min 10 % for 2 min, 10 % to 55 % in 20 min, 55 % for 5 min, 55 % to 100 % in 2 min and 100 % until complete elution of all material. All values correspond to the percentage of the organic phase.

Sep Pak C18 columns: Single use Sep-Pak Vac RC (500 mg C18 cartridges from Waters (Baden-Dättwil, Switzerland) were used in combination with an Econo Pump Model EP-1 and an Econo UV Monitor Model EM-1 both from Bio-Rad (Hercules CA, USA) always according to the following protocol. Conditioning of the column with 10 ml MeOH (flow: 3 mL/min) and equilibration with 30 ml H_2O (3 mL/min). The sample was loaded to the column at neutral pH in aqueous solution (2 mL/min) and washed with 20 ml of H_2O (2 mL/min). Finally the product was eluted using MeOH/H_2O (80:20, 2 mL/min).

PD MiniTrap G-25 columns: Single use PD MiniTrap G-25 Size exclusion columns from GE Healthcare (Uppsala, Sweden) for desating of protein solutions were applies according to manufacturers instructions. Columns were equilibrated with total 8 mL of desired final buffer, the sample was loaded on the column with a volume of 0.5 mL

and eluted with 1 mL of the desired final buffer.

Mass spectrometry: ESI-MS analysis of small molecules and lanthanide complexes was performed on a Bruker Daltonics Esquire 3000 plus spectrometer. All compounds were applied with a concentration of 10 µg/mL to 1 µg/mL, or even lower, dissolved in either pure methanol (MeOH), in a MeOH/H_2O/TFA mixture or using properly diluted fractions direct from HPLC. Mass spectrometric analysis of protein samples were performed on a Bruker Daltonics microTOF ESI/time of flight (TOF)-MS spectrometer combined with an Agilent HPLC system with autosampler. Samples were diluted into an 0.1 % TFA solution to a final concentration of 0.1 mg/mL or below. 40 µL were applied directly to the spectrometer trough the hplc system.

Polymerase chain reaction (PCR): PCRs were carried out in an Mastercycler Gradient from Eppendorf (Schönenbuch, Switzerland).

UV spectroscopy: UV spectra for the determination of DNA concentrations were recorded on a Thermo Fisher Scientific NanoDrop 1000 spectrometer. Concentrations of proteins, M8-SPy and LnM8-SPy complexes were determined on a Agilent Technologies 8453 UV-Visible Diode Array spectrophotometer using cuvettes suitable for 50 µL sample volume from Hellma Analytics (Müllheim, Germany). Determination of cell growth was performed on a Varian Cary 50 Scan UV-Vis spectrometer.

Gel electrophoresis: Sodium dodecyl sulfate polyacrylamide gel electrophoresis (SDS-PAGE) were performed on Bio-Rad Mini-PROTEAN and Sub-Cell systems, respectively. The gels were analysed using a Molecular Image Gel Doc XR (Reinach, Switzerland).

Protein expression: Expression of protein in shaking flasks were performed either in an Infors HT Ecotron (Bottmingen, Switzerland) or a New Brunswick Scientific

INNOVA 44 (Edison NJ, USA). Expression of triple labelled protein was carried out in an 2 L Infors HT Labforce 5 Cell fermenter (Bottmingen, Switzerland) equipped with pH sensor, pO_2 sensor and four peristaltic pump channels.

Protein purification: Chromatografic purification of proteins was carried out on an ÄKTA prime plus from GE Healthcare (Glattbrugg, Switzerland).

Centrifugation: Centrifugation steps were carried out on the following centrifuges: An Heraeus Multifuge 4KR centrifuge equipped with a swinging bucket rotor (4440 rpm correspond to 5346 × g), a Sorvall RC-6 plus centrifuge equipped with a fixed angel rotor either for 6 × 250 mL samples (14 000 rpm correspond to 30 000 × g) or for 6 × 1 L samples (9500 rpm correspond to 16 880 × g), a Heraeus Fresco 21 centrifuge for eppendorf samples (14 800 rpm correspond to 21 100 × g) all from Thermo Fisher Scientific (Waltham, MA USA) or a Universal 320 from Hettich (Tuttlingen, Germany) equipped with a rotor for 12 × 15 mL falcon tubes (12 000 rpm correspond to 13 201 × g).

Lyophilization: Lyophilization steps were carried out in a Labonco benchtop lyophiliser FreeZone 2.5 L (Kansas City, MO USA).

Ultrapure water: Ultrapure water was obtained either from a Merck Millipore Milli-Q Reference water purification system (Molsheim, France) or from a Labtec ELGA Purelab ultra water purification system (Villmergen, Switzerland).

5.2 Protein expression

The site directed mutation and the expression of all the double mutants of hCA-II both uniform ^{15}N labelled and selective ^{15}N leucine labelled were performed in collaboration with Dr. Elisa S. Pereira Nogueira and are described as well in her PhD thesis[39]. Throughout the whole thesis the numbering system for the residues of hCA-I was used for hCA-II, where Thr-125 is followed directly by Lys-127. hCA-I has an additional alanine residue at the position 126 which is missing for hCA-II.[40]

All solutions used were either heated in an autoclave at 121 °C for 15 min or filter-sterilised using a 0.22 µm sterile filter.

5.2.1 pACA plasmid

The pACA plasmid used for the production of hCA-II was generous gift from Prof. Carol A. Fierke (University of Michigan, USA).[44] It consists of the hCA-II gene[45] behind a T7 RNA polymersae promoter, a f1 origin of replication,[46] and an amp^r gene as well as a cm^r gene in a pMa5-8 vector.[47] The gene for hCA-II has an alanine instead of a serine at position 2 which does not affect the expression of the protein nor its catalytic activity. This plasmid was used as a template for single point mutations by PCR.

5.2.2 Site-directed mutagenesis

Plasmid amplification:

The plasmid containing the gene for hCA-II was amplified by transformation into *E. coli* DH5α cells (genotype: F$^-$ Φ 80*lac* ZΔM15Δ(*lac*ZYA-*arg*F) U169 *rec*A1 *end*A1 *hsd*R17 (r_K^-, m_K^+) *pho*A *sup*E44 λ-*thi*-1 *gyr*A96 *rel*A1), according to the Invitrogen protocol with minor changes. 50 µL DH5α chemically competent cells were allowed to thaw on ice. 10 ng of the plasmid were mixed gently with the cells and incubated on ice during 30 min. Then the cells were heat-shocked by keeping the tube for exactly 20 s in a 42 °C water bath without shaking and then immediately place the tube on ice for 2 min. 950 µL of pre-warmed Super Optimal Broth with Catabolic repressor (SOC) medium were added and incubated for 2 h in a shaking inkubator (37 °C, 250 rpm). 20 µL to 200 µL of the medium from the transformation were spread on a pre-warmed lysogeny

broth (LB) (LB-Miller) plate (containing 60 µg/mL ampicillin (amp) and 34 µg/mL chloramphenicol (cm)). Different volumes were applied to ensure that at least one plate will have well spread colonies. The plates were incubated upside down at 37 °C over night. Three colonies were selected for extraction of the plasmid using a Promega AG Wizard Plus SV Miniprep DNA purification system (Dübendorf, Switzerland), which were analysed by sequencing at Microsynth AG (Balgach. Switzerland).

Site-directed mutagenesis:

hCA-II double and triple mutants were prepared by site-directed mutagenesis using the wt hCA-II plasmid (pACA) as initial template for the first mutation and for the final double and triple mutants plasmids already containing one respectively two mutations were used. The site-directed mutagenesis steps were carried out according to the procedure described by *Zheng et al.*[24] and primer candidates were tested *in silico* to minimise hairpin formation.[81] Resulting primers were ordered from Microsynth (Balgach, Switzerland) and are listed in Table 5.1

Only the C206S mutant was used for further mutation steps resulting in the plasmids for the following protein mutants (see table 5.2).

5.2.3 Transformation of plasmids for protein expression

For protein expression the desired plasmid was transformed into *E. coli* BL21(DE3)pLysS cells (genotype: F$^-$ *ompT lon hsdS*$_B$ (r_B^-, m_B^-) *dcm gal* λ(DE3) [pLysS (cm^r)] (produced in house).
100 µL of ultra-competent *E. coli* BL21(DE3)pLysS cells were allowed to thaw on ice, 8 µl dithiothreitol (DTT) (200 mM) and 3 µL of the plasmid (0.2 µg to 0.5 µg of DNA) were added and mixed gently. The mixture was kept on ice for 15 min and then plated on pre-warmed LB plates (containing 60 µg/mL amp and 34 µg/mL cm and 2 % w/v glucose). The plates were incubated upside down at 37 °C over night. When only chemical competent cells were available the following steps lead to the desired result. As far as the 15 min incubation on ice the protocol followed the same steps as above, then the cells were heat-shocked (30 s to 60 s at 42 °C followed by 2 min on ice). 900 µL LB

Table 5.1: List of primers (f: forward, r: reverse)

Mutant		Primers (5' → 3')	T_m (°C)	Length (bases)
C206A	f	CTT CTG GAG gct GTG ACC TGG ATT GTG CTG AAG	67.3	33
	r	CCA GGT CAC agc CTC CAG AAG AGG AGG AGG GG	69.7	29
C206S	f	CTT CTG GAG tct GTG ACC TGG ATT GTG CTC AAG	66.1	33
	r	CCA GGT CAC aga CTC CAG AAG AGG AGG GG	68.1	29
S50C	f	CTG TCT GTT tgc TAT GAT CAA GCG ACT TCC CTG	64.4	33
	r	TTG ATC ATA gca AAC AGA CAG GGG CTT CAG	62.5	30
S166C	f	GTG CTG GAT tgc ATT AAA ACA AAG GGG AAG AGT GC	64.5	35
	r	GT TTT AAT gca ATC CAG CAC ATC AAC AAC	58.2	29
S173C	f	AAG GGC AAA tgc GCT GAC TTC ACT AAC TTC G	63.5	31
	r	GAA GTC AGC gca TTT GCC CTT TGT TTT AAT G	61.0	31
S217C	f	AAG GAA CCC ATC tcg GTC AGC AGC GAG CAG GTG	69.8	33
	r	GCT GCT GAC gca GAT GGG TTC CTT GAG CAC AAT CC	69.0	35
S220C	f	AGC GTC AGC tgc GAG CAA GTG TTG AAA TTC CG	66.0	32
	r	CAC TTG CTC gca GCT GAC GCT GAT GGG TTC	67.8	30

medium (or SOC medium) were added and the mixture was incubated for 1 h at 37 °C in a shaking incubator (250 rpm) The cells were spun down in a centrifuge at top speed for 20 s, 950 µL of the supernatant was discarded and the cells were resuspended in the remaining 50 µL. Finally the cells were spread on a pre-warmed LB plate (containing 60 µg/mL amp and 34 µg/mL cm and 0.2 % w/v glucose) and were incubated upside down at 37 °C over night.

Table 5.2: Yields [mg/L] of hCA-II mutants for a given isotope labelling scheme according to conditions given in section 5.2.4 to 5.2.6 and their calculated and determined masses (calculated mass corresponds to protein without N-terminal methionine).

Mutant	**Yield [mg/L]**	**Calculated Mass [Da]**	**Determined Mass [Da]**
unif. ^{15}N hCA-II_S50C_C206S	95	29452	29447
unif. ^{15}N hCA-II_S166C_C206S	95	29452	29449
unif. ^{15}N hCA-II_S173C_C206S	85	29452	29450
unif. ^{15}N hCA-II_S217C_C206S	60	29452	29450
unif. ^{15}N hCA-II_S220C_C206S	80	29452	29450
unif. ^{15}N hCA-II_S50C_S166C_C206S	33	29469	29467
unif. ^{15}N hCA-II_S50C_S217C_C206S	1 [a]	29469	29522 [b]
unif. ^{15}N hCA-II_S50C_S220C_C206S	7 [a]	29469	29523 [b] (100 %), 29467 (90 %)
unif. ^{15}N hCA-II_S166C_S217C_C206S	7 [a]	29469	29523 [b]
sel. ^{15}N-Leu hCA-II_S50C_C206S	230	29125	29116
sel. ^{15}N-Leu hCA-II_S166C_C206S	140	29125	29116
sel. ^{15}N-Leu hCA-II_S173C_C206S	180	29125	29116
sel. ^{15}N-Leu hCA-II_S217C_C206S	180	29125	29117
sel. ^{15}N-Leu hCA-II_S220C_C206S	165	29125	29117
unif. ^{2}H ^{13}C ^{15}N hCA-II_S50C_C206S	84	32763	32157 [c]

[a] Bacteriophage contamination was assumed to be responsible for low expression level. [b] Mass difference possibly caused by N-terminal acetylation or similar modification. [c] Corresponds to a deuteration level of 85 %.

5.2.4 Expression of uniform ^{15}N labelled hCA-II mutants in 1 L shaking flasks

All double mutants and all triple hCA-II mutants mentioned in table 5.2 with the exception of hCA-II_S50C_S166C_C206S were expressed under the following conditions. With the difference that for the double mutants LB medium and for the triple mutants main culture medium was used for the pre-culture.

Inoculum

Early in the morning 15 mL of LB medium (containing 100 µg/mL amp and 34 µg/mL cm and 2 % w/v glucose) in a 75 mL baffled shaking flask were inoculated with a tip dipped into a single colony from the transformation. The mixture was incubated at 37 °C for 6 h to 7 h at 250 rpm.

Pre-culture

The inoculum was centrifuged at 5346 × g for 10 min at 4 °C, the supernatant was discarded and the pellet was resuspended in 2.5 mL pre-culture medium. Early in the evening either 50 mL LB medium (containing 60 µg/mL amp and 34 µg/mL cm and 0.2 % w/v glucose) or 50 mL of main culture medium (see below) in a 250 mL baffled shaking flask were inoculated with the 2.5 mL of resuspended inoculum. In the case of LB medium the culture was incubated overnight at 37 °C, 250 rpm until the optical density at 600 nm (OD_{600}) reached around 6.0. In the case of main culture medium the culture was incubated overnight too, at a temperature between 25 °C to 33 °C in order to reach a final OD_{600} of 1.0 to 2.0. In the next morning the pre-culture was centrifuged at 5346 × g for 10 min at 4 °C, the supernatant was discarded and the pellet was resuspended in 50 mL main culture medium.

Main culture

1 L of main culture medium in 3 L baffled shaking flasks was inoculated with the cells from the pre-culture. The medium was consisting of phosphate buffer (2 g/L Na_2HPO_4, 1 g/L KH_2PO_4, pH adjusted to 7.2) 0.5 g/L NaCl, 1 g/L $^{15}NH_4Cl$ (filter-sterilised), 2 mM $MgSO_4$, 0.1 mM $CaCl_2$, 0.2 % w/v glucose, 0.5 mM $ZnSO_4$, 100 µg/mL amp, 34 µg/mL

cm, 1X BME vitamin solution (using a 100X stock solution from Sigma-Aldrich, Buchs, Switzerland) and 1X of a trace element solution (using a 200X stock solution consisting of: 6 g/L $CaCl_2 \cdot 2H_2O$, 6 g/L $FeSO_4 \cdot 7H_2O$, 1.15 g/L $MnCl_2 \cdot 4H_2O$, 0.8 g/L $CoCl_2 \cdot 6H_2O$, 0.7 g/L $ZnSO_4 \cdot 7H_2O$, 0.3 g/L $CuCl_2 \cdot 2H_2O$, 0.02 g/L H_3BO_4, 0.25 g/L $(NH_4)_6Mo_7O_{24} \cdot 4H_2O$ and 5 g/L EDTA disodium salt). The culture was incubated at 37 °C in a shaking incubator at 250 rpm until OD_{600} reached around 0.6. Then the temperature was decreased to 25 °C and the expression was induced when OD_{600} reached 1.0 to 1.3 by the addition of 250 µM Isopropyl-β-D-thiogalactopyranosid (IPTG) and 450 µM $ZnSO_4$. The cells were incubated for 4 h to 6 h after the induction and the OD_{600} was monitored continuously. 1 mL samples were taken before induction and then every hour until the end of expression. All samples were kept on ice and were treated the same way as the main culture after the end of the expression. To prevent the leaking of the labelling the expression was not left for more than 6 h after the induction, even if the OD_{600} was still increasing. Cells were harvested by centrifugation at 4 °C and 5346 × g for 15 min. The supernatant was deactivated by the addition of NaClO and the cell pellet was kept overnight at −20 °C.

5.2.5 Expression of selective ^{15}N leucine labelled hCA-II mutants

All double mutants listet in table 5.2 were expressed ^{15}N leucine labelled.

Inoculum

The inoculum followed the same procedure as described in section 5.2.4.

Pre-culture

The inoculum was centrifuged at 5346 × g for 10 min at 4 °C, the supernatant was discarded and the pellet was resuspended in 2.5 mL pre-culture medium. Early in the evening 50 mL LB medium (containing 60 µg/mL amp and 34 µg/mL cm and 0.2 % w/v glucose) in a 250 mL baffled shaking flask were inoculated with the 2.5 mL of resuspended inoculum. The culture was incubated overnight at 37 °C, 250 rpm until the OD_{600} reached around 6.0. In the next morning the pre-culture was centrifuged

at 5346 × g for 10 min at 4 °C, the supernatant was discarded and the pellet was resuspended in 20 mL main culture medium.

Main culture

1 L of main culture medium in 3 L baffled shaking flasks was inoculated with the cells from the pre-culture. The medium was consisting of phosphate buffer (4.5 g/L Na_2HPO_4, 3 g/L KH_2PO_4, pH adjusted to 7.2) 0.5 g/L NaCl, 1 g/L, amino acid mix (see table 5.3), 0.2 % w/v glucose, 2 mM $MgSO_4$, 0.1 mM $CaCl_2$, 10 µM $ZnSO_4$, 100 µg/mL amp, 34 µg/mL cm, 1X BME vitamin solution (using a 100X stock solution from Sigma-Aldrich, Buchs, Switzerland) and 1X of a trace element solution (using a 200X stock solution consisting of: 6 g/L $CaCl_2 \cdot 2H_2O$, 6 g/L $FeSO_4 \cdot 7H_2O$, 1.15 g/L $MnCl_2 \cdot 4H_2O$, 0.8 g/L $CoCl_2 \cdot 6H_2O$, 0.7 g/L $ZnSO_4 \cdot 7H_2O$, 0.3 g/L $CuCl_2 \cdot 2H_2O$, 0.02 g/L H_3BO_3, 0.25 g/L $(NH_4)_6Mo_7O_{24} \cdot 4H_2O$ and 5 g/L EDTA disodium salt). The culture was incubated at 37 °C in a shaking incubator at 250 rpm until OD_{600} reached around 0.8. Then the temperature was decreased to 25 °C and the expression was induced when OD_{600} reached 1.0 to 1.3 by the addition of 250 µM IPTG, 450 µM $ZnSO_4$ and 60 mg ^{15}N leucine dissolved in 50 mL main culture medium (filter sterilised). The cells were incubated for 4 h to 6 h after the induction and the OD_{600} was monitored continuously. 1 mL samples were taken before induction and then every hour until the end of expression. All samples were kept on ice and were treated the same way as the main culture after the end of the expression. Cells were harvested by centrifugation at 4 °C and 5346 × g for 15 min. The supernatant was deactivated by the addition of NaClO and the cell pellet was kept overnight at −20 °C.

5.2.6 Uniform ^2H, ^{13}C, ^{15}N labelled hCA-II_S50C_C206S

Only hCA-II_S50C_C206S was expressed in triple labelled medium. The same protocol with only $^{15}NH_4Cl$ as the sole labelled compound in the medium was applied to express uniform ^{15}N labelled hCA-II_S50C_S166C_C206S.
For expression of triple labelled protein all solutions were prepared in D_2O apart from the BME vitamin solution and the trace element solution where only small volumes

Table 5.3: Recipe for amino acid mixture. The amino acids are listed in the order they were mixed.

Order	Amino acid	mg/L
1	Alanine	500
2	Arginine	400
3	Aspartic acid	400
4	Glutamic acid	650
5	Glycine	550
6	Histidine	100
7	Isoleucine	230
8	Lysine-HCl	420
9	Methionine	250
10	Proline	100
11	Serine	2100
12	Threonine	230
13	Valine	230
14	Phenylalanine	130
15	Tryptophan	50
16	Asparagine	-
17	Cysteine-HCl	50
18	Tyrosine	170
19	Glutamine	400
	Leucine (^{15}N labelled)	60

^{15}N labelled leucine was not added to the medium until the time of induction.

were added to the medium. All solutions were filter sterilised (not autoclaved) and used directly after preparation.

Inoculum

The inoculum followed the same procedure as described in section 5.2.4, no labelled compounds were used in this step.

Pre-culture

The inoculum was centrifuged at 5346 × g for 10 min at 4 °C, the supernatant was discarded and the pellet was resuspended in 2.5 mL pre-culture medium. Early in the evening 50 mL of main culture medium (see below), with 0.375 % w/v D_7-^{13}C-glucose instead of 0.08 %, in a 250 mL baffled shaking flask were inoculated with the 2.5 mL of resuspended inoculum. The culture was incubated overnight at a temperature between 30 °C to 37 °C in order to reach a final OD_{600} of 1.0 to 2.0. In the next morning the pre-culture was centrifuged at 5346 × g for 10 min at 4 °C, the supernatant was discarded and the pellet was resuspended in 50 mL main culture medium.

Main culture

All parts of the fermenter with 2 L working volume were autoclaved and dried properly. The medium for the main culture was consisting of phosphate buffer (9 g/L Na_2HPO_4, 13 g/L KH_2PO_4, 10 g/L K_2HPO_4, 2.4 g/L K_2SO_4, pH adjusted to 7.2), 1 g/L $^{15}NH_4Cl$ (filter-sterilised), 0.08 % w/v D_7-^{13}C-glucose, 5 mM $MgSO_4$, 500 µM $ZnSO_4$, 100 µg/mL amp, 34 µg/mL cm, 1X BME vitamin solution (using a 100X stock solution from Sigma-Aldrich, Buchs, Switzerland) and 1X of a trace element solution (using a 200X stock solution consisting of: 6 g/L $CaCl_2 \cdot 2H_2O$, 6 g/L $FeSO_4 \cdot 7H_2O$, 1.15 g/L $MnCl_2 \cdot 4H_2O$, 0.8 g/L $CoCl_2 \cdot 6H_2O$, 0.7 g/L $ZnSO_4 \cdot 7H_2O$, 0.3 g/L $CuCl_2 \cdot 2H_2O$, 0.02 g/L H_3BO_3, 0.25 g/L $(NH_4)_6Mo_7O_{24} \cdot 4H_2O$ and 5 g/L EDTA disodium salt). 1 L of main culture medium was inoculated in the fermenter with the cells from the pre-culture. The fermentation was initiated at 37 °C with the stirring at 250 rpm and an oxygen level kept between 50 % to 90 %. Antifoam solution was applied manually, if required. The glucose level was

monitored using Merckoquant Glucose-Test strips (from Merck, Darmstadt, Germany). After around 3 h, when the all initial glucose was consumed (also indicated by a short drop, followed by an increase of the oxygen level) a slow feed containing a total amount of 5.5 g D_7-^{13}C-glucose and 0.5 g $^{15}NH_4Cl$ was applied with such a feed rate that 60 % of the glucose is delivered over night to the culture. In the morning, the OD_{600} was around 3.0 to 3.5, the temperature was decreased to 20 °C and protein expression was induced by the addition of of 250 µM IPTG and 450 µM $ZnSO_4$. 1 mL samples were taken before induction and then every hour until the end of expression. All samples were kept on ice and were treated the same way as the main culture after the end of the expression. The remaining 40 % of the feed was delivered to the culture over a period of 5 h to 6 h. 3 h after induction 0.5 mM phenylmethanesulfonylfluoride (PMFS) was added. When all glucose is consumed the cells are harvested by centrifugation at 4 °C and 5346 × g for 15 min. The supernatant was deactivated by the addition of NaClO and the cell pellet was kept overnight at −20 °C.

5.2.7 Protein purification

All cell pellets from the different expressions were treated the same way. In order to obtain the protein in the reduced state with regard to the free thiol group, all buffers used for purification were prepared with 1 mM DTT, or in the case of dialysis buffer with at least 100 µM DTT. If no DTT was used the protein was obtained with glutathione bound to the thiol.

Cell lysis

Lysis of the cells was achieved by three cycles of freezing and thawing of the cell pellet, which activated the gene encoding for T7 lysozyme. The pellet was resuspended in 25 mL lysis buffer (50 mM Tris-SO_4, pH 8.0, 50 mM NaCl, 0.5 mM $ZnSO_4$, 1 mM DTT and 10 µg/mL PMFS). The resuspension was shaken vigorously (300 rpm) at room temperature (RT) for 30 min then Deoxyribonuclease I (DNase I) (1 µg/L) was added and the mixture was shaken for another 30 min. The lysate was centrifuged at 16 880 × g for 30 min at 4 °C. The supernatant was recovered and the pellet was resuspended

another two times in 25 mL lysis buffer (followed by 30 min shaking and cenrifugation each time) to extract as much protein as possible. The total 75 mL solution from the extraction was filtered trough a 0.45 µm filter and used directly for affinity chromatography.

Inhibitor affinity chromatography

Affinity chromatography was performed using 25 mL of *p*-amino-ethylbenzene sulfonamide agarose resin packed into a XK 16 column (GE Healthcare, Glattbrugg, Switzerland). The collumn was equilibrated with 5 column volume (CV) activity buffer (50 mM Tris-SO_4, pH 8.0, 0.5 mM $ZnSO_4$, 1 mM DTT) and the protein in 75 mL lysis buffer was loadet onto the column at a slow flow rate (1 mL/min. Then the column was washed with 5 CV of wash buffer (50 mM Na_2SO_4, 50 mM $NaClO_4$, 25 mM Tris-SO_4, pH 8.8, 1 mM DTT) and the protein was was eluted with 10 CV of elution buffer (200 mM $NaClO_4$, 100 mM NaAc, pH 5.6, 1 mM DTT). 10 mL fractions were collected and those containing the protein (detected by UV absorption were pooled and dialysed at 4 °C against activity buffer for 12 h, followed by deionised H_2O for 24 h and finally against ultrapure water for another 24 h. Dialysis buffer contained 100 µM DTT and were exchanged at least three times a day. The resulting solution was frozen in liquid nitrogen and lyophilised. The resulting protein was stored at 4 °C.

5.2.8 Protein analysis by gel electrophoresis

Sample preparation

The Samples taken during the expression were lysed by tree cycles of freezing and thawing of the cell pellet, which activated the gene encoding for T7 lysozyme. The pellet was resuspended in ultrapure water. For each sample 40 µL water times the OD_{600} at the time of sampling was used to normalize the concentration over the number of cells. 1 µL of DNase I (1 mg/mL dissolved in 5 mM Tris-HCl pH 7.5, 75 mM $MgCl_2$ and 50 % v/v glycerol). The samples were vortexed and shaken vigorously (300 rpm) at RT for 30 min to 60 min. The samples were centrifuged at 21 100 × g for 5 min at RT. The soluble fraction (supernatant) was separated and the insoluble fraction (pellet)

was dissolved in 8 M urea (again 40 µL urea solution times the OD_{600} was used). Each sample fraction (soluble and insoluble) as well as a positive control (around 5 µg to 20 µg pure hCA-II dissolved in 20 µL water) were mixed with 4 µL 6X loading buffer (100 mM Tris-HCl pH 6.8, 2 % v/v β-mercaptoethanol, 20 % w/v sucrose, 0.012 % w/v bromophenol blue and 60 mM). The samples were heated to 98 °C for 5 min and then loaded immediately on a 12 % acrylamide gel.

SDS-PAGE

A 12 % acrylamide running gel for gel electrophoresis was prepared as follows. 5 mL ultrapure water, 6 mL of 30 %/0.8 % w/v acrylamide/bis-acrylamide, 3.8 mL of 1.5 M Tris-HCl pH 8.8, 75 µL of 20 % w/v sodium dodecyl sulfate (SDS), 100 µL of 15 % w/v ammonium peroxodisulfate (APS) and 6 µL of tetramethylethylenediamine (TEMED) were mixed well and the solution was directly poured into a chamber between glass plates and left for polymerisation for 30 min. A 5 % acrylamide stacking gel was prepared by mixing 3.4 mL ultrapure water, 1 mL of 30 %/0.8 % w/v acrylamide/bis-acrylamide, 1.5 mL of 0.5 M Tris-HCl pH 6.8, 30 µL of 20 % w/v SDS, 40 µL of 15 % w/v APS and 6 µL of TEMED. The solution was poured directly after preparation on top of the running gel and a comb was inserted into the solution in order to prepare the spaces required for loading the different samples onto the gel. The stacking gel again left for 30 min for polymerisation. To keep the gel from dryness, the gel was clamped into the holder and the holder was placed in a tank containing SDS buffer (25 mM Tris-HCl, 0.192 M glycine and 0.1 % SDS). Then 20 µL of each sample were loaded onto the gel and 6 µL of the protein marker (Prestained Protein Marker, Broad Range, from New England BioLabs Inc., Bioconcept, Allschwil, Switzerland). The gel ran at 200 V until the blue front line reached the end of the gel (after about 1.5 h). The gel was transferred into a container with 100 mL of staining solution (25 % w/v Coomassie Brilliant Blue R-250, 50 % v/v MeOH, 7.5 % v/v glacial acetic acid) and was rocked gently for 1 h. Then the gel was placed in 100 mL of a destaining solution (20 % v/v MeOH and 7.5 % v/v glacial acetic acid) and was rocked gently until the protein pattern appeared (around 3 h or longer). The gel was left in water overnight and a Kimwipe towel was placed in the solution to absorb the stain in the solution.

5.2.9 Refolding of hCA-II_S50C_C206S

For denaturation the hCA-II was dissolved in 5 M GdmCl, 100 mM Tris-SO_4, 1 mM TCEP at pH 7.5 to obtain a final protein concentration of 14.25 µM. Protein concentration was controlled by UV absorption at 280 nm (ε_{280} =54 700 M^{-1} cm^{-1})[37] after every step of the protocol. Refolding of the protein was initialised by fast dilution of the whole sample into 100 mM Tris-SO_4 buffer at pH 7.5 containing 10 µM TCEP to obtain a final concentration of 0.3 M GdmCl and 0.855 µM of protein. The resulting solution was stirred for 3 h to allow the protein to subsequently refold. To reduce the large sample volume the protein solution was loaded on a sulafonamide affinity column according to the same conditions as described above in section 5.2.7 with the exception that instead of buffer exchange to the described the activity buffer the protein was loaded directly in the present buffer after the dilution onto the column. The resulting fractions containing the protein were pooled and dialysed at 4 °C against activity buffer for 12 h, followed by deionised H_2O for 24 h and finally against ultrapure water for another 24 h. All dialysis buffer contained 10 µM TCEP. The final solution was concentrated using 15 ml Vivaspin ultrafiltration tubes (MW.co. 10 kDa) to a volume of 2 mL by successive addition of the protein solution. The final buffer exchange to 10 mM PO_4^{3-} pH 6.8 was carried out using a 4 mL Amicon ultrafiltration tube to obtain a final volume of 280 µL.

5.3 Ln-M8-SPy Synthesis

The following synthesis was carried out according to published procedures with minor adjustments given in the protocols below. The analytical data was in accordance to the literature. (*R*)-Bn-lactic acid-OTf (**2**) and (*R*)-^{t}Bu-lactic acid-OTf (**4**) were taken from stocks kept at −20 °C which were synthesized according to the literature.[28]

5.3.1 Synthesis of M4cyclen-Bn-lactate, **3**

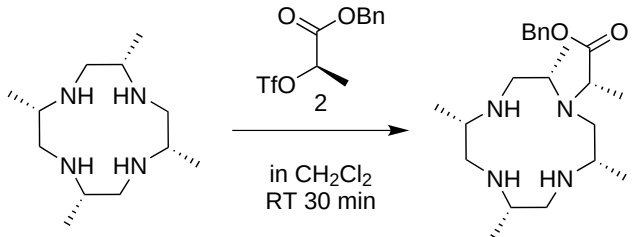

M4cyclen, **1** (402.2 mg, 1.76 mmol, 1 eq.) was dissolved in 50 mL of CH_2Cl_2 and (*R*)-Bn-lactic acid-OTf, **2** (385.5 mg, 1.76 mmol, 0.7 eq.) in 2 mL of CH_2Cl_2 was added during 30 min and the reaction was monitored by ESI-MS. NEt_3 (1 mL, 7.21 mmol, 4.1 eq.) was added to quench the reaction and volatile material was removed under reduced pressure. The resulting oil was purified by flash column chromatography (25 g SiO_2, ethyl acetate (EtOAc):ethanol (EtOH):NEt_3 10:1:0.4). The fractions were analysed by ESI-MS, and those containing the product were combined and evaporated to yield a yellowish waxy solid (396.7 mg, 1.02 mmol, 82 %).
$C_{22}H_{38}N_4O_2$, **FW**: 390.57 g/mol **ESI-MS**: *m/z* 391.3 $[M+H]^+$.

5.3.2 Synthesis of (*8S*) ^{t}Bu$_3$-M4DOTMA-Bn, 5

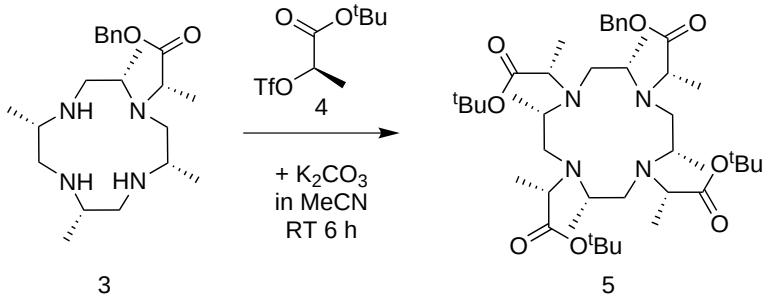

M4cyclen-Bn-lactate, **3** (400 mg, 1.03 mmol) was dissolved in 15 mL AcN under argon atmosphere. (*R*)-^{t}Bu-lactic acid-OTf, **4** (1.11 g, 3.99 mmol, 3.9 eq.) in 6 mL AcN and freshly powdered K_2CO_3 was added and the resulting mixture was stirred for 6 h, until

completion of the reaction was indicated by ESI-MS. NEt_3 (200 µL, 1.44 mmol, 1.4 eq.) was added to quench the excess reagent and after an additional 10 min of stirring, the mixture was filtered trough celite. Removal of volatile material under reduced pressure yielded a waxy yellowish solid that was purified by flash column chromatography (25 g SiO_2, $CHCl_3$/EtOH 9:1) to yield a off-white waxy solid (1.06 g, 90 %). $C_{43}H_{74}N_4O_8$, **FW**: 775.09 g/mol **ESI-MS**: *m/z* 797.7 $[M+Na]^+$.

5.3.3 Synthesis of $^tBu_3$-M4DOTMA-OH, 6

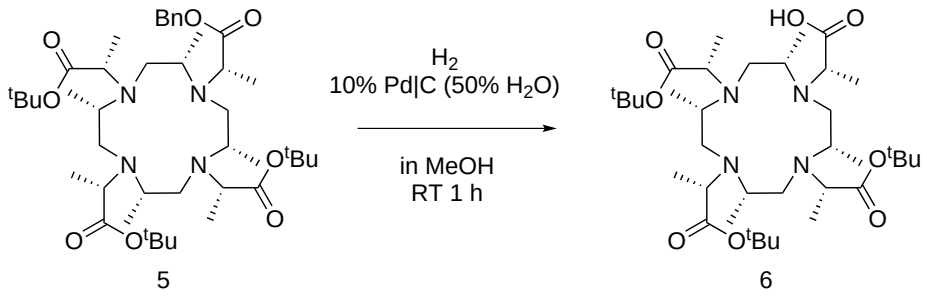

$^tBu_3$-M4DOTMA-Bn, **5** (100.6 mg, 0.13 mmol) was dissolved in 5 mL MeOH under argon atmosphere and palladium on carbon (30.8 mg, 10 % Pd, 50 % H_2o) as hydrogenation catalyst was added. The mixture was stirred while a total amount of 500 mL of hydrogen gas was allowed to bubble gently trough the solution at atmospheric pressure over a period of 1 h and the reaction was monitored by ESI-MS. After completion of the reaction the mixture was filtrated through celite and volatile material was removed under reduced pressure, yielding a colourless glassy solid which was used for the next reaction step without further purification (84.1 mg, 0.12 mmol, 94 %). $C_{36}H_{68}N_4O_8$, **FW**: 684.95 g/mol, **ESI-MS**: *m/z* 685.7 (47 %, $[M+H]^+$), 707.6 (100 %, $[M+Na]^+$).

5.3.4 Synthesis of M8-SPy, 8

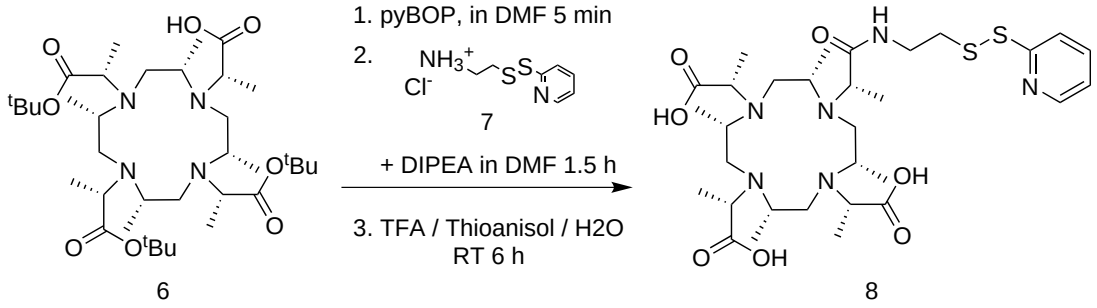

$^{t}Bu_3$-M4DOTMA-OH, **6** (84.1 mg, 0.12 mmol) dissolved in 1.6 mL DMF was activated with pyBOP (64.2 mg, 0.12 mmol, 1 eq.) in 0.8 mL DMF for 2 min under argon atmosphere to yield a pale yellow solution. Then a mixture of 2-(pyridyldithio)-ethylamine hydrochloride, **7** (27.5 mg, 0.12 mmol, 1 eq.) and DIPEA (42.8 µL, 0.24 mmol, 2 eq.) in 2 mL DMF was added and the resulting solution stirred at RT under argon atmosphere until ESI-MS indicated complete consumtion of the starting material after 1 h. Then 5 mL EtOAc and 5 mL sat. aq. Na_2CO_3 were added and vigorously mixed. After phase separation, the aqueous layer was extracted with additional 5 mL EtOAc. The combined organic layers were extracted twice with 5 mL sat. aq. Na_2CO_3 and dried over Na_2SO_4. Volatile material was removed under reduced pressure to yield a yellow oil. This oil was immediately used for the following deprotection, otherwise the overall yield was very low. The oil was dissolved in 4 mL deprotection mixture (TFA/thioanisol/H_2O 92:6:2) and stirred under argon. The right reaction time of the deprotection step was crucial because apart from the deprotection a second reaction, (either a cleavage of the disulfide bond or a decomposition of the DOTA backbone) reducing the amount of desired product, could be observed. The reaction was followed by ESI-MS in order to monitor the signal intensity of the product peaks. In order to obtain comparable results the intensity of the product peak was normalised by the intensity of a peak at m/z 515 which is expected to be byproduct of the initial coupling reaction. After 6 h the intensity of the signals corresponding to the product started to reach a plateau and the reaction was interrupted by removal of the solvent under reduced pressure. The residue was dissolved in 10 mL H_2O and purified by HPLC. Eight different fractions were isolated thereof the fourth one eluting at 42 % organic phase

of contained the desired product. Organic solvent in the hplc fraction was removed under reduced pressure and the pH of the resulting aqueous solution was adjusted to 5.4 by the addition of ammonium acetate. The concentration of the product was determined by UV spectroscopy (ε_{280} =4232 M^{-1} cm^{-1}). Yield: 34.6 mg, 50.6 µmol, 42 %. $C_{31}H_{52}N_6O_7S_2$, **FW**: 684.91 g/mol, **ESI-MS**: m/z = 685.4 (100 % $[M+H]^+$, 343.3 (15 %, $[M+2H]^{2+}$), 707.3 (12 %, $[M+Na]^+$).

5.3.5 Synthesis for [Ln(M8-SPy)] complexes

The following complexation was carried out with different Lanthanide metals therefore a general synthesis protocol is given and the details for the different complexes are summarised in the table below. As ligands both, (*8S*) M8-SPy, synthesized as described above, and (*4R4S*)-M8-SPy, synthesized by Dr. Roché Walliser during his masters thesis[57] according an analogous synthesis, were used.

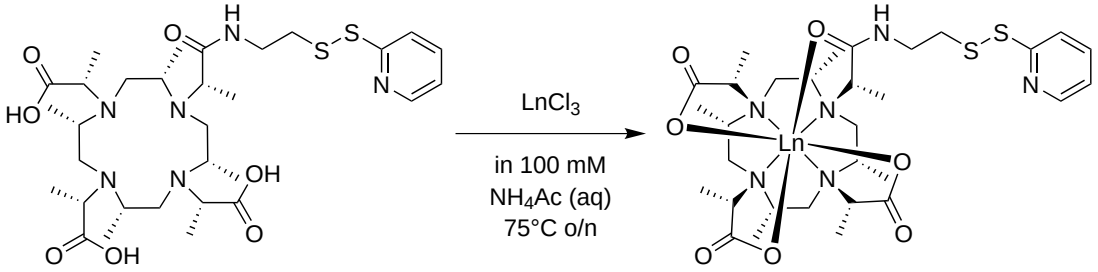

M8-SPy, 8 [Ln(M8-SPy)]

To an aqueous solution of M8-SPy, **9** (2 mM to 4 mM) and ammonium acetate (100 mM) three equivalents of the desired lanthanide chloride or lanthanide bromide were added. The mixture was stirred at 75 °C over night and completion of the reaction was confirmed by ESI-MS. The product was purified by HPLC where in the case of the (*8S*) ligand two different fractions could be isolated, one eluting at 39 % of the organic solvent and the second at 43 %, both showing the desired mass of the product in the ESI-MS spectrum. The ratio of the two fractions depends on the lanthanide metal. For Gd a ration of 8:2 was observed for the earlier to the later fraction, for Dy 6:4, for Tm 0.5:9.5 and for Lu only the second fraction was observable. When substituted to a protein no differences could be observed between the two fractions (both pro-

tein samples show exactly the same ^{15}N-HSQC spectrum). In the case of the (*4R4S*) ligand only one fraction was observed. The fractions containing the product were further purified using a single use Sep-Pak C18 column to yield the product as a glassy solid after removing the solvent under reduced pressure. For further use the product was dissolved in 1 mL H_2O, the concentration was determined by UV spectroscopy (ε_{280} =4232 M^{-1} cm^{-1}) and the solution was stored at −20 °C.

Table 5.4: Specific conditions for the complexation of M8-SPy using different lanthanide metals and analytic data

Product	**M8-SPy**	**Yield**	**ESI-MS**
	[mg]	**[mg] (%)**	***m/z* (rel. Int., [Assignment])**
LuM8-SPy (*8S*)	5	5.5 (88 %)	857.3 (100 % $[M+H]^+$), 858.3 (42 %), 859.3 (17 %), 860.4 (4 %), 861.4 (1 %), 429.2 (25 % $[M+2H]^{2+}$) [a]
TmM8-SPy (*8S*)	5	5.8 (93 %)	873.6 (100 % $[M+Na]^+$), 874.6 (36 %), 875.6 (12 %)
DyM8-SPy (*8S*)	10	7.5 (60 %)	868.4 (100 % $[M+Na]^+$), 867.4 (95 %), 866.4 (66 %), 865.4 (42 %), 869.4 (38 %), 870.4 (13 %), 864.4 (4 %), 871.4 (4 %), 846.4 (14 % $[M+H]^+$) [a], 884.3 (9 % $[M+K]^+$)[a]
GdM8-SPy (*8S*)	5	5.6 (91 %)	862.3 (100 % $[M+Na]^+$), 864.3 (72 %), 861.3 (66 %), 860.3 (63 %), 859.3 (37 %), 863.3 (33 %), 865.3 (23 %), 866.3 (7 %), 858.3 (4 %), 442.6 (23 % $[M+H+Na]^{2+}$]) [a]
GdM8-SPy (*4R4S*)	5	2.7 (44 %)	862.2 (100 % $[M+Na]^+$), 864.2 (67 %), 861.2 (64 %), 860.2 (64 %), 859.2 (33 %), 863.2 (32 %), 865.2 (18 %), 866.2 (8 %), 858.2 (2 %), 442.6 (13 % $[M+H+Na]^{2+}$) [a]

[a] Only the relative intensity of the main isotopomer is given, the intensity distribution of the corresponding isotopomers is the same as for the main species.

5.4 Protein tagging

The general protocol for the tagging of the protein with the individual LnM8-SPy compound is given in the following section. And the individual conditions for the different samples are listed afterwards.

5.4.1 General procedure for M8 tagging

2 mg to 5 mg of protein were dissolved in 200 µL to 500 µL of 10 mM PO_4^{3-} pH 6.8 to yield a 300 µM to 350 µM solution. The concentration was confirmed by UV absorption at 280 nm (ε_{280} =54 700 M^{-1} cm^{-1})[37]. 100 mM TCEP solution at neutral pH was added to obtain a final concentration of 1 mM TCEP. The sample was kept at 4 °C overnight. The full reduction of the protein was confirmed by ESI-MS (in the case of not complete reduction concentrations of up to 10 mM TCEP in the protein sample were successfully applied). The buffer was exchanged to 10 mM PO_4^{3-}, 100 µM TCEP pH 6.8 by ultrafiltration using 4 mL Amicon Ultrafiltration tubes (MW.co. 10 kDa) in 3 to 4 centrifugation steps. In each step the spinning time was adjusted that the sample volume did not decrease below 500 µL to avoid the aggregation of the protein. The TCEP concentration was further decreased using a PD MiniTrap G-25 desalting column and the protein was eluted directly into 3 eq. of the desired LnM8-SPy in aqueous solution (for the double cystein mutants 6 eq. of LnM8-SPy were used). To ensure complete tagging of the protein, the solution was kept under agitation at 4 °C overnight. The reaction was monitored with ESI-MS. The excess of LnM8-SPy was removed by ultrafiltration with 10 mM PO_4^{3-} pH 6.8 in 3 to 4 centrifugation steps to ensure that more than 99 % of the LnM8-SPy has been removed. Appart from the last step again the sample volume was not allowed to decrease below 500 µL. In the final step the sample volume was reduced to around 250 µL. The sample was removed and the centrifugation tube was washed 2 times to obtain a final volume of 280 µL. 5 % D_2O were added and the pH was adjusted to 6.80. The concentration was determined again by UV absorption and the sample was transferred into a shigemi NMR tube.

5.4.2 Specific conditions

Table 5.5: Specific conditions for the tagging of hCA-II with the corresponding LnM8-SPy complex.

Product	**Protein** [a] **[mg]**	**Concentration** [b] **[µM]**	**Yield [%]**	**ESI-MS [*m/z*]**
unif. ^{15}N hCA-II_S50C_C206S-GdM8 (*8S*)	2.2	200	74	30175
unif. ^{15}N hCA-II_S50C_C206S-DyM8 (*8S*)	3.8	120	20	30179
unif. ^{15}N hCA-II_S50C_C206S-TmM8 (*8S*)	3	90	25	30187
unif. ^{15}N hCA-II_S50C_C206S-LuM8 (*8S*)	2.2	180	67	30193
sel. ^{15}N-Leu hCA-II_S50C_C206S-DyM8 (*8S*)	6.4	620	79	29849
sel. ^{15}N-Leu hCA-II_S50C_C206S-TmM8 (*8S*)	5.8	560	79	29856
sel. ^{15}N-Leu hCA-II_S50C_C206S-LuM8 (*8S*)	6.0	550	75	29862
unif. ^{15}N hCA-II_S166C_C206S-GdM8 (*8S*)	2.4	230	79	30178
unif. ^{15}N hCA-II_S166C_C206S-DyM8 (*8S*)	2.4	220	76	30180
unif. ^{15}N hCA-II_S166C_C206S-TmM8 (*8S*)	3.9	320	68	30189
unif. ^{15}N hCA-II_S166C_C206S-LuM8 (*8S*)	2.6	210	68	30195
sel. ^{15}N-Leu hCA-II_S166C_C206S-TmM8 (*8S*)	2.1	230	78	29857
sel. ^{15}N-Leu hCA-II_S166C_C206S-LuM8 (*8S*)	2.9	240	67	29864
unif. ^{15}N hCA-II_S173C_C206S-TmM8 (*8S*)	5	340	56	30190
sel. ^{15}N-Leu hCA-II_S173C_C206S-TmM8 (*8S*)	4.1	440	87	29859
sel. ^{15}N-Leu hCA-II_S173C_C206S-LuM8 (*8S*)	6.1	520	70	29864
unif. ^{15}N hCA-II_S217C_C206S-GdM8 (*8S*)	2.3	210	75	30180
unif. ^{15}N hCA-II_S217C_C206S-DyM8 (*8S*)	2.3	240	86	30184
unif. ^{15}N hCA-II_S217C_C206S-TmM8 (*8S*)	3.4	280	68	30192
unif. ^{15}N hCA-II_S217C_C206S-LuM8 (*8S*)	2.0	200	82	30199
sel. ^{15}N-Leu hCA-II_S217C_C206S-TmM8 (*8S*)	3.5	240	60	29859

continued on next page ...

Product	**Protein** [a] **[mg]**	**Concentration** [b] **[μM]**	**Yield [%]**	**ESI-MS [*m/z*]**
sel. ^{15}N-Leu hCA-II_S217C_C206S-LuM8 (*8S*)	4.9	400	67	29864
unif. ^{15}N hCA-II_S220C_C206S-GdM8 (*8S*)	2.3	140	50	30179
unif. ^{15}N hCA-II_S220C_C206S-DyM8 (*8S*)	2.3	220	79	30182
unif. ^{15}N hCA-II_S220C_C206S-TmM8 (*8S*)	3.5	240	57	30190
unif. ^{15}N hCA-II_S220C_C206S-LuM8 (*8S*)	2.3	200	72	30195
sel. ^{15}N-Leu hCA-II_S220C_C206S-TmM8 (*8S*)	2.5	270	88	29857
sel. ^{15}N-Leu hCA-II_S220C_C206S-LuM8 (*8S*)	5.0	500	81	29863
unif. ^{15}N hCA-II_S50C_S166C_C206S-GdM8$_2$ (*8S*)	4.3	190	36	30922
unif. ^{15}N hCA-II_S50C_S217C_C206S-GdM8$_2$ (*8S*)	0.6	70 [c]	17	29975
unif. ^{15}N hCA-II_S50C_S220C_C206S-GdM8$_2$ (*8S*)	2.4	120	41	30979 [d]
unif. ^{15}N hCA-II_S166C_S217C_C206S-GdM8$_2$ (*8S*)	2.4	60	19	30979
unif. ^{2}H ^{13}C ^{15}N hCA-II_S50C_C206S-TmM8 (*8S*)	4.5	330	66	32952
unif. ^{2}H ^{13}C ^{15}N hCA-II_S50C_C206S-LuM8 (*8S*)	6.2	460	67	32902

[a] Initial amount of protein used for the reaction, [b] Final concentration of the NMR sample (Volume = 280 μL if not further specified), [c] Sample volume was 50 μL, [d] Second peak with 90 % intensity at *m/z*=30923 was observable.

5.5 hCA-II inhibitor complexes

The following inhibitors (see figure 5.1) were used to form hCA-II-Inhibitor complexes: *N*-(2,3-Difluorobenzyl)-4-sulfamoylbenzamide (**9**) abbreviated as F2-Inh, [(Cp*)Ir(2,6-difluoro-N-((4-(4-sulfamoylphenyl)pyridin-2-yl)methyl)benzenesulfonamide)Cl]Cl (**10**) abbreviated as F2-Complex and 2,2,5,5-tetramethyl-3-((4-sulfamoylphenyl)carbamoyl)-2,5-dihydro-1*H*-pyrrol-1-oxyl (**11**) abbreviated as NOX-Inh.

F2-Inh and F2-Complex were synthesized by Dr. Fabien W. Monnard, and are described in his PhD. thesis.[60] NOX-Inh was synthesized by Guido Grassi from the ETH

Zürich, Switzerland.

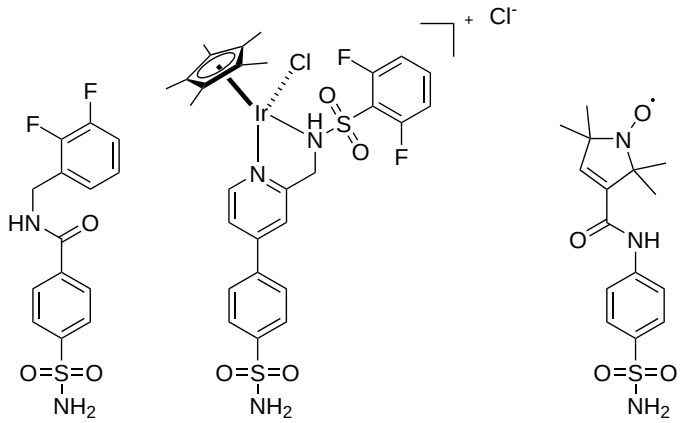

Figure 5.1: sulfonamide based inhibitors used for the preparation of hCA-II-inhibitor complexes.

5.5.1 F2-Inh ⊂ hCA-II

To a protein sample 1.1 eq. of F2-Inh (24 mM) dissolved in deuterated dimethyl sulfoxide (DMSO-D_6) were added and the sample was stirred well. The excess of inhibitor was removed by ultrafiltration using 4 mL Amicon ultrafiltration tubes (MW.co. 10 kDa). 2 µL of 100 µM TFA as internal standard for fluorine chemical shift and 5 % v/v D_2O were added and the pH was adjusted to 6.80.

5.5.2 F2-Complex ⊂ hCA-II

F2-Complex appeared to be poorly soluble in DMSO-D_6 unless it was acidified by bubbling HCl (g) through the solvent. A 27 mM stock solution was prepared which was stored at −20 °C. 1.1 eq. of F2-complex were added to a protein sample and excess of inhibitor was removed by ultrafiltration using 4 mL Amicon ultrafiltration tubes (MW.co. 10 kDa). 2 µL of 100 µM TFA as internal standard for fluorine chemical shift and 5 % v/v D_2O were added and the pH was adjusted to 6.80.

5.5.3 NOX-Inh ⊂ hCA-II

To a protein sample 1.1 eq. of F2-Inh (24 mM) dissolved in DMSO-D_6 were added ans the sample was stirred well. The excess of inhibitor was removed by ultrafiltration using 4 mL Amicon ultrafiltration tubes (MW.co. 10 kDa). After 3 cycles of ultrafiltration, addition of 5 % D_2O and pH adjustment to 6.80, the ^{15}N-HSQC spectrum showed that only 0.8 eq. of the inhibitor retained in the protein, indicated by a shift of a peak at 9.47 ppm in ^{1}H dimension and 119.1 ppm in ^{15}N dimension. This sample was concentrated to 200 µM if necessary using again Amicon ultrafiltration tubes but without further dilution before the run, to avoid further influence on the inhibitor concentration. Two samples were prepared from this solution, one with the given 0.8 eq. of the inhibitor and another with total 1.1 eq. of inhibitor. After addition of 50 % v/v glycerol these samples were used for EPR spectroscopy.

5.6 NMR experiments

A handwritten ^{1}H-^{15}N-HSQC experiment with selective pulses and gradients for water suppression was used for the characterisation of the protein samples and for the determination of the PCSs and PRE. A IPAP variant of the ^{15}N-HSQC experiment with additional ^{13}C decoupling during ^{15}N evolution was used for the determination of RDC. TROSY based HSQC experiments were used to record ^{1}H-^{15}N-HSQC spectra[82], as well as the determination of T_1[83], T_2[83] times andheteronuclear nuclear Overhauser effects (hetNOEs)[83,84]. For backbone assignment of triple labelled hCA-II_S50C_C206S-LuM8, TROSY based HNCO[85,86], HNCA[50], HNCOCA[85,86], HNCACO[85,86] and HNCACB[50] experiments were used. The parameters used for set up these experiments, as well as detail of the samples used, are given in tables 5.6 and 5.7. 1D ^{19}F experiments of hCA-II-Inhibitor complexes were recorded with an Offset of −135 ppm and a SW of 40 ppm for F2-Inh and with an Offset of −115 ppm and a SW of 100 ppm for F2-Complex. ^{1}H-^{19}F HOESY experiments were carried out with a mixing time of 0.5 s, a SW of 3.5 ppm in the indirect dimension, and a TD of 80 points in the indirect dimension using a standard pulsesequence delivered by Bruker.

Table 5.6: Parameters for the 2D NMR experiments.

Parameter		**^{15}N HSQC**	**IPAP ^{15}N HSQC**	**^{15}N TROSY**	**^{15}N TROSY T1** [a]	**^{15}N TROSY T2** [b]	**hetNOE**
NS		32 - 512	16 - 48	4	8	16	36
SW	F1	2000	2045	2270	2000	2000	2000
[Hz]	F2	10822	14423	12019	11261	10823	11261
Offset	F1	116.5	116.5	116.6	116.5	116.6	116.5
[ppm]	F2	4.7	4.69	4.74	4.74	4.74	4.7
TD	F1	200	600	256	256	256	512
[points]	F2	2048	2048	2048	2048	2048	2048
AQ	F1	50	147	56	64	64	128
[ms]	F2	95	71	85	91	91	91
Nucleus	F1	^{15}N	^{15}N	^{15}N	^{15}N	^{15}N	^{15}N
	F2	^{1}H	^{1}H	^{1}H	^{1}H	^{1}H	^{1}H

[a] Delays [ms] for T_1 time determination of individual experiments were set to 16, 40, 80, 400, 800, 1600, 3200, 6400, 8000, [b] Delays [ms] for T_2 time determination of individual experiments were set to 16, 32, 64, 128, 256.

Table 5.7: Parameters for the 3D NMR experiments used for backbone assignment of hCA-II_S50C_C206S

Parameter		**HNCO**	**HNCA**	**HNCOCA**	**HNCACO**	**HNCACB**
NS		8	16	32	32	36
SW	F1	2113	1947	5634	2113	1947
[Hz]	F2	2128	5585	1946	2270	10566
	F3	12019	11261	11261	11261	11261
Offset	F1	175	116.5	175	175	116.5
[ppm]	F2	116.5	56	116.5	116.5	45
	F3	4.74	4.74	4.74	4.74	4.74
TD	F1	80	80	88	88	80
[points]	F2	80	88	88	88	84
	F3	2048	2048	2048	2048	2048
AQ	F1	19	20	8	21	21
[ms]	F2	19	8	23	19	4
	F3	85	91	91	91	91
Nucleus	F1	13C	15N	13C	13C	15N
	F2	15N	13C	15N	15N	13C
	F3	1H	1H	1H	1H	1H

5.7 Tensor and PCS position determination

For reproducibility of the tensors determined in Numbat[18], the following random seed numbers were used for every tensor of a specific protein mutant: hCA-II_S50C_C206S: 301, hCA-II_S166C_C206S: 840, hCA-II_S217C_C206S: 129 and hCA-II_S220C_C206S: 615. For the position calculation, based on PCS, in Matlab[63] the seed of the random number generator was set to 688 for every position determination.

Bibliography

1. HESSE, M., H. MEIER, and B. ZEEH: *Spectroskopische Methoden in der organischen Chemie*. 7. Auflage. Thieme, 2005 (cit. on p. 1).
2. WÜTHRICH, K.: 'The way to NMR structures of proteins'. *Nat. Struct. Biol.* (2001), vol. 8(11): pp. 923–925 (cit. on p. 1).
3. GÖBL, C., T. MADL, B. SIMON, and M. SATTLER: 'NMR approaches for structural analysis of multidomain proteins and complexes in solution'. *Prog. Nucl. Magn. Reson. Spectrosc.* (2014), vol. 80: pp. 26–63 (cit. on pp. 1, 2).
4. KENDREW, J. C., G. BODO, H. M. DINTZIS, R. G. PARRISH, H. WYCKOFF, and D. C. PHILLIPS: 'A Three-Dimensional Model of the Myoglobin Molecule Obtained by X-Ray Analysis'. *Nature* (1958), vol. 181: pp. 662–666 (cit. on p. 1).
5. BERMAN, H. M., J. WESTBROOK, Z. FENG, G. GILLILAND, T. N. BHAT, H. WEISSIG, I. N. SHINDYALOV, and P. E. BOURNE: 'The Protein Data Bank'. *Nucleic Acids Res.* (2000), vol. 28(1): pp. 235–242 (cit. on pp. 1, 81).
6. OHKI, S. and M. KAINOSHO: 'Stable isotope labeling methods for protein NMR spectroscopy'. *Prog. Nucl. Magn. Reson. Spectrosc.* (2008), vol. 53(4): pp. 208–226 (cit. on p. 2).
7. NIETLISPACH, D., R. T. CLOWES, R. W. BROADHURST, Y. ITO, J. KEELER, M. KELLY, J. ASHURST, H. OSCHKINAT, P. J. DOMAILLE, and E. D. LAUE: 'An Approach to the Structure Determination of Larger Proteins Using Triple Resonance NMR Experiments in Conjunction with Random Fractional Deuteration'. *J. Am. Chem. Soc.* (1996), vol. 118(2): pp. 407–415 (cit. on p. 2).

8. MILO, R and R. PHILLIPS: *Cell Biology by the Numbers*. 1st. GS Garland Science, 2015 (cit. on p. 2).

9. JACKSON, J. A., J. F. LEMONS, and H. TAUBE: 'Nuclear Magnetic Resonance Studies on Hydration of Cations'. *The Journal of Chemical Physics* (1960), vol. 32(2): pp. 553–555 (cit. on p. 2).

10. DWEK, R. A., R. E. RICHARDS, K. G. MORALLEE, E. NIEBOER, R. J. P. WILLIAMS, and A. V. XAVIER: 'The Lanthanide Cations as Probes in Biological Systems'. *Eur. J. Biochem.* (1971), vol. 21(2): pp. 204–209 (cit. on p. 2).

11. CLORE, G. M. and J. IWAHARA: 'Theory, Practice, and Applications of Paramagnetic Relaxation Enhancement for the Characterization of Transient Low-Population States of Biological Macromolecules and Their Complexes'. *Chem. Rev.* (2009), vol. 109(9): pp. 4108–4139 (cit. on p. 3).

12. KEIZERS, P. H., A. SARAGLIADIS, Y. HIRUMA, M. OVERHAND, and M. UBBINK: 'Design, Synthesis, and Evaluation of a Lanthanide Chelating Protein Probe: CLaNP-5 Yields Predictable Paramagnetic Effects Independent of Environment'. *J. Am. Chem. Soc.* (2008), vol. 130(44): pp. 14802–14812 (cit. on p. 3).

13. OTTING, G.: 'Protein NMR Using Paramagnetic Ions'. *Annu. Rev. Biophys.* (2010), vol. 39(1): pp. 387–405 (cit. on p. 3).

14. BERTINI, I., C. LUCHINAT, and G. PARIGI: 'Magnetic susceptibility in paramagnetic NMR'. *Prog. Nucl. Magn. Reson. Spectrosc.* (2002), vol. 40(3): pp. 249–273 (cit. on pp. 3, 4, 76).

15. HASS, M. AS and M. UBBINK: 'Structure determination of protein-protein complexes with long-range anisotropic paramagnetic NMR restraints'. *Curr. Opin. Struct. Biol.* (2014), vol. 24(0): pp. 45–53 (cit. on p. 3).

16. RINALDELLI, M., A. CARLON, E. RAVERA, G. PARIGI, and C. LUCHINAT: 'FANTEN: a new web-based interface for the analysis of magnetic anisotropy-induced NMR data'. English. *J. Biomol. NMR* (2015), vol. 61(1): pp. 21–34 (cit. on pp. 4, 76, 77).

17. PRESTEGARD, J. H., C. M. BOUGAULT, and A. I. KISHORE: 'Residual Dipolar Couplings in Structure Determination of Biomolecules'. *Chem. Rev.* (2004), vol. 104(8): pp. 3519–3540 (cit. on p. 5).

18. SCHMITZ, C., M. J. STANTON-COOK, X. SU, G. OTTING, and T. HUBER: 'Numbat: an interactive software tool for fitting Chi-tensors to molecular coordinates using pseudocontact shifts'. English. *J. Biomol. NMR* (2008), vol. 41(3): pp. 179–189 (cit. on pp. 5, 25, 30, 49, 70, 71, 93, 133).

19. CORNILESCU, G. and A. BAX: 'Measurement of Proton, Nitrogen, and Carbonyl Chemical Shielding Anisotropies in a Protein Dissolved in a Dilute Liquid Crystalline Phase'. *J. Am. Chem. Soc.* (2000), vol. 122(41): pp. 10143–10154 (cit. on pp. 5, 71, 96).

20. JOHN, M., A. Y. PARK, G. PINTACUDA, N. E. DIXON, and G. OTTING: 'Weak Alignment of Paramagnetic Proteins Warrants Correction for Residual CSA Effects in Measurements of Pseudocontact Shifts'. *J. Am. Chem. Soc.* (2005), vol. 127(49): pp. 17190–17191 (cit. on pp. 5, 30, 97).

21. GOCHIN, M. and H. RODER: 'Protein structure refinement based on paramagnetic NMR shifts: Applications to wild-type and mutant forms of cytochrome c'. *Protein Sci.* (1995), vol. 4(2): pp. 296–305 (cit. on p. 5).

22. ALLEGROZZI, M., I. BERTINI, M. B. L. JANIK, Y. LEE, G. LIU, and C.< LUCHINAT: 'Lanthanide-Induced Pseudocontact Shifts for Solution Structure Refinements of Macromolecules in Shells up to 40 Å from the Metal Ion'. *J. Am. Chem. Soc.* (2000), vol. 122(17): pp. 4154–4161 (cit. on p. 5).

23. BERTINI, I., M. B. L. JANIK, Y. LEE, C. LUCHINAT, and A. ROSATO: 'Magnetic Susceptibility Tensor Anisotropies for a Lanthanide Ion Series in a Fixed Protein Matrix'. *J. Am. Chem. Soc.* (2001), vol. 123(18): pp. 4181–4188 (cit. on pp. 5, 49, 87).

24. ZHENG, L., U. BAUMANN, and J.-L. REYMOND: 'An efficient one-step site-directed and site-saturation mutagenesis protocol'. *Nucleic Acids Res.* (2004), vol. 32(14): e115 (cit. on pp. 5, 17, 110).

25. RODRIGUEZ-CASTAÑDA, F., P. HABERZ, A. LEONOV, and C. GRIESINGER: 'Paramagnetic tagging of diamagnetic proteins for solution NMR'. *Magn. Reson. Chem.* (2006), vol. 44(S1): S10–S16 (cit. on p. 6).

26. ROCKLAGE, S. M. and A. D. WATSON: 'Chelates of gadolinium and dysprosium as contrast agents for MR imaging'. *J. Magn. Reson. Imaging* (1993), vol. 3(1): pp. 167–178 (cit. on p. 6).

27. KEIZERS, P. H., J. F. DESREUX, M. OVERHAND, and M. UBBINK: 'Increased Paramagnetic Effect of a Lanthanide Protein Probe by Two-Point Attachment'. *J. Am. Chem. Soc.* (2007), vol. 129(30): pp. 9292–9293 (cit. on pp. 6, 82).

28. HÄUSSINGER, D., J. HUANG, and S. GRZESIEK: 'DOTA-M8: An Extremely Rigid, High-Affinity Lanthanide Chelating Tag for PCS NMR Spectroscopy'. *J. Am. Chem. Soc.* (Oct. 2009), vol. 131(41): pp. 14761–14767 (cit. on pp. 6, 11, 13, 27, 77, 80, 83, 84, 86, 121).

29. AIME, S., M. BOTTA, M. FASANO, MARQUES M. P. M., C. F. G. C. GERALDES, D. PUBANZ, and A. E. MERBACH: 'Conformational and Coordination Equilibria on DOTA Complexes of Lanthanide Metal Ions in Aqueous Solution Studied by 1H-NMR Spectroscopy'. *Inorg. Chem.* (1997), vol. 36(10): pp. 2059–2068 (cit. on p. 6).

30. YAGI, H., K. B. PILLA, A. MALECKIS, B. GRAHAM, T. HUBER, and G. OTTING: 'Three-Dimensional Protein Fold Determination from Backbone Amide Pseudocontact Shifts Generated by Lanthanide Tags at Multiple Sites'. *Structure* (2013), vol. 21(6): pp. 883–890 (cit. on pp. 9, 49, 91, 102).

31. YU, F., V. M. CANGELOSI, M. L. ZASTROW, M. TEGONI, J. S. PLEGARIA, A. G. TEBO, C. S. MOCNY, L. RUCKTHONG, H. QAYYUM, and V. L. PECORARO: 'Protein Design: Toward Functional Metalloenzymes'. *Chem. Rev.* (2014), vol. 114(7): pp. 3495–3578 (cit. on p. 10).

32. WARD, T. R.: 'Artificial Metalloenzymes Based on the Biotin-Avidin Technology: Enantioselective Catalysis and Beyond'. *Acc. Chem. Res.* (2011), vol. 44(1): pp. 47–57 (cit. on p. 10).

33. KÖHLER, V., Y. M. WILSON, M. DÜRRENBERGER, D. GHISLIERI, E. CHURAKOVA, T. QUINTO, L. KNÖRR, D. HÄUSSINGER, F. HOLLMANN, N. J. TURNER, and T. R. WARD: 'Synthetic cascades are enabled by combining biocatalysts with artificial metalloenzymes'. *Nat Chem* (2013), vol. 5(2): pp. 93–99 (cit. on p. 10).

34. MONNARD, F. W., T. HEINISCH, E. S. NOGUEIRA, T. SCHIRMER, and T. R. WARD: 'Human Carbonic Anhydrase II as a host for piano-stool complexes bearing a sulfonamide anchor'. *Chem. Commun.* (29 2011), vol. 47: pp. 8238–8240 (cit. on p. 10).

35. MONNARD, F. W., E. S. NOGUEIRA, T. HEINISCH, T. SCHIRMER, and T. R. WARD: 'Human carbonic anhydrase II as host protein for the creation of artificial metalloenzymes: the asymmetric transfer hydrogenation of imines'. *Chem. Sci.* (8 2013), vol. 4: pp. 3269–3274 (cit. on pp. 10, 68).

36. HEINISCH, T., M. PELLIZZONI, M. DÜRRENBERGER, C. E. TINBERG, V. KÖHLER, J. KLEHR, D. HÄUSSINGER, D. BAKER, and T. R. WARD: 'Improving the Catalytic Performance of an Artificial Metalloenzyme by Computational Design'. *J. Am. Chem. Soc.* (2015), vol. 137(32): pp. 10414–10419 (cit. on pp. 10, 96).

37. KRISHNAMURTHY, V. M., G. K. KAUFMAN, A. R. URBACH, I. GITLIN, K. L. GUDIKSEN, D. B. WEIBEL, and G. M. WHITESIDES: 'Carbonic Anhydrase as a Model for Biophysical and Physical-Organic Studies of Proteins and Protein-Ligand Binding'. *Chem. Rev.* (2008), vol. 108(3): pp. 946–1051 (cit. on pp. 11, 18, 57, 83, 89, 93, 121, 127).

38. WANG, J., M. SÁNCHEZ-ROSELLÓ, J. L. ACEÑA, C. del POZO, A. E. SOROCHINSKY, S. FUSTERO, V. A. SOLOSHONOK, and H. LIU: 'Fluorine in Pharmaceutical Industry: Fluorine-Containing Drugs Introduced to the Market in the Last Decade (2001-2011)'. *Chem. Rev.* (2014), vol. 114(4): pp. 2432–2506 (cit. on pp. 11, 103).

39. PEREIRA NOGUEIRA, E. S.: 'Novel apapproach for the creation of artificial metalloenzymes'. PhD thesis. University of Basel, Faculty of Science, 2013 (cit. on pp. 13, 109).

40. HENDERSON, L. E., D. HENRIKSSON, and P. O. NYMAN: 'Primary structure of human carbonic anhydrase C.' *J. Biol. Chem.* (1976), vol. 251(18): pp. 5457–5463 (cit. on pp. 13, 109).

41. OPINA, A. C. L., M. STRICKLAND, Y. LEE, N. TJANDRA, A. R. BYRD, R. E. SWENSON, and O. VASALATIY: 'Analysis of the isomer ratios of polymethylated-DOTA complexes and the implications on protein structural studies'. *Dalton Trans.* (11 2016), vol. 45: pp. 4673–4687 (cit. on pp. 15, 85).

42. MAARTENSSON, L. G., B. H. JONSSON, P. O. FRESKGAARD, A. KIHLGREN, M. SVENSSON, and U. CARLSSON: 'Characterization of folding intermediates of human carbonic anhydrase II: probing substructure by chemical labeling of sulfhydryl groups introduced by site-directed mutagenesis'. *Biochemistry* (1993), vol. 32(1): pp. 224–231 (cit. on p. 15).

43. KREBS, J. F. and C. A. FIERKE: 'Determinants of catalytic activity and stability of carbonic anhydrase II as revealed by random mutagenesis.' *J. Biol. Chem.* (1993), vol. 268(2): pp. 948–954 (cit. on p. 15).

44. NAIR, S. K., T. L. CALDERONE, D. W. CHRISTIANSON, and C. A. FIERKE: 'Altering the mouth of a hydrophobic pocket. Structure and kinetics of human carbonic anhydrase II mutants at residue Val-121.' *J. Biol. Chem.* (1991), vol. 266(26): pp. 17320–17325 (cit. on pp. 17, 109).

45. MURAKAMI, H., G. P. MARELICH, J. H. GRUBB, J. W. KYLE, and W. S. SLY: 'Cloning, expression, and sequence homologies of cDNA for human carbonic anhydrase II'. *Genomics* (1987), vol. 1(2): pp. 159–166 (cit. on pp. 17, 109).

46. ROSENBERG, A. H., B. N. LADE, C. DAO-SHAN, S. LIN, J. J. DUNN, and F. W. STUDIER: 'Vectors for selective expression of cloned DNAs by T7 RNA polymerase'. *Gene* (1987), vol. 56(1): pp. 125–135 (cit. on pp. 17, 109).

47. STUDIER, F. W. and B. A. MOFFATT: 'Use of bacteriophage T7 RNA polymerase to direct selective high-level expression of cloned genes'. *J. Mol. Biol.* (1986), vol. 189(1): pp. 113–130 (cit. on pp. 17, 109).

48. VENTERS, R. A., B. T. FARMER II, C. A. FIERKE, and L. D. SPICER: 'Characterizing the Use of Perdeuteration in NMR Studies of Large Proteins:13C,15N and 1H Assignments of Human Carbonic Anhydrase II'. *J. Mol. Biol.* (1996), vol. 264(5): pp. 1101–1116 (cit. on pp. 18, 87).

49. CARLSSON, U., L. E. HENDERSON, and S. LINDSKOG: 'Denaturation and reactivation of human carbonic anhydrases in guanidine hydrochloride and urea'. *Biochimica et Biophysica Acta (BBA) - Protein Structure* (1973), vol. 310(2): pp. 376–387 (cit. on pp. 22, 88).

50. SALZMANN, M., G. WIDER, K. PERVUSHIN, H. SENN, and K. WÜTHRICH: 'TROSY-type Triple-Resonance Experiments for Sequential NMR Assignments of Large Proteins'. *J. Am. Chem. Soc.* (1999), vol. 121(4): pp. 844–848 (cit. on pp. 23, 131).

51. LI, Y., A. ROY, and Y. ZHANG: 'HAAD: A Quick Algorithm for Accurate Prediction of Hydrogen Atoms in Protein Structures'. *PLoS One* (Aug. 2009), vol. 4(8): e6701 (cit. on p. 24).

52. PELLECCHIA, M., D. S. SEM, and K. WÜTHRICH: 'Nmr in drug discovery'. *Nat. Rev. Drug Discovery* (2002), vol. 1(3): pp. 211–209 (cit. on p. 37).

53. SAIO, T., K. OGURA, H. KUMETA, Y. KOBASHIGAWA, K. SHIMIZU, M. YOKOCHI, K. KODAMA, H. YAMAGUCHI, H. TSUJISHITA, and F. INAGAKI: 'Ligand-driven conformational changes of MurD visualized by paramagnetic NMR'. *Sci. Rep.* (2015), vol. (cit. on p. 49).

54. CRICK, D. J., J. X. WANG, B. GRAHAM, J. D. SWARBRICK, H. R. MOTT, and D. NIETLISPACH: 'Integral membrane protein structure determination using pseudo-contact shifts'. *J. Biomol. NMR* (2015), vol. 61(3): pp. 197–207 (cit. on pp. 49, 91, 98).

55. BERTINI, I., C. DEL BIANCO, I. GELIS, N. KATSAROS, C. LUCHINAT, G. PARIGI, M. PEANA, A. PROVENZANI, and M. A. ZORODDU: 'Experimentally exploring the conformational space sampled by domain reorientation in calmodulin'. *Proc. Natl. Acad. Sci. U. S. A.* (2004), vol. 101(18): pp. 6841–6846 (cit. on p. 49).

56. SCHMITZ, C., M. JOHN, A. Y. PARK, N. E. DIXON, G. OTTING, G. PINTACUDA, and T. HUBER: 'Efficient (CHI) tensor determination and NH assignment of paramagnetic proteins'. English. *J. Biomol. NMR* (2006), vol. 35(2): pp. 79–87 (cit. on p. 49).

57. WALLISER, R. M.: 'PCS NMR-Spectroscopy on a Series of Lanthanide derivatives of DOTA-M8'. MA thesis. University of Basel, 2012 (cit. on pp. 54, 85, 125).

58. OTTING, G.: 'Prospects for lanthanides in structural biology by NMR'. English. *J. Biomol. NMR* (2008), vol. 42(1): pp. 1–9 (cit. on pp. 55, 80, 86).

59. KIM, C., J. S. CHANG, J. B. DOYON, T. T. BAIRD JR., C. A. FIERKE, A. JAIN, and D. W. CHRISTIANSON: 'Contribution of Fluorine to Protein-Ligand Affinity in the Binding of Fluoroaromatic Inhibitors to Carbonic Anhydrase II'. *J. Am. Chem. Soc.* (2000), vol. 122(49): pp. 12125–12134 (cit. on pp. 57, 96).

60. MONNARD, F. W.: 'Human Carbonic Anhydrase II: a Novel Scaffold for Artificial Metalloenzymes'. PhD thesis. University of Basel, 2013 (cit. on pp. 57, 129).

61. DOYON, J. B., E. A. M. HANSEN, C KIM, J. S. CHANG, D. W. CHRISTIANSON, R. D. MADDER, J. G. VOET, T. A. BAIRD JR, C. A. FIERKE, and A. JAIN: 'Linear Free Energy Relationships Implicate Three Modes of Binding for Fluoroaromatic Inhibitors to a Mutant of Carbonic Anhydrase II'. *Org. Lett.* (2000), vol. 2(9): pp. 1189–1192 (cit. on p. 58).

62. DOYON, J. B., E. A. M. HANSEN, C. KIM, J. S. CHANG, D. W. CHRISTIANSON, R. D. MADDER, J. G. VOET, T. A. BAIRD JR, C. A. FIERKE, and A. JAIN: 'Linear Free Energy Relationships Implicate Three Modes of Binding for Fluoroaromatic Inhibitors to a Mutant of Carbonic Anhydrase II'. *Org. Lett.* (2000), vol. 2(16): pp. 2557–2558 (cit. on p. 58).

63. *MATLAB version 8.5.0.197613 (R2015a)*. The Mathworks, Inc. Natick, Massachusetts, 2015 (cit. on pp. 64, 133).

64. RABER, H. and M. MEHRING: '19F Chemical shift tensor in fluorobenzene compounds'. *Chem. Phys.* (1977), vol. 26(1): pp. 123–130 (cit. on pp. 71, 96).

65. DÜRR, U. H. N., S. L. GRAGE, R. WITTER, and A. S. ULRICH: 'Solid state 19F NMR parameters of fluorine-labeled amino acids. Part I: Aromatic substituents'. *J. Magn. Reson.* (2008), vol. 191(1): pp. 7–15 (cit. on pp. 71, 96).

66. ULRICH, E. L. et al.: 'BioMagResBank'. *Nucleic Acids Res.* (2008), vol. 36(suppl 1): pp. D402–D408 (cit. on p. 75).

67. KOEHLER, J. and J. MEILER: 'Expanding the utility of NMR restraints with paramagnetic compounds: Background and practical aspects'. *Prog. Nucl. Magn. Reson. Spectrosc.* (2011), vol. 59(4): pp. 360–389 (cit. on pp. 76, 98).

68. OTTIGER, M., F. DELAGLIO, and A. BAX: 'Measurement of J and Dipolar Couplings from Simplified Two-Dimensional NMR Spectra'. *J. Magn. Reson.* (1998), vol. 131(2): pp. 373–378 (cit. on p. 76).

69. KEIZERS, P. H. and M. UBBINK: 'Paramagnetic tagging for protein structure and dynamics analysis'. *Prog. Nucl. Magn. Reson. Spectrosc.* (2011), vol. 58(1-2): pp. 88–96 (cit. on p. 77).

70. PINTACUDA, G., M. A. KENIRY, T. HUBER, A. Y. PARK, N. E. DIXON, and G. OTTING: 'Fast Structure-Based Assignment of 15N HSQC Spectra of Selectively 15N-Labeled Paramagnetic Proteins'. *J. Am. Chem. Soc.* (2004), vol. 126(9): pp. 2963–2970 (cit. on p. 77).

71. PETERS, F., M. MAESTRE-MARTINEZ, A. LEONOV, L. KOVAČIČ, S. BECKER, R. BOELENS, and C. GRIESINGER: 'Cys-Ph-TAHA: a lanthanide binding tag for RDC and PCS enhanced protein NMR'. *J. Biomol. NMR* (2011), vol. 51(3): pp. 329–337 (cit. on p. 77).

72. MICHALCZYK, R., C. J. UNKEFER, J. BACIK, T. E. SCHRADER, A. OSTERMANN, A. Y. KOVALEVSKY, R. MCKENNA, and S. Z. FISHER: 'Joint neutron crystallographic and NMR solution studies of Tyr residue ionization and hydrogen bonding: Implications for enzyme-mediated proton transfer'. *Proceedings of the National Academy of Sciences* (2015), vol. 112(18): pp. 5673–5678 (cit. on p. 81).

73. CLEMENTE-JUAN, J. M., E. CORONADO, and A. GAITA-ARIÑO: *Lanthanide and Actinides in Molecular Magnetism*. Ed. by LAYFIELD, R. A. and M. MURUGESU. 1. edition. Wiley-VCH, 2015 (cit. on p. 86).

74. HIRUMA, Y., M. A.S. HASS, Y. KIKUI, W. LIU, B. ÖLMEZ, S. P. SKINNER, A. BLOK, A. KLOOSTERMAN, H. KOTEISHI, F. LÖHR, H. SCHWALBE, M. NOJIRI, and M. UBBINK: 'The Structure of the Cytochrome P450cam-Putidaredoxin Complex Determined by Paramagnetic NMR Spectroscopy and Crystallography'. *J. Mol. Biol.* (2013), vol. 425(22): pp. 4353–4365 (cit. on p. 91).

75. BANCI, L., I. BERTINI, G. CAVALLARO, A. GIACHETTI, C. LUCHINAT, and G. PARIGI: 'Paramagnetism-Based Restraints for Xplor-NIH'. *J. Biomol. NMR* (2004), vol. 28(3): pp. 249–261 (cit. on p. 91).

76. SKINNER, S. P., M. MOSHEV, M. A. S. HASS, and M. UBBINK: 'PARAssign—paramagnetic NMR assignments of protein nuclei on the basis of pseudocontact shifts'. *J. Biomol. NMR* (2013), vol. 55(4): pp. 379–389 (cit. on p. 91).

77. CAVANAGH, J., W. J. FAIRBROTHER, A. G. PALLMER III, M. RANCE, and N. J. SKELTON: *Protein NMR Spectroscopy*. second edition. Elsevier Academic Press, 2007 (cit. on p. 96).

78. BERTINI, I., I. C. FELLI, and C. LUCHINAT: 'High Magnetic Field Consequences on the NMR Hyperfine Shifts in Solution'. *J. Magn. Reson.* (1998), vol. 134(2): pp. 360–364 (cit. on p. 97).

79. ZHOU, Y., J. WANG, Z. GU, S. WANG, W. ZHU, J. L. ACEÑA, V. A. SOLOSHONOK, K. IZAWA, and H. LIU: 'Next Generation of Fluorine-Containing Pharmaceuticals, Compounds Currently in Phase II-III Clinical Trials of Major Pharmaceutical Companies: New Structural Trends and Therapeutic Areas'. *Chem. Rev.* (2016), vol. 116(2): pp. 422–518 (cit. on p. 103).

80. EBRIGHT, Y. W., Y. CHEN, P. S. PENDERGRAST, and R. H. EBRIGHT: 'Incorporation of an EDTA-metal complex at a rationally selected site within a protein: application to EDTA-iron DNA affinity cleaving with catabolite gene activator protein (CAP) and Cro'. *Biochemistry* (1992), vol. 31(44): pp. 10664–10670 (cit. on p. 105).

81. KIBBE, W. A.: 'OligoCalc: an online oligonucleotide properties calculator'. *Nucleic Acids Res.* (2007), vol. 35(suppl 2): W43–W46 (cit. on p. 110).

82. PERVUSHIN, K., R. RIEK, G. WIDER, and K. WÜTHRICH: 'Attenuated T2 relaxation by mutual cancellation of dipole-dipole coupling and chemical shift anisotropy indicates an avenue to NMR structures of very large biological macromolecules in solution'. *Proc. Natl. Acad. Sci. U. S. A.* (1997), vol. 94(23): pp. 12366–12371 (cit. on p. 131).

83. ZHU, G., Y. XIA, L. K. NICHOLSON, and K. H. SZE: 'Protein Dynamics Measurements by TROSY-Based NMR Experiments'. *J. Magn. Reson.* (2000), vol. 143(2): pp. 423–426 (cit. on p. 131).

84. RENNER, C., M. SCHLEICHER, L. MORODER, and T. A. HOLAK: 'Practical aspects of the 2D 15N-{1H}-NOE experiment'. English. *J. Biomol. NMR* (2002), vol. 23(1): pp. 23–33 (cit. on p. 131).

85. SALZMANN, M., K. PERVUSHIN, G. WIDER, H. SENN, and K. WÜTHRICH: 'TROSY in triple-resonance experiments: New perspectives for sequential NMR assignment of large proteins'. *Proceedings of the National Academy of Sciences* (1998), vol. 95(23): pp. 13585–13590 (cit. on p. 131).

86. SALZMANN, M., G. WIDER, K. PERVUSHIN, and K. WÜTHRICH: 'Improved sensitivity and coherence selection for [15N,1H]-TROSY elements in triple resonance experiments'. English. *J. Biomol. NMR* (1999), vol. 15(2): pp. 181–184 (cit. on p. 131).

List of Figures

List of Tables

APPENDIX A

Tabels and figures

A.1 Backbone assignment

Table A.1: Backbone chemical shifts of hCA-II_S50C_C206S-LuM8. All values are given in ppm.

Residue	HN	N	CO	Cα	Cβ	Residue	HN	N	CO	Cα	Cβ
P21[a]	N/A	…	175.7	62.2	28.0	A142	8.77	123.9	173.7	47.9	18.5
I22	7.92	121.1	171.7	58.0	35.4	V143	7.16	124.8	170.2	56.7	28.1
A23	8.55	123.3	176.8	50.4	15.6	L144	8.35	128.7	170.2	49.7	41.3
K24	7.07	115.3	173.6	52.0	27.8	G145	9.80	114.7	168.0	40.8	N/A
G25	8.17	109.3	171.5	41.9	N/A	I146	9.02	124.7	182.0	56.0	39.2
E26	9.24	118.2	173.6	53.7	27.3	F147	9.99	129.3	172.0	55.1	36.6
R27	8.71	122.0	172.6	50.2	27.9	L148	8.10	120.7	172.3	52.1	39.4
Q28	7.58	115.9	175.2	52.2	28.6	K149	8.85	119.8	171.8	49.8	32.7
S29	7.94	118.3	181.8	54.2	60.5	V150	8.32	121.8	175.2	59.4	27.9
P30	N/A	…	170.2	59.0	29.7	G151	8.97	118.5	169.9	43.7	N/A
V31	6.14	107.5	171.0	56.0	32.2	S152	8.22	125.0	170.1	55.5	60.5
D32	8.19	118.7	172.0	50.2	39.1	A153	8.24	121.5	174.8	49.3	15.6
I33	8.59	129.0	170.2	58.0	33.6	K154	8.59	124.4	174.0	48.5	29.0
D34	7.40	128.7	175.4	49.2	38.0	P155	N/A	…	…	…	…
T35	10.15	122.7	174.4	62.2	65.8	G156	…	…	…	…	N/A
H36	8.67	119.3	173.7	54.7	25.5	L157	7.42	117.3	175.3	50.6	40.5
T37	7.51	109.2	172.5	58.7	66.6	Q158	7.65	122.8	173.7	56.2	24.5
A38	7.34	128.0	173.7	49.3	14.4	K159	8.71	116.3	176.7	56.4	30.0
K39	7.98	123.1	174.0	51.8	30.8	V160	6.89	113.6	173.5	61.5	28.3
Y40	8.57	127.1	172.2	53.9	34.3	V161	7.15	114.8	175.6	62.5	27.8
D41	7.61	129.4	171.3	46.0	39.3	D162	8.26	117.9	174.7	53.6	37.4
P42	N/A	…	173.9	59.7	28.2	V163	7.00	114.5	174.7	58.0	29.8
S43	8.35	115.6	172.7	56.2	60.7	L164	6.92	122.1	175.9	54.3	36.2
L44	6.86	123.5	174.6	52.1	37.2	D165	8.08	116.6	175.3	53.7	36.7
K45	7.42	123.6	172.0	51.2	28.0	S166	7.85	114.0	171.9	57.0	60.9
P46	N/A	…	175.1	60.0	28.0	I167	7.27	117.0	171.7	55.8	34.5
L47	8.84	127.0	173.1	52.0	39.9	K168	7.25	117.9	173.0	57.4	30.0
S48	8.45	122.0	168.8	54.2	60.3	T169	6.44	99.6	171.4	55.3	68.3
V49	8.13	126.7	172.7	58.1	27.8	K170	7.34	121.0	175.0	54.8	28.1

[a] Residues 1 to 20 were not assigned.

continued on next page …

Table A.1 – continued from previous page

Residue	HN	N	CO	Cα	Cβ	Residue	HN	N	CO	Cα	Cβ
S50	8.38	127.4	172.0	50.1	36.4	G171	8.74	117.3	172.2	41.4	N/A
Y51	8.73	123.9	174.0	49.8	35.2	K172	7.68	120.7	172.3	53.0	30.0
D52	8.61	122.2	173.9	55.0	37.2	S173	8.21	114.2	170.2	53.6	63.8
Q53	7.93	114.9	172.4	51.4	25.1	A174	8.90	123.9	173.5	47.9	18.3
A54	7.26	120.6	175.3	50.4	15.9	D175	8.48	122.4	173.1	52.8	37.8
T55	9.26	121.1	170.4	57.6	68.7	F176	7.88	125.8	170.7	54.7	36.1
S56	9.88	127.0	170.8	55.9	60.6	T177	7.97	115.4	171.8	57.3	68.0
L57	8.81	118.0	175.4	52.5	42.0	N178	9.58	115.9	171.5	51.4	33.9
R58	7.07	115.3	169.0	52.0	30.3	F179	8.14	119.4	171.9	55.3	37.6
I59	8.91	122.6	169.7	54.7	38.2	D180	7.89	128.6	173.2	46.6	37.9
L60	8.56	124.1	172.1	51.2	41.6	P181	N/A	…	174.2	60.9	27.7
N61	8.31	121.5	173.8	48.8	35.5	R182	8.19	118.7	176.4	56.2	25.7
N62	7.90	123.7	174.1	48.4	35.3	G183	7.16	103.3	171.2	42.8	N/A
G63	9.56	109.7	170.2	42.1	N/A	L184	7.10	117.8	170.5	50.6	38.1
H64	…	…	…	…	…	L185	6.49	113.6	174.1	49.7	37.7
A65	8.46	123.9	172.6	49.0	16.5	P186	N/A	…	171.9	59.0	28.7
F66	7.07	110.5	171.2	52.0	38.5	E187	8.03	116.9	174.2	55.4	26.3
N67	8.85	121.2	172.4	47.3	36.6	S188	7.50	111.9	173.0	53.5	61.0
V68	8.53	122.4	172.5	58.3	27.2	L189	8.51	126.2	173.7	50.3	37.1
E69	8.35	124.3	173.4	52.1	28.7	D190	7.30	122.4	174.2	52.7	36.9
F70	8.51	119.5	172.2	53.8	38.5	Y191	8.64	119.4	169.8	53.8	39.8
D71	8.32	117.4	173.5	51.4	38.0	W192	9.42	117.6	174.3	54.7	27.9
D72	8.82	132.1	173.8	49.8	37.0	T193	9.57	115.6	168.1	55.3	67.5
S73	8.59	116.1	171.4	57.7	60.9	Y194	7.90	126.0	168.3	53.2	36.0
Q74	7.53	118.1	172.7	50.4	30.1	P195	N/A	…	174.1	58.6	27.8
D75	8.76	123.4	172.0	51.8	35.6	G196	9.23	111.2	171.3	43.0	N/A
K76	7.85	124.6	172.5	54.7	31.0	S197	8.56	120.5	173.2	53.9	67.1
A77	7.93	122.9	172.2	48.1	15.6	L198	7.89	118.7	177.4	52.3	39.9
V78	8.23	117.3	169.8	55.2	33.1	T199	…	…	…	…	…
L79	8.84	123.2	171.8	49.7	42.4	T200	6.84	109.2	169.2	53.4	65.8
K80	8.28	120.4	172.0	51.4	33.2	P201	N/A	…	…	…	…
G81	8.92	107.0	171.4	41.2	N/A	P202	N/A	…	172.3	61.0	30.2
G82	6.97	109.5	171.4	41.4	N/A	L203	9.01	120.9	170.8	53.9	33.4
P83	N/A	…	172.6	59.5	28.4	L204	5.80	111.7	176.3	52.3	37.9
L84	7.66	120.9	174.3	51.4	37.5	E205	8.55	125.4	174.1	52.8	22.9
D85	8.95	125.6	173.0	50.0	38.0	C206	7.34	114.1	170.7	52.9	63.1
G86	7.79	110.1	170.3	41.2	N/A	V207	7.09	117.2	173.6	58.3	32.2
T87	8.35	116.9	170.0	59.5	67.0	T208	8.22	125.8	170.3	60.2	64.9
Y88	8.30	126.1	172.6	52.1	36.0	W209	8.10	129.7	173.9	55.5	27.7
R89	8.48	123.4	173.3	52.5	29.8	I210	8.65	127.8	170.7	58.0	35.9
L90	8.40	124.4	172.0	52.7	38.0	V211	9.60	128.8	172.7	58.0	30.0
I91	…	…	…	…	…	L212	8.80	126.9	173.9	52.2	36.0
Q92	7.15	115.6	172.3	51.8	26.4	K213	7.26	122.8	174.2	54.5	28.9
F93	8.47	113.9	169.7	52.8	41.3	E214	8.77	122.2	172.1	50.4	27.2
H94	8.06	113.5	168.3	52.6	28.6	P215	N/A	…	176.1	58.6	29.7
F95	9.01	117.6	169.8	52.7	40.1	I216	8.81	114.0	171.7	56.9	37.4
H96	8.62	115.6	171.6	51.2	28.0	S217	7.95	117.0	170.1	53.8	61.7
W97	9.39	119.6	172.7	55.5	28.0	V218	8.41	116.4	172.0	55.7	30.3
G98	7.94	108.4	172.1	41.0	N/A	S219	8.28	116.4	174.1	53.2	62.4
S99	8.26	112.4	170.7	55.4	59.4	S220	9.17	117.7	174.0	58.8	62.5
L100	7.21	119.5	174.8	50.4	41.7	E221	8.27	118.9	175.8	56.6	25.8
D101	8.76	120.9	173.6	54.0	36.8	Q222	7.40	118.4	173.6	56.3	24.8
G102	7.54	103.3	169.6	42.3	N/A	V223	7.23	115.2	174.8	61.4	27.9
Q103	7.71	115.5	168.6	50.1	27.2	L224	7.87	121.3	176.6	55.1	37.9
G104	8.11	106.6	168.2	43.0	N/A	K225	6.77	115.5	176.9	55.2	27.8
S105	7.21	108.2	170.0	55.0	60.0	F226	6.98	119.2	173.1	55.5	30.2
E106	8.16	119.5	175.0	55.4	27.1	R227	6.55	109.5	172.5	53.9	26.1
H107	10.56	118.2	170.9	56.9	25.5	K228	6.72	114.6	175.2	52.0	29.2

[a] Residues 1 to 20 were not assigned.

continued on next page …

Table A.1 – continued from previous page

Residue	HN	N	CO	Cα	Cβ	Residue	HN	N	CO	Cα	Cβ
T108	7.22	109.8	170.7	56.2	68.3	L229	6.97	119.7	173.3	52.6	40.2
V109	7.50	119.0	174.4	57.9	30.1	N230	8.78	118.8	171.8	48.8	38.1
D110	9.57	132.8	173.6	53.3	35.8	F231	8.75	117.5	173.9	56.2	37.7
K111	9.72	110.4	173.1	55.0	26.5	N232	8.03	111.0	172.9	50.1	37.8
K112	8.10	125.1	172.1	53.5	29.0	G233	8.54	105.2	171.7	40.9	N/A
K113	7.84	122.4	173.9	51.9	31.7	E234	8.26	121.9	174.9	54.9	26.1
Y114	8.06	121.8	170.8	54.6	36.0	G235	8.94	114.6	171.0	42.1	N/A
A115	7.44	121.3	175.2	50.6	15.9	E236	7.23	120.5	170.6	50.6	26.5
A116	8.01	112.5	172.7	48.2	18.7	P237	N/A	…	173.8	60.1	…
E117	9.30	121.4	170.2	52.8	32.5	E238	8.12	123.7	174.1	54.8	27.4
L118	9.77	130.9	171.8	50.0	39.9	E239	8.89	130.3	172.5	52.2	29.5
H119	8.87	125.6	171.0	49.0	29.9	L240	8.62	126.3	173.1	53.0	38.0
L120	8.90	124.1	172.0	52.5	38.5	M241	8.50	123.5	168.3	50.9	28.3
V121	9.07	126.9	170.9	60.8	29.3	V242	6.59	115.4	171.7	56.0	34.1
H122	8.41	124.6	…	50.8	37.8	D243	7.01	115.2	172.2	53.3	34.8
W123	8.95	119.5	171.4	50.6	30.3	N244	8.26	119.8	170.4	47.5	32.4
N124	8.94	120.3	174.3	50.3	35.6	W245	6.35	114.7	170.2	47.9	29.3
T125	8.07	117.9	174.0	60.9	65.3	R246	10.29	127.3	171.1	49.5	29.1
K127	7.81	123.4	174.6	55.1	28.4	P247	N/A	…	173.3	58.7	29.4
Y128	7.56	116.1	174.3	54.7	35.1	A248	7.86	120.7	174.3	50.3	14.9
G129	7.73	107.9	170.5	44.7	N/A	Q249	8.58	122.5	170.1	48.5	24.9
D130	7.30	116.8	171.4	49.5	39.6	P250	N/A	…	174.6	59.5	28.0
F131	7.48	120.1	172.5	58.3	36.1	L251	8.55	126.3	176.0	54.1	38.6
G132	7.95	105.0	173.9	43.3	N/A	K252	8.74	115.1	174.0	54.4	25.9
K133	7.50	120.1	176.4	54.8	29.3	N253	8.57	120.2	172.2	50.6	34.7
A134	7.80	123.8	176.8	52.1	16.3	R254	7.17	119.1	171.7	52.9	30.8
V135	7.80	113.9	171.0	60.7	27.6	Q255	8.46	118.7	172.0	51.2	28.0
Q136	6.44	113.9	173.5	51.9	26.1	I256	8.79	124.8	173.5	58.0	34.1
Q137	7.54	119.6	172.7	49.2	25.2	K257	8.66	127.0	172.4	51.3	32.5
P138	N/A	…	173.5	61.9	28.3	A258	8.23	124.0	173.7	46.3	18.7
D139	7.77	115.0	175.6	48.8	35.7	S259	8.84	116.9	169.4	55.7	60.4
G140	8.15	108.7	171.7	45.3	N/A	F260	6.51	118.4	168.4	50.3	38.7
L141	8.63	116.1	174.5	49.3	43.3	K261	7.62	124.9	178.7	54.0	30.0

[a] Residues 1 to 20 were not assigned.

A.2 PCS spectra

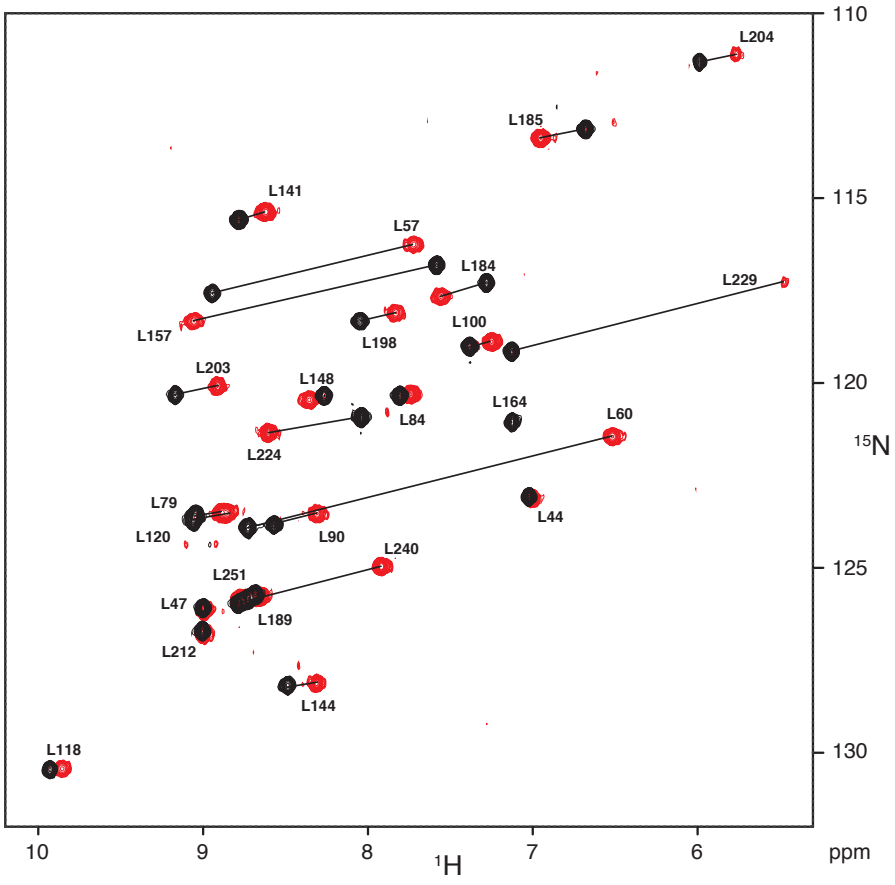

Figure A.1: Overlay of the ^{1}H-^{15}N-HSQC spectra (600 MHz, 298 K) of selective ^{15}N leucine labelled hCA-II_S166C_C206S-LuM8 (black) and hCA-II_S166C_C206S-TmM8 (red). Assignment and PCS are indicated.

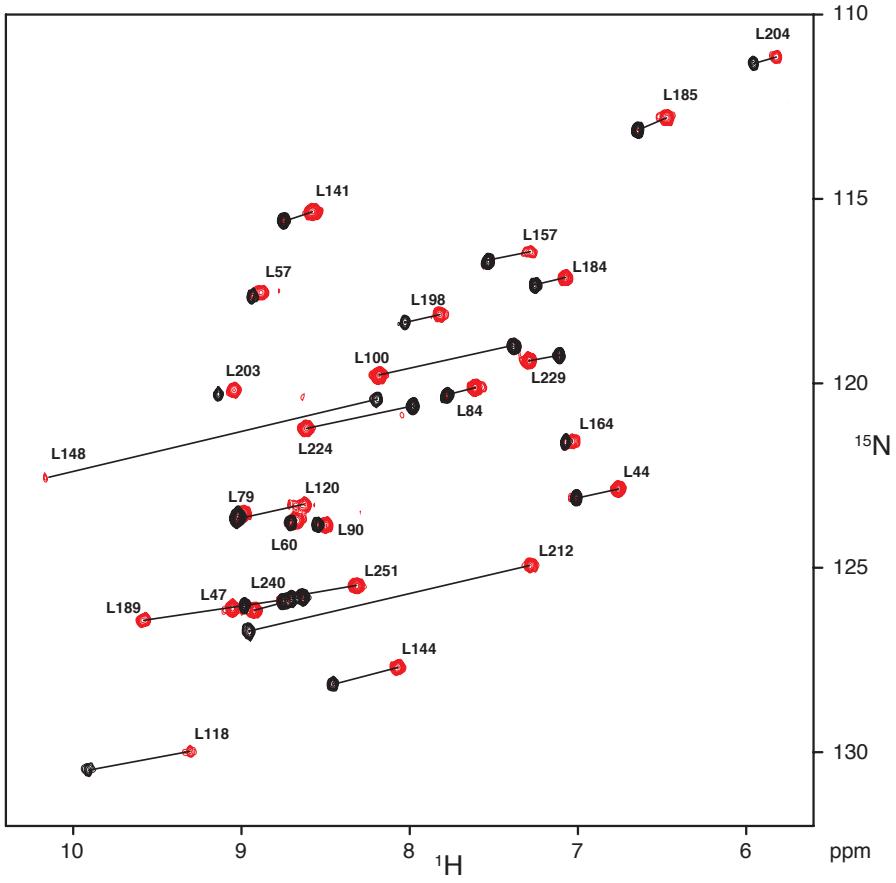

Figure A.2: Overlay of the ^{1}H-^{15}N-HSQC spectra (600 MHz, 298 K) of selective ^{15}N leucine labelled hCA-II_S217C_C206S-LuM8 (black) and hCA-II_S217C_C206S-TmM8 (red). Assignment and PCS are indicated.

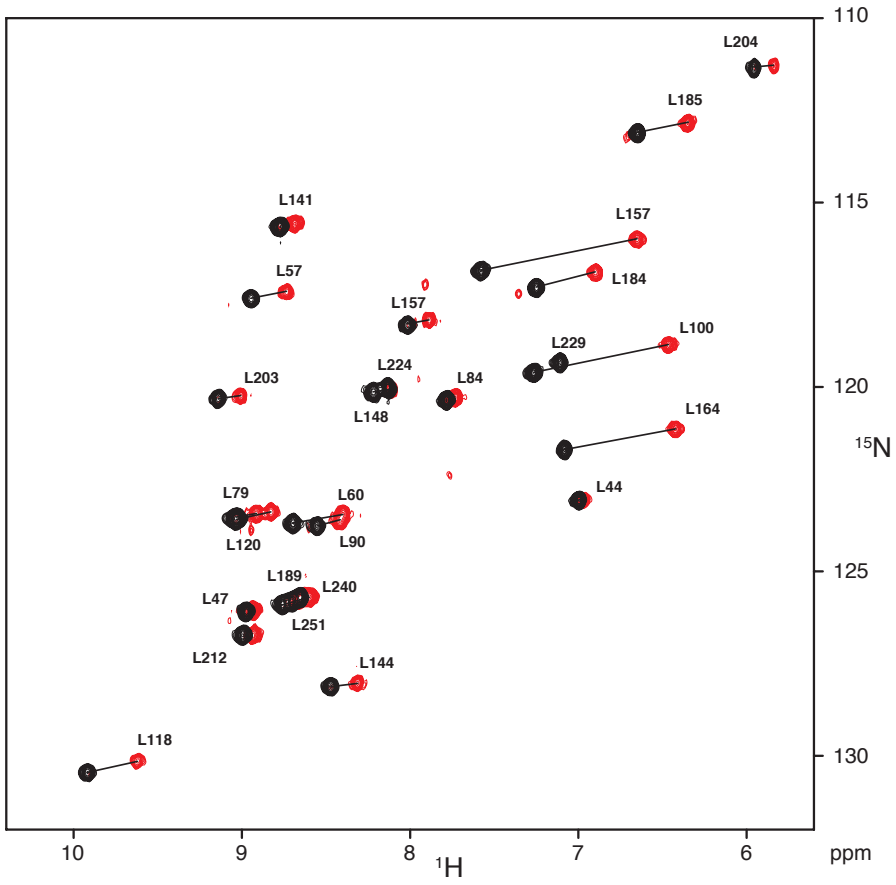

Figure A.3: Overlay of the ^{1}H-^{15}N-HSQC spectra (600 MHz, 298 K) of selective ^{15}N leucine labelled hCA-II_S220C_C206S-LuM8 (black) and hCA-II_S220C_C206S-TmM8 (red). Assignment and PCS are indicated.

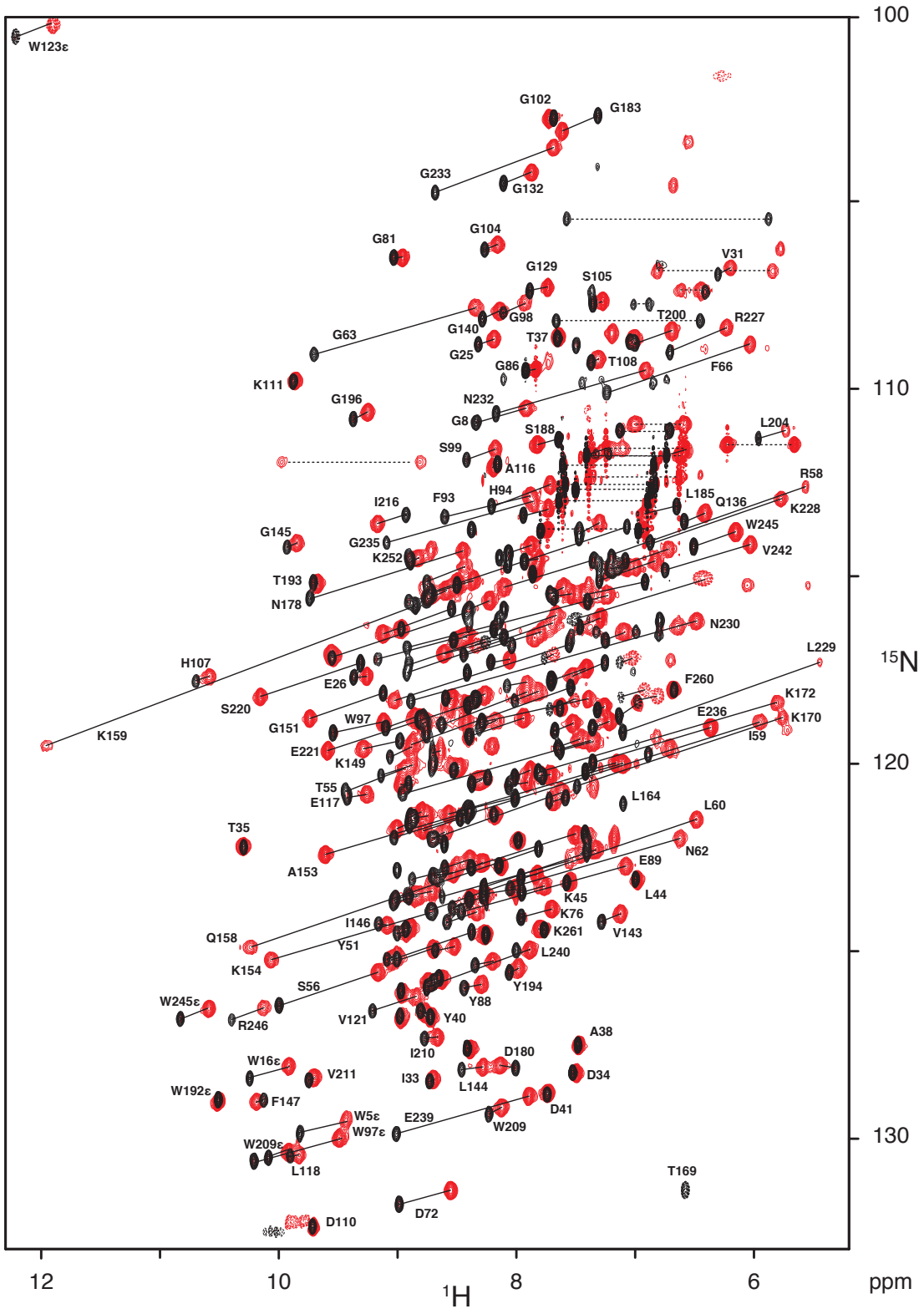

Figure A.4: Overlay of the ^{1}H-^{15}N-HSQC spectra (600 MHz, 298 K) of uniform ^{15}N labelled hCA-II_S166C_C206S-LuM8 (black) and hCA-II_S166C_C206S-TmM8 (red). Aliased signals with negative intensity are shown with dashed contour lines. Assignment and PCS are indicated with solid and NH_2 groups with dashed lines.

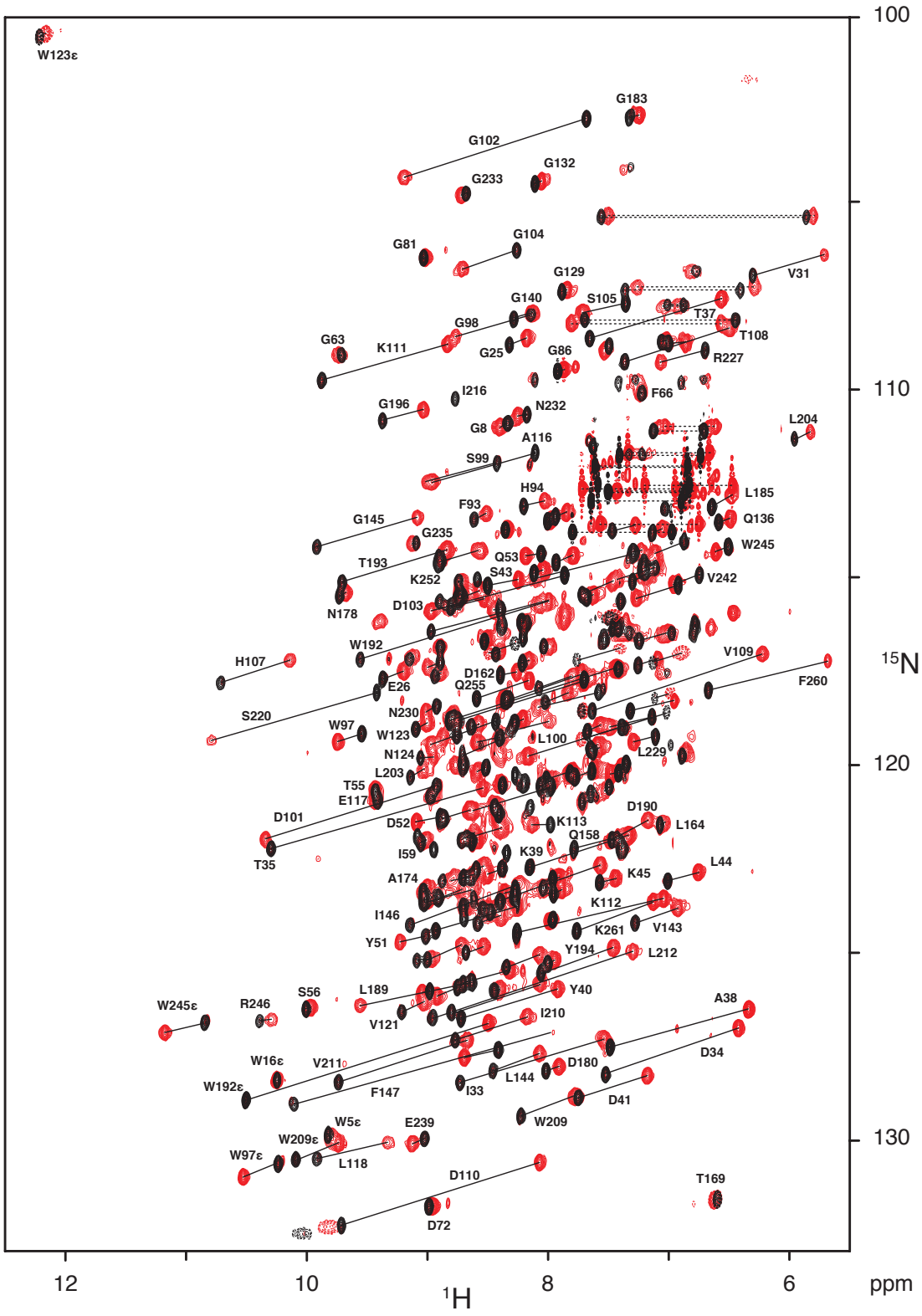

Figure A.5: Overlay of the ^{1}H-^{15}N-HSQC spectra (600 MHz, 298 K) of uniform ^{15}N labelled hCA-II_S217C_C206S-LuM8 (black) and hCA-II_S217C_C206S-TmM8 (red). Aliased signals with negative intensity are shown with dashed contour lines. Assignment and PCS are indicated with solid and NH_2 groups with dashed lines.

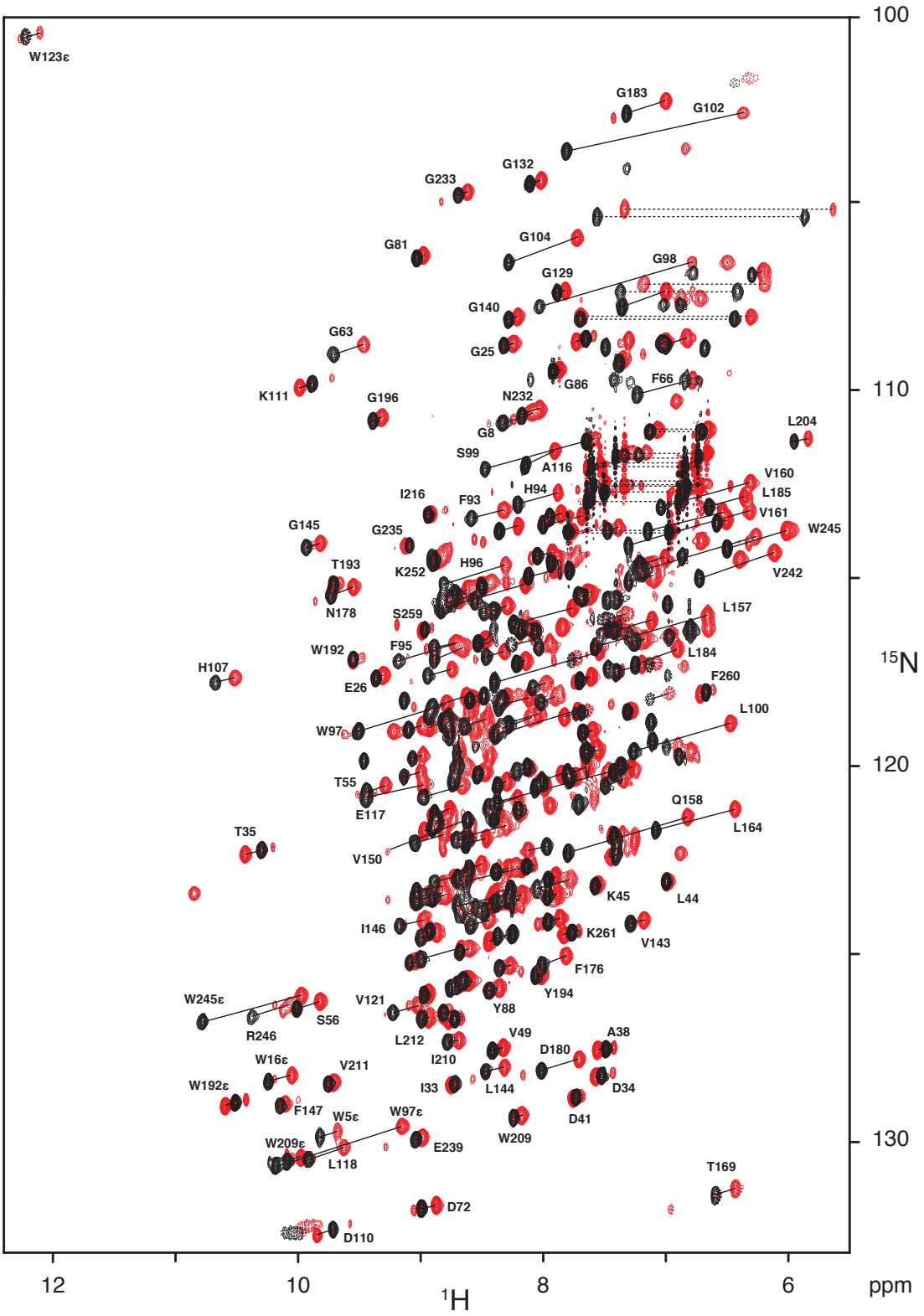

Figure A.6: Overlay of the ^{1}H-^{15}N-HSQC spectra (600 MHz, 298 K) of uniform ^{15}N labelled hCA-II_S220C_C206S-LuM8 (black) and hCA-II_S220C_C206S-TmM8 (red). Aliased signals with negative intensity are shown with dashed contour lines. Assignment and PCS are indicated with solid and NH_2 groups with dashed lines.

Table A.2: PCS of all four hCA-II mutants. Shifts which were excluded from tensor calculation are marked. All values are given in ppm.

Residue [a]	S50C		S166C		S217C		S220C	
	HN	N	HN	N	HN	N	HN	N
I22	−0.010 [b]	0.167 [b]	−0.150 [c]	−0.085 [c]	−0.089	−0.136	−0.082	−0.051
A23	0.032 [b]	0.052 [b]	−0.163	−0.094	−0.100	−0.137	−0.094	−0.093
K24	0.019	0.063	−0.132	−0.061	−0.096	−0.098	…	…
G25	0.026	0.033	−0.124	−0.146	−0.141	−0.189	−0.080	−0.045
E26	0.053	0.101	−0.102	−0.034	−0.171	−0.205	−0.057	−0.069
R27	0.055	0.090	−0.111	−0.066	−0.220	−0.220	−0.068	−0.038
Q28	0.094	0.060	−0.102	−0.167	−0.252	−0.361	−0.076	−0.057
S29	0.094	0.235 [d]	−0.160	−0.098	−0.270	−0.303	−0.111	−0.102
V31	0.135	0.083	−0.096	−0.178	−0.592	−0.538	−0.087	−0.080
D32	0.128	−0.006 [d]	−0.072	−0.112	−0.616	−0.660	−0.038	−0.061
I33	0.165	0.131	−0.022	−0.058	−1.192	−1.165	0.033	0.034
D34	0.200	0.166	−0.020	0.010	−1.099	−1.239	0.051	0.034
T35	0.189	0.143	0.014	−0.021	−1.752	−1.612	0.136	0.118
H36	0.207 [b]	0.126 [b]	0.013	0.000	−1.380	−1.384	0.117	0.148
T37	0.214	0.242	0.000	−0.045	−1.087	−1.054	0.080	0.082
A38	0.261	0.206	0.001	−0.003	−1.146	−1.017	0.070	0.020
K39	0.360	0.376	−0.011	0.024	−0.817	−0.857	0.036	0.048
Y40	0.410	0.493	0.005	0.005	−0.800	−0.782	0.051	0.026
D41	0.653	0.571	0.002	−0.037	−0.571	−0.585	0.023	0.029
S43	0.779	0.879	−0.005	−0.042	−0.249	−0.160	0.005	−0.005
L44	1.039	1.213	−0.010	0.024	−0.252	−0.237	−0.001	0.003
K45	1.949	1.928	−0.020	−0.026	−0.130	−0.114	−0.019	−0.022
L47	3.001 [b]	3.747 [b]	0.000	0.051	0.066	0.062	−0.035	−0.044
S48	…	…	−0.037	−0.082	0.072	0.105	−0.063	−0.071
V49	…	…	−0.015	0.026	0.284	0.207	−0.088	−0.077
S50	…	…	−0.088	−0.134	0.124	0.145	−0.107	−0.111
Y51	…	…	−0.068	−0.079	0.216	0.150	−0.130	−0.138
D52	…	…	−0.093	−0.191	0.204	0.116	−0.124	−0.111
Q53	…	…	−0.181	−0.209	0.129	0.061	−0.121	−0.083
A54	−3.566 [b]	−2.908 [b]	−0.254	−0.227	0.066	0.031	−0.145	−0.122
T55	−1.195	−1.220	−0.493	−0.596	0.004	−0.057	−0.151	−0.186
S56	−0.746	−0.698	−0.824	−0.885	−0.034	−0.043	−0.189	−0.196
L57	−0.396	−0.341	−1.216	−1.318	−0.047	−0.091	−0.196	−0.172
R58	−0.296	−0.319	−1.623 [c]	−1.880 [c]	−0.057	−0.056	−0.209	−0.264 [d]
I59	−0.205	−0.174	−3.301	−2.859	−0.040	−0.072	−0.241	−0.213
L60	−0.216	−0.304 [d]	−2.226	−2.466	−0.022	−0.021	−0.290	−0.259
N61	−0.118	−0.130	…	…	…	…	−0.239	−0.236
N62	−0.112	−0.120	−1.424	−1.325	0.003 [b]	0.019 [b]	−0.267	−0.230
G63	−0.082	0.012	−1.353	−1.248	0.026	−0.010	−0.247	−0.270
H64	…	…	…	…	…	…	…	…
A65	…	…	−1.065	−0.904	…	…	…	…
F66	−0.149	−0.079	−1.196	−1.299	0.011	−0.019	−0.447	−0.395
N67	−0.207	−0.200	−1.580	−1.409	−0.016	−0.026	−0.315	−0.297
V68	−0.346	−0.338	−1.049	−1.224	…	…	−0.412	−0.362
E69	−0.338	−0.482	−1.378	−1.217	−0.056	−0.072	−0.238	−0.217
F70	−0.488	−0.513	−0.708	−0.869	−0.058	−0.075	−0.182	−0.196
D71	−0.433 [b]	−0.157 [b]	−0.648	−0.601	−0.032	−0.086	−0.148	−0.148
D72	−0.343 [b]	−0.426 [b]	−0.425	−0.372	−0.022	−0.011	−0.119	−0.082
S73	0.132	0.068	−0.351	−0.381	−0.010	−0.063	−0.105	−0.141
Q74	0.677 [b]	0.772 [b]	−0.286	−0.331	0.000	0.025	−0.094	−0.109

[a] Residues 1 to 20 (not assigned) and proline residues 21, 30, 42, 46, 83, 138, 155, 181, 186, 195, 201, 202, 215, 237, 247 and 250 (no resonance in ^{1}H-^{15}N-HSQC) were omitted. [b] PCS which were excluded from tensor calculation for set 1. [c] PCS excluded for set 2, additionally to set 1. [d] PCS excluded for set 3, additionally to set 1 and 2.

continued on next page …

Table A.2 – continued from previous page

Residue [a]	S50C		S166C		S217C		S220C	
	HN	N	HN	N	HN	N	HN	N
D75	…	…	−0.176	−0.066 [d]	−0.018	0.010	−0.163	−0.116
K76	…	…	−0.250	−0.229	0.021	0.029	−0.100	−0.105
A77	…	…	−0.259	−0.129	0.018	0.059	−0.115	−0.117
V78	…	…	−0.167	−0.255	0.060	0.004	−0.113	−0.130
L79	…	…	−0.152	−0.144 [d]	−0.022	−0.073	−0.109	−0.101
K80	…	…	−0.074	−0.105	0.012	−0.034	−0.079	−0.112
G81	…	…	−0.066	0.001	−0.010	−0.014	−0.053	−0.076
G82	4.147 [b]	3.804 [b]	−0.027	−0.090	−0.040	−0.037	−0.033	−0.035
L84	2.332 [d]	1.941 [d]	−0.063	−0.037	−0.167	−0.215	−0.050	−0.029
D85	0.929	1.117	−0.069	−0.077	−0.125	−0.042	−0.045	−0.042
G86	1.082	0.737	−0.078	−0.043	−0.050	−0.044	−0.052	−0.036
T87	−1.097 [b]	−0.668 [b]	−0.110	−0.103	−0.024	−0.048	−0.062	−0.097
Y88	0.837 [b]	0.016 [b]	−0.136	−0.101	−0.042	−0.046	−0.083	−0.072
R89	−1.027 [b]	−1.328 [b]	−0.203	−0.246	−0.062	−0.072	−0.098	−0.126
L90	−1.632	−1.318	−0.253	−0.339	−0.049	0.023	−0.134	−0.145
I91	…	…	…	…	…	…	…	…
Q92	−0.415	−0.419	−0.462	−0.524	−0.116	−0.198	−0.199	−0.179
F93	−0.415	−0.433	−0.708	−0.556	−0.099 [b]	−0.161 [b]	−0.267	−0.215
H94	−0.233	−0.182	−0.484	−0.572	−0.173	−0.149	−0.324	−0.306
F95	−0.192 [b]	−0.234 [b]	−0.651	−0.533	−0.030	−0.066	−0.470	−0.451
H96	−0.062	0.024 [d]	−0.310	−0.412	−0.028	0.021	−0.501 [c]	−0.515 [c]
W97	−0.042	−0.055	−0.415	−0.290	0.201	0.214	−0.711	−0.726
G98	−0.061	−0.113	−0.172	−0.265	0.629	0.575	−1.252 [c]	−1.188 [c]
S99	−0.024	−0.041	−0.235	−0.290	0.589	0.495	−0.901 [b]	−0.815 [b]
L100	−0.023	−0.078	−0.133	−0.162	0.781	0.770	−0.786	−0.741
D101	−0.030	−0.057	0.074	−0.006	1.413 [d]	1.407 [d]	…	…
G102	−0.014	−0.032	0.047	0.004	1.506	1.557	−1.441 [b]	−1.016 [b]
Q103	−0.016	0.000	−0.018	−0.084	1.107	0.951	…	…
G104	−0.001	0.050	−0.100	−0.145	0.450	0.500	−0.558 [b]	−0.649 [b]
S105	−0.003	−0.029	−0.076	−0.078	0.361	0.244	−0.356	−0.419
E106	0.005	0.159 [d]	−0.130	−0.148	−0.314	−0.208	−0.238	−0.305
H107	0.092	0.161	−0.101	−0.128	−0.574	−0.601	−0.156	−0.128
T108	0.115	−0.005	−0.054	−0.091	−0.864	−0.890	−0.031	−0.060
V109	0.106	0.072	0.004	−0.047	−1.409 [d]	−1.520 [d]	0.138	0.119
D110	0.155	0.111	0.004	0.003	−1.642 [d]	−1.682 [d]	0.130	0.133
K111	0.108	0.056	−0.008	−0.029	−1.039 [d]	−0.964 [d]	0.102	0.097
K112	0.091	0.053	0.018	−0.019	−1.216 [b]	−0.902 [b]	0.195	0.199
K113	0.046	0.049	0.010	0.006	0.157 [b]	−0.005 [b]	0.155	0.107
Y114	0.026	−0.037	0.000	0.024	…	…	−0.006 [c]	0.082 [c]
A115	−0.014	−0.002	0.109	0.096	…	…	…	…
A116	−0.032	0.012	0.042	0.080	0.856 [b]	0.776 [b]	−0.237 [c]	−0.379 [c]
E117	−0.057	0.011	−0.148	−0.052	0.019	−0.032	−0.469	−0.334
L118	−0.065	−0.056	−0.068	−0.030	−0.585	−0.437	−0.288	−0.303
H119	−0.148	0.039 [c]	−0.299	−0.291	−0.278	−0.396	−0.326	−0.247
L120	−0.065	−0.170	−0.184	−0.148	−0.390	−0.285	−0.194	−0.170
V121	−0.292	−0.275	−0.358	−0.386	−0.183	−0.302	−0.204	−0.177
H122	−0.050	−0.065	−0.244	−0.280	−0.187	−0.221	−0.138	−0.128
W123	−0.528	−0.415	−0.270	−0.232	−0.093	−0.172	−0.113	−0.106
N124	−0.320	−0.516	−0.175	−0.294	−0.107	−0.027	−0.086	−0.091
T125	−1.262	−1.159	−0.151	−0.067	−0.052	−0.062	−0.074	−0.074
K127	−1.193	−1.268	−0.129	−0.072	−0.048	−0.037	−0.063	−0.092
Y128	−0.850	−0.917 [d]	−0.141	−0.074	−0.057	−0.077	−0.062	−0.075

[a] Residues 1 to 20 (not assigned) and proline residues 21, 30, 42, 46, 83, 138, 155, 181, 186, 195, 201, 202, 215, 237, 247 and 250 (no resonance in ^{1}H-^{15}N-HSQC) were omitted. [b] PCS which were excluded from tensor calculation for set 1. [c] PCS excluded for set 2, additionally to set 1. [d] PCS excluded for set 3, additionally to set 1 and 2.

continued on next page …

Table A.2 – continued from previous page

Residue [a]	S50C		S166C		S217C		S220C	
	HN	N	HN	N	HN	N	HN	N
G129	−0.756	−0.625	−0.143	−0.096	−0.039	−0.053	−0.067	−0.042
D130	−0.445	−0.490	−0.163	−0.244	−0.047	−0.058	−0.074	−0.067
F131	−0.359	−0.282	−0.252	−0.231	−0.052	−0.089	−0.085	−0.091
G132	−0.243	−0.236	−0.228	−0.297	−0.055	−0.077	−0.092	−0.094
K133	−0.260	−0.255	−0.174	−0.249	−0.058	−0.122	−0.076	−0.090
A134	−0.311	−0.256	−0.181	−0.178	−0.068	−0.123	−0.081	−0.055
V135	−0.211	−0.230 [d]	−0.199	−0.140	−0.091	−0.111	−0.092	−0.084
Q136	−0.162	−0.089	−0.167	−0.230	−0.091	−0.111	−0.078	−0.092
Q137	−0.140	−0.161	−0.148	−0.195	−0.108	−0.182	−0.076	−0.059
D139	−0.062	−0.046	−0.111	−0.073	−0.140	−0.175	−0.059	−0.084
G140	−0.043	−0.036	−0.134	−0.211	−0.147	−0.157	−0.074	−0.073
L141	0.036	−0.010	−0.159	−0.220	−0.173	−0.234	−0.083	−0.081
A142	0.135	0.295	−0.191	−0.140	−0.191	−0.237	−0.106	−0.089
V143	0.392	0.409	−0.150	−0.214	−0.353	−0.398	−0.109	−0.094
L144	0.175	0.240	−0.172	−0.078	−0.380	−0.464	−0.152	−0.124
G145	0.304	0.127	−0.076	−0.114	−0.831	−0.788	−0.113	−0.110
I146	0.037	0.091	−0.065	0.025	−0.895	−1.081	−0.192	−0.140
F147	0.058	−0.026	0.070	0.036	−2.143 [c]	−1.916 [c]	−0.039	−0.052
L148	−0.024	−0.020	0.106	0.090	1.956 [b]	2.110 [b]	−0.104 [b]	−0.073 [b]
K149	−0.067	−0.021	0.316	0.204	…	…	…	…
V150	−0.051	−0.034	0.321	0.298	…	…	0.655 [b]	0.846 [b]
G151	−0.107	−0.064	0.627	0.669	…	…	…	…
S152	−0.122	−0.099	0.686	0.741	…	…	…	…
A153	−0.178	−0.258	1.219	1.136	…	…	−0.956 [b]	−0.842 [b]
K154	−0.237	−0.256	1.351	1.281	…	…	…	…
G156	…	…	…	…	…	…	…	…
L157	−0.433	−0.458	1.475	1.494	…	…	−0.916 [d]	−0.841 [d]
Q158	−0.403	−0.342	2.423	2.608	−0.360	−0.302	−0.974	−0.971
K159	−0.431	−0.371	3.115	3.731	−0.276	−0.248	−0.687	−0.657
V160	−0.384	−0.366	1.663 [c]	1.813 [c]	…	…	−0.731	−0.665
V161	−0.291	−0.368	…	…	−0.066	−0.036	−0.988 [b]	−0.916 [b]
D162	−0.264	−0.248	…	…	−0.132	−0.084	−0.855	−0.818
V163	−0.236	−0.247	…	…	−0.079	−0.112	−0.608	−0.490
L164	−0.194	−0.182	…	…	−0.012	−0.005	−0.644	−0.557
D165	−0.138	−0.144	…	…	−0.010	0.016	−0.477	−0.417
S166	−0.139	−0.126	…	…	−0.024	−0.030	−0.315	−0.236
I167	−0.136	−0.098	−11.203 [b]	−10.446 [b]	0.039	−0.028	−0.298	−0.274
K168	−0.098	−0.089	−7.403 [b]	−6.021 [b]	0.016	−0.013	−0.204	−0.204
T169	−0.082	−0.077	−3.833	−3.513	0.029	0.020	−0.161	−0.173
K170	−0.063	−0.041	−1.722	−1.836	0.035	0.091	−0.148	−0.180
G171	−0.103	−0.005	−1.681 [d]	−1.393	0.008	−0.012	−0.178	−0.093
K172	−0.080	−0.054	−1.996 [c]	−1.842 [c]	−0.010	−0.030	−0.158	−0.187
S173	−0.089	−0.103	…	…	−0.010	−0.023	−0.152	−0.133
A174	−0.143	−0.075	…	…	−0.025	−0.102	−0.210	−0.129
D175	−0.120	−0.155	…	…	−0.045	−0.088	−0.165	−0.125
F176	−0.224	−0.314	…	…	−0.052	−0.081	−0.195	−0.248
T177	−0.283	−0.349	…	…	−0.073	−0.081	−0.205	−0.210
N178	−0.481	−0.557	−1.283	−1.278	−0.051	−0.085	−0.184	−0.225
F179	−0.703	−0.747	−0.885	−0.618	−0.069	−0.104	−0.238	−0.264
D180	−1.028	−1.191	0.139	−0.073	−0.106	−0.114	−0.305	−0.305
R182	−1.995	−1.801	0.085	0.138	0.024	0.009	−0.248	−0.209
G183	−1.296	−1.218	0.307	0.410	−0.079	−0.068	−0.319	−0.334
L184	−0.901	−0.769	0.281	0.349	−0.163	−0.179	−0.344	−0.401

[a] Residues 1 to 20 (not assigned) and proline residues 21, 30, 42, 46, 83, 138, 155, 181, 186, 195, 201, 202, 215, 237, 247 and 250 (no resonance in ^{1}H-^{15}N-HSQC) were omitted. [b] PCS which were excluded from tensor calculation for set 1. [c] PCS excluded for set 2, additionally to set 1. [d] PCS excluded for set 3, additionally to set 1 and 2.

continued on next page …

Table A.2 – continued from previous page

Residue [a]	S50C		S166C		S217C		S220C	
	HN	N	HN	N	HN	N	HN	N
L185	−0.757	−0.580	0.281	0.195	−0.167	−0.333	−0.290	−0.273
E187	−0.057	−0.028	0.260	0.196	…	…	−0.007	−0.001
S188	0.126	0.130	0.188	0.144	…	…	−0.018	−0.025
L189	0.471 [c]	0.425 [c]	0.099	0.108	0.927	0.614	−0.025	−0.012
D190	0.558 [d]	0.611 [d]	0.005	0.059	−0.297 [b]	−0.527 [b]	0.014	−0.014
Y191	0.831	0.749	0.019	0.061	−1.046 [c]	−1.063 [c]	…	…
W192	0.567	0.608	0.008	−0.074	−1.559	−1.547	0.002	0.033
T193	0.591	0.646	−0.030	0.025	−0.865	−0.864	−0.006	0.015
Y194	0.502	0.551	−0.070	−0.117	−0.596	−0.678	−0.046	−0.019
G196	0.225	0.220	−0.116	−0.186	−0.335	−0.291	−0.072	−0.088
S197	0.123	0.278 [c]	−0.150	0.049 [d]	−0.306	−0.240	−0.085	0.028 [d]
L198	−0.011 [b]	−0.044 [b]	−0.194	−0.245	−0.188	−0.259	−0.116	−0.154
T199	…	…	…	…	…	…	…	…
T200	…	…	−0.305	−0.339	−0.142	−0.028	−0.182	−0.177
L203	0.002	0.136 [d]	−0.257	−0.291	−0.111	−0.212	−0.135	−0.118
L204	−0.028	−0.078	−0.217	−0.216	−0.130	−0.176	−0.113	−0.071
E205	−0.004	−0.035	−0.151	−0.119	−0.145	−0.167	−0.083	−0.095
C206	0.031	0.032	−0.163 [c]	−0.333 [c]	−0.191	−0.150	−0.092	−0.097
V207	0.108	0.155	−0.151	−0.232	−0.232	−0.209	−0.085	−0.085
T208	0.307	0.385	−0.137	−0.110	−0.275	−0.329	−0.085	−0.063
W209	0.418	0.469	−0.101	−0.186	−0.456	−0.513	−0.067	−0.061
I210	0.532	0.659	−0.101	−0.045	−0.595	−0.632	−0.091	−0.042
V211	0.540	0.459	−0.038	−0.074	−1.062	−1.108	−0.040	−0.032
L212	0.328	0.495	−0.003	0.071	−1.656	−1.761	−0.056	0.002
K213	0.416	0.326	0.061	0.118	…	…	0.042	0.112
E214	0.260	0.210	0.115	0.142	…	…	0.071	0.073
I216	−0.061	−0.102	0.248	0.234	…	…	−0.022	−0.018
S217	−0.152	−0.155	0.514	0.429	…	…	…	…
V218	−0.131	−0.103	0.585	0.658	…	…	…	…
S219	−0.184	−0.159	1.143	1.136	…	…	…	…
S220	−0.108	−0.112	0.850	0.897	1.370 [b]	1.267 [b]	…	…
E221	−0.121	−0.103	1.191	1.196	0.539 [b]	0.595 [b]	…	…
Q222	−0.150	−0.122	1.345	1.563	0.504	0.395	…	…
V223	−0.145	−0.160	0.760	0.718	0.818 [b]	0.603 [b]	…	…
L224	−0.114	−0.148	0.570	0.422	0.652	0.620	…	…
K225	−0.131	−0.121	0.523	0.347	0.346	0.338	…	…
F226	−0.130	−0.130	−0.144	−0.368	0.349	0.269	…	…
R227	−0.103	−0.160	−0.466	−0.663	0.372	0.315	…	…
K228	−0.098	−0.129	−1.091	−1.159	0.243	0.322	…	…
L229	−0.095	−0.037	−1.652	−1.877	0.183	0.138	−0.632 [d]	−0.467 [d]
N230	−0.080	−0.064	−2.396	−2.143	0.093	0.151	−0.282	−0.309
F231	−0.060	−0.052	−1.234	−1.323	0.108	0.129	−0.231	−0.311
N232	−0.046	−0.031	−1.250	−1.151	0.079	0.035	−0.143	−0.169
G233	−0.047	−0.072	−0.987	−1.209	0.039	0.039	−0.074	−0.081
E234	−0.046	−0.057	−1.285	−1.276	0.020	0.097	−0.051	−0.054
G235	−0.033	−0.028	−1.229	−1.090 [d]	0.034	0.014	0.031	0.023
E236	−0.037	−0.069	−0.983	−0.932	0.044	0.099	0.011	0.019
E238	−0.027	−0.055	−0.932	−1.002	0.093	0.110	0.118	0.109
E239	−0.049	−0.027	−1.108	−1.012	0.105	0.129	−0.053	−0.047
L240	−0.043	−0.075	−0.858	−1.013	0.172	0.236	−0.154	−0.224
M241	−0.066	−0.006	−1.149	−1.162	0.169	0.075	−0.561	−0.437
V242	−0.053	−0.068	−0.708	−0.686	0.215	0.253	−0.610	−0.706
D243	−0.055	−0.072	−0.412	−0.484	0.349	0.341	−0.871	−0.837

[a] Residues 1 to 20 (not assigned) and proline residues 21, 30, 42, 46, 83, 138, 155, 181, 186, 195, 201, 202, 215, 237, 247 and 250 (no resonance in ^{1}H-^{15}N-HSQC) were omitted. [b] PCS which were excluded from tensor calculation for set 1. [c] PCS excluded for set 2, additionally to set 1. [d] PCS excluded for set 3, additionally to set 1 and 2.

continued on next page …

Table A.2 – continued from previous page

Residue [a]	S50C		S166C		S217C		S220C	
	HN	N	HN	N	HN	N	HN	N
N244	−0.040	−0.042	−0.450	−0.485	0.193	0.111	−0.663	−0.620
W245	−0.027	−0.135	−0.344	−0.395	0.107	0.136	−0.487	−0.474
R246	−0.022	−0.052	−0.264	−0.326	−0.089 [b]	−0.042 [b]	−0.303	−0.332
A248	0.051	0.023	−0.121	−0.187	−0.205	−0.213	−0.163	−0.193
Q249	0.105	0.071	−0.096	−0.171	−0.280	−0.268	−0.100	−0.094
L251	0.112	0.121	−0.068	−0.082	−0.385	−0.363	−0.041	−0.084
K252	0.098	0.071	−0.058	−0.084	−0.321	−0.292	−0.029	−0.049
N253	0.118	0.114	−0.060	−0.014	−0.304	−0.353	−0.028	−0.016
R254	0.155	0.157	−0.052	−0.089	−0.362	−0.276	−0.023	−0.022
Q255	0.248	0.232	−0.048	0.012	−0.431	−0.477	−0.012	−0.024
I256	0.287	0.347	−0.028	−0.041	−0.666	−0.692	0.007	0.011
K257	0.477	0.450	−0.034	0.065	−0.729	−0.779	−0.002	0.037
A258	0.539	0.559	−0.006	−0.043	−0.830	−0.959	0.027	0.012
S259	0.759	0.727	0.011	−0.008	−0.973	−0.809	0.021	0.032
F260	0.655	0.673	0.023	0.004	−0.985	−0.786	0.047	0.051
K261	0.542	0.524	0.047	−0.034	−0.633	−0.785	0.066	0.066

[a] Residues 1 to 21 (not assigned) and proline residues 21, 30, 42, 46, 83, 138, 155, 181, 186, 195, 201, 202, 215, 237, 247 and 250 (no resonance in ^{1}H-^{15}N-HSQC) were omitted. [b] PCS which were excluded from tensor calculation for set 1. [c] PCS excluded for set 2, additionally to set 1. [d] PCS excluded for set 3, additionally to set 1 and 2.

Table A.3: ^{1}H-^{15}N HSQC peak assignments for untagged, LuM8 tagged and TmM8 tagged hCA-II mutants S50C and S166C. All values are given in ppm.

Residue [a]	S50C		S50C-Lu		S50C-Tm		S166C		S166C-Lu		S166C-Tm	
	HN	N	HN	N	HN	N	HN	N	HN	N	HN	N
I22	8.07	120.4	8.07	120.4	8.06	120.6	8.06	120.4	8.06	120.6	7.91	120.5
A23	8.67	123.0	8.67	123.0	8.71	123.0	8.67	123.0	8.70	123.0	8.54	122.9
K24	7.21	114.8	7.21	114.8	7.23	114.8	7.20	114.7	7.21	114.8	7.08	114.7
G25	8.32	108.8	8.32	108.8	8.34	108.8	8.31	108.8	8.32	108.8	8.20	108.7
E26	9.37	117.7	9.37	117.7	9.42	117.8	9.36	117.7	9.37	117.7	9.27	117.7
R27	8.87	121.4	8.87	121.4	8.92	121.5	8.86	121.4	8.86	121.5	8.75	121.4
Q28	7.71	115.5	7.71	115.5	7.81	115.5	7.71	115.5	7.71	115.5	7.61	115.3
S29	8.07	117.8	8.07	117.8	8.16	118.1	8.05	117.8	8.08	117.9	7.92	117.8
V31	6.30	107.0	6.30	107.0	6.44	107.1	6.30	107.0	6.30	106.9	6.21	106.8
D32	8.33	118.3	8.33	118.3	8.46	118.3	8.35	118.3	8.35	118.3	8.27	118.2
I33	8.73	128.5	8.73	128.5	8.90	128.6	8.72	128.5	8.73	128.5	8.71	128.4
D34	7.53	128.2	7.53	128.2	7.73	128.4	7.53	128.2	7.53	128.2	7.50	128.2
T35	10.30	122.3	10.30	122.3	10.49	122.4	10.29	122.2	10.30	122.2	10.31	122.2
H36	8.80	118.9	8.80	118.9	9.01	119.0	8.81	118.8	8.82	118.8	8.83	118.8
T37	7.65	108.6	7.65	108.6	7.86	108.8	7.64	108.6	7.65	108.7	7.65	108.6
A38	7.49	127.6	7.49	127.6	7.75	127.8	7.48	127.5	7.48	127.5	7.48	127.5
K39	8.15	122.7	8.15	122.7	8.51	123.1	8.14	122.7	8.15	122.7	8.14	122.7
Y40	8.72	126.7	8.72	126.7	9.13	127.2	8.72	126.8	8.72	126.8	8.73	126.8
D41	7.76	128.9	7.76	128.9	8.41	129.4	7.74	128.8	7.74	128.8	7.74	128.8
S43	8.50	115.2	8.50	115.2	9.28	116.1	8.49	115.2	8.50	115.2	8.50	115.2
L44	7.01	123.1	7.01	123.1	8.05	124.3	6.99	123.1	7.00	123.1	6.99	123.1
K45	7.58	123.2	7.58	123.2	9.53	125.2	7.57	123.2	7.58	123.2	7.56	123.2
L47	8.98	126.4	8.98	126.4	11.98	130.2	8.97	126.1	8.97	126.1	8.97	126.1

[a] Residues 1 to 20 (not assigned) and proline residues 21, 30, 42, 46, 83, 138, 155, 181, 186, 195, 201, 202, 215, 237, 247 and 250 (no resonance in ^{1}H-^{15}N-HSQC) were omitted.

continued on next page ...

Table A.3 – continued from previous page

Residue [a]	S50C		S50C-Lu		S50C-Tm		S166C		S166C-Lu		S166C-Tm	
	HN	N	HN	N	HN	N	HN	N	HN	N	HN	N
S48	8.58	121.4	8.58	121.4	…	…	8.52	120.2	8.53	120.2	8.49	120.1
V49	8.27	126.2	8.27	126.2	…	…	8.41	127.6	8.41	127.6	8.40	127.6
S50	8.52	127.0	8.52	127.0	…	…	8.37	122.8	8.38	122.8	8.29	122.6
Y51	8.90	123.5	8.90	123.5	…	…	8.99	124.6	9.00	124.5	8.93	124.4
D52	8.74	121.7	8.74	121.7	…	…	8.88	121.4	8.90	121.5	8.80	121.3
Q53	8.05	114.4	8.05	114.4	…	…	8.05	114.4	8.07	114.4	7.88	114.2
A54	7.40	120.1	7.40	120.1	3.83	117.2	7.42	120.2	7.42	120.2	7.16	120.0
T55	9.40	120.8	9.40	120.8	8.21	119.6	9.43	120.7	9.44	120.7	8.95	120.1
S56	10.02	126.6	10.02	126.6	9.28	125.9	9.99	126.5	10.00	126.4	9.17	125.6
L57	8.94	117.5	8.94	117.5	8.54	117.2	8.92	117.6	8.92	117.6	7.70	116.3
R58	7.21	114.8	7.21	114.8	6.92	114.4	7.20	114.7	7.20	114.5	5.57	112.6
I59	9.05	122.1	9.05	122.1	8.84	121.9	9.02	122.0	9.03	122.0	5.73	119.1
L60	8.72	123.9	8.72	123.9	8.50	123.6	8.71	123.9	8.72	123.9	6.49	121.5
N61	8.45	121.2	8.45	121.2	8.33	121.1	…	…	…	…	…	…
N62	8.05	123.3	8.05	123.3	7.94	123.2	8.06	123.4	8.05	123.3	6.63	122.0
G63	9.71	108.9	9.71	108.9	9.63	108.9	9.74	109.0	9.70	109.1	8.35	107.8
H64	…	…	…	…	…	…	…	…	…	…	…	…
A65	…	…	…	…	…	…	…	…	8.62	123.5	7.56	122.6
F66	7.23	110.1	7.23	110.1	7.08	110.0	7.23	110.1	7.24	110.1	6.04	108.8
N67	9.00	120.8	9.00	120.8	8.80	120.6	8.99	120.8	8.95	120.8	7.37	119.4
V68	8.70	122.0	8.70	122.0	8.36	121.7	8.68	122.0	8.68	122.0	7.63	120.8
E69	8.49	124.0	8.49	124.0	8.16	123.5	8.45	124.0	8.46	123.9	7.09	122.7
F70	8.65	119.1	8.65	119.1	8.16	118.6	8.63	119.0	8.63	119.0	7.92	118.1
D71	8.46	117.0	8.46	117.0	8.02	116.8	8.44	117.1	8.44	117.1	7.80	116.5
D72	8.97	131.6	8.97	131.6	8.63	131.2	8.98	131.7	8.99	131.7	8.56	131.4
S73	8.76	115.6	8.76	115.6	8.89	115.7	8.72	115.5	8.72	115.5	8.37	115.1
Q74	7.66	117.5	7.66	117.5	8.34	118.3	7.70	117.7	7.71	117.8	7.42	117.4
D75	8.86	123.0	8.86	123.0	…	…	8.87	123.1	8.88	123.1	8.70	123.0
K76	8.01	124.2	8.01	124.2	…	…	7.96	124.1	7.96	124.1	7.71	123.9
A77	8.08	122.5	8.08	122.5	…	…	8.26	123.4	8.27	123.5	8.01	123.3
V78	8.37	116.7	8.37	116.7	…	…	8.39	115.9	8.40	115.9	8.23	115.6
L79	8.98	122.8	8.98	122.8	…	…	9.02	123.6	9.03	123.6	8.87	123.5
K80	8.42	119.9	8.42	119.9	…	…	8.37	120.5	8.37	120.5	8.30	120.4
G81	9.06	106.6	9.06	106.6	…	…	9.03	106.5	9.03	106.5	8.97	106.5
G82	7.13	109.0	7.13	109.0	11.28	112.8	7.04	108.7	7.04	108.7	7.02	108.7
L84	7.80	120.3	7.80	120.3	10.13	122.2	7.78	120.3	7.78	120.3	7.72	120.3
D85	9.08	125.2	9.08	125.2	10.01	126.3	9.08	125.2	9.09	125.2	9.02	125.1
G86	7.92	109.5	7.92	109.5	9.00	110.3	7.91	109.5	7.92	109.5	7.84	109.5
T87	8.50	116.4	8.50	116.4	7.40	115.7	8.52	116.7	8.53	116.7	8.42	116.6
Y88	8.44	125.8	8.44	125.8	9.28	125.9	8.43	126.0	8.44	126.0	8.30	125.9
R89	8.63	123.0	8.63	123.0	7.60	121.6	8.60	122.8	8.60	122.8	8.40	122.5
L90	8.55	124.1	8.55	124.1	6.92	122.8	8.54	123.9	8.54	123.9	8.28	123.5
I91	…	…	…	…	…	…	…	…	…	…	…	…
Q92	7.30	115.2	7.30	115.2	6.89	114.8	7.30	115.2	7.30	115.1	6.84	114.6
F93	8.63	113.5	8.63	113.5	8.22	113.1	8.62	113.5	8.60	113.4	7.89	112.9
H94	8.22	113.1	8.22	113.1	7.98	112.9	8.21	113.0	8.21	113.1	7.72	112.6
F95	9.18	117.3	9.18	117.3	8.99	117.0	9.16	117.3	9.16	117.2	8.51	116.7
H96	8.74	115.0	8.74	115.0	8.68	115.0	8.73	115.1	8.76	115.2	8.45	114.7
W97	9.53	119.1	9.53	119.1	9.48	119.1	9.53	119.2	9.54	119.2	9.13	118.9
G98	8.10	108.0	8.10	108.0	8.04	107.9	8.10	108.0	8.11	108.0	7.94	107.7
S99	8.41	111.9	8.41	111.9	8.39	111.8	8.41	111.9	8.42	111.9	8.18	111.6
L100	7.35	119.0	7.35	119.0	7.32	118.9	7.35	119.0	7.36	119.0	7.23	118.9
D101	8.91	120.5	8.91	120.5	8.88	120.5	8.90	120.5	8.91	120.5	8.98	120.5
G102	7.69	102.8	7.69	102.8	7.67	102.7	7.68	102.8	7.69	102.8	7.73	102.8
Q103	7.87	114.9	7.87	114.9	7.85	114.9	7.86	114.9	7.86	114.9	7.85	114.9
G104	8.27	106.3	8.27	106.3	8.27	106.3	8.26	106.3	8.27	106.3	8.17	106.1

[a] Residues 1 to 20 (not assigned) and proline residues 21, 30, 42, 46, 83, 138, 155, 181, 186, 195, 201, 202, 215, 237, 247 and 250 (no resonance in ^{1}H-^{15}N-HSQC) were omitted.

continued on next page …

Table A.3 – continued from previous page

Residue [a]	S50C		S50C-Lu		S50C-Tm		S166C		S166C-Lu		S166C-Tm	
	HN	N	HN	N	HN	N	HN	N	HN	N	HN	N
S105	7.36	107.7	7.36	107.7	7.35	107.7	7.35	107.7	7.36	107.7	7.28	107.7
E106	8.31	119.0	8.31	119.0	8.31	119.1	8.29	119.0	8.31	119.0	8.18	118.8
H107	10.69	117.8	10.69	117.8	10.78	117.9	10.68	117.8	10.69	117.8	10.59	117.7
T108	7.38	109.3	7.38	109.3	7.49	109.3	7.37	109.3	7.37	109.3	7.32	109.2
V109	7.64	118.5	7.64	118.5	7.74	118.6	7.63	118.5	7.63	118.5	7.63	118.5
D110	9.71	132.3	9.71	132.3	9.87	132.4	9.71	132.3	9.72	132.3	9.72	132.3
K111	9.88	109.8	9.88	109.8	9.99	109.9	9.87	109.8	9.88	109.8	9.87	109.8
K112	8.26	124.6	8.26	124.6	8.35	124.6	8.25	124.6	8.26	124.6	8.27	124.6
K113	7.98	122.0	7.98	122.0	8.03	122.1	7.98	122.1	7.98	122.0	7.99	122.1
Y114	8.20	121.4	8.20	121.4	8.22	121.3	8.18	121.3	8.19	121.3	8.19	121.4
A115	7.58	120.9	7.58	120.9	7.57	120.9	7.58	120.9	7.59	120.9	7.69	121.0
A116	8.16	112.0	8.16	112.0	8.13	112.0	8.15	112.0	8.16	112.0	8.20	112.1
E117	9.44	120.9	9.44	120.9	9.38	120.9	9.41	120.8	9.41	120.9	9.27	120.8
L118	9.90	130.5	9.90	130.5	9.83	130.4	9.89	130.4	9.90	130.5	9.84	130.4
H119	9.00	125.1	9.00	125.1	8.86	125.2	9.00	125.2	9.00	125.2	8.71	124.9
L120	9.03	123.7	9.03	123.7	8.97	123.6	9.02	123.6	9.03	123.6	8.84	123.5
V121	9.22	126.6	9.22	126.6	8.93	126.3	9.22	126.6	9.21	126.6	8.85	126.2
H122	8.55	124.1	8.55	124.1	8.50	124.0	8.58	124.2	8.58	124.2	8.34	123.9
W123	9.10	119.1	9.10	119.1	8.57	118.7	9.10	119.1	9.10	119.0	8.83	118.8
N124	9.08	120.0	9.08	120.0	8.76	119.4	9.06	119.8	9.06	119.8	8.89	119.5
T125	8.21	117.4	8.21	117.4	6.94	116.2	8.21	117.3	8.22	117.3	8.06	117.2
K127	7.96	122.9	7.96	122.9	6.77	121.7	7.96	123.0	7.96	123.0	7.83	123.0
Y128	7.69	115.6	7.69	115.6	6.84	114.7	7.68	115.6	7.69	115.6	7.54	115.5
G129	7.88	107.3	7.88	107.3	7.13	106.7	7.88	107.4	7.89	107.4	7.74	107.3
D130	7.45	116.3	7.45	116.3	7.00	115.8	7.46	116.3	7.46	116.3	7.30	116.1
F131	7.63	119.6	7.63	119.6	7.28	119.3	7.63	119.6	7.63	119.6	7.38	119.4
G132	8.11	104.5	8.11	104.5	7.87	104.3	8.10	104.5	8.11	104.5	7.88	104.2
K133	7.65	119.6	7.65	119.6	7.39	119.3	7.65	119.5	7.65	119.6	7.47	119.3
A134	7.95	123.4	7.95	123.4	7.64	123.1	7.95	123.4	7.95	123.4	7.77	123.3
V135	7.94	113.4	7.94	113.4	7.73	113.1	7.94	113.4	7.94	113.4	7.74	113.2
Q136	6.59	113.5	6.59	113.5	6.43	113.4	6.58	113.5	6.59	113.5	6.42	113.3
Q137	7.68	119.1	7.68	119.1	7.54	119.0	7.67	119.1	7.68	119.1	7.53	118.9
D139	7.92	114.6	7.92	114.6	7.86	114.6	7.92	114.6	7.93	114.6	7.82	114.5
G140	8.28	108.1	8.28	108.1	8.24	108.1	8.28	108.1	8.29	108.1	8.15	107.9
L141	8.76	115.6	8.76	115.6	8.79	115.6	8.76	115.6	8.75	115.6	8.59	115.4
A142	8.90	123.5	8.90	123.5	9.03	123.8	8.90	123.5	8.91	123.5	8.72	123.4
V143	7.28	124.2	7.28	124.2	7.68	124.6	7.27	124.2	7.28	124.2	7.13	124.0
L144	8.48	128.4	8.48	128.4	8.66	128.6	8.45	128.2	8.46	128.2	8.29	128.1
G145	9.96	114.4	9.96	114.4	10.26	114.5	9.93	114.2	9.93	114.2	9.85	114.1
I146	9.14	124.2	9.14	124.2	9.17	124.3	9.14	124.3	9.16	124.3	9.10	124.3
F147	10.13	129.0	10.13	129.0	10.19	128.9	10.12	129.0	10.13	129.0	10.20	129.0
L148	8.24	120.3	8.24	120.3	8.22	120.3	8.23	120.4	8.24	120.4	8.35	120.4
K149	8.98	119.3	8.98	119.3	8.92	119.3	8.97	119.4	8.98	119.4	9.30	119.6
V150	8.48	121.4	8.48	121.4	8.43	121.4	8.47	121.4	8.47	121.5	8.79	121.7
G151	9.13	118.2	9.13	118.2	9.02	118.1	9.12	118.2	9.12	118.1	9.75	118.8
S152	8.37	124.6	8.37	124.6	8.25	124.5	8.36	124.5	8.38	124.5	9.06	125.2
A153	8.39	121.1	8.39	121.1	8.21	120.9	8.38	121.2	8.40	121.3	9.61	122.4
K154	8.72	123.9	8.72	123.9	8.48	123.6	8.71	123.9	8.72	123.9	10.07	125.2
G156	…	…	…	…	…	…	…	…	…	…	…	…
L157	7.56	116.8	7.56	116.8	7.13	116.3	7.55	116.8	7.55	116.8	9.03	118.3
Q158	7.80	122.4	7.80	122.4	7.40	122.0	7.80	122.3	7.82	122.3	10.24	124.9
K159	8.85	115.8	8.85	115.8	8.42	115.5	8.85	115.9	8.85	115.8	11.96	119.5
V160	7.04	113.2	7.04	113.2	6.66	112.8	7.04	113.3	7.07	113.7	8.73	115.5
V161	7.30	114.5	7.30	114.5	7.01	114.1	7.28	114.6	7.30	114.7	…	…
D162	8.40	117.5	8.40	117.5	8.14	117.3	8.41	117.6	8.42	117.6	…	…
V163	7.15	113.9	7.15	113.9	6.91	113.7	7.15	115.1	7.08	114.6	…	…

[a] Residues 1 to 20 (not assigned) and proline residues 21, 30, 42, 46, 83, 138, 155, 181, 186, 195, 201, 202, 215, 237, 247 and 250 (no resonance in ^{1}H-^{15}N-HSQC) were omitted.

continued on next page …

Table A.3 – continued from previous page

Residue [a]	S50C		S50C-Lu		S50C-Tm		S166C		S166C-Lu		S166C-Tm	
	HN	N	HN	N	HN	N	HN	N	HN	N	HN	N
L164	7.08	121.7	7.08	121.7	6.88	121.5	7.05	120.9	7.10	121.1	…	…
D165	8.23	116.2	8.23	116.2	8.09	116.1	8.15	115.9	8.15	116.2	…	…
S166	8.01	113.5	8.01	113.5	7.87	113.4	…	…	…	…	…	…
I167	7.43	116.4	7.43	116.4	7.29	116.3	…	…	8.14	114.5	-3.06	104.1
K168	7.41	117.5	7.41	117.5	7.31	117.4	…	…	7.71	117.8	0.28	111.8
T169	6.59	131.5	6.59	131.5	6.51	131.4	6.58	131.4	6.58	131.4	2.74	127.9
K170	7.49	120.5	7.49	120.5	7.42	120.5	7.47	120.5	7.49	120.6	5.77	118.8
G171	8.91	116.9	8.91	116.9	8.81	116.9	8.92	116.9	8.92	116.9	7.24	115.5
K172	7.81	120.2	7.81	120.2	7.73	120.2	7.81	120.2	7.81	120.2	5.82	118.4
S173	8.36	113.7	8.36	113.7	8.27	113.6	8.37	113.8	8.38	113.8	…	…
A174	9.03	123.3	9.03	123.3	8.89	123.2	8.99	123.1	9.00	122.8	…	…
D175	8.63	122.1	8.63	122.1	8.51	121.9	8.62	122.1	8.61	122.2	…	…
F176	8.03	125.4	8.03	125.4	7.80	125.0	7.99	125.2	8.00	125.0	…	…
T177	8.11	114.8	8.11	114.8	7.83	114.5	8.10	114.9	8.07	114.7	…	…
N178	9.72	115.5	9.72	115.5	9.24	114.9	9.72	115.5	9.74	115.6	8.46	114.3
F179	8.28	118.8	8.28	118.8	7.58	118.1	8.28	118.9	8.29	118.9	7.41	118.3
D180	8.04	128.0	8.04	128.0	7.01	126.8	8.02	128.1	8.00	128.1	8.14	128.0
R182	8.33	118.3	8.33	118.3	6.34	116.5	8.35	118.3	8.35	118.3	8.43	118.4
G183	7.31	102.7	7.31	102.7	6.01	101.5	7.31	102.7	7.31	102.7	7.62	103.1
L184	7.24	117.3	7.24	117.3	6.34	116.5	7.25	117.3	7.26	117.3	7.54	117.7
L185	6.64	113.2	6.64	113.2	5.88	112.6	6.65	113.1	6.65	113.1	6.93	113.3
E187	8.18	116.3	8.18	116.3	8.13	116.3	8.18	116.4	8.19	116.4	8.45	116.6
S188	7.64	111.3	7.64	111.3	7.76	111.5	7.63	111.3	7.64	111.3	7.83	111.5
L189	8.65	125.7	8.65	125.7	9.12	126.1	8.65	125.7	8.65	125.7	8.75	125.8
D190	7.43	121.9	7.43	121.9	7.98	122.5	7.42	121.9	7.42	121.9	7.43	121.9
Y191	8.77	119.0	8.77	119.0	9.60	119.7	8.76	118.9	8.77	118.9	8.79	118.9
W192	9.55	117.2	9.55	117.2	10.11	117.8	9.54	117.2	9.55	117.2	9.56	117.1
T193	9.71	115.2	9.71	115.2	10.30	115.8	9.71	115.2	9.71	115.2	9.68	115.2
Y194	8.05	125.5	8.05	125.5	8.55	126.1	8.04	125.5	8.06	125.6	7.99	125.5
G196	9.38	110.8	9.38	110.8	9.60	111.0	9.37	110.8	9.37	110.8	9.26	110.6
S197	8.70	120.0	8.70	120.0	8.82	120.3	…	…	8.70	120.0	8.55	120.0
L198	8.03	118.3	8.03	118.3	8.02	118.3	8.01	118.4	8.02	118.3	7.82	118.1
T199	…	…	…	…	…	…	…	…	…	…	…	…
T200	6.98	108.8	6.98	108.8	6.98	108.6	6.97	108.7	7.00	108.8	6.70	108.4
L203	9.12	120.2	9.12	120.2	9.13	120.3	9.13	120.3	9.14	120.3	8.88	120.0
L204	5.95	111.4	5.95	111.4	5.92	111.3	5.95	111.4	5.96	111.3	5.74	111.1
E205	8.68	125.0	8.68	125.0	8.68	125.0	8.68	125.0	8.68	125.0	8.53	124.9
C206	7.46	113.7	7.46	113.7	7.49	113.8	7.46	113.7	7.47	113.9	7.31	113.6
V207	7.25	116.7	7.25	116.7	7.36	116.8	7.24	116.7	7.25	116.7	7.10	116.5
T208	8.35	125.3	8.35	125.3	8.65	125.7	8.34	125.4	8.35	125.4	8.21	125.3
W209	8.24	129.3	8.24	129.3	8.65	129.8	8.23	129.3	8.23	129.3	8.13	129.2
I210	8.78	127.2	8.78	127.2	9.31	127.9	8.76	127.3	8.77	127.3	8.67	127.3
V211	9.75	128.4	9.75	128.4	10.29	128.9	9.74	128.4	9.75	128.4	9.71	128.4
L212	8.95	126.5	8.95	126.5	9.28	127.0	8.97	126.7	8.98	126.7	8.98	126.8
K213	7.41	122.4	7.41	122.4	7.83	122.7	7.40	122.4	7.41	122.3	7.47	122.4
E214	8.90	121.6	8.90	121.6	9.16	121.8	8.90	121.5	8.90	121.6	9.02	121.7
I216	8.93	113.4	8.93	113.4	8.87	113.3	8.92	113.4	8.93	113.4	9.18	113.6
S217	8.10	116.7	8.10	116.7	7.94	116.5	8.09	116.7	8.10	116.6	8.62	117.1
V218	8.55	115.8	8.55	115.8	8.42	115.7	8.54	115.8	8.54	115.9	9.13	116.5
S219	8.42	115.9	8.42	115.9	8.24	115.8	8.42	115.9	8.42	116.0	9.56	117.1
S220	9.32	117.3	9.32	117.3	9.21	117.2	9.31	117.3	9.31	117.3	10.16	118.2
E221	8.41	118.4	8.41	118.4	8.29	118.3	8.42	118.4	8.41	118.5	9.60	119.6
Q222	7.55	117.9	7.55	117.9	7.39	117.8	7.54	118.0	7.54	118.0	8.89	119.5
V223	7.38	114.7	7.38	114.7	7.24	114.6	7.37	114.7	7.35	114.6	8.11	115.3
L224	8.03	120.9	8.03	120.9	7.91	120.8	8.02	120.9	8.01	120.9	8.58	121.3
K225	6.92	115.0	6.92	115.0	6.79	114.9	6.91	115.2	6.92	115.1	7.44	115.5

[a] Residues 1 to 20 (not assigned) and proline residues 21, 30, 42, 46, 83, 138, 155, 181, 186, 195, 201, 202, 215, 237, 247 and 250 (no resonance in ^{1}H-^{15}N-HSQC) were omitted.

continued on next page …

Table A.3 – continued from previous page

Residue [a]	S50C		S50C-Lu		S50C-Tm		S166C		S166C-Lu		S166C-Tm	
	HN	N	HN	N	HN	N	HN	N	HN	N	HN	N
F226	7.13	118.7	7.13	118.7	7.00	118.6	7.13	118.7	7.13	118.7	6.99	118.4
R227	6.70	109.1	6.70	109.1	6.60	108.9	6.70	109.1	6.71	109.0	6.24	108.4
K228	6.86	114.1	6.86	114.1	6.76	114.0	6.86	114.2	6.87	114.1	5.78	112.9
L229	7.11	119.3	7.11	119.3	7.01	119.3	7.10	119.2	7.10	119.2	5.45	117.3
N230	8.92	118.4	8.92	118.4	8.84	118.4	8.91	118.4	8.89	118.3	6.49	116.2
F231	8.89	117.2	8.89	117.2	8.83	117.1	8.90	117.2	8.90	117.4	7.67	116.0
N232	8.17	110.6	8.17	110.6	8.12	110.6	8.16	110.7	8.17	110.7	6.92	109.5
G233	8.68	104.8	8.68	104.8	8.64	104.7	8.68	104.8	8.68	104.8	7.70	103.6
E234	8.40	121.3	8.40	121.3	8.36	121.2	8.40	121.3	8.40	121.3	7.11	120.0
G235	9.09	114.1	9.09	114.1	9.05	114.1	9.09	114.1	9.09	114.1	7.86	113.0
E236	7.35	120.0	7.35	120.0	7.32	119.9	7.35	120.0	7.36	120.0	6.37	119.0
E238	8.27	123.3	8.27	123.3	8.24	123.2	8.27	123.3	8.27	123.3	7.34	122.3
E239	9.03	130.0	9.03	130.0	8.98	130.0	9.01	129.9	9.01	129.9	7.90	128.9
L240	8.75	126.0	8.75	126.0	8.71	125.9	8.75	126.0	8.75	126.0	7.90	125.0
M241	8.63	123.0	8.63	123.0	8.56	123.0	8.66	123.0	8.66	123.1	7.51	121.9
V242	6.74	114.8	6.74	114.8	6.69	114.8	6.74	114.8	6.75	114.8	6.04	114.1
D243	7.16	114.8	7.16	114.8	7.10	114.7	7.14	114.7	7.14	114.8	6.73	114.3
N244	8.40	119.3	8.40	119.3	8.36	119.2	8.39	119.3	8.40	119.3	7.95	118.8
W245	6.50	114.2	6.50	114.2	6.47	114.1	6.50	114.2	6.51	114.2	6.16	113.8
R246	10.44	127.0	10.44	127.0	10.42	126.9	10.38	126.8	10.40	126.8	10.13	126.5
A248	8.02	120.3	8.02	120.3	8.07	120.3	8.01	120.4	8.01	120.4	7.89	120.2
Q249	8.70	122.0	8.70	122.0	8.81	122.1	8.70	122.0	8.71	122.0	8.61	121.8
L251	8.70	125.9	8.70	125.9	8.81	126.0	8.70	125.9	8.70	125.8	8.63	125.8
K252	8.89	114.6	8.89	114.6	8.99	114.6	8.89	114.6	8.89	114.6	8.83	114.5
N253	8.70	119.7	8.70	119.7	8.82	119.8	8.70	119.6	8.71	119.7	8.65	119.7
R254	7.31	118.5	7.31	118.5	7.47	118.7	7.31	118.6	7.32	118.6	7.26	118.5
Q255	8.60	118.2	8.60	118.2	8.85	118.5	8.59	118.3	8.59	118.2	8.55	118.3
I256	8.94	124.4	8.94	124.4	9.22	124.8	8.92	124.4	8.93	124.4	8.90	124.4
K257	8.81	126.6	8.81	126.6	9.28	127.0	8.80	126.6	8.81	126.6	8.77	126.7
A258	8.40	123.6	8.40	123.6	8.93	124.2	8.39	123.6	8.40	123.6	8.39	123.6
S259	8.98	116.5	8.98	116.5	9.74	117.2	8.96	116.4	8.97	116.4	8.98	116.4
F260	6.67	118.0	6.67	118.0	7.32	118.7	6.66	118.0	6.67	118.0	6.69	118.0
K261	7.77	124.4	7.77	124.4	8.31	125.0	7.76	124.4	7.76	124.4	7.81	124.4

[a]Residues 1 to 21 (not assigned) and proline residues 21, 30, 42, 46, 83, 138, 155, 181, 186, 195, 201, 202, 215, 237, 247 and 250 (no resonance in ^{1}H-^{15}N-HSQC) were omitted.

Table A.4: ^{1}H-^{15}N HSQC peak assignments for untagged, LuM8 tagged and TmM8 tagged hCA-II mutants S217C and S220C. All values are given in ppm.

Residue [a]	S217C		S217C-Lu		S217C-Tm		S220C		S220C-Lu		S220C-Tm	
	HN	N	HN	N	HN	N	HN	N	HN	N	HN	N
I22	8.07	120.5	8.06	120.6	7.98	120.4	8.07	120.4	8.07	120.6	7.98	120.5
A23	8.69	123.0	8.70	123.0	8.60	122.9	8.67	122.9	8.70	123.0	8.60	122.9
K24	7.21	114.7	7.21	114.8	7.11	114.7	7.20	114.7	7.21	114.7	…	…
G25	8.32	108.8	8.32	108.8	8.18	108.6	8.31	108.8	8.32	108.8	8.24	108.8
E26	9.37	117.7	9.37	117.7	9.20	117.5	9.37	117.7	9.36	117.7	9.31	117.6
R27	8.87	121.4	8.87	121.4	8.65	121.2	8.86	121.4	8.87	121.5	8.80	121.5
Q28	7.71	115.5	7.72	115.5	7.46	115.1	7.71	115.5	7.71	115.4	7.64	115.4

[a] Residues 1 to 20 (not assigned) and proline residues 21, 30, 42, 46, 83, 138, 155, 181, 186, 195, 201, 202, 215, 237, 247 and 250 (no resonance in ^{1}H-^{15}N-HSQC) were omitted.

continued on next page …

Table A.4 – continued from previous page

Residue [a]	S217C		S217C-Lu		S217C-Tm		S220C		S220C-Lu		S220C-Tm	
	HN	N	HN	N	HN	N	HN	N	HN	N	HN	N
S29	8.07	117.9	8.08	117.9	7.81	117.6	8.05	117.8	8.09	117.9	7.98	117.8
V31	6.31	107.0	6.30	107.0	5.71	106.4	6.30	107.0	6.30	106.9	6.21	106.9
D32	8.35	118.3	8.35	118.3	7.73	117.6	8.35	118.3	8.33	118.2	8.30	118.2
I33	8.73	128.5	8.73	128.5	7.54	127.3	8.73	128.5	8.72	128.5	8.75	128.5
D34	7.53	128.2	7.52	128.2	6.43	127.0	7.54	128.2	7.52	128.2	7.57	128.3
T35	10.30	122.2	10.30	122.2	8.54	120.6	10.29	122.3	10.30	122.2	10.43	122.3
H36	8.81	118.8	8.82	118.8	7.44	117.4	8.80	118.8	8.81	118.8	8.93	119.0
T37	7.65	108.6	7.66	108.6	6.57	107.6	7.64	108.6	7.65	108.6	7.73	108.7
A38	7.49	127.5	7.49	127.5	6.34	126.5	7.48	127.6	7.49	127.5	7.56	127.6
K39	8.15	122.7	8.15	122.7	7.34	121.9	8.13	122.7	8.14	122.7	8.17	122.7
Y40	8.72	126.7	8.72	126.8	7.92	126.0	8.72	126.7	8.72	126.7	8.77	126.8
D41	7.75	128.8	7.75	128.9	7.18	128.3	7.74	128.9	7.73	128.8	7.75	128.8
S43	8.50	115.2	8.50	115.2	8.25	115.1	8.50	115.2	8.50	115.2	8.51	115.2
L44	7.00	123.1	7.01	123.1	6.76	122.9	6.99	123.1	6.99	123.1	6.99	123.1
K45	7.58	123.2	7.58	123.1	7.45	123.0	7.58	123.2	7.58	123.2	7.56	123.2
L47	8.98	126.0	8.98	126.0	9.05	126.1	8.97	126.1	8.97	126.1	8.94	126.0
S48	8.52	120.1	8.52	120.1	8.59	120.2	8.53	120.2	8.54	120.2	8.47	120.2
V49	8.42	127.6	8.41	127.6	8.70	127.8	8.41	127.6	8.41	127.6	8.33	127.5
S50	8.38	122.8	8.38	122.8	8.51	122.9	8.37	122.8	8.38	122.8	8.28	122.7
Y51	9.01	124.6	9.02	124.6	9.23	124.7	9.00	124.6	9.00	124.6	8.87	124.4
D52	8.89	121.4	8.89	121.4	9.10	121.5	8.89	121.4	8.89	121.3	8.76	121.2
Q53	8.06	114.4	8.06	114.4	8.19	114.4	8.05	114.4	8.05	114.4	7.93	114.3
A54	7.42	120.2	7.42	120.2	7.48	120.2	7.42	120.2	7.43	120.2	7.28	120.0
T55	9.43	120.7	9.43	120.7	9.43	120.7	9.44	120.7	9.44	120.7	9.29	120.5
S56	10.00	126.5	10.01	126.5	9.97	126.5	10.01	126.5	10.01	126.5	9.82	126.3
L57	8.93	117.6	8.94	117.6	8.89	117.6	8.93	117.6	8.94	117.6	8.75	117.4
R58	7.21	114.7	7.21	114.8	7.15	114.7	7.20	114.7	7.21	114.7	7.01	114.5
I59	9.05	122.1	9.06	122.1	9.02	122.0	9.04	122.1	9.05	122.0	8.81	121.8
L60	8.71	123.8	8.70	123.8	8.68	123.7	8.70	123.8	8.70	123.7	8.41	123.5
N61	8.44	121.2	8.45	121.1	…	…	8.44	121.2	8.45	121.1	8.21	120.9
N62	8.06	123.4	8.04	123.3	8.04	123.3	8.05	123.4	8.05	123.3	7.78	123.0
G63	9.74	109.1	9.71	109.1	9.74	109.1	9.72	108.9	9.71	109.1	9.46	108.8
H64	…	…	…	…	…	…	…	…	…	…	…	…
A65	…	…	8.61	123.6	…	…	…	…	8.63	123.5	…	…
F66	7.22	110.1	7.22	110.1	7.23	110.1	7.23	110.1	7.23	110.1	6.78	109.7
N67	9.01	120.8	8.97	120.8	8.96	120.8	9.01	120.8	8.97	120.8	8.66	120.5
V68	8.72	122.0	8.72	122.0	…	…	8.70	122.0	8.71	122.0	8.30	121.6
E69	8.48	124.0	8.48	123.9	8.42	123.8	8.47	123.9	8.48	123.9	8.24	123.7
F70	8.64	119.0	8.64	119.0	8.58	118.9	8.64	119.0	8.64	119.0	8.46	118.8
D71	8.44	117.0	8.44	117.0	8.40	117.0	8.45	117.1	8.46	117.1	8.32	117.0
D72	8.99	131.8	8.99	131.8	8.97	131.8	8.99	131.8	8.99	131.8	8.87	131.7
S73	8.73	115.5	8.73	115.5	8.72	115.4	8.72	115.5	8.72	115.5	8.62	115.3
Q74	7.70	117.7	7.70	117.7	7.70	117.8	7.70	117.7	7.70	117.7	7.61	117.6
D75	8.87	123.0	8.88	123.1	8.86	123.1	8.87	123.1	8.89	123.1	8.73	123.0
K76	7.96	124.1	7.96	124.1	7.98	124.2	7.96	124.2	7.96	124.2	7.86	124.0
A77	8.27	123.4	8.28	123.5	8.29	123.5	8.27	123.5	8.29	123.5	8.17	123.4
V78	8.40	115.9	8.39	115.9	8.45	115.9	8.39	115.9	8.40	115.9	8.29	115.7
L79	9.02	123.7	9.02	123.6	9.00	123.5	9.02	123.6	9.03	123.6	8.92	123.5
K80	8.38	120.5	8.38	120.6	8.39	120.5	8.37	120.5	8.37	120.5	8.29	120.4
G81	9.03	106.5	9.03	106.5	9.02	106.5	9.03	106.5	9.03	106.5	8.98	106.4
G82	7.05	108.7	7.06	108.7	7.02	108.7	7.04	108.8	7.03	108.8	7.00	108.7
L84	7.78	120.3	7.78	120.3	7.61	120.1	7.78	120.3	7.79	120.3	7.74	120.3
D85	9.09	125.2	9.09	125.2	8.96	125.2	9.09	125.3	9.09	125.2	9.05	125.2
G86	7.92	109.5	7.92	109.5	7.87	109.5	7.92	109.5	7.92	109.5	7.87	109.5
T87	8.53	116.7	8.53	116.7	8.50	116.7	8.53	116.8	8.53	116.7	8.47	116.6
Y88	8.44	126.0	8.45	126.0	8.41	126.0	8.43	126.0	8.44	126.0	8.36	125.9

[a] Residues 1 to 20 (not assigned) and proline residues 21, 30, 42, 46, 83, 138, 155, 181, 186, 195, 201, 202, 215, 237, 247 and 250 (no resonance in ^{1}H-^{15}N-HSQC) were omitted.

continued on next page …

Table A.4 – continued from previous page

Residue [a]	S217C		S217C-Lu		S217C-Tm		S220C		S220C-Lu		S220C-Tm	
	HN	N	HN	N	HN	N	HN	N	HN	N	HN	N
R89	8.60	122.8	8.60	122.8	8.54	122.7	8.60	122.8	8.60	122.7	8.50	122.6
L90	8.55	123.9	8.54	123.8	8.49	123.9	8.55	123.8	8.55	123.8	8.42	123.6
I91	…	…	…	…	…	…	…	…	…	…	…	…
Q92	7.31	115.2	7.30	115.1	7.19	114.9	7.30	115.3	7.30	115.1	7.10	114.9
F93	8.64	113.6	8.61	113.5	8.52	113.3	8.63	113.5	8.59	113.4	8.32	113.2
H94	8.20	113.0	8.20	113.1	8.03	113.0	8.20	113.0	8.21	113.0	7.88	112.7
F95	9.17	117.3	9.15	117.2	9.12	117.1	9.19	117.3	9.18	117.2	8.71	116.8
H96	8.73	115.0	8.74	115.1	8.72	115.1	8.74	115.1	8.81	115.2	8.31	114.7
W97	9.53	119.1	9.55	119.2	9.75	119.4	9.52	119.1	9.51	119.1	8.79	118.3
G98	8.13	108.0	8.14	108.0	8.77	108.6	8.09	108.0	8.03	107.8	6.78	106.6
S99	8.42	111.9	8.43	112.0	9.01	112.5	8.41	111.9	8.47	112.1	7.57	111.3
L100	7.37	119.0	7.39	119.0	8.17	119.8	7.32	119.1	7.26	119.6	6.48	118.9
D101	8.92	120.6	8.93	120.6	10.34	122.0	8.86	120.5	8.74	120.4	…	…
G102	7.69	102.8	7.68	102.8	9.19	104.3	7.71	102.9	7.81	103.6	6.37	102.6
Q103	7.87	114.9	7.86	114.9	8.97	115.9	7.86	115.0	7.79	114.8	…	…
G104	8.27	106.3	8.26	106.3	8.71	106.8	8.27	106.3	8.28	106.6	7.73	106.0
S105	7.36	107.7	7.36	107.7	7.72	108.0	7.35	107.7	7.36	107.8	7.00	107.4
E106	8.31	119.0	8.31	119.0	8.00	118.8	8.32	119.0	8.34	119.0	8.10	118.7
H107	10.69	117.8	10.71	117.8	10.14	117.2	10.68	117.8	10.67	117.8	10.52	117.7
T108	7.37	109.3	7.37	109.3	6.50	108.4	7.37	109.3	7.38	109.3	7.35	109.2
V109	7.63	118.6	7.64	118.6	6.23	117.0	7.64	118.6	7.69	118.6	7.83	118.7
D110	9.72	132.3	9.72	132.3	8.07	130.6	9.71	132.4	9.72	132.3	9.85	132.5
K111	9.87	109.8	9.88	109.8	8.84	108.8	9.88	109.8	9.89	109.8	9.99	109.9
K112	8.26	124.5	8.26	124.5	7.04	123.6	8.25	124.6	8.25	124.5	8.44	124.7
K113	7.98	121.8	7.98	121.6	8.14	121.6	7.98	122.1	7.97	122.1	8.13	122.3
Y114	8.18	121.3	8.15	121.1	…	…	8.19	121.4	8.20	121.2	8.20	121.2
A115	7.59	120.9	7.65	120.8	…	…	7.59	120.9	7.71	121.0	7.26	122.0
A116	8.15	111.9	8.11	111.7	8.96	112.5	8.16	112.1	8.15	112.0	7.91	111.6
E117	9.41	120.8	9.41	120.9	9.43	120.9	9.42	120.8	9.45	120.8	8.98	120.5
L118	9.90	130.4	9.92	130.5	9.33	130.1	9.90	130.5	9.92	130.5	9.63	130.2
H119	9.00	125.1	9.00	125.2	8.72	124.8	9.00	125.2	9.00	125.1	8.67	124.9
L120	9.02	123.7	9.02	123.6	8.63	123.3	9.02	123.6	9.03	123.6	8.83	123.4
V121	9.23	126.6	9.21	126.6	9.03	126.3	9.23	126.6	9.23	126.6	9.02	126.4
H122	8.58	124.2	8.58	124.2	8.40	124.0	8.58	124.3	8.59	124.2	8.45	124.1
W123	9.10	119.1	9.10	119.0	9.00	118.9	9.10	119.1	9.10	119.0	8.99	118.9
N124	9.06	119.8	9.06	119.8	8.95	119.8	9.06	119.8	9.07	119.8	8.98	119.7
T125	8.22	117.3	8.22	117.3	8.16	117.2	8.21	117.3	8.22	117.3	8.14	117.2
K127	7.96	123.0	7.96	123.0	7.91	123.0	7.95	123.0	7.96	123.0	7.90	122.9
Y128	7.68	115.6	7.68	115.5	7.63	115.5	7.68	115.6	7.69	115.5	7.62	115.4
G129	7.89	107.4	7.89	107.4	7.85	107.3	7.88	107.4	7.89	107.4	7.82	107.4
D130	7.46	116.3	7.47	116.3	7.42	116.3	7.46	116.3	7.47	116.3	7.39	116.3
F131	7.64	119.6	7.63	119.6	7.58	119.5	7.64	119.6	7.65	119.6	7.56	119.5
G132	8.11	104.5	8.11	104.5	8.06	104.4	8.11	104.6	8.11	104.5	8.02	104.4
K133	7.66	119.5	7.65	119.6	7.59	119.5	7.65	119.6	7.65	119.6	7.57	119.5
A134	7.95	123.4	7.96	123.4	7.89	123.3	7.95	123.5	7.96	123.5	7.88	123.4
V135	7.94	113.4	7.94	113.4	7.85	113.3	7.94	113.4	7.95	113.4	7.86	113.3
Q136	6.59	113.5	6.59	113.5	6.50	113.4	6.58	113.5	6.58	113.5	6.50	113.5
Q137	7.67	119.1	7.68	119.1	7.57	118.9	7.67	119.1	7.68	119.1	7.60	119.1
D139	7.93	114.6	7.93	114.6	7.79	114.4	7.92	114.6	7.94	114.6	7.88	114.5
G140	8.29	108.1	8.29	108.1	8.14	108.0	8.28	108.1	8.28	108.1	8.21	108.0
L141	8.74	115.5	8.75	115.6	8.58	115.4	8.76	115.6	8.77	115.6	8.69	115.6
A142	8.90	123.5	8.91	123.6	8.72	123.3	8.90	123.5	8.90	123.5	8.80	123.4
V143	7.27	124.2	7.28	124.2	6.93	123.8	7.28	124.2	7.29	124.2	7.18	124.1
L144	8.45	128.1	8.46	128.1	8.08	127.7	8.46	128.2	8.47	128.1	8.32	128.0
G145	9.93	114.2	9.92	114.2	9.09	113.4	9.93	114.2	9.93	114.2	9.82	114.1
I146	9.15	124.3	9.14	124.3	8.25	123.2	9.14	124.3	9.17	124.3	8.98	124.1

[a] Residues 1 to 20 (not assigned) and proline residues 21, 30, 42, 46, 83, 138, 155, 181, 186, 195, 201, 202, 215, 237, 247 and 250 (no resonance in ^{1}H-^{15}N-HSQC) were omitted.

continued on next page …

Table A.4 – continued from previous page

Residue [a]	S217C		S217C-Lu		S217C-Tm		S220C		S220C-Lu		S220C-Tm	
	HN	N	HN	N	HN	N	HN	N	HN	N	HN	N
F147	10.13	129.0	10.10	129.0	7.96	127.1	10.14	129.0	10.15	129.0	10.11	129.0
L148	8.24	120.4	8.20	120.5	10.16	122.6	8.23	120.3	8.22	120.1	8.11	120.1
K149	9.00	120.1	9.08	121.9	…	…	8.97	119.3	8.93	118.6	…	…
V150	8.48	121.9	8.27	120.3	…	…	8.47	120.8	8.62	121.4	9.27	122.3
G151	9.09	117.6	7.64	120.2	…	…	9.07	117.6	9.14	118.3	…	…
S152	8.26	124.0	8.34	122.3	…	…	8.38	124.5	8.37	124.5	…	…
A153	8.21	119.5	…	…	…	…	8.40	121.3	8.38	121.0	7.42	120.2
K154	8.73	123.9	8.70	124.1	…	…	8.71	124.0	8.67	123.9	…	…
G156	…	…	…	…	…	…	…	…	…	…	…	…
L157	7.54	116.8	7.53	116.7	…	…	7.55	116.7	7.58	116.8	6.66	116.0
Q158	7.80	122.2	7.79	122.2	7.43	121.9	7.80	122.4	7.80	122.3	6.83	121.4
K159	8.80	115.8	8.81	115.8	8.53	115.5	8.84	115.9	8.83	115.8	8.15	115.2
V160	7.04	113.2	7.03	113.2	…	…	7.03	113.2	7.04	113.1	6.31	112.5
V161	7.30	114.4	7.30	114.3	7.23	114.3	7.30	114.5	7.31	114.1	6.32	113.2
D162	8.41	117.6	8.40	117.6	8.26	117.5	8.40	117.6	8.40	117.8	7.55	117.0
V163	7.14	113.9	7.14	113.8	7.06	113.7	7.14	113.9	7.15	113.8	6.54	113.3
L164	7.08	121.6	7.07	121.6	7.06	121.6	7.07	121.7	7.08	121.7	6.44	121.1
D165	8.22	116.2	8.22	116.2	8.21	116.2	8.23	116.3	8.24	116.2	7.76	115.8
S166	8.01	113.5	8.00	113.5	7.98	113.5	8.00	113.6	8.00	113.6	7.69	113.4
I167	7.42	116.4	7.42	116.4	7.46	116.3	7.42	116.5	7.42	116.4	7.12	116.1
K168	7.42	117.5	7.42	117.4	7.44	117.4	7.42	117.5	7.40	117.5	7.20	117.3
T169	6.59	131.5	6.60	131.6	6.63	131.6	6.58	131.4	6.59	131.4	6.43	131.2
K170	7.49	120.5	7.50	120.6	7.53	120.7	7.48	120.5	7.49	120.5	7.34	120.4
G171	8.92	116.9	8.89	116.9	8.90	116.9	8.91	116.9	8.89	116.9	8.71	116.8
K172	7.81	120.2	7.82	120.2	7.81	120.2	7.81	120.2	7.80	120.2	7.64	120.0
S173	8.36	113.8	8.36	113.7	8.35	113.7	8.36	113.8	8.36	113.8	8.21	113.6
A174	9.03	123.3	9.03	123.4	9.01	123.3	9.02	123.4	9.03	123.4	8.82	123.3
D175	8.63	122.0	8.63	122.0	8.59	122.0	8.63	122.1	8.63	122.1	8.47	121.9
F176	8.01	125.3	8.00	125.3	7.95	125.2	8.01	125.3	8.01	125.3	7.81	125.0
T177	8.12	114.9	8.12	114.9	8.04	114.8	8.12	114.9	8.12	114.9	7.92	114.7
N178	9.73	115.5	9.73	115.5	9.68	115.4	9.73	115.5	9.73	115.5	9.55	115.2
F179	8.28	118.9	8.28	118.9	8.21	118.8	8.27	118.9	8.28	118.9	8.05	118.6
D180	8.02	128.1	8.02	128.1	7.91	128.0	8.02	128.1	8.01	128.1	7.71	127.8
R182	8.35	118.3	8.35	118.3	8.37	118.3	8.35	118.3	8.36	118.4	8.11	118.2
G183	7.32	102.7	7.33	102.8	7.25	102.7	7.31	102.7	7.32	102.6	7.00	102.3
L184	7.26	117.3	7.26	117.4	7.09	117.2	7.25	117.3	7.25	117.3	6.91	116.9
L185	6.66	113.2	6.64	113.1	6.48	112.8	6.65	113.1	6.65	113.1	6.36	112.8
E187	8.20	116.4	8.18	116.3	…	…	8.18	116.4	8.19	116.4	8.18	116.4
S188	7.64	111.3	7.62	111.6	…	…	7.64	111.3	7.65	111.4	7.63	111.3
L189	8.65	125.7	8.63	125.8	9.56	126.4	8.66	125.7	8.65	125.7	8.63	125.7
D190	7.42	121.9	7.47	122.0	7.18	121.5	7.43	121.9	7.42	121.9	7.44	121.8
Y191	8.77	118.9	8.75	118.8	7.70	117.8	8.77	118.9	8.76	119.2	…	…
W192	9.55	117.2	9.56	117.2	8.00	115.6	9.54	117.2	9.55	117.2	9.55	117.2
T193	9.71	115.2	9.71	115.1	8.84	114.3	9.71	115.2	9.71	115.2	9.71	115.2
Y194	8.05	125.5	8.06	125.5	7.46	124.9	8.04	125.5	8.06	125.6	8.02	125.6
G196	9.37	110.8	9.37	110.8	9.04	110.5	9.38	110.8	9.39	110.8	9.32	110.7
S197	…	…	8.70	120.0	8.40	119.8	…	…	8.70	120.0	8.62	120.0
L198	8.04	118.3	8.02	118.3	7.83	118.1	8.03	118.4	8.02	118.3	7.90	118.2
T199	…	…	…	…	…	…	…	…	…	…	…	…
T200	6.99	108.8	7.00	108.8	6.86	108.8	6.97	108.7	7.00	108.8	6.82	108.6
L203	9.13	120.2	9.14	120.3	9.03	120.1	9.13	120.3	9.14	120.3	9.00	120.2
L204	5.95	111.3	5.96	111.3	5.83	111.1	5.94	111.4	5.95	111.4	5.84	111.3
E205	8.69	125.0	8.68	125.0	8.54	124.8	8.68	125.0	8.68	125.0	8.60	124.9
C206	7.46	113.7	7.47	113.8	7.28	113.6	7.46	113.7	7.47	113.8	7.38	113.7
V207	7.24	116.7	7.25	116.7	7.01	116.5	7.25	116.7	7.25	116.7	7.17	116.6
T208	8.34	125.4	8.35	125.4	8.07	125.1	8.34	125.4	8.35	125.4	8.27	125.3

[a] Residues 1 to 20 (not assigned) and proline residues 21, 30, 42, 46, 83, 138, 155, 181, 186, 195, 201, 202, 215, 237, 247 and 250 (no resonance in ^{1}H-^{15}N-HSQC) were omitted.

continued on next page …

Table A.4 – continued from previous page

Residue [a]	S217C		S217C-Lu		S217C-Tm		S220C		S220C-Lu		S220C-Tm	
	HN	N	HN	N	HN	N	HN	N	HN	N	HN	N
W209	8.23	129.3	8.23	129.3	7.77	128.8	8.23	129.3	8.24	129.4	8.18	129.3
I210	8.76	127.3	8.77	127.3	8.18	126.7	8.76	127.3	8.78	127.3	8.69	127.3
V211	9.75	128.5	9.74	128.4	8.68	127.3	9.75	128.5	9.75	128.5	9.71	128.4
L212	8.97	126.8	8.96	126.7	7.30	125.0	8.97	126.7	8.99	126.7	8.94	126.7
K213	7.41	122.4	7.40	122.2	…	…	7.41	122.4	7.41	122.3	7.45	122.4
E214	8.91	121.7	8.95	122.3	…	…	8.90	121.6	8.90	121.7	8.97	121.7
I216	8.91	113.0	8.77	110.2	…	…	8.93	113.4	8.94	113.3	8.92	113.3
S217	8.15	119.8	7.72	121.0	…	…	8.07	116.5	8.07	116.4	…	…
V218	8.55	115.6	8.59	115.1	…	…	8.52	115.6	8.56	115.6	…	…
S219	8.42	116.0	8.38	116.3	…	…	…	…	…	…	…	…
S220	9.32	117.4	9.42	118.1	10.79	119.3	…	…	…	…	…	…
E221	8.41	118.6	8.44	118.8	8.98	119.4	8.51	118.1	8.48	118.1	…	…
Q222	7.57	118.1	7.58	118.1	8.08	118.5	7.53	118.0	7.47	117.4	…	…
V223	7.33	114.6	7.30	114.3	8.11	114.9	7.39	114.9	7.47	115.6	…	…
L224	7.98	120.6	7.98	120.6	8.63	121.2	7.96	120.7	8.13	120.0	…	…
K225	6.93	115.2	6.92	115.2	7.27	115.6	6.90	114.9	6.99	115.7	…	…
F226	7.16	118.8	7.14	118.7	7.49	119.0	7.11	118.7	7.12	118.8	…	…
R227	6.71	109.0	6.70	109.0	7.07	109.3	6.70	109.1	6.68	108.9	…	…
K228	6.88	114.1	6.87	114.1	7.12	114.4	6.85	114.2	6.87	114.4	…	…
L229	7.11	119.3	7.11	119.2	7.29	119.4	7.10	119.4	7.11	119.3	…	…
N230	8.92	118.4	8.92	118.4	9.02	118.6	8.92	118.5	8.90	118.4	8.62	118.1
F231	8.90	117.2	8.89	117.3	9.00	117.4	8.89	117.1	8.89	117.2	8.66	116.9
N232	8.17	110.6	8.18	110.7	8.26	110.7	8.17	110.6	8.18	110.7	8.03	110.5
G233	8.68	104.8	8.68	104.8	8.72	104.8	8.68	104.8	8.69	104.8	8.62	104.7
E234	8.41	121.3	8.41	121.3	8.43	121.4	8.40	121.3	8.41	121.4	8.36	121.3
G235	9.09	114.1	9.10	114.1	9.13	114.1	9.09	114.1	9.09	114.1	9.12	114.2
E236	7.36	120.0	7.35	120.0	7.40	120.1	7.35	120.0	7.36	120.0	7.38	120.0
E238	8.27	123.3	8.27	123.3	8.37	123.4	8.27	123.3	8.27	123.3	8.39	123.4
E239	9.03	130.0	9.02	130.0	9.13	130.1	9.03	130.0	9.04	129.9	8.99	129.9
L240	8.75	125.9	8.75	125.9	8.92	126.2	8.76	126.0	8.76	125.9	8.61	125.7
M241	8.63	123.0	8.64	123.0	8.81	123.1	8.62	123.0	8.65	123.1	8.08	122.6
V242	6.75	114.9	6.75	114.9	6.96	115.2	6.73	114.8	6.73	115.0	6.11	114.3
D243	7.12	114.7	7.11	114.8	7.46	115.1	7.15	114.7	7.14	114.7	6.27	113.9
N244	8.39	119.2	8.40	119.3	8.59	119.4	8.39	119.3	8.38	119.2	7.72	118.5
W245	6.51	114.2	6.51	114.2	6.61	114.3	6.49	114.2	6.50	114.2	6.01	113.7
R246	10.36	126.7	10.39	126.8	10.30	126.8	10.36	126.7	10.38	126.7	10.08	126.3
A248	8.02	120.4	8.01	120.4	7.81	120.2	8.02	120.3	8.01	120.4	7.85	120.2
Q249	8.70	122.0	8.67	122.0	8.39	121.7	8.70	122.0	8.71	122.0	8.61	121.9
L251	8.71	125.8	8.70	125.8	8.32	125.5	8.70	125.9	8.70	125.8	8.66	125.7
K252	8.89	114.6	8.90	114.6	8.57	114.3	8.89	114.6	8.89	114.6	8.87	114.5
N253	8.71	119.7	8.71	119.7	8.41	119.3	8.70	119.7	8.71	119.7	8.68	119.6
R254	7.32	118.6	7.32	118.6	6.96	118.3	7.31	118.6	7.31	118.6	7.29	118.5
Q255	8.60	118.2	8.59	118.2	8.16	117.8	8.60	118.3	8.60	118.3	8.59	118.2
I256	8.93	124.4	8.93	124.4	8.26	123.7	8.93	124.4	8.93	124.4	8.94	124.4
K257	8.81	126.6	8.80	126.6	8.07	125.8	8.81	126.6	8.81	126.6	8.81	126.6
A258	8.40	123.6	8.40	123.6	7.57	122.7	8.38	123.6	8.39	123.6	8.42	123.6
S259	8.97	116.4	8.97	116.5	8.00	115.6	8.97	116.4	8.97	116.4	8.99	116.4
F260	6.67	118.0	6.67	118.0	5.69	117.2	6.66	118.0	6.67	118.0	6.72	118.1
K261	7.77	124.4	7.76	124.4	7.13	123.6	7.77	124.5	7.77	124.4	7.83	124.5

[a] Residues 1 to 21 (not assigned) and proline residues 21, 30, 42, 46, 83, 138, 155, 181, 186, 195, 201, 202, 215, 237, 247 and 250 (no resonance in ^{1}H-^{15}N-HSQC) were omitted.

Table A.5: Arginine sidechain NH assignment of LuM8 and TmM8 tagged hCA-II mutants S50C and S166C as well as the corresponding PCS. All values are given in ppm.

Residue	S50C-Lu		S50C-Tm		PCS		S166C-Lu		S166C-Tm		PCS	
	He	Ne	He	Ne	He	Ne	He	Ne	He	Ne	He	Ne
R27	7.14	117.3	7.24	117.4	0.103	0.167	7.13	117.3	7.03	117.2	-0.101	-0.117
R58	7.49	116.1	7.36	116.0	-0.125	-0.163	7.50	116.1	6.44	115.0	-1.058	-1.098
R89	7.72	118.5	…	…	…	…	7.72	118.5	7.52	118.3	-0.197	-0.245
R182	8.27	116.8	…	…	…	…	8.26	116.8	8.35	116.8	0.089	0.078
R227	6.97	118.3	6.92	118.2	-0.053	-0.058	6.97	118.3	6.81	118.2	-0.161	-0.156
R246	7.09	118.2	7.14	118.2	0.050	0.039	7.12	118.2	6.93	118.0	-0.185	-0.239
R254	7.77	117.2	7.90	117.4	0.133	0.179	7.76	117.2	7.69	117.1	-0.076	-0.099

Table A.6: Arginine sidechain NH assignment of LuM8 and TmM8 tagged hCA-II mutants S217C and S220C as well as the corresponding PCS. All values are given in ppm.

Residue	S217C-Lu		S217C-Tm		PCS		S220C-Lu		S220C-Tm		PCS	
	He	Ne	He	Ne	He	Ne	He	Ne	He	Ne	He	Ne
R27	7.13	117.3	6.90	117.0	-0.234	-0.268	7.13	117.3	7.07	117.3	-0.058	-0.047
R58	7.49	116.1	7.47	116.1	-0.025	-0.048	7.49	116.1	7.33	116.0	-0.156	-0.122
R89	7.72	118.6	7.72	118.6	-0.006	-0.004	7.73	118.6	7.64	118.5	-0.092	-0.101
R182	8.27	116.8	8.49	117.0	0.218	0.238	8.26	116.8	8.06	116.6	-0.200	-0.155
R227	7.02	118.6	7.73	119.3	0.713	0.713	6.99	117.6	…	…	…	…
R246	7.12	118.2	7.00	118.1	-0.116	-0.129	7.13	118.2	6.97	118.1	-0.157	-0.164
R254	7.76	117.2	7.40	116.9	-0.362	-0.312	7.77	117.2	7.72	117.1	-0.044	-0.057

Table A.7: Tryptophan sidechain NH assignment of LuM8 and TmM8 tagged hCA-II mutants S50C and S166C as well as the corresponding PCS. All values are given in ppm.

Residue	S50C-Lu		S50C-Tm		PCS		S166C-Lu		S166C-Tm		PCS	
	He	Ne	He	Ne	He	Ne	He	Ne	He	Ne	He	Ne
W5	9.82	129.9	9.76	129.7	-0.062	-0.129	9.82	129.9	9.44	129.5	-0.381	-0.358
W16	10.26	128.5	10.23	128.3	-0.036	-0.168	10.24	128.4	9.92	128.1	-0.322	-0.334
W97	10.22	130.6	10.13	130.5	-0.083	-0.120	10.21	130.6	9.50	130.0	-0.708	-0.616
W123	12.23	133.5	11.64	132.9	-0.588	-0.643	12.22	133.5	11.91	133.2	-0.306	-0.321
W192	10.51	129.0	10.87	129.4	0.352	0.368	10.51	129.0	10.52	129.0	0.011	0.050
W209	10.08	130.5	10.22	130.6	0.142	0.077	10.09	130.5	9.92	130.4	-0.164	-0.150
W245	10.82	126.8	10.81	126.7	-0.007	-0.048	10.83	126.8	10.60	126.5	-0.232	-0.282

Table A.8: Tryptophan sidechain NH assignment of LuM8 and TmM8 tagged hCA-II mutants S217C and S220C as well as the corresponding PCS. All values are given in ppm.

Residue	S217C-Lu		S217C-Tm		PCS		S220C-Lu		S220C-Tm		PCS	
	He	Ne	He	Ne	He	Ne	He	Ne	He	Ne	He	Ne
W5	9.83	129.9	9.80	129.9	-0.030	0.060	9.82	129.9	9.68	129.7	-0.146	-0.162
W16	10.25	128.4	10.25	128.4	0.001	-0.009	10.24	128.4	10.05	128.2	-0.191	-0.160
W97	10.24	130.6	10.53	131.0	0.291	0.345	10.18	130.6	9.16	129.6	-1.025	-1.044
W123	12.22	133.5	12.16	133.4	-0.052	-0.089	12.22	133.5	12.11	133.4	-0.116	-0.107
W192	10.51	128.9	8.50	126.9	-2.008	-2.062	10.51	129.0	10.60	129.0	0.083	0.091
W209	10.09	130.5	9.74	130.1	-0.350	-0.428	10.09	130.5	9.98	130.4	-0.113	-0.105
W245	10.85	126.9	11.18	127.1	0.331	0.256	10.78	126.8	9.98	126.1	-0.802	-0.694

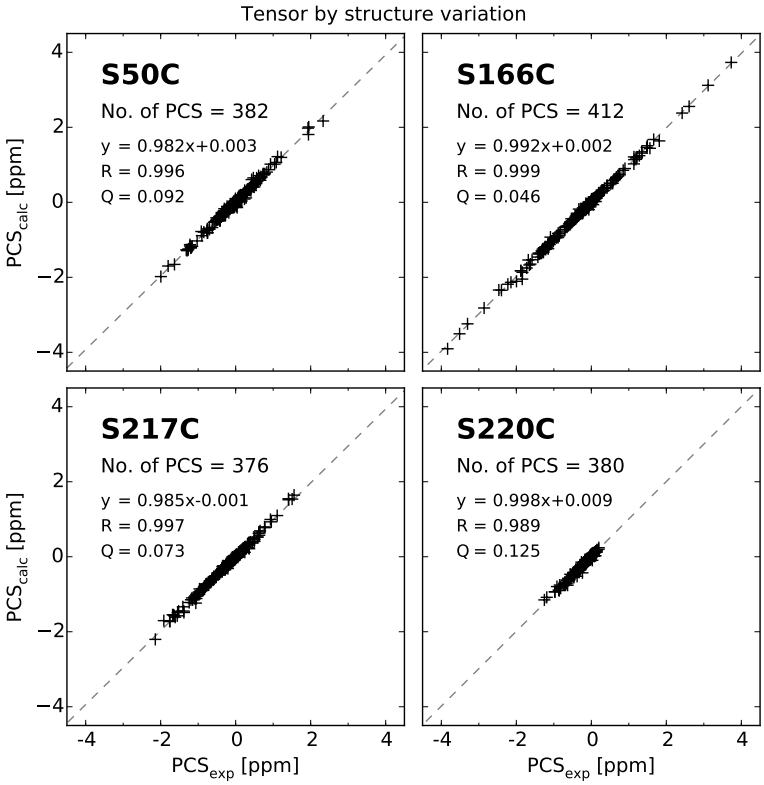

Figure A.7: Correlation of experimental and back calculated PCS obtained from tensors determined with the given type of *Monte-Carlo* protocol using the PCS of set 1.

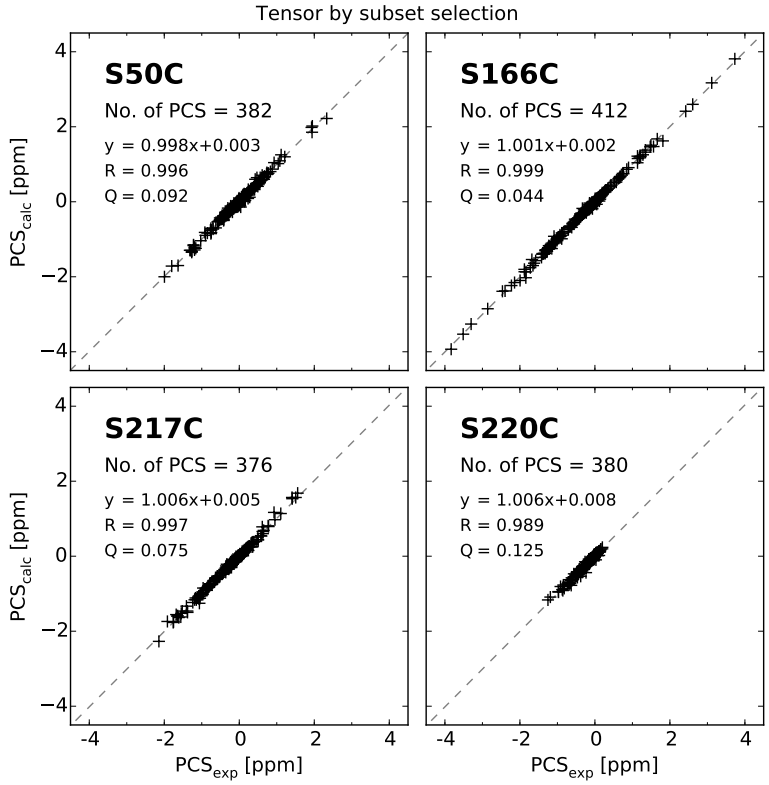

Figure A.8: Correlation of experimental and back calculated PCS obtained from tensors determined with the given type of *Monte-Carlo* protocol using the PCS of set 1.

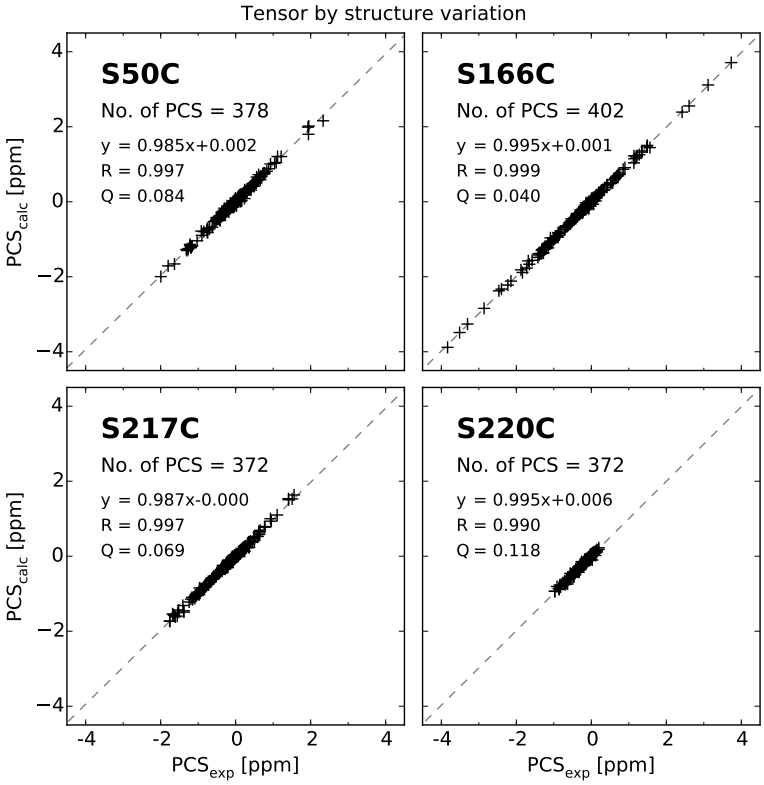

Figure A.9: Correlation of experimental and back calculated PCS obtained from tensors determined with the given type of *Monte-Carlo* protocol using the PCS of set 2.

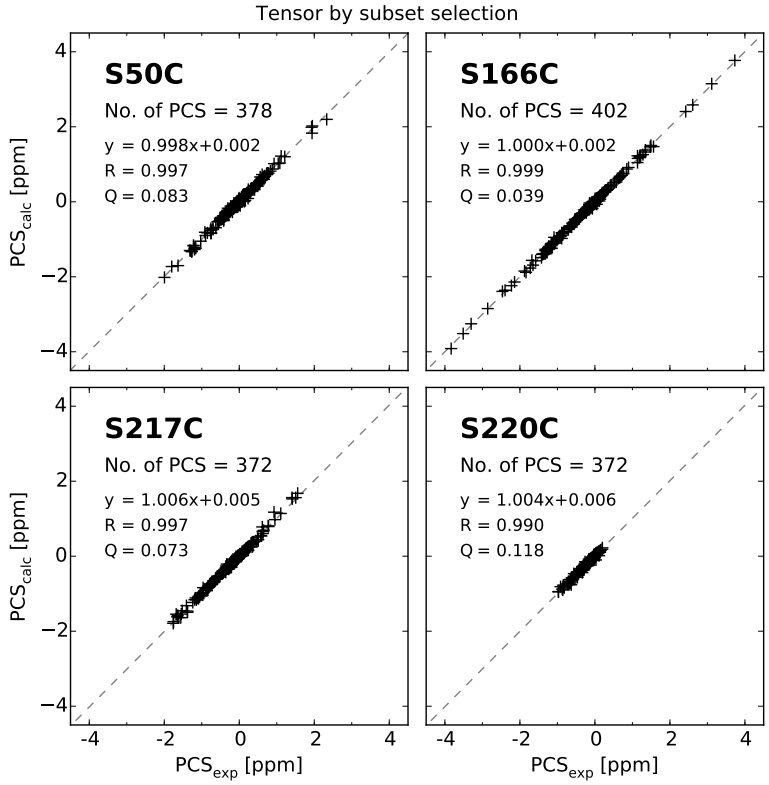

Figure A.10: Correlation of experimental and back calculated PCS obtained from tensors determined with the given type of *Monte-Carlo* protocol using the PCS of set 2.

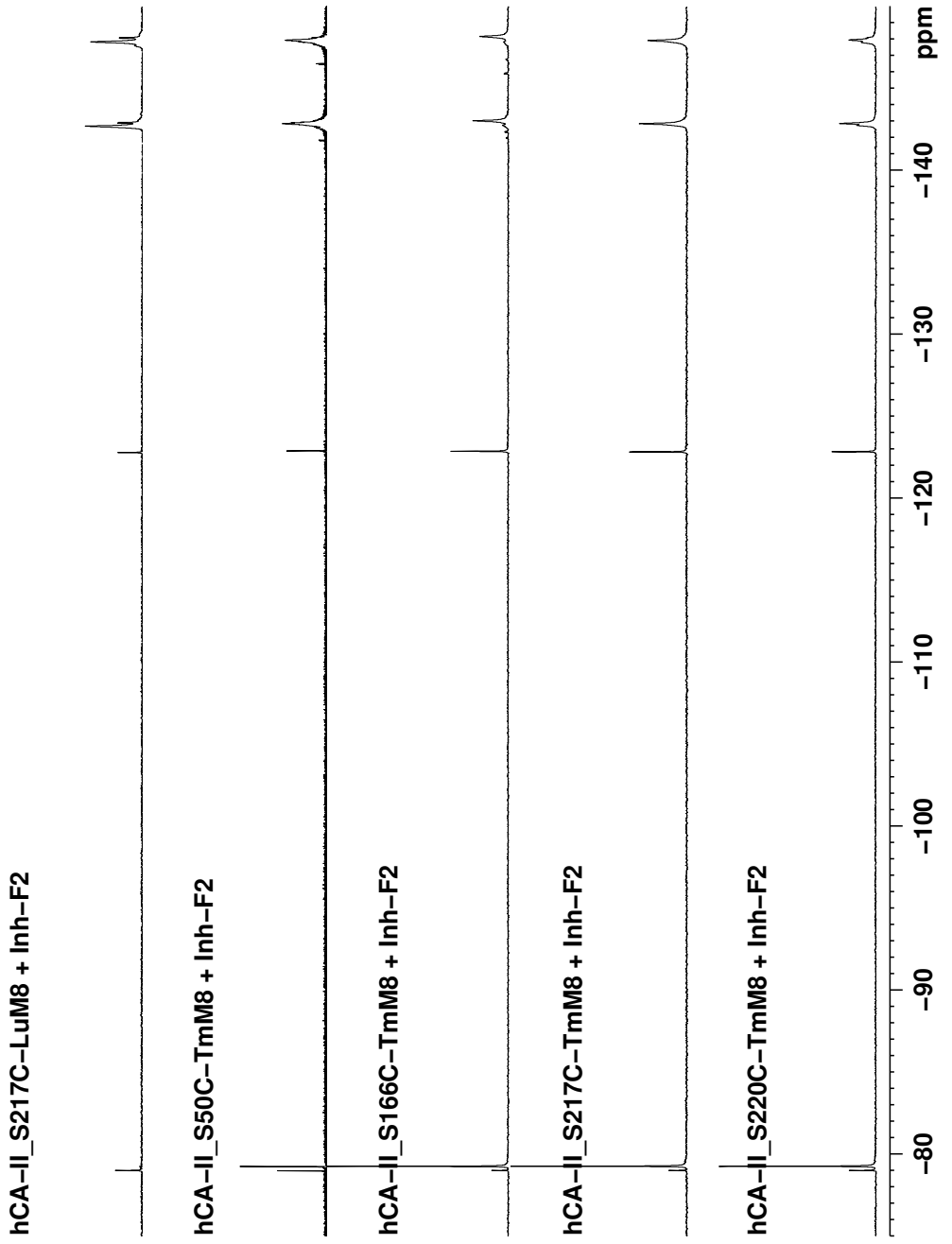

Figure A.11: 1D ^{19}F NMR spectra (600.000 MHz, 298.000 K) F2-Inh in the presence of different hCA-II constructs. All relevant fluorine signals are displayed.

Publications

Scientific publications

1. RICKHAUS, M., L. M. BANNWART, M. NEUBURGER, H. GSELLINGER, **K. ZIMMERMANN**, D. HÄUSSINGER, and M. MAYOR: 'Inducing Axial Chirality in a Geländer Oligomer by Length Mismatch of the Oligomer Strands'. *Angewandte Chemie International Edition* (2014), vol. 53(52): pp. 14587–14591.

2. SCHMIDT, P., L. ZHOU, K. TISHINOV, **K. ZIMMERMANN**, and D. GILLINGHAM: 'Dialdehydes Lead to Exceptionally Fast Bioconjugations at Neutral pH by Virtue of a Cyclic Intermediate'. *Angewandte Chemie International Edition* (2014), vol. 53(41): pp. 10928–10931.

3. FEI, N., D. HÄUSSINGER, S. BLUMLI, B.-J. LAVENTIE, L. D. BIZZINI, **K. ZIMMERMANN** ., U. JENAL, and D. GILLINGHAM: 'Catalytic carbene transfer allows the direct customization of cyclic purine dinucleotides'. *Chem. Commun.* (2014), vol. 50(62): pp. 8499–8502.

4. GARBUIO, L., **K. ZIMMERMANN**, D. HÄUSSINGER, and M. YULIKOV: 'Gd(III) complexes for electron-electron dipolar spectroscopy: Effects of deuteration, pH and zero field splitting'. *Journal of Magnetic Resonance* (2015), vol. 259: pp. 163–173.

Submissions to international conferences

1. **ZIMMERMANN K.**, H. GSELLINGER, and D. HÄUSSINGER: 'DOTA-M8 - a highly rigid lanthanide chelating tag, inducing very large pseudocontact shifts in proteins'. *WWMR 2010, joint EUROMAR 2010 and 17th ISMAR conference*. 2010.
2. **ZIMMERMANN K.**, E. S. NOGUEIRA, H. GSELLINGER, and D. HÄUSSINGER: 'PCS NMR of DOTA-M8 tagged human Carbonic Anhydrase II'. *EUROMAR 2011*. 2011.
3. **ZIMMERMANN K.**, E. S. NOGUEIRA, F. W. MONNARD, and D. HÄUSSINGER: 'Protein - Ligand Interaction in an Artficial Metalloenzyme Monitored by Pseudo Contact Shift 19F-NMR Spectroscopy'. *EUROMAR 2012*. 2012.
4. **ZIMMERMANN K.**, F. W. MONNARD, E. S. NOGUEIRA, and D. HÄUSSINGER: 'Structural Investigation of an Artificial Metalloenzyme by Pseudo Contact Shift 19F-NMR Spectroscopy'. *EUROMAR 2013*. 2013.
5. HÄUSSINGER, D., **K. ZIMMERMANN**, T. MÜNTENER, and M. YULIKOV: 'Rigid, High-Affinity Lanthanide Chelating Tags Monitor Protein-Ligand Interactions by NMR (PCS, PRE AND RDC), DEER-EPR AND FRET'. *EUROMAR 2015*. 2015.

Acknowledgments

I am very grateful to the following people with whom I had contact, with whom I collaborated or with whom I somehow differently interacted during the time of this thesis. Everyone mentioned supported me in a different way but each and any of you contributed substantially to this thesis. If the following lines may not sound like sincere thanks, then it is a mere lack of skill to express myself properly in English.
I am very thankful to:

PD Dr. Daniel Häussinger for giving me the opportunity to contribute to such a very interesting topic during my thesis. For excellent mentoring and for every support during the whole time i spent at this University and particular during this thesis. Especially mentioning also the all the memorable group trips and for brining me to the highest heights so far, at least to those reachable on foot. I learnt a lot for my life.

Prof. Dr. Thomas R. Ward for being the Faculty Representative and for providing laboratory equipment for protein expression.

Prof. Dr. Catherine Housecroft for spontaneous co-examination of this thesis.

Dr. Elisa Nogueira for the good collaboration for teaching me a lot about molecular biology and for preparation of most of the protein that was used in this thesis.

Dr. Fabien Monnard for the good collaboration and for the preparation of the sulfonamide ligands that were essential for this thesis.

Livia Knörr for expression of protein samples and for supporting my own attempts of doing such expressions by myself.

Dr. Heiko Gsellinger for the very good time we had already during the master thesis and as well as during this thesis and especially for numerous humorous situations.

Dr. Luca Garbuio, Dr. Sahand Razzaghi and Dr. Maxim Yulikov for the collaboration and for providing me insights into a more "electronic" part of spectroscopy.

Dr. Michel Rickhaus for allowing me to carry out a challenging assignment of a "Geländer"-like molecule.

Dr. Pascal Schmidt and Na Fei for very interesting NMR projects about dialdehydes and dinucleotides.

Dr. Roché Walliser, Thomas Müntener and Florian Lüttin for the effort and contribution during their master thesis in our group. Especially to Roché for the synthesis of M8-SPy lignand.

To all students that spent either a Wahlpraktikum or a Schlussversuch in our group for their contributions and for their interest. I'm sorry for not mentioning everyone by name, but the almost exponential growth students spending their Wahlpraktikum in our group made it impossible for me to keep track of everyone. And instead of forgetting someone I prefer to threat everyone equally. The only one I have to mention by name is Simone Grendelmeier for her contribution to the protein assignment.

The group of Prof. Dr. Hermann Wegner for sharing the group seminar with us, before they moved to Giessen. And especially to Dr. Luca Schweighauser, Dr. Anne-Florence Tran Van, Silas Götz and Dr. Miroslav Sisa for sharing the basement lab.

Heiko Gsellinger, Jonas Schönle, Ewald Schönhofer, Roché Walliser, Thomas Müntener,

Annabell Bonn, Simone Grendelmeier, Steffen Müller, Florian Lüttin, all the Members of the Constable/Housecroft group and the Wenger group with whom I spent time during breaks, aperos and other occasions.

Jonas Schönle, Ewald Schönhofer, Larissa Pauli, Lukas Jundt, for good time already during the studies and for becoming friends.

All the secretaries and the technical for keeping everything running behind the scenes.

Liselotte Siegfried and Dominik Siefrig for maintaining the supply with liquid nitrogen.

Dr. Sandro Gabutti, Dr. Nicolas Jenny, Dr. Gero Harzmann, Dr. Kiril Tischinov and Cederic Stress for maintaining the ESI-MS.

Dr. R. A. Byrd for a gift of tetramethylcyclen.

Prof. Carol A. Fierke for the generous gift of the pACA plasmid used for the production of hCA-II.

Prof. Dr. S. Grzesiek for poviding ESI-MS time.

You, who I have forgotten to mention, and for reading these lines.

The Swiss National Science Foundation (Grant No. SNF 200021_130263) as well as the Department of Chemistry for financial support .

My family, for all the support ever since I can remember.

Kathrin the most important person of my life, for all the time we spent together.

And of course, to everyone who tried to kick my ∗∗∗.